NONALCOHOLIC FATTY LIVER DISEASE THERAPY: EXPLORING MOLECULAR MECHANISMS OF WELL-DEFINED COMPOSITION FROM NATURAL PLANTS

EDITED BY: Wenji Zhang, Menghao Huang and Runping Liu
PUBLISHED IN: Frontiers in Pharmacology

frontiers Research Topics

ISSN 1664-8714
ISBN 978-2-83250-400-0
DOI 10.3389/978-2-83250-400-0

About Frontiers

Frontiers is more than just an open-access publisher of scholarly articles: it is a pioneering approach to the world of academia, radically improving the way scholarly research is managed. The grand vision of Frontiers is a world where all people have an equal opportunity to seek, share and generate knowledge. Frontiers provides immediate and permanent online open access to all its publications, but this alone is not enough to realize our grand goals.

Frontiers Journal Series

The Frontiers Journal Series is a multi-tier and interdisciplinary set of open-access, online journals, promising a paradigm shift from the current review, selection and dissemination processes in academic publishing. All Frontiers journals are driven by researchers for researchers; therefore, they constitute a service to the scholarly community. At the same time, the Frontiers Journal Series operates on a revolutionary invention, the tiered publishing system, initially addressing specific communities of scholars, and gradually climbing up to broader public understanding, thus serving the interests of the lay society, too.

Dedication to Quality

Each Frontiers article is a landmark of the highest quality, thanks to genuinely collaborative interactions between authors and review editors, who include some of the world's best academicians. Research must be certified by peers before entering a stream of knowledge that may eventually reach the public - and shape society; therefore, Frontiers only applies the most rigorous and unbiased reviews.
Frontiers revolutionizes research publishing by freely delivering the most outstanding research, evaluated with no bias from both the academic and social point of view. By applying the most advanced information technologies, Frontiers is catapulting scholarly publishing into a new generation.

What are Frontiers Research Topics?

Frontiers Research Topics are very popular trademarks of the Frontiers Journals Series: they are collections of at least ten articles, all centered on a particular subject. With their unique mix of varied contributions from Original Research to Review Articles, Frontiers Research Topics unify the most influential researchers, the latest key findings and historical advances in a hot research area! Find out more on how to host your own Frontiers Research Topic or contribute to one as an author by contacting the Frontiers Editorial Office: frontiersin.org/about/contact

NONALCOHOLIC FATTY LIVER DISEASE THERAPY: EXPLORING MOLECULAR MECHANISMS OF WELL-DEFINED COMPOSITION FROM NATURAL PLANTS

Topic Editors:
Wenji Zhang, Crops Research Institute, Guangdong Academy of Agricultural Science, China
Menghao Huang, Indiana University Bloomington, United States
Runping Liu, Beijing University of Chinese Medicine, China

Citation: Zhang, W., Huang, M., Liu, R., eds. (2022). Nonalcoholic Fatty Liver Disease Therapy: Exploring Molecular Mechanisms of Well-defined Composition From Natural Plants. Lausanne: Frontiers Media SA.
doi: 10.3389/978-2-83250-400-0

Table of Contents

frontiers | Frontiers in Pharmacology

TYPE Editorial
PUBLISHED 20 September 2022
DOI 10.3389/fphar.2022.1006750

OPEN ACCESS

EDITED AND REVIEWED BY
Angelo A Izzo,
University of Naples Federico II, Italy

*CORRESPONDENCE
Wenji Zhang,
zhangwenji@gdaas.cn
Menghao Huang,
huangmen@iu.edu

SPECIALTY SECTION
This article was submitted to Gastrointestinal and Hepatic Pharmacology, a section of the journal Frontiers in Pharmacology

RECEIVED 29 July 2022
ACCEPTED 02 August 2022
PUBLISHED 20 September 2022

CITATION
Zhang W, Huang M and Liu R (2022), Editorial: Nonalcoholic fatty liver disease therapy: Exploring molecular mechanisms of well-defined composition from natural plants. *Front. Pharmacol.* 13:1006750. doi: 10.3389/fphar.2022.1006750

Editorial: Nonalcoholic fatty liver disease therapy: Exploring molecular mechanisms of well-defined composition from natural plants

Wenji Zhang[1]*, Menghao Huang[2]* and Runping Liu[3]

[1]Guangdong Provincial Engineering & Technology, Research Center for Tobacco Breeding & Comprehensive Utilization, Key Laboratory of Crop Genetic Improvement of Guangdong Province, Crops Research Institute, Guangdong Academy of Agricultural Sciences, Guangzhou, China, [2]Indiana University School of Medicine, Indianapolis, IN, United States, [3]Beijing University of Chinese Medicine, Beijing, China

KEYWORDS

nonalcoholic fatty liver disease, Natural plants, NAFLD, NASH, Well-defined Compositio

Editorial on the Research Topic
Nonalcoholic fatty liver disease therapy: Exploring molecular mechanisms of well-defined composition from natural plants

Nonalcoholic fatty liver disease (NAFLD), a global public health problem in recent years with an incidence rate of approximately 25%, may bring a progressive disease of non-alcoholic steatohepatitis (NASH), cirrhosis, or even hepatocellular carcinoma (Fan et al., 2017; Younossi, 2019). Ever greater attention has been paid to treating NAFLD, and except for the crucial intervention of lifestyle modification, the treatments of drugs and health products have become particularly important in our current world of fast-paced modern life (Zhu et al., 2020). At present, the main adjuvant clinical therapies usually include pioglitazone and vitamin E treatment, but the applicability of these is weak because the long-term effects have yet to be determined (Majumdar et al., 2021). So far, no drugs specifically targeting NAFLD have been approved by the FDA. People have been exploring drugs to treat NAFLD over the past two decades.

Substances from plants including tea, flaxseed, cinnamon, silybin, soy, ginger, and licorice are playing an increasingly promising role in the treatment and prevention of NAFLD (Yan et al., 2020). However, previous research was much more focused on plant-derived extracts or mixtures, which due to the unclear constituents or the lack of standardized product progress, is still a long way from drug development. Therefore, this Research Topic, Nonalcoholic Fatty Liver Disease Therapy: Exploring Molecular Mechanisms of Well-defined Composition from Natural Plants, is inclined to and encourages pharmacological research about NAFLD using well-defined compositions. We hope to discover and collect novel

natural compounds, active ingredients, combination formulas, or prescriptions in plants with therapeutic selectivity that can be used for NAFLD, or NASH. Meanwhile, the novel discovery of molecular pathogenic mechanisms of NAFLD studies was also reported.

In this Research Topic, the aurantio-obtusin from Cassia semen (Zhou et al.), pterostilbene from blueberries and grapes (Tan et al.), the combination of bicyclol from *Schisandra chinensis* and berberine from *Coptis chinensis* and *Berberis vulgaris* (Li et al.), artemether from artemisinin (Xu et al.), scoparone from Artemisia scoparia Waldst. etKit and Artemisia capillaris Thunb. (Jiang et al.), nootkatone from Alpiniae oxyphyllae Fructus (Yong et al.), Limonin from lemon (Wang et al.) and theaflavin-3,3′-digallate from black tea (Zhou et al.), attenuated NAFLD/NASH mainly by regulating lipid metabolism and liver inflammation to varying degrees. There are also a lot of new pathways involved. For example, Aurantio-obtusin ameliorates hepatic steatosis *via* AMPK/autophagy- and AMPK/TFEB-mediated suppression of lipid accumulation; bicyclol enhanced lipolysis and β-oxidation through restoring the p62-Nrf2-CES2 signaling axis and p62-Nrf2-PPARα signaling axis, respectively; scoparone downregulated the activation of JNK/Sab signaling, improved hepatosteatosis and inflammation, especially mitochondrial dysfunction; theaflavin-3,3′-digallate was speculated to attenuate leptin-deficient induced NAFLD via Fads1/PPARδ/Fabp4 axis. In particular, berberine and theaflavin-3,3′-digallate also protected NAFLD *in vivo* through regulating gut microbiota which is a hot issue of concern, for example, berberine enriches lipid metabolism-related Bacteroidaceae (family) and *Bacteroides* (genus); theaflavin-3,3′-digallate increased the abundance of Prevotellaceae_UCG-001, norank_f_Ruminococcaceae, and GCA-900066575 and significantly decreased that of Parvibacter. Noticeably, with the multiple targets, the ganweikang tablet (Ma et al.), based on traditional Chinese medicine theory and clinical experience, was verified to improve NAFL and NASH by modulating inflammation, apoptosis, and fatty acid oxidation by inhibiting NFκB, caspase-8, and activating PPARα. In addition, artemether, the combination of bicyclol and berberine, and pterostilbene, also mediated the development of liver fibrosis *in vivo*, which protects liver injury more broadly. These results have a direct impact on the treatment of NAFLD and provided promising candidates for its therapy.

The pathophysiological mechanisms of NAFLD is a complex, "multiple-hit theory" that has gradually been posited to explain the pathogenesis of NAFLD, including visceral obesity and lipodystrophy-like phenotype, diabetes, insulin resistance, *de novo* lipogenesis, gut dysbiosis, genetic factors, epigenetic modifications, etc (Zhang et al., 2022). Great progress has been made on the alleviating effect of plant-derived composition on fatty liver disease, but the research on its mechanism is not comprehensive and in-depth, and its clinical application needs to be evaluated based on the "multiple-hit theory".

Author contributions

WZ wrote the draft, MH and RL revised and polished the manuscript.

Funding

This work was supported by the National Natural Science Foundation of China (grant number 81903319); the Special Fund for Scientific Innovation Strategy-Construction of High Level Academy of Agriculture Science (grant number R2018YJ-YB3002); the Foundation of Director of Crops Research Institute, Guangdong Academy of Agricultural Sciences (grant number 202205).

Conflict of interest

The authors declare that the research was conducted in the absence of any commercial or financial relationships that could be construed as a potential conflict of interest.

Publisher's note

References

Fan, J. G., Kim, S. U., and Wong, V. W. (2017). New trends on obesity and NAFLD in Asia. *J. Hepatol.* 67, 862–873. doi:10.1016/j.jhep.2017.06.003

Majumdar, A., Verbeek, J., and Tsochatzis, E. A. (2021). Non-alcoholic fatty liver disease: Current therapeutic options. *Curr. Opin. Pharmacol.* 61, 98–105. doi:10.1016/j.coph.2021.09.007

Yan, T., Yan, N., Wang, P., Xia, Y., Hao, H., Wang, G., et al. (2020). Herbal drug discovery for the treatment of nonalcoholic fatty liver disease. *Acta Pharm. Sin. B* 10, 3–18. doi:10.1016/j.apsb.2019.11.017

Younossi, Z. M. (2019). Non-alcoholic fatty liver disease - a global public health perspective. *J. Hepatol.* 70, 531–544. doi:10.1016/j.jhep.2018.10.033

Zhang, W., Lin, H., Cheng, W., Huang, Z., and Zhang, W. (2022). Protective effect and mechanism of plant-based monoterpenoids in non-alcoholic fatty liver diseases. *J. Agric. Food Chem.* 70, 4839–4859. doi:10.1021/acs.jafc.2c00744

Zhu, J. Z., Yi, H. W., Huang, W., Pang, T., Zhou, H. P., and Wu, X. D. (2020). Fatty liver diseases, mechanisms, and potential therapeutic plant medicines. *Chin. J. Nat. Med.* 18, 161–168. doi:10.1016/S1875-5364(20)30017-0

frontiers in Pharmacology

ORIGINAL RESEARCH
published: 11 January 2022
doi: 10.3389/fphar.2021.826628

Aurantio-Obtusin Attenuates Non-Alcoholic Fatty Liver Disease Through AMPK-Mediated Autophagy and Fatty Acid Oxidation Pathways

*Fei Zhou[1†], Mingning Ding[1†], Yiqing Gu[2], Guifang Fan[2], Chuanyang Liu[3], Yijie Li[1], Rong Sun[4,5], Jianzhi Wu[1], Jianchao Li[4,6], Xiaoyong Xue[1], Hongjuan Li[1] and Xiaojiaoyang Li[1]**

[1]School of Life Sciences, Beijing University of Chinese Medicine, Beijing, China, [2]School of Chinese Materia Medica, Beijing University of Chinese Medicine, Beijing, China, [3]School of Traditional Chinese Medicine, Beijing University of Chinese Medicine, Beijing, China, [4]The Second Hospital of University, Jinan, China, [5]Advanced Medical Research Institute, Shandong University, Jinan, China, [6]Shandong University of Traditional Chinese Medicine, Jinan, China

OPEN ACCESS

Edited by:
Menghao Huang,
Indiana University school of medicine, United States

Reviewed by:
Hu Li,
Chinese Academy of Medical Sciences and Peking Union Medical College, China
Hongzhi Du,
Hubei University of Chinese Medicine, China

***Correspondence:**
Xiaojiaoyang Li
xiaojiaoyang.li@bucm.edu.cn

[†]These authors have contributed equally to this work

Specialty section:
This article was submitted to Gastrointestinal and Hepatic Pharmacology, a section of the journal Frontiers in Pharmacology

Received: 01 December 2021
Accepted: 21 December 2021
Published: 11 January 2022

Citation:
Zhou F, Ding M, Gu Y, Fan G, Liu C, Li Y, Sun R, Wu J, Li J, Xue X, Li H and Li X (2022) Aurantio-Obtusin Attenuates Non-Alcoholic Fatty Liver Disease Through AMPK-Mediated Autophagy and Fatty Acid Oxidation Pathways. Front. Pharmacol. 12:826628. doi: 10.3389/fphar.2021.826628

Nonalcoholic fatty liver disease (NAFLD), manifested as the aberrant accumulation of lipids in hepatocytes and inflammation, has become an important cause of advanced liver diseases and hepatic malignancies worldwide. However, no effective therapy has been approved yet. Aurantio-obtusin (AO) is a main bioactive compound isolated from *Cassia* semen that has been identified with multiple pharmacological activities, including improving adiposity and insulin resistance. However, the ameliorating effects of AO on diet-induced NAFLD and underlying mechanisms remained poorly elucidated. Our results demonstrated that AO significantly alleviated high-fat diet and glucose-fructose water (HFSW)-induced hepatic steatosis in mice and oleic acid and palmitic acid (OAPA)-induced lipid accumulation in hepatocytes. Remarkably, AO was found to distinctly promote autophagy flux and influence the degradation of lipid droplets by inducing AMPK phosphorylation. Additionally, the induction of AMPK triggered TFEB activation and promoted fatty acid oxidation (FAO) by activating PPARα and ACOX1 and decreasing the expression of genes involved in lipid biosynthesis. Meanwhile, the lipid-lowing effect of AO was significantly prevented by the pretreatment with inhibitors of autophagy, PPARα or ACOX1, respectively. Collectively, our study suggests that AO ameliorates hepatic steatosis *via* AMPK/autophagy- and AMPK/TFEB-mediated suppression of lipid accumulation, which opens new opportunities for pharmacological treatment of NAFLD and associated complications.

Keywords: aurantio-obtusin, nonalcoholic fatty liver disease, autophagy, AMPK, PPARα, ACOX1

Abbreviations: AO, Aurantio-obtusin; ACOX1, acyl-CoA oxidase 1; AMPK, AMP-activated protein kinase; ATG5, autophagy-related protein 5; CC, compound C; CPT1α, carnitine palmitoyl transferase 1 alpha; FASN, fatty acid synthase; FFA, free fatty acids; HFSW, high-fat diet and glucose-fructose water; LC3, microtubule-associated protein 1 light chain 3; MPH, mouse primary hepatocyte; mTOR, mechanistic target of rapamycin; OAPA, oleic acid and palmitic acid; PPARα, peroxisome proliferator-activated receptor alpha; SREBP1, sterol regulatory element binding protein 1; TC, total cholesterol; TFEB, transcription factor EB; TG, triglycerides; TRCDA, 10,12-Tricosadiynoic acid; ULK, unc-51-like kinases.

INTRODUCTION

Nonalcoholic fatty liver disease (NAFLD), characterized by excess hepatic fat accumulation, inflammation and oxidative stress, has become a burgeoning worldwide epidemic liver disease, affecting approximately one-quarter of the entire global population (Diehl and Day, 2017). Moreover, NAFLD not only encompasses a cascade of conditions including nonalcoholic steatohepatitis (NASH), advanced liver fibrosis, cirrhosis and even hepatocellular carcinoma (HCC) but also confers a high risk for type 2 diabetes, cardiovascular complications and various extrahepatic malignancies (Dixon et al., 2001; Loomba et al., 2020). So far, the underlying mechanism driving NAFLD development remains obscure. An increasing number of studies have pointed out that the pathophysiology of NAFLD is complex and multifactorial. Progress over the last decade was substantial in the roles of lipotoxicity, oxidative stress, inflammation, genetics and metabolism in NAFLD pathogenesis (Marra and Svegliati-Baroni, 2018). Furthermore, gut microbiome and various dietary components as other gastrointestinal hits with proinflammatory potential have been demonstrated (Tilg et al., 2021). Among these pathogenic factors, lipotoxicity, resulting from excessive accumulation of harmful lipids and hepatocyte injury, has gained remarkable attention and represents a critical step in NAFLD progression (Marra and Svegliati-Baroni, 2018).

Autophagy is a genetically programmed and evolutionarily conserved self-eating catabolic process whereby injurious organelles and intracellular components are degraded within lysosome. Under pathological circumstances, autophagy plays a critical role in maintaining cellular and metabolic homeostasis by eliminating damaged organelles, misfolded proteins as well as accumulated lipid droplets (Singh et al., 2009). Recently, insufficient autophagy was regarded as the fundamental cellular defect in the pathogenesis of NAFLD. Notably, the dysregulation of hepatic autophagy has been implicated in NAFLD and NASH patients (Czaja, 2016). In experimental animals, the blockade of autophagy using selective inhibitors or specific siRNAs targeting autophagy-related genes like autophagy-related protein 5 (ATG5, *Atg5*) promoted the hepatic accumulation of lipid droplets and triglycerides (TG) and accelerated liver injury (Ni et al., 2012; Zhou et al., 2018). Furthermore, the enhancement of autophagy accelerated fatty acid oxidation (FAO), improved mitochondrial function and protected against palmitate lipotoxicity in murine hepatocytes (Mwangi et al., 2019). However, whether autophagy in NAFLD could be targetable by any pharmacological therapies remains unclear.

At present, therapeutic approaches of NAFLD mainly include dietary restrain or taking medicines inhibiting lipid biogenesis, removing excessive lipid droplets, and inhibiting inflammation or cell apoptosis in livers (Mao et al., 2016). Notably, the primary therapeutic strategy for NAFLD is targeting intrahepatic lipid accumulation, such as the agonists of FAO including peroxisome proliferator-activated receptor alpha (PPARα) agonists, acyl-coenzyme A oxidase 1 (Acox1) agonists and inhibitors of *de novo* lipogenesis including fatty acid synthase (FASN) inhibitors. Although most representative next-generation PPARα or pan-PPARs agonists like elafibranor and pioglitazone have been found to efficiently induce the resolution of NASH patients, most of them have been withdrawn from the market owing to severe side effects such as weight gain, bone fractures, peripheral edema and even congestive heart failure (Friedman et al., 2018; Boeckmans et al., 2019). Besides, a variety of synthetic inhibitors, including apoptosis signaling kinase 1 (ASK1) inhibitors, galectin three antagonists and nonsteroidal FXR agonists, have been reported to improve advanced NASH patients in clinical trials; however, their applications are still restricted due to unexpected adverse effects like pruritus (Sumida and Yoneda, 2018). Recently, autophagy represents a novel therapeutic target for NAFLD by clearing excessive lipid droplets and suppressing hepatic inflammation, while the unclear and double-edged effects of autophagy raise concerns as well (Mao et al., 2016). Despite these tough challenges, there is as yet no Food and Drug Administration (FDA)-approved pharmacotherapy, and it remains a pressing need to discover interventions to mitigate the risk of hepatic steatosis.

Unlike the above strategies that mainly focused on one single target, natural products derived from traditional Chinese medicine (TCM) with multiple-targeting and promising hepatoprotective effects represent the rich source of lead compounds for drug discovery against liver steatosis. Aurantio-obtusin (AO), the main characteristic bioactive ingredient isolated from *Cassiae* semen that has a long history of usage for thousands of years, exerts a broad spectrum of pharmacological activities, including anti-inflammatory, anti-allergic, anti-hypertensive, antioxidant and immunoregulatory effects (Kim et al., 2015; Kwon et al., 2018; Tejero et al., 2019). Recently, increasing studies have begun to focus on the unique effects of AO on improving metabolic diseases. Under the challenge of high fat and sweet sugar, AO was found to improve adiposity and insulin resistance by downregulating the expression of lipid metabolism-related genes and suppressing inflammatory cytokines expression in white adipose tissue (Guo et al., 2021). Although the above results pointed out the possibility of AO-induced hepatoprotective effects against liver steatosis, researchers temporarily focused on the anti-obesity effect of AO while paid less attention to its lipid-reducing effect and deeper mechanism involved in NAFLD. These insightful preliminary results and existing questions encourage us to further investigate the potential protective effects of AO on diet-induced hepatic steatosis.

In the current study, we investigated the therapeutic effects and underlying mechanisms of AO in a high-fat diet (HFD) and glucose-fructose water (HFSW)-induced NAFLD mouse model and oleic acid and palmitic acid (OAPA)-treated mouse primary hepatocytes (MPHs). AO markedly promoted autophagy flux, triggered transcription factor EB (TFEB) activation, subsequently inhibited lipid *de novo* synthesis and accelerated FAO in livers by inducing AMP-activated protein kinase (AMPK) phosphorylation, which were prevented by pretreatment with the inhibitors of autophagy, PPARα or ACOX1, respectively. Taken together, our findings provide experimental evidence supporting the possibility of developing AO-based medicines

for the pharmacological treatment of NAFLD and associated metabolic disorders.

MATERIALS AND METHODS

Materials

AO (PS0100-0250) was purchased from Push Bio-Technology (Chengdu, China). Oleic acid (C4977) was obtained from APExBIO (Houston, United States). Palmitic acid (P101061) was purchased from Aladdin (Shanghai, China). 3-methyladenine (3-MA) (S2767) and compound C (CC) (HY-13418A) were obtained from Selleck (Houston, United States). 10,12-Tricosadiynoic acid (TRCDA), glucose (B21882) and fructose (B21896) were purchased from Yuanye Bio-Technology (Shanghai, China). Williams' Medium E with L-glutamine (W4125), collagenase from *Clostridium* histolyticum (C5138), collagen type I from rat tail (C3867), dexamethasone (D1756), 0.1% L-Thyroxine (T-073) and other cell culture material were purchased from Sigma (St. Louis, United States). Goat anti-mouse IgG (H + L) Highly Cross-Adsorbed secondary antibody (Alexa Fluor Plus 488) (Ul287767) was obtained from Thermo Fisher Scientific (Waltham, United States) and goat anti-rabbit IgG (H + L), F (ab')2 Fragment (Alexa Fluor 594 Conjugate) (8889S) was purchased from Cell Signaling Technology (Danvers, United States).

Animal Study

C57BL/6J (8-week-old, male) mice were obtained from Vital River Laboratory Animal Technology (Beijing, China). Mice were kept under 12 h light-dark cycle at a consistent temperature (22 ± 2 C) with free access to water and standard chow. All animals were accepted 1 week of adaptive feeding before the experiment and sacrificed after 8-weeks treatment. For *in vivo* experiments, the doses of AO (5,10 and 15 mg/kg) were selected based on recent publications (Xu et al., 2019; Guo et al., 2021). In chronic HFSW experiment (n = 6), mice were divided into five groups: 1) control group (chow diet); 2) NAFLD model group [HFSW, Western diet-42% Kcal from fat and 0.2% cholesterol (TD.88137, Harlan Laboratories, Inc., Indianapolis, IN, United States) plus with a high sugar solution (D-fructose: 23.1 g/L and D-glucose: 18.9 g/L) in drinking water (Li et al., 2021)]; (3–5) HFSW diet with AO administration group. Mice in groups (2–5) were first fed with the HFSW diet for 4 weeks to induce liver steatosis followed by orally given different doses of AO (5, 10 and 15 mg/kg) or vehicle control for another 4 weeks. In the ACOX1 inhibitor experiment, mice were divided into five groups at random (n = 6): 1) control group; 2) HFSW diet group; 3) HFSW diet with AO administration group; 4) HFSW diet with TRCDA administration group; 5) HFSW diet with AO and TRCDA administration group. Mice from groups (4)–5) were intragastrically administrated with TRCDA (1 mg/kg) for 8 weeks and mice from groups (3)–5) orally administrated with AO (10 mg/kg) in the last 4 weeks. Body weight, food intake and water consumption were measured every 2 days. At the end of treatment, mice were anesthetized and shaved in the thorax and abdomen area for measuring body temperature using Tau two VPC thermal imaging camera (FLIR Systems, United States). After sacrificed, mice serum and liver tissues were collected for further experiments.

All animal studies and procedures were approved by the Institutional Animal Care and Use Committee of Beijing University of Chinese Medicine and were carried out in accordance with all guidelines.

Measurement of Serum Alanine Transaminase and Aspartate Transaminase

Mice serum was collected after sacrificed. ALT assay kit (C009-2-1) and AST assay kit (C010-2-1) were obtained from Nanjing Jiancheng Bioengineering Institute (Nanjing, China) and used to measure serum ALT and AST levels according to the manufacturer's instructions.

Measurement of Total TG and Total Cholesterol

Mouse serum was collected by centrifugation and liver samples were homogenized by anhydrous ethanol for obtaining supernatant. Cell samples were lysed in RIPA lysis buffer and prepared the supernatant for following detection. TG and TC from different samples were measured using TG assay Kit (A110-1-1) and TC assay kit (A111-1-1) from Nanjing Jiancheng Bioengineering Institute (Nanjing, China).

Histopathologic Analysis

Mice liver tissues were fixed with 4% formaldehyde for 7 days, dehydrated by ethyl alcohol, embedded by paraffin and cut into 5 μM sections. For hematoxylin and eosin (HE) staining, paraffin sections were dewaxed by xylene, rehydrated by ethyl alcohol, stained by hematoxylin and eosin and dehydrated by ethyl alcohol. The images of all sections were captured by Aperio Versa (Leica, Wetzlar, Germany).

Oil-Red Staining

Oil-red staining was performed as previous established conditions (Li et al., 2021). Oil-red powder was first dissolved in isopropanol solution (0.5 g/ml). Freshly cut sections from frozen livers and hepatocytes were fixed in 4% formaldehyde, washed in PBS solution and subsequently stained by Oil-red solution for 30 min. The image was captured by Aperio Versa (Leica, Wetzlar, Germany).

Isolation and Culture of Mouse Primary Hepatocytes

MPHs were isolated by a two-step collagenase perfusion method as previously described (Li et al., 2017). After seeded in 6-well plates or different dishes that pre-coated with collagen, MPHs were cultured in Williams' Medium E containing with 0.1% dexamethasone and 0.1% L-Thyroxine for further experiments.

Cell Treatment

For *in intro* experiments, the doses of AO were chosen according to our CCK8 data. For the time course experiment, MPHs were

treated with DMSO or AO (25 μM) for 0.5, 1, 2, 4 and 6 h. For the dose course experiment with or without OAPA, MPHs were first treated with OAPA (OA: 250 μM, PA: 500 μM) or not and then treated with different dosages of AO (12.5, 25 and 50 μM) for 24 h. For inhibitor experiments with or without OAPA, MPHs were first treated CC (10 μM), 3-MA (5 mM), TRCDA (10 μM) or GW6771 (10 μM) for 1.5 h, respectively, then treated with OAPA or not and AO (25 μM) for another 2 h or 24 h.

HepG2 Cells Transfection

HepG2 cells were obtained from ATCC and were seeded in a 6-well plate at 30×10^4 cells/well for 24 h. After attachment, cells were cultured with complete medium (CM) (1% Penicillin-Streptomycin and 10% FBS) containing HBLV-mcherry-EGFP-LC3-PURO (MOI = 20) (HanBio Technology, China) and polybrene (5 μg/ml) for 8 h. After virus infection, cell culture medium was changed into fresh CM for 16 h and then replaced with selection medium (CM containing 2.5 μg/ml puromycin). After 1 week of selection, cells were treated with AO (25 μM) or DMSO for 3 and 5 h. Live cell images were captured by Olympus FV3000 confocal laser scanning microscopy (Tokyo, Japan).

Quantitative Real-Time RT-PCR

Liver tissues were homogenized and lysed by TRIzol reagent. Total RNA from mouse livers were extracted by chloroform, isopropanol and 75% ethyl alcohol and dissolved in DNase/RNase-free water. Total RNA of cell samples was extracted with Fast Pure Cell/Tissue Total RNA isolation kit (RC101-01, Vazyme Biotech). The mRNA expression was detected by quantitative real-time PCR (qPCR) using AceQ universal SYBR qPCR Master Mix (Q511-02, Vazyme Biotech). Further inquiries of primers for qPCR can be directed to the corresponding author.

Western Blot Analysis

Western blot analysis was carried out as previously described (Li et al., 2021). Briefly, liver tissues and cell samples were lysed in RIPA lysis buffer. The equivalent protein was prepared, separated with SDS-PAGE gel and successively incubated with relative primary antibodies at 4 C overnight. After incubated with secondary antibodies, all bands were developed using ECL western bolting reagents and imaged by ChemiDocTM Touch Imaging System (Bio-Rad, Hercules, CA). Detailed information of primary antibodies was provided in **Supplementary Table S1**.

Statistical Analysis

All results were repeated at least three times and presented as mean ± SEM. One-way ANOVA was employed to compare the differences between multiple groups using GraphPad Prism 8 (Graph-Pad, San Diego, CA). p value ≤ 0.05 was considered statistically significant.

RESULTS

AO Ameliorates Hepatic Steatosis in HFSW-Fed Mice

To identify the hepatoprotective effects and detailed mechanisms of AO on fatty liver, mice were first fed with an HFSW diet for 4 weeks to induce liver steatosis followed by administration with different doses of AO (5, 10 and 15 mg/kg) or vehicle control for additional 4 weeks with continuous HFSW diet (**Figure 1A**). The body weight and the intake of food and water were recorded every 2 days. As shown in **Figure 1B** and **Supplementary Figure S1A**, AO significantly reduced the HFSW-induced body weight and body weight gain without affecting the amount of average calorie and water intake. Moreover, analysis of the raw tissues of liver, spleen and adipose showed that AO slightly decreased the organ coefficients of spleen and adipose but had no obvious influence on livers (**Supplementary Figure S1B–1D**). Serum biochemistry assays then demonstrated that AO significantly decreased the serum ALT and AST levels in HFSW mice (**Figure 1C**, **left** and **middle panel**). As expected, HFSW also significantly increased the serum levels of blood glucose, which were markedly reversed by medium dose and high dose of AO (**Figure 1C**, **right panel**). More intuitively, we examined the accumulation of abdominal fat and measured the thoracoabdominal temperature and found that AO resulted in a less weight of white adipose tissue and a greater liver temperature than that in the HFSW group (**Figure 1D**), suggesting that AO improved metabolic syndrome of HFSW mice. As illustrated in **Figure 1E** and **Supplementary Figure S1E**, HFSW also significantly elevated the serum and hepatic lipid accumulation, as evidenced by increased levels of TG and TC. As expected, AO administration markedly reduced hepatic TG and TC as well as serum TG levels. In line with the above findings, histological examination depicted that AO significantly and dose-dependently reduced the HSFW-caused lipid droplet accumulation and extensive steatosis, as indicated by decreased number and size of lipid droplets in hepatocytes (**Figure 1F** and **Supplementary Figure S1F**). These results suggested that AO exerted beneficial effects on hepatic steatosis.

AO Regulates Lipid Metabolism and Autophagy in HFSW-Fed Mice

Considering that inflammatory response toward hepatocyte damage is a decisive step in the development of NAFLD, we examined the levels of several major inflammatory cytokines and chemokines for immune cell recruitment. As shown in **Figure 2A**, HFSW significantly increased the levels of *Ccl2* and *Tgfb1* in livers, which were then markedly downregulated under AO administration. However, the effect of AO on HFSW-induced *Tnf* and *IL-6* was minimal (**data not shown**). Once out of control, persistent inflammation will disturb the bile acid homeostasis and lead to a cumulative result-liver fibrosis, which in turn, reinforces a vicious cycle of NAFLD damage (Chavez-Talavera et al., 2017). Cholesterol metabolism enzyme cholesterol 7-alpha-hydroxylase (CYP7A1, *Cyp7a1*), a primary rate-limiting enzyme that promotes the conversion of cholesterol into bile acids, was downregulated by HFSW probably due to a compensatory mechanism but was markedly reduced under all doses of AO (**Figure 2B**). Next, we measured the mRNA expression of genes involved in ECM accumulation and liver fibrosis like *Fn1* and collagen type I (COL1A1, *Col1a1*). Although the *Fn1* level was almost unchanged before or after AO treatment (**Supplementary Figure S2A**, **left panel**), the administration of

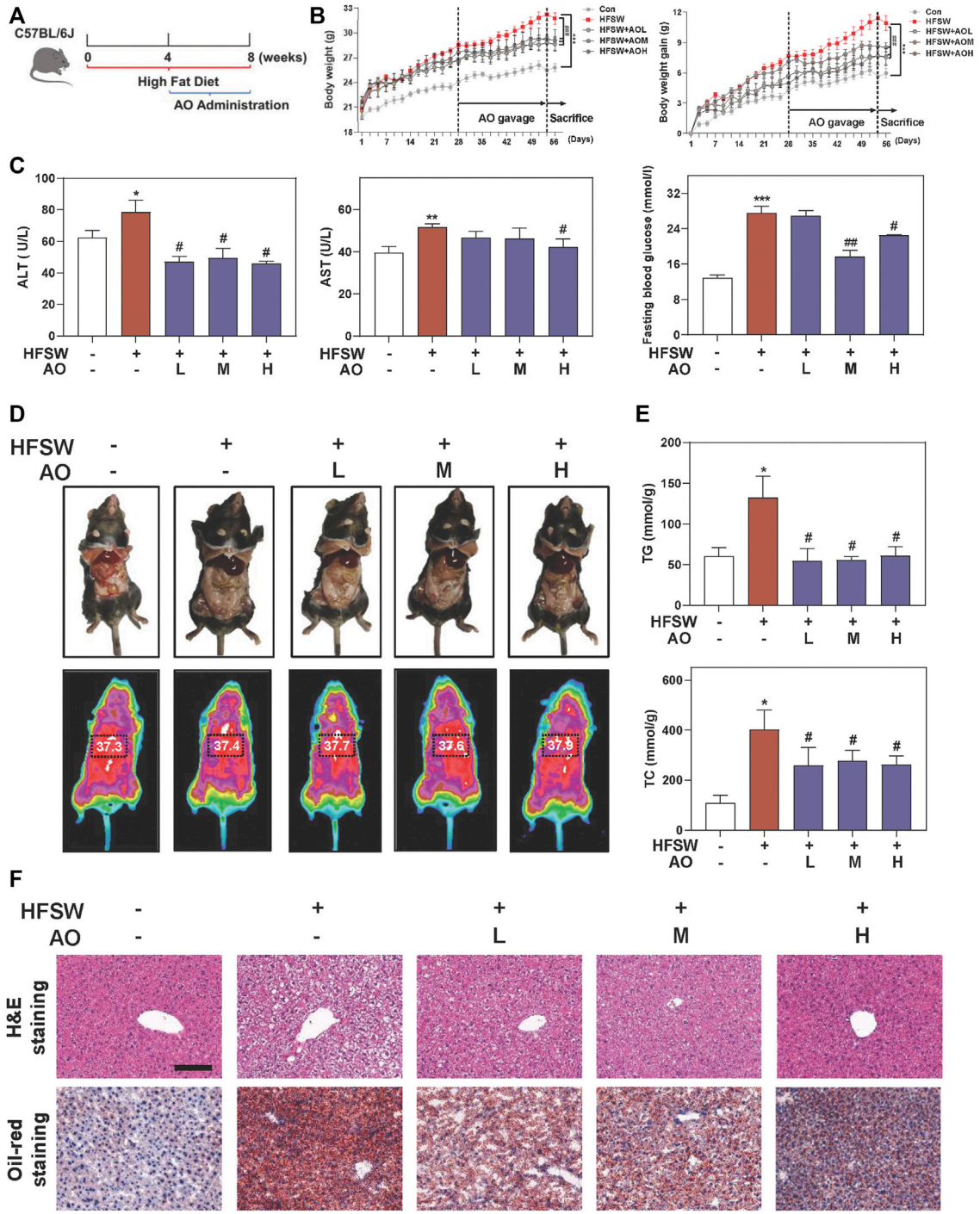

FIGURE 1 | AO ameliorates hepatic steatosis in HFSW-fed mice. Mice were fed with chow diet or HFSW diet for 8 weeks and administered with different dosages (5, 10, and 15 mg/kg) of AO by gavage from Week 5 **(A)** Schematic diagram of *in vivo* experimental design **(B)** Body weight and Body weight gain **(C)** Levels of serum ALT and AST and fasting blood glucose **(D)** Representative images of epididymal fat and thoracoabdominal temperature **(E)** Hepatic TG and TC levels **(F)** Representative images of H&E and oil red O staining. Scale bar = 100 μm. Statistical significance: $^{*}p < 0.05$, $^{**}p < 0.01$, $^{***}p < 0.001$, compared with control group; $^{\#}p < 0.05$, $^{\#\#}p < 0.01$, compared with HFSW group (n = 6).

AO significantly decreased the mRNA level of *Col1a1* upon HFSW feeding (**Figure 2C**). Subsequently, the most prominent genes involved in lipid synthesis and metabolism such as *Fasn* and key regulators of FAO (*Ppara* and *Acox1*) were also determined after AO treatment. As depicted in **Figure 2D** and **Supplementary Figure S2A**, **right panel**, AO didn't affect the

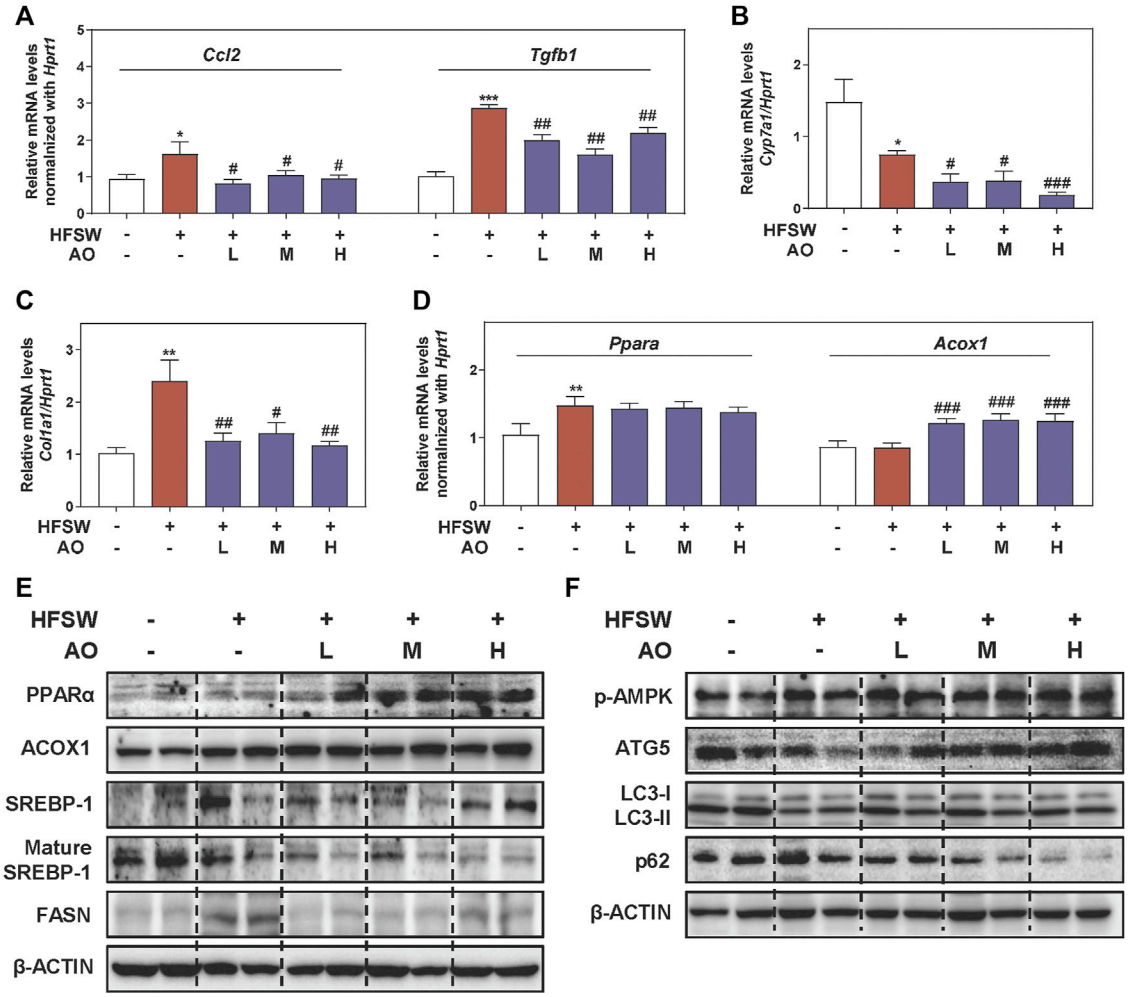

FIGURE 2 | AO improves lipid metabolism and activates autophagy pathway in HFSW-fed mice. Mice were treated with the same method as described in **Figure 1**. Relative mRNA levels of **(A)** *Ccl2* and *Tgfb1*, **(B)** *Cyp7a1*, **(C)** *Col1a1* and **(D)** *Ppara* and *Acox1* in liver tissues were determined by qPCR and normalized using *Hprt1* as an internal control. The protein levels of **(E)** PPARα, ACOX1, SREBP-1, mature SREBP-1, FASN, **(F)** p-AMPK, ATG5, LC3-II/LC3-I and p62 in the liver were determined by western blot using β-ACTIN as a loading control. Statistical significance: $^{*}p < 0.05$, $^{**}p < 0.01$, $^{***}p < 0.001$, compared with control group; $^{\#}p < 0.05$, $^{\#\#}p < 0.01$, $^{\#\#\#}p < 0.001$, compared with HFSW group (n = 6).

Ppara and *Fasn* levels caused by HFSW but significantly elevated the *Acox1* level in the fatty liver. We next analyzed representative proteins in pathways coordinating lipid homeostasis. PPARα contributes to the transcriptional regulation of essential genes involved in *de nova* fatty acid biosynthesis, including *Srebp1* and *Fasn* (Shen et al., 2020). As shown in **Figure 2E** and **Supplementary Figure S2B**, the protein levels of PPARα and ACOX1 were increased while FASN and the transformation of uncleaved SREBP-1 into mature SREBP-1 were decreased in AO-treated mice than their respective levels in HFSW mice, providing the potential explanation for the increased FAO and liver temperature after AO administration in **Figure 1D**. However, the expression of carnitine palmitoyl transferase 1alpha (CPT1α, *Cpt1a*), another important target responsible for mitochondrial oxidation, was almost unchanged after AO treatment (**Supplementary Figure S2C**). A series of other and our studies recently reported the important role of AMPK played in maintaining physiological functions and alleviating fatty liver, which might attribute to the regulation of autophagy and lipid metabolism (Zhao et al., 2020; Wu et al., 2021). As depicted in **Figure 2F** and **Supplementary Figure S2D**, the phosphorylation of AMPK was markedly increased after AO administration. We also observed that AO resulted in a significant increase of LC3-II/LC3-I and ATG5 levels and a decrease of p62 level in livers compared with the HFSW group. These findings together with those presented in **Figure 1** supported that AO inhibited fatty acid synthesis, promoted FAO and activated AMPK signaling and autophagy in response to lipid challenge.

AO Alleviates Lipid Accumulation in Fat-Overloaded MPHs

To further investigate lipid-lowering effects of AO on hepatocytes and gain detailed insight into the working mechanisms, we

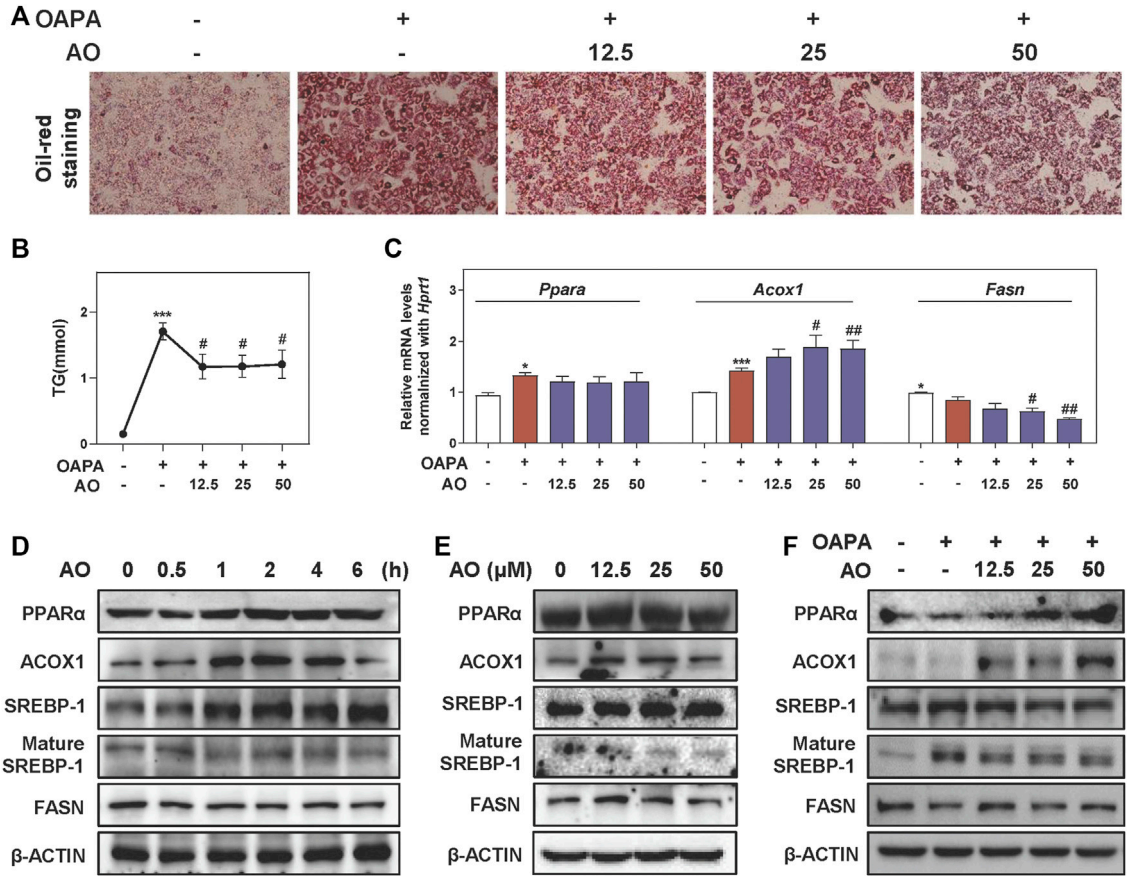

FIGURE 3 | AO alleviates lipid accumulation in fat-overloaded MPHs. MPHs were incubated with OAPA (OA: 250 μM, PA: 500 μM) and treated with different dosages (12.5, 25 and 50 μM) of AO for 24 h **(A)** Representative images of oil red O staining of MPHs **(B)** TG levels of MPHs **(C)** Relative mRNA levels of *Ppara*, *Acox1* and *Fasn* in MPHs were determined by qPCR and normalized using *Hprt1* as an internal control **(D)** MPHs were treated with AO (25 μM) at different time points **(E** and **F)** MPHs were treated with different concentrations of AO for 24 h with or without OAPA **(D, E** and **F)** The protein levels of PPARα, ACOX1, SREBP-1, mature SREBP-1 and FASN in MPHs were determined by western blot using β-ACTIN as a loading control. Statistical significance: $^{*}p < 0.05$, $^{***}p < 0.001$, compared with control group; $^{\#}p < 0.05$, $^{\#\#}p < 0.01$, compared with OAPA group (n = 3).

freshly isolated MPHs and further established an OAPA-induced steatosis *in vitro* model to mimic the *in vivo* environment. Our CCK-8 assay showed that AO had no obvious influence on MPH cell viability even at 200 μM (**Supplementary Figure S3A**). As shown in **Figure 3A**, the increased number and size of lipid droplets in hepatocytes were observed after the OAPA insult, which were distinctly and dose-dependently reversed by AO treatment (from 12.5 to 50 μM). Therefore, doses below 50 μM of AO were selected for the following *in vitro* assays. Next, the TG contents in MPHs were measured with 11.2 times higher upon OAPA treatment than the control group, while AO at all doses markedly decreased intracellular TG contents (**Figure 3B**). As illustrated in **Figure 3C**, AO maintained or enhanced the expression of *Ppara* and *Acox1* and significantly decreased the mRNA levels of *Fasn* in fat-loaded hepatocytes. Again, the gene expression of *Cpt1a* was not changed after AO treatment (**Supplementary Figure S3B**). Additionally, we examined the expression of targets involved in lipid metabolism at different time points or doses and found that AO significantly induced the activation of PPARα and ACOX1 after 1 h treatment and peaked at 4 h and decreased the levels of mature SREBP-1 and FASN at 1 h (**Figures 3D,E** and **Supplementary Figure S3C, D**). Furthermore, we determined the lipid-lowing effects of AO with the presence of overloaded fat. As expected, the protein level of lipid oxidation targets such as PPARα and ACOX1 were prominently increased and a lipogenic target like SREBP-1 maturation was decreased in response to various concentrations of AO when compared with the OAPA treatment alone (**Figure 3F** and **Supplementary Figure S3E**). Consistent with **Figure 3E**, AO also decreased the protein expression of FASN even in the presence of OAPA. These findings suggested that AO remarkedly inhibited lipid accumulation in hepatocytes.

AO Rapidly Triggers Autophagy Flux in Hepatocytes

After observing that AO inhibited the lipid accumulation in MPHs, we further explored whether this lipid-lowing effect of AO was related to autophagy activation and was consistent

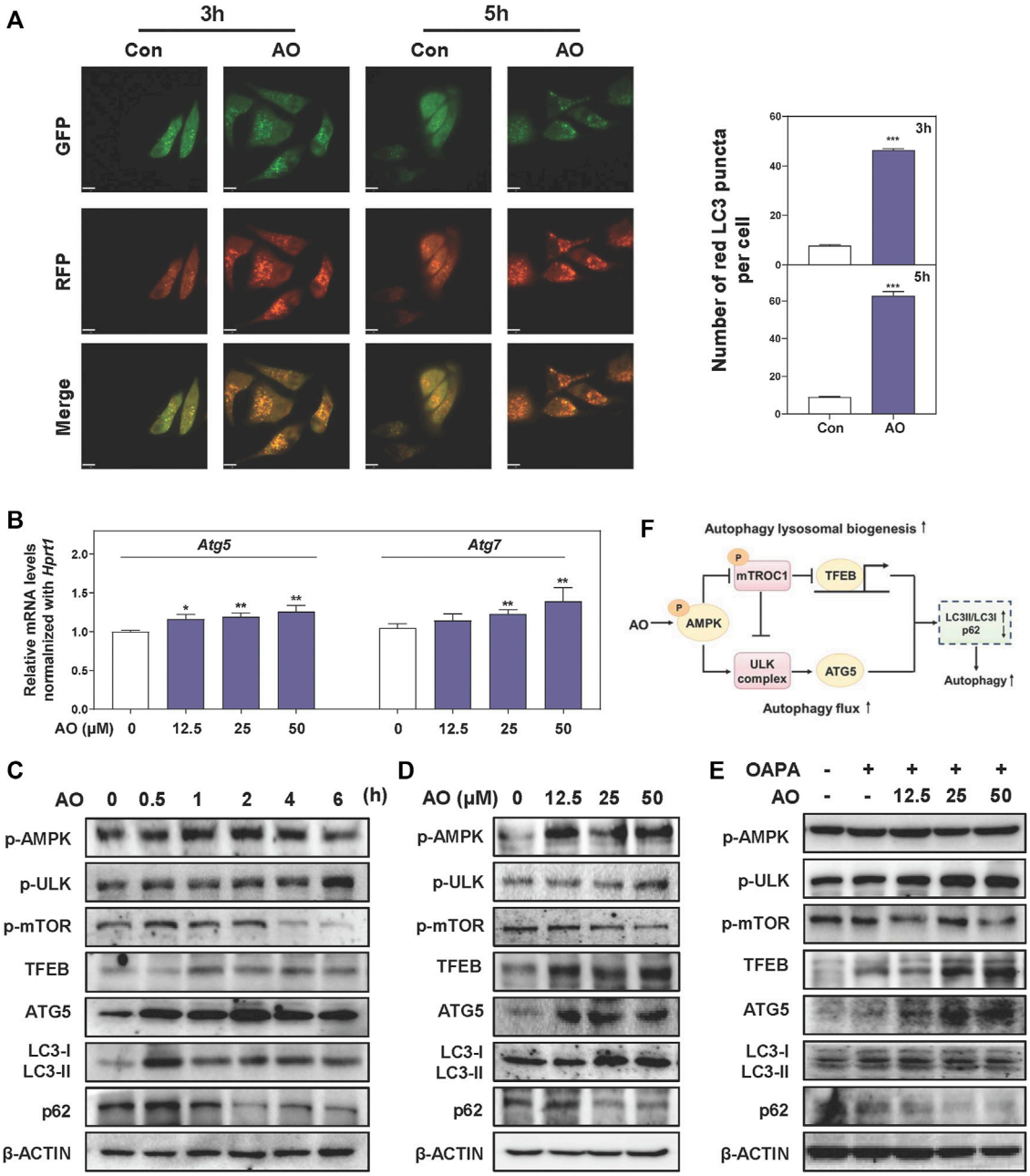

FIGURE 4 | AO rapidly triggers autophagy flux in hepatocytes **(A)** MPHs were treated with AO (25 μM) for 3 and 5 h. The mean numbers of red puncta representing autolysosomes were plotted **(B)** Relative mRNA levels of *Atg5* and *Atg7* in MPHs were determined by qPCR and normalized using *Hprt1* as an internal control **(C)** MPHs were treated with AO (25 μM) at different time points **(D** and **E)** MPHs were treated with different concentrations of AO with or without OAPA **(C, D** and **E)** The protein levels of p-AMPK, p-ULK, p-mTOR, TFEB, ATG5, LC3-II/LC3-I and p62 in MPHs were determined by western blot using β-ACTIN as a loading control **(F)** Schematic diagram that linked AO with the regulation of autophagy. Statistical significance: $^{*}p < 0.05$, $^{**}p < 0.01$, $^{***}p < 0.001$, compared with control group (n = 3).

with our *in vivo* findings. To examine whether AO itself affects the autophagic flux, we constructed an mRFP-GFP-LC3 reporter and transfected it into hepatocytes. As shown in **Figure 4A**, co-fluorescence staining of autolysosomes (red fluorescent puncta) and autophagosomes (yellow fluorescent puncta) exhibited that the number of red fluorescent puncta was sustainably increased by AO at 3 and 5 h, suggesting that AO effectively promoted autophagy flux in hepatocytes. As expected, AO significantly increased the mRNA levels of *Atg5* and *Atg7* in MPHs (**Figure 4B**). The oncogenic TFEB is considered to be the most important regulator of the transcription of genes responsible for the lysosomal-autophagy pathway (Settembre et al., 2011). As shown in **Figure 4C**, AO significantly increased the phosphorylation

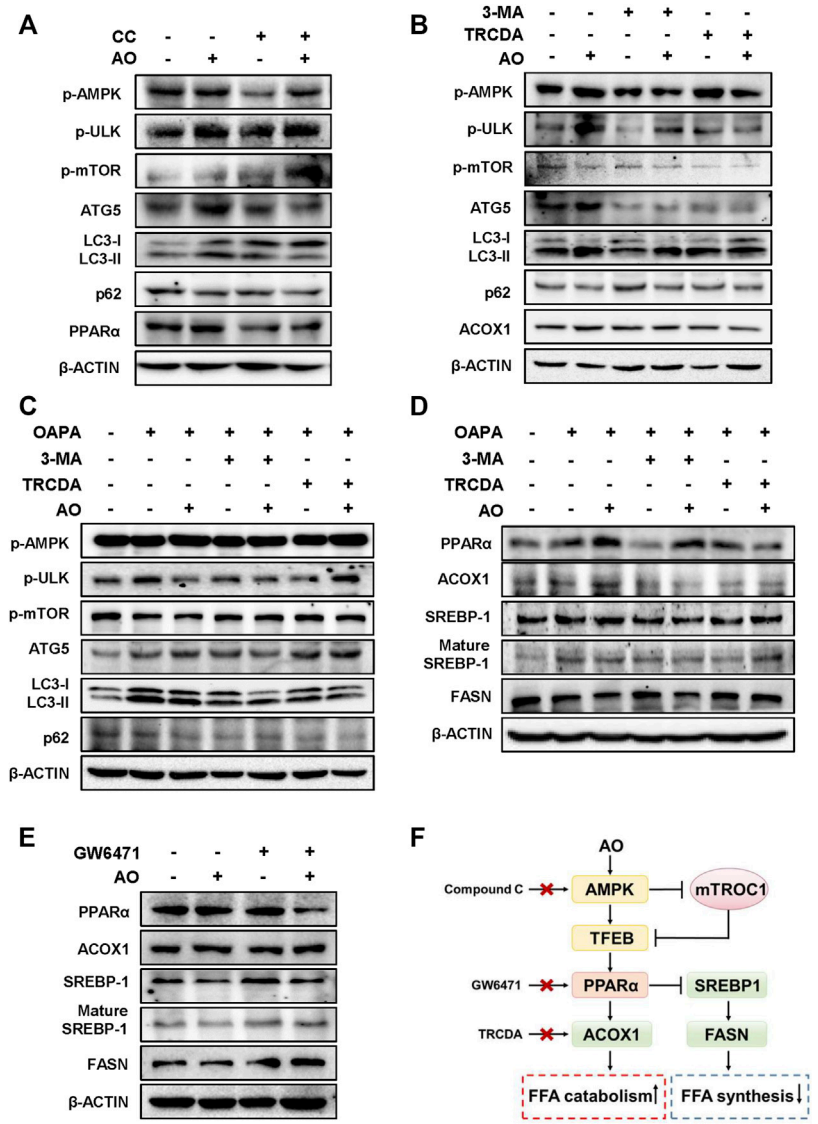

FIGURE 5 | AO alleviates lipid accumulation in hepatocytes by promoting AMPK-mediated protective autophagy **(A)** MPHs were pre-treated with CC (10 μM) for 1.5 h and then administrated with AO (25 μM) for another 2 h **(B)** After pretreatment with 3-MA (5 mM) or TRCDA (10 μM) for 1.5 h, MPHs were administrated with AO (25 μM) for another 2 h **(C** and **D)** After pretreatment with 3-MA (5 mM) or TRCDA (10 μM) for 1.5 h, MPHs were administrated with AO (25 μM) for another 24 h with or without OAPA treatment **(E)** After pre-treated with GW6471 (10 μM) for 1.5 h, MPHs were administrated with AO (25 μM) for another 2 h **(A** to **E)** The protein levels of p-AMPK, p-ULK, p-mTOR, ATG5, LC3-II/LC3-I, p62 and PPARα, ACOX1, SREBP-1, mature SREBP-1 and FASN in MPHs were determined by western blot using β-ACTIN as a loading control **(F)** The pathway of AO in regulating FFA catabolism and synthesis.

of AMPK and ULK at 0.5 h and peaked at 1 h, activated TFEB at 1 h and decreased the phosphorylation of mTOR, a downstream effector of AMPK, at 1 h and almost vanished at 4 h. Moreover, AO significantly resulted in the increase of LC3-II/I conversion and ATG5 and the decline of p62 in hepatocytes (**Figure 4C** and **Supplementary Figure S4A**). Consistent with the results above, the protein expressions of p-AMPK, p-ULK, TFEB, ATG5 and LC3-II were significantly increased while phosphorylated mTOR and p62 were markedly downregulated by AO treatment at different doses (**Figure 4D** and **Supplementary Figure S4B**). Given the strong influence of AO itself on autophagy activation, we next examined whether AO promoted autophagy exposure to high amounts of fatty acids. As depicted in **Figure 4E** and **Supplementary Figure S4C**, interestingly, OAPA exposure resulted in a compensatory increase of p-AMPK and TFEB but had no effect on ULK and mTOR phosphorylation, which were significantly enhanced by AO administration. As expected, AO significantly promoted the expression of autophagy-related proteins including ATG5 and LC3-II/LC3-I, while decreased the level of p62 compared with the OAPA group. These results suggested that AO rapidly triggered AMPK phosphorylation and promoted the autophagic flux in hepatocytes (**Figure 4F**).

AO Alleviates Lipid Accumulation in Hepatocytes by Promoting AMPK-Mediated Protective Autophagy

We next applied different inhibitors of autophagy- or lipid metabolism-related targets and investigated their influences on the lipid-lowering effects of AO in hepatocytes. Firstly, the protein levels of p-AMPK and autophagy-related targets were examined after AO treatment with or without the presence of CC, a widely used AMPK inhibitor. In agreement with our anticipation, CC markedly prevented AO-induced AMPK phosphorylation, p-mTOR inhibition, PPARα induction and autophagic activity, as evidenced by decreased levels of ATG5, LC3-II and increased level of p62 (**Figure 5A** and **Supplementary Figure S5A**). Given the decisive role of AMPK in AO-induced autophagy activation, we next examined whether 3-MA, a specific inhibitor that blocks the formation of autophagosomes, had any effect on AMPK, autophagy- and lipid metabolism-related targets after AO treatment. As shown in **Figure 5B** and **Supplementary Figure S5B**, without affecting the phosphorylation of AMPK and ULK, 3-MA distinctly inhibited AO-induced autophagy flux, as evidenced by decreased LC3-II and ATG5 levels and increased p-mTOR and p62 levels. We also applied TRCDA, an inhibitor of Acox1 and found that AO failed to induce ACOX1 expression but still maintained the activation of phosphorylated AMPK and its downstream autophagy-related pathways with the presence of TRCDA (**Figure 5B** and **Supplementary Figure S5B**). Under the exposure to OAPA, 3-MA still inhibited the activation of autophagy caused by AO treatment, while TRCDA had no obvious effect on AO-induced autophagy activation, again, indicating that autophagy flux was triggered prior to ACOX1 induction (**Figure 5C** and **Supplementary Figure S5C**). After confirming that AO specifically activated autophagy under both normal and lipid-overload conditions, we next investigated whether the inhibition of autophagy had any effect on the lipid-reducing effect of AO in MPHs. As shown in **Figure 5D** and **Supplementary Figure S5D**, pretreated with 3-MA significantly blocked AO-induced upregulation of PPARα and ACOX1 and downregulation of SREBP-1 maturation, but exerted no effect on FASN expression. It was interesting to note that TRCDA slightly decreased PPARα and reversed the declined FASN level caused by AO, indicating complicated regulatory relationships between ACOX1 and FASN in hepatocytes. Both peroxisomal ACOX1 and mitochondrial CPT1α were regulated by the activation of PPARα-PGC1α transcription factor complex (Boeckmans et al., 2019). We then measured the changes of lipid metabolism-related targets after AO treatment with or without the presence of the PPARα inhibitor, GW6471. In accordance with our hypothesis, GW6471 significantly inhibited AO-induced upregulation of PPARα, causing distinct upregulation of mature SREBP-1 and FASN expression in hepatocytes (**Figure 5E** and **Supplementary Figure S5E**). Collectively, these results suggested that AO alleviated hepatic lipid accumulation and promoted FAO by promoting AMPK-mediated protective autophagy (**Figure 5F**).

Inhibition of ACOX1 Blunted AO-Mediated Protective Effects Against Steatosis

We further focused on the common and paramount downstream target ACOX1 and identified whether AO-induced hepatoprotective effects depended on the ACOX1 activation. Based on our preliminary experiments, long-term administration of TRCDA (8 weeks) showed a better inhibitory effect on hepatic ACOX1 than short-term intervention (4 weeks) (**data not shown**). Therefore, mice were continuously treated with TRCDA accompanied with HFSW diet for 8 weeks and were co-administered with AO (10 mg/kg) during the last 4 weeks (**Figure 6A**). Although AO significantly inhibited the increase of body weight and weight gain induced by HFSW, TRCDA significantly elevated the body weight even in the presence of AO without affecting the amount of average calorie and water intake (**Figure 6B** and **Supplementary Figure S6A**). Serum biochemical examinations further showed that TRCDA significantly impaired the hepatoprotective effect of AO on fatty livers (**Figure 6C**). Moreover, the serum levels of TG and TC were distinctly reduced after AO treatment when compared with the HFSW group, which were significantly elevated by TRCDA (**Figure 6D**). It was interesting to note that additional administration of TRCDA obviously increased the weights of epididymal white adipose tissue and liver temperature when compared with the HFSW + AO group (**Figure 6E**). Furthermore, results of H&E, Oil-red staining and gross images of livers also showed that TRCDA remarkably increased the size and number of AO-declined lipid droplets (**Figure 6F** and **Supplementary Figure S6B**).

Inhibition of ACOX1 Blocks the Lipid-Lowering Effect of AO *via* Disturbing Lipid Metabolism

Previous studies reported that NAFLD mice caused by gene variation were in a proinflammatory and fibrotic state, accompanied by abnormal altered genes including ACOX1 (Dongiovanni et al., 2020). As shown in **Figure 7A, B**, and **Supplementary Figure S6C**, AO distinctly decreased the HFSW-induced levels of *Ccl2*, *Tgfb1* and *Col1a1* in livers, while TRCDA administration markedly reversed these changes and even increased the levels of *Fn1* and *Fasn* to a certain extent. We also noticed a significant elevation of the mRNA expression of *cyp7a1* in the HFSW + AO + TRCDA group when compared with the HFSW + AO group (**Figure 7C**). Considering the tight correlation between ACOX1 and PPARα, we next investigated whether the inhibition of ACOX1 had any influence on PPARα expression. As shown in **Figure 7D**, TRCDA markedly increased *Ppara* expression while decreased the level of *Acox1* induced by AO. Furthermore, the effects of ACOX1 inhibition on the autophagy signaling and lipid homeostasis were also investigated. As performed in

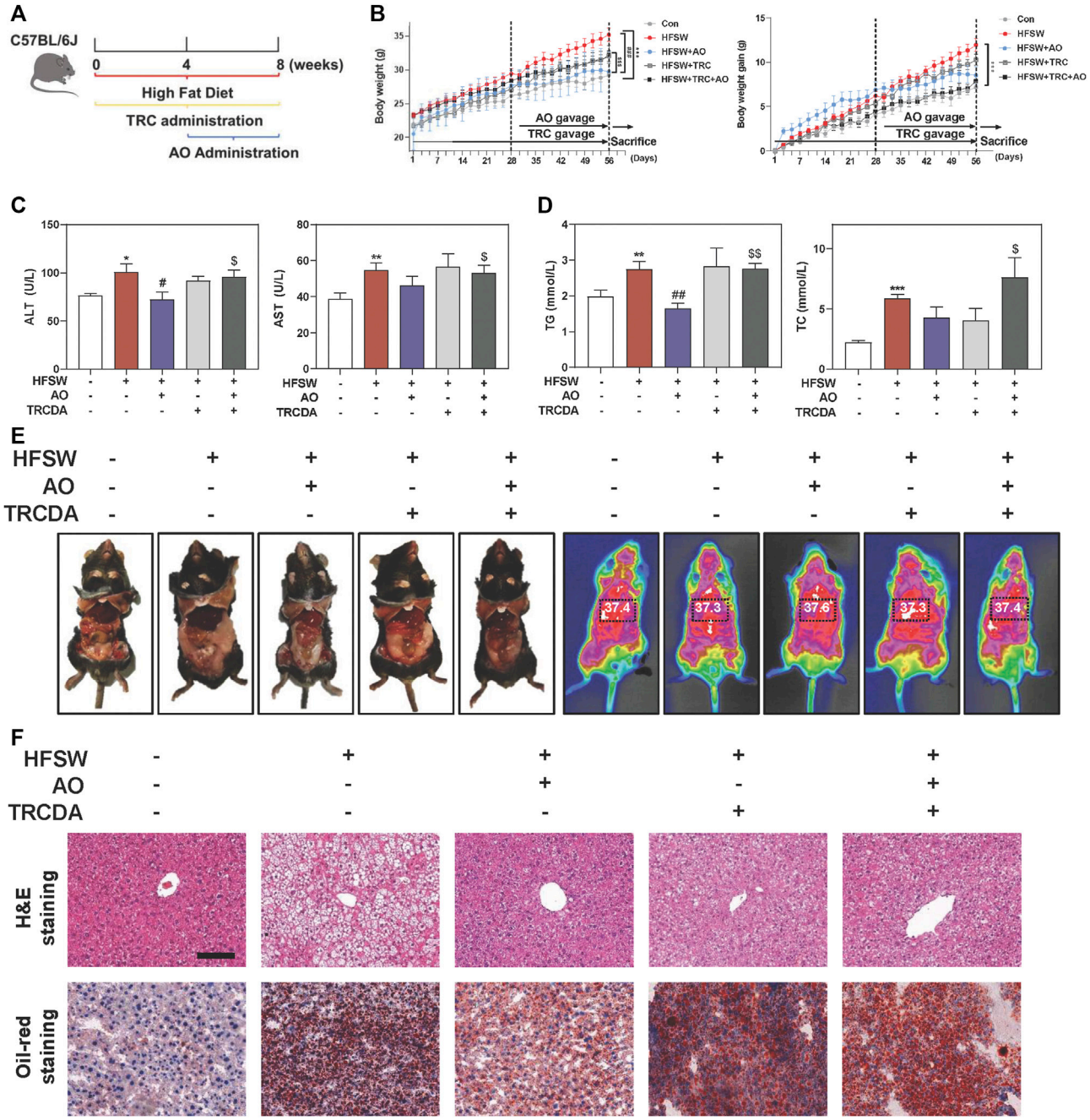

FIGURE 6 | Inhibition of ACOX1 suppressed AO-mediated protective effects against NAFLD. Mice were fed chow diet or HFSW diet for 8 weeks, and administered with TRCDA (1 mg/kg) during the whole 8 weeks of HFSW diet followed by administration with AO (10 mg/kg) from Week 5 **(A)** Schematic diagram of *in vivo* experimental design **(B)** Body weight and Body weight gain **(C)** Serum ALT and AST levels **(D)** Serum TG and TC levels **(E)** Representative images of epididymal fat and thoracoabdominal temperature **(F)** Representative images of H&E and oil red O staining. Scale bar = 100 μm. Statistical significance: $^{*}p < 0.05$, $^{**}p < 0.01$, $^{***}p < 0.001$, compared with control group; $^{\#}p < 0.05$, $^{\#\#}p < 0.01$, compared with HFSW group; $^{\$}p < 0.05$, $^{\$\$}p < 0.01$, compared with HFSW + AO group (n = 6).

Figure 7E and **Supplementary Figure S6D**, without affecting AMPK phosphorylation, TRCDA distinctly promoted AO-induced autophagy activation, as evidenced by a higher level of p-ULK, ATG5 and LC3-II/LC3-I and a lower level of p-mTOR and p62 compared to HFSW + AO group. These results indicated that the inhibition of ACOX1 not only didn't block the AO-induced autophagy activation but even enhanced this process. In consistent with our results *in vitro*, TRCDA significantly reversed AO-suppressed FASN expression and SREBP-1 maturation in livers. Additionally, the expression of PPARα was slightly decreased in the HFSW + AO + TRCDA group when compared with the HFSW + AO group (**Figure 7F**

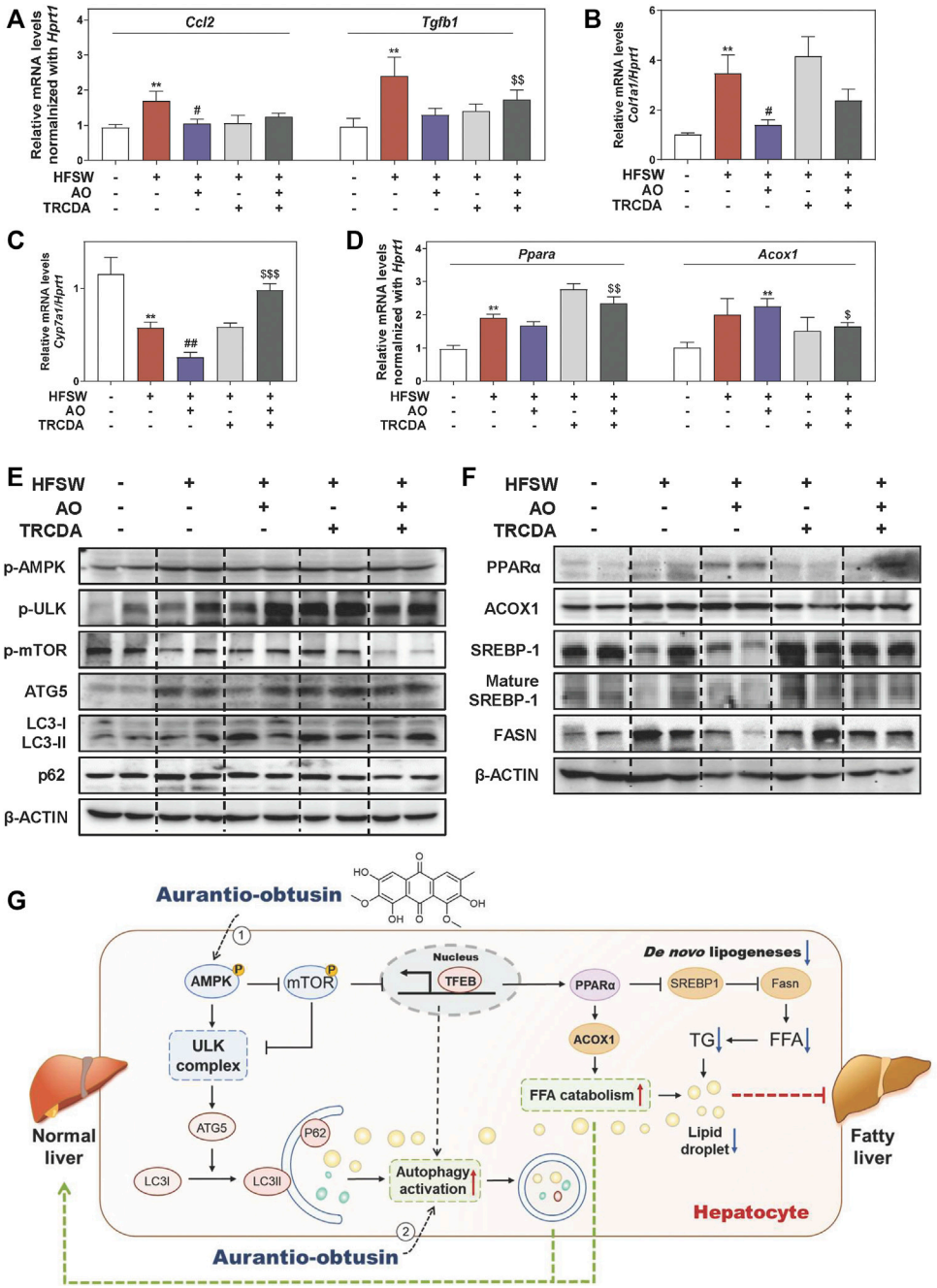

FIGURE 7 | Inhibition of ACOX1 deteriorates the AO-ameliorated liver steatosis *via* accelerating liver inflammation and fibrosis and disturbing lipid metabolism. Relative mRNA levels of **(A)** *Ccl2* and *Tgfb1*, **(B)** *Col1a1*, **(C)** *Cyp7a1*, **(D)** *Ppara* and *Acox1* in liver tissues were determined by qPCR and normalized using *Hprt1* as an internal control. The protein levels of **(E)** p-AMPK, p-ULK, p-mTOR, ATG5, LC3-II/LC3-I, p62, **(F)** PPARα, ACOX1, SREBP-1, mature SREBP-1 and FASN in the liver were determined by western blot using β-ACTIN as a loading control, **(G)** Schematic diagram of the proposed mechanisms underlying the protective effects of AO on autophagy and lipid accumulation during NAFLD. Statistical significance: $^{**}p < 0.01$, compared with control group; $^{\#}p < 0.05$, $^{\#\#}p < 0.01$, compared with HFSW group; $^{\$}p < 0.05$, $^{\$\$}p < 0.01$, $^{\$\$\$}p < 0.001$, compared with HFSW + AO group (n = 6).

and **Supplementary Figure S6E**). Collectively, our study provided critical evidence that the inhibition of ACOX1 aggravated HFSW-induced liver steatosis by promoting lipid *de novo* synthesis and inhibiting lipid consumption even in the case of autophagy activation (**Figure 7G**).

DISCUSSION

NAFLD affects about 20–30% of the adult population in developed countries and is inevitably becoming the next major health epidemic (Maya-Miles et al., 2021; Wegermann et al.,

2021). Although a variety of therapeutic drugs curing NAFLD has been proposed, almost all of them have failed in the clinical trial, leading to an urgent requirement of novel therapeutic options. *Cassiae* semen is a prestigious and traditional drug that has been used for thousands of years in Asian history for treating various cardiovascular or digestive diseases. In the current study, we focused on AO, the main characteristic bioactive ingredient isolated from *Cassiae* semen, and found that AO significantly alleviated hepatic steatosis both in the HFSW-induced NAFLD mouse model and OAPA-treated lipid accumulation *in vitro* model, owing to the declined lipid *de novo* synthesis and elevated lipid consumption. Mechanistically, AO significantly activated the autophagy flux in hepatocytes through the phosphorylation of AMPK and the following activation of TFEB, which further improved the lipid metabolism by promoting the expression of PPARα and ACOX1 and inhibiting the maturation of SREBP-1 and downstream FASN expression (**Figure 7G**).

With the development of in-depth study of pathogenesis on NAFLD, the strong correlation between autophagy and hepatic lipid metabolism has been emphasized. Autophagy is responsible for the degradation of lipid droplets and critical for maintaining cellular energy homeostasis. Previous studies reported that the induction of hepatic autophagy effectively mitigated hepatic lipid accumulation in obese mice (L. Yang et al., 2010). Meanwhile, the increased production of unsaturated fatty acids was demonstrated to activate autophagy in multiple cell types (O'Rourke et al., 2013; Tu et al., 2014; B. Yang et al., 2020). In consistent with the *in vitro* experiments of oleate-induced autophagy activation by other studies (Singh et al., 2009), we found that HFSW feeding promoted the activation of autophagy to some extent by a compensatory mechanism. As shown in **Figures 2**, **4**, AO efficiently improved hepatic lipid metabolism accompanied by increased autophagy flux and remarkable activation of ATG5. Previous studies have demonstrated that ATG5 could be activated under the phosphorylation of signal transducer and activator of transcription 3 (STAT3), the acetylation of p21 activated kinase 1 (PAK1) and induced hypoxia-inducible factor (Feng et al., 2021). Interestingly, we found that AO rapidly promoted the phosphorylation of STAT3 in hepatocytes (**Supplementary Figure S7A**). Therefore, we speculated that the activation of ATG5 induced by AO might be attributed to STAT3 phosphorylation, but detailed mechanisms remain to be identified in further studies. Furthermore, our results showed that AO markedly increased the ratio of LC3II/LC3I and decreased the level of p62. In addition, the function of AO on promoting autophagy and ameliorating lipid metabolism was suppressed by a classic early phase autophagy inhibitor, 3-MA. These data suggested that AO might participate in the regulation of the whole process of autophagy to modulate lipid metabolism and serve as a potent autophagy activator.

AMPK, an evolutionarily conserved serine/threonine-protein kinase, acts as an energy sensor and regulates a variety of metabolic processes (Paquette et al., 2021). Previous studies reported that AMPK directly promoted intracellular autophagy by phosphorylating the essential autophagy-related proteins including ULK and mTORC1 (Chen et al., 2020; Paquette et al., 2021; Wirth et al., 2013), and mTORC1 inhibited the interaction between AMPK and ULK1 (Loffler et al., 2011). In our study, we demonstrated that AO markedly increased the phosphorylation of AMPK and ULK and decreased the phosphorylation of mTOR (**Figures 2**, **4**). Additionally, CC markedly blocked AO-induced upregulation of p-AMPK and p-ULK and downregulation of p-mTOR (**Figure 5A**). It has been previously reported that AMPK activated TFEB, a transcription factor that controls lysosomal biogenesis, and promoted the formation of autophagosomes (Settembre et al., 2011; Yoo et al., 2021). Here, we observed a significant increased level of TFEB under the challenges of various doses of AO in hepatocytes (**Figure 4**). Furthermore, Park *et al.* found that TFEB activation attenuated methionine choline-deficient diet-induced steatosis by increasing the FAO-related genes including *Ppara*, *Acox1* and *Cpt1a* (Park et al., 2020). Although there was no obvious change on *Cpt1a* level after AO treatment when compared with the control group, AO markedly increased the expression of PPARα and ACOX1, accompanied with increased TFEB level (**Figure 3E**). Taken together, our study provided critical evidence that AO activated autophagy and improved lipid metabolism by upregulating the expression of a series of autophagy-related proteins including AMPK, mTORC1, ULK as well as TFEB.

Previous studies reported that the induction of autophagy contributed to PPARα activation by promoting the degradation of NCoR1 (nuclear receptor co-repressor 1) (Saito et al., 2019). Additionally, it has also been reported that activated PPARα promoted the process of autophagy by up-regulating the expression of autophagy-related genes (Yu et al., 2020). A PPARα agonist, fenofibrate, was also found to activate AMPK pathway and promote TFEB nuclear translocation (Yoo et al., 2021). These findings suggest a complicated and interactive relationship between autophagy and PPARα. Interestingly, our results also identified that the inhibition of autophagy by 3-MA completely blocked AO-induced PPARα activation (**Figure 5**). In addition, previous studies have shown that AO increased the level of PPARγ in white tissues to improve obesity and insulin resistance (Guo et al., 2021), suggesting the potential activities of AO targeting PPAR family proteins. Similarly, we found that PPAR inhibitor GW6471 markedly eliminated AO-induced decreased level of FASN and mature SREBP-1 (**Figure 5E**), indicating AO exerted its lipid-lowering function in a PPARα-related manner.

ACOX1 has been well-characterized as the first step of peroxisomal β-oxidation and is responsible for the shortening of very long-chain fatty acids. Existing studies have suggested that the regulation of ACOX1 was largely under the control of activated PPARα (Misra and Reddy, 2014), while in the absence of ACOX1, unmetabolized ACOX1 substrates were reported to cause sustained activation of PPARα (Jia et al., 2014). Based on our *in vivo* and *in vitro* results, AO markedly stimulated lipid consumption and attenuated liver steatosis accompanied by the activation of PPARα and ACOX1 (**Figures 2**, **3**). By using GW6471, we demonstrated that ACOX1 expression induced by AO was likely dependent on PPARα signaling. Whereas, enzymatic inhibition of ACOX1 by TRCDA slightly decreased AO-induced PPARα expression (**Figures 5**, **7**). Meanwhile, the enhanced autophagy flux in response to ACOX1 inhibition was probably attributed to accumulated free fatty acids

(**Figure 7**). Moreover, Anyuan He and his colleagues recently reported that hepatic Acox1 deficiency markedly led to lowered total cytosolic acetyl-CoA levels, resulting in impaired activation of mTORC1 (He et al., 2020a; He et al., 2020b), providing another explanation for enhanced autophagy after TRCDA administration. Interestingly, it is worth noting that the expression of FASN was also increased in liver-specific Acox1 knockout mice (He et al., 2020a), which was also consistent with our finding in **Figure 7F**, again, indicating the complex balance between lipid synthesis and lipid consumption in fatty liver.

CONCLUSION

Insufficient therapeutic strategy for treating NAFLD remains a huge challenge of human public health. In the current study, we demonstrated that AO promoted autophagy flux and alleviated liver steatosis in an HFSW-fed NAFLD mouse model and OAPA-treated mouse primary hepatocytes by inducing the phosphorylation of AMPK and TFEB, which subsequently increased the expression of targets involved in lipid degradation and decreased the expression of targets involved in lipid biosynthesis. The inhibition of autophagy or genes responsible for lipid peroxidation markedly blocked AO-induced lipid-lowering and hepatoprotective effects. As illustrated in **Figure 7G**, our study not only provides insights into the complicated mechanisms underlying the anti-steatosis activities of AO but also offers vital evidence inspiring the development of AO structure-based innovative drug candidates for the treatment of NAFLD and related complications.

DATA AVAILABILITY STATEMENT

The original contributions presented in the study are included in the article/**Supplementary Material**, further inquiries can be directed to the corresponding author.

ETHICS STATEMENT

The animal study was reviewed and approved by All animal studies and procedures were approved by the Institutional Animal Care and Use Committee of Beijing University of Chinese Medicine and were carried out in accordance with all guidelines.

AUTHOR CONTRIBUTIONS

XL designed the research. FZ, MD, YG, GF, CL, YL, RS, JW, JL, XX and HL performed and analyzed the research. FZ and MD wrote the manuscript and revised the figures.

FUNDING

This work was supported by grants from Beijing Municipal Science Technology Commission (Grant NO. 7212174 to XL). Young Talents Promotion Project of China Association of Traditional Chinese Medicine (Grant NO. 2020-QNRC2-01 to XL); Innovation Team and Talents Cultivation Program of National Administration of Traditional Chinese Medicine (Grant NO. ZYYCXTD-C-202006 to XL); Beijing Nova Program of Science; Technology (Grant NO. Z191100001119088 to XL); National Natural Science Foundation of China (Grant NO. 82004045 to XL).

SUPPLEMENTARY MATERIAL

The Supplementary Material for this article can be found online at: https://www.frontiersin.org/articles/10.3389/fphar.2021.826628/full#supplementary-material

REFERENCES

Boeckmans, J., Natale, A., Rombaut, M., Buyl, K., Rogiers, V., De Kock, J., et al. (2019). Anti-NASH Drug Development Hitches a Lift on PPAR Agonism. *Cells* 9 (1), 37. doi:10.3390/cells9010037

Chávez-Talavera, O., Tailleux, A., Lefebvre, P., and Staels, B. (2017). Bile Acid Control of Metabolism and Inflammation in Obesity, Type 2 Diabetes, Dyslipidemia, and Nonalcoholic Fatty Liver Disease. *Gastroenterology* 152 (7), 1679–e3. doi:10.1053/j.gastro.2017.01.055

Chen, P., Wang, Y., Chen, L., Song, N., and Xie, J. (2020). Apelin-13 Protects Dopaminergic Neurons against Rotenone-Induced Neurotoxicity through the AMPK/mTOR/ULK-1 Mediated Autophagy Activation. *Int. J. Mol. Sci.* 21 (21), 8376. doi:10.3390/ijms21218376

Czaja, M. J. (2016). Function of Autophagy in Nonalcoholic Fatty Liver Disease. *Dig. Dis. Sci.* 61 (5), 1304–1313. doi:10.1007/s10620-015-4025-x

Diehl, A. M., and Day, C. (2017). Cause, Pathogenesis, and Treatment of Nonalcoholic Steatohepatitis. *N. Engl. J. Med.* 377 (21), 2063–2072. doi:10.1056/NEJMra1503519

Dixon, J. B., Bhathal, P. S., and O'Brien, P. E. (2001). Nonalcoholic Fatty Liver Disease: Predictors of Nonalcoholic Steatohepatitis and Liver Fibrosis in the Severely Obese. *Gastroenterology* 121 (1), 91–100. doi:10.1053/gast.2001.25540

Dongiovanni, P., Crudele, A., Panera, N., Romito, I., Meroni, M., De Stefanis, C., et al. (2020). β-Klotho Gene Variation Is Associated with Liver Damage in Children with NAFLD. *J. Hepatol.* 72 (3), 411–419. doi:10.1016/j.jhep.2019.10.011

Feng, X., Zhang, H., Meng, L., Song, H., Zhou, Q., Qu, C., et al. (2021). Hypoxia-induced Acetylation of PAK1 Enhances Autophagy and Promotes Brain Tumorigenesis via Phosphorylating ATG5. *Autophagy* 17 (3), 723–742. doi:10.1080/15548627.2020.1731266

Friedman, S. L., Neuschwander-Tetri, B. A., Rinella, M., and Sanyal, A. J. (2018). Mechanisms of NAFLD Development and Therapeutic Strategies. *Nat. Med.* 24 (7), 908–922. doi:10.1038/s41591-018-0104-9

Guo, C. Y., Liao, W. T., Qiu, R. J., Zhou, D. S., Ni, W. J., Yu, C. P., et al. (2021). Aurantio-obtusin Improves Obesity and Insulin Resistance Induced by High-Fat Diet in Obese Mice. *Phytother Res.* 35 (1), 346–360. doi:10.1002/ptr.6805

He, A., Chen, X., Tan, M., Chen, Y., Lu, D., Zhang, X., et al. (2020a). Acetyl-CoA Derived from Hepatic Peroxisomal β-Oxidation Inhibits Autophagy and Promotes Steatosis via mTORC1 Activation. *Mol. Cel* 79 (1), 30–e4. e34. doi:10.1016/j.molcel.2020.05.007

He, A., Dean, J. M., Lu, D., Chen, Y., and Lodhi, I. J. (2020b). Hepatic Peroxisomal β-oxidation Suppresses Lipophagy via RPTOR Acetylation and MTOR Activation. *Autophagy* 16 (9), 1727–1728. doi:10.1080/15548627.2020.1797288

Jia, Y., Viswakarma, N., and Reddy, J. K. (2014). Med1 Subunit of the Mediator Complex in Nuclear Receptor-Regulated Energy Metabolism, Liver Regeneration, and Hepatocarcinogenesis. *Gene Expr.* 16 (2), 63–75. doi:10.3727/105221614X13919976902219

Kim, M., Lim, S. J., Lee, H. J., and Nho, C. W. (2015). Cassia Tora Seed Extract and its Active Compound Aurantio-Obtusin Inhibit Allergic Responses in IgE-Mediated Mast Cells and Anaphylactic Models. *J. Agric. Food Chem.*, 63(41), 9037–9046. doi:10.1021/acs.jafc.5b03836

Kwon, K. S., Lee, J. H., So, K. S., Park, B. K., Lim, H., Choi, J. S., et al. (2018). Aurantio-obtusin, an Anthraquinone from Cassiae Semen, Ameliorates Lung Inflammatory Responses. *Phytother Res.* 32 (8), 1537–1545. doi:10.1002/ptr.6082

Li, X., Ge, J., Li, Y., Cai, Y., Zheng, Q., Huang, N., et al. (2021). Integrative Lipidomic and Transcriptomic Study Unravels the Therapeutic Effects of Saikosaponins A and D on Non-alcoholic Fatty Liver Disease. *Acta Pharm. Sin B* 11 (11), 3527–3541. doi:10.1016/j.apsb.2021.03.018

Li, X., Liu, R., Yang, J., Sun, L., Zhang, L., Jiang, Z., et al. (2017). The Role of Long Noncoding RNA H19 in Gender Disparity of Cholestatic Liver Injury in Multidrug Resistance 2 Gene Knockout Mice. *Hepatology* 66 (3), 869–884. doi:10.1002/hep.29145

Löffler, A. S., Alers, S., Dieterle, A. M., Keppeler, H., Franz-Wachtel, M., Kundu, M., et al. (2011). Ulk1-mediated Phosphorylation of AMPK Constitutes a Negative Regulatory Feedback Loop. *Autophagy* 7 (7), 696–706. doi:10.4161/auto.7.7.15451

Loomba, R., Lim, J. K., Patton, H., and El-Serag, H. B. (2020). AGA Clinical Practice Update on Screening and Surveillance for Hepatocellular Carcinoma in Patients with Nonalcoholic Fatty Liver Disease: Expert Review. *Gastroenterology* 158 (6), 1822–1830. doi:10.1053/j.gastro.2019.12.053

Mao, Y., Yu, F., Wang, J., Guo, C., and Fan, X. (2016). Autophagy: a New Target for Nonalcoholic Fatty Liver Disease Therapy. *Hepat. Med.* 8, 27–37. doi:10.2147/HMER.S98120

Marra, F., and Svegliati-Baroni, G. (2018). Lipotoxicity and the Gut-Liver axis in NASH Pathogenesis. *J. Hepatol.* 68 (2), 280–295. doi:10.1016/j.jhep.2017.11.014

Maya-Miles, D., Ampuero, J., Gallego-Durán, R., Dingianna, P., and Romero-Gómez, M. (2021). Management of NAFLD Patients with Advanced Fibrosis. *Liver Int.* 41 (Suppl. 1), 95–104. doi:10.1111/liv.14847

Misra, P., and Reddy, J. K. (2014). Peroxisome Proliferator-Activated Receptor-α Activation and Excess Energy Burning in Hepatocarcinogenesis. *Biochimie* 98, 63–74. doi:10.1016/j.biochi.2013.11.011

Mwangi, S. M., Li, G., Ye, L., Liu, Y., Reichardt, F., Yeligar, S. M., et al. (2019). Glial Cell Line-Derived Neurotrophic Factor Enhances Autophagic Flux in Mouse and Rat Hepatocytes and Protects against Palmitate Lipotoxicity. *Hepatology* 69 (6), 2455–2470. doi:10.1002/hep.30541

Ni, H. M., Bockus, A., Boggess, N., Jaeschke, H., and Ding, W. X. (2012). Activation of Autophagy Protects against Acetaminophen-Induced Hepatotoxicity. *Hepatology* 55 (1), 222–232. doi:10.1002/hep.24690

O'Rourke, E. J., Kuballa, P., Xavier, R., and Ruvkun, G. (2013). ω-6 Polyunsaturated Fatty Acids Extend Life Span through the Activation of Autophagy. *Genes Dev.* 27 (4), 429–440. doi:10.1101/gad.205294.112

Paquette, M., El-Houjeiri, L., Zirden, P., Puustinen, P., Blanchette, P., Jeong, H., et al. (2021). AMPK-dependent Phosphorylation Is Required for Transcriptional Activation of TFEB and TFE3. *Autophagy* 17 (12), 3957–3975. doi:10.1080/15548627.2021.1898748

Park, H. S., Song, J. W., Park, J. H., Lim, B. K., Moon, O. S., Son, H. Y., et al. (2020). TXNIP/VDUP1 Attenuates Steatohepatitis via Autophagy and Fatty Acid Oxidation. *Autophagy* 17 (9), 2549–2564. doi:10.1080/15548627.2020.1834711

Saito, T., Kuma, A., Sugiura, Y., Ichimura, Y., Obata, M., Kitamura, H., et al. (2019). Autophagy Regulates Lipid Metabolism through Selective Turnover of NCoR1. *Nat. Commun.* 10 (1), 1567. doi:10.1038/s41467-019-08829-3

Settembre, C., Di Malta, C., Polito, V. A., Garcia Arencibia, M., Vetrini, F., Erdin, S., et al. (2011). TFEB Links Autophagy to Lysosomal Biogenesis. *Science* 332 (6036), 1429–1433. doi:10.1126/science.1204592

Shen, S., Faouzi, S., Souquere, S., Roy, S., Routier, E., Libenciuc, C., et al. (2020). Melanoma Persister Cells Are Tolerant to BRAF/MEK Inhibitors via ACOX1-Mediated Fatty Acid Oxidation. *Cell Rep* 33 (8), 108421. doi:10.1016/j.celrep.2020.108421

Singh, R., Kaushik, S., Wang, Y., Xiang, Y., Novak, I., Komatsu, M., et al. (2009). Autophagy Regulates Lipid Metabolism. *Nature* 458 (7242), 1131–1135. doi:10.1038/nature07976

Sumida, Y., and Yoneda, M. (2018). Current and Future Pharmacological Therapies for NAFLD/NASH. *J. Gastroenterol.* 53 (3), 362–376. doi:10.1007/s00535-017-1415-1

Tejero, J., Shiva, S., and Gladwin, M. T. (2019). Sources of Vascular Nitric Oxide and Reactive Oxygen Species and Their Regulation. *Physiol. Rev.* 99 (1), 311–379. doi:10.1152/physrev.00036.2017

Tilg, H., Adolph, T. E., and Moschen, A. R. (2021). Multiple Parallel Hits Hypothesis in Nonalcoholic Fatty Liver Disease: Revisited after a Decade. *Hepatology* 73 (2), 833–842. doi:10.1002/hep.31518

Tu, Q. Q., Zheng, R. Y., Li, J., Hu, L., Chang, Y. X., Li, L., et al. (2014). Palmitic Acid Induces Autophagy in Hepatocytes via JNK2 Activation. *Acta Pharmacol. Sin* 35 (4), 504–512. doi:10.1038/aps.2013.170

Wegermann, K., Suzuki, A., Mavis, A. M., Abdelmalek, M. F., Diehl, A. M., and Moylan, C. A. (2021). Tackling Nonalcoholic Fatty Liver Disease: Three Targeted Populations. *Hepatology* 73 (3), 1199–1206. doi:10.1002/hep.31533

Wirth, M., Joachim, J., and Tooze, S. A. (2013). Autophagosome Formation-Tthe Role of ULK1 and Beclin1-Pi3kc3 Complexes in Setting the Stage. *Semin. Cancer Biol.* 23 (5), 301–309. doi:10.1016/j.semcancer.2013.05.007

Wu, J., Xue, X., Fan, G., Gu, Y., Zhou, F., Zheng, Q., et al. (2021). Ferulic Acid Ameliorates Hepatic Inflammation and Fibrotic Liver Injury by Inhibiting PTP1B Activity and Subsequent Promoting AMPK Phosphorylation. *Front. Pharmacol.* 12, 754976. doi:10.3389/fphar.2021.754976

Xu, L., Li, J., Tang, X., Wang, Y., Ma, Z., and Gao, Y. (2019). Metabolomics of Aurantio-Obtusin-Induced Hepatotoxicity in Rats for Discovery of Potential Biomarkers. *Molecules* 24 (19), 3452. doi:10.3390/molecules24193452

Yang, B., Zhou, Y., Wu, M., Li, X., Mai, K., and Ai, Q. (2020). ω-6 Polyunsaturated Fatty Acids (Linoleic Acid) Activate Both Autophagy and Antioxidation in a Synergistic Feedback Loop via TOR-dependent and TOR-independent Signaling Pathways. *Cell Death Dis* 11 (7), 607. doi:10.1038/s41419-020-02750-0

Yang, L., Li, P., Fu, S., Calay, E. S., and Hotamisligil, G. S. (2010). Defective Hepatic Autophagy in Obesity Promotes ER Stress and Causes Insulin Resistance. *Cell Metab* 11 (6), 467–478. doi:10.1016/j.cmet.2010.04.005

Yoo, J., Jeong, I. K., Ahn, K. J., Chung, H. Y., and Hwang, Y. C. (2021). Fenofibrate, a PPARα Agonist, Reduces Hepatic Fat Accumulation through the Upregulation of TFEB-Mediated Lipophagy. *Metabolism* 120, 154798. doi:10.1016/j.metabol.2021.154798

Yu, S., Wang, Z., Ding, L., and Yang, L. (2020). The Regulation of TFEB in Lipid Homeostasis of Non-alcoholic Fatty Liver Disease: Molecular Mechanism and Promising Therapeutic Targets. *Life Sci.* 246, 117418. doi:10.1016/j.lfs.2020.117418

Zhao, P., Sun, X., Chaggan, C., Liao, Z., In Wong, K., He, F., et al. (2020). An AMPK-Caspase-6 axis Controls Liver Damage in Nonalcoholic Steatohepatitis. *Science* 367 (6478), 652–660. doi:10.1126/science.aay0542

Zhou, S., Gu, J., Liu, R., Wei, S., Wang, Q., Shen, H., et al. (2018). Spermine Alleviates Acute Liver Injury by Inhibiting Liver-Resident Macrophage Pro-inflammatory Response through ATG5-dependent Autophagy. *Front. Immunol.* 9, 948. doi:10.3389/fimmu.2018.00948

Conflict of Interest: The authors declare that the research was conducted in the absence of any commercial or financial relationships that could be construed as a potential conflict of interest.

Publisher's Note: All claims expressed in this article are solely those of the authors and do not necessarily represent those of their affiliated organizations, or those of the publisher, the editors and the reviewers. Any product that may be evaluated in this article, or claim that may be made by its manufacturer, is not guaranteed or endorsed by the publisher.

frontiers in Pharmacology

ORIGINAL RESEARCH
published: 24 January 2022
doi: 10.3389/fphar.2022.833705

Limonin, an AMPK Activator, Inhibits Hepatic Lipid Accumulation in High Fat Diet Fed Mice

*Si-wei Wang[1], Tian Lan[1], Hang-fei Chen[2], Hao Sheng[3], Chun-yi Xu[2], Li-feng Xu[1], Fang Zheng[1] and Feng Zhang[1]**

[1]Core Facility, The Quzhou Affiliated Hospital of Wenzhou Medical University, Quzhou People's Hospital, Quzhou, China, [2]Zhejiang Chinese Medical University, Hangzhou, China, [3]Zhejiang University School of Medicine, Hangzhou, China

NAFLD is the most prevalent liver disease in human history. The treatment is still limited yet. In the current study, we reported that limonin inhibited hepatic lipid accumulation and fatty acid synthesis in HFD fed mice. Using AMPK inhibitor and AMPK deficient *C. elegans*, we revealed the effect was dependent on the activation of AMPK. We found that limonin activated AMPK through inhibition of cellular energy metabolism and increasing ADP:ATP ratio. Furthermore, the treatment of limonin induced AMPK mediated suppression of the transcriptional activity of SREBP1/2. Our study suggests that limonin may a promising therapeutic agent for the treatment of NAFLD.

Keywords: limonin, AMPK, lipid accumulation, NAFLD, SREBP

OPEN ACCESS

Edited by:
Menghao Huang,
Indiana University School of Medicine, United States

Reviewed by:
Hu Li,
Chinese Academy of Medical Sciences and Peking Union Medical College, China
Chuanpeng Dong,
Purdue University Indianapolis, United States
Jinan Li,
Indiana University School of Medicine, United States

****Correspondence:***
Feng Zhang
felix.f.zhang@outlook.com

Specialty section:
This article was submitted to Gastrointestinal and Hepatic Pharmacology, a section of the journal Frontiers in Pharmacology

Received: *12 December 2021*
Accepted: *06 January 2022*
Published: *24 January 2022*

Citation:
Wang S-w, Lan T, Chen H-f, Sheng H, Xu C-y, Xu L-f, Zheng F and Zhang F (2022) Limonin, an AMPK Activator, Inhibits Hepatic Lipid Accumulation in High Fat Diet Fed Mice. Front. Pharmacol. 13:833705. doi: 10.3389/fphar.2022.833705

INTRODUCTION

Non-alcoholic fatty liver disease (NAFLD), which is also called metabolic associated fatty liver disease (MAFLD) (Eslam et al., 2020), is characterized by pathological accumulation of triglycerides (TG) and other lipids in hepatocytes (Heeren and Scheja 2021; Ooi et al., 2021). It can progress to nonalcoholic steatohepatitis (NASH) and fibrosis, which eventually lead to liver cirrhosis, hepatocellular carcinoma. Although a variety of small molecule chemical drugs are undergoing clinical trials (Zhu et al., 2021), the treatment for NAFLD is still limited.

AMP-activated protein kinase (AMPK) is a key metabolic regulator that senses energy status and controls energy expenditure and storage, whose activation has been proposed to be therapeutically beneficial for the treatment of NAFLD (Garcia et al., 2019; Zhao et al., 2020). AMPK is activated in response to energy stress by sensing increases in AMP: ATP and ADP: ATP ratios and inhibited by adenosine triphosphate (ATP) (Garcia and Shaw 2017). Liver specific AMPK knockout can aggravate hepatic lipid accumulation, steatosis, inflammation, fibrosis and hepatocyte apoptosis (Garcia et al., 2019; Zhao et al., 2020). Hepatic activation of AMPK by the synthetic polyphenol protects against hepatic steatosis by suppressing sterol regulatory element binding protein 1 (SREBP1) activity (Li et al., 2011). Activating AMPK also inhibit hepatic cholesterol synthesis by suppression of SREBP2 activity (Tang et al., 2016). Our previous study showed that activation of AMPK by flavonoids could ameliorate hepatic steatosis in mice (Wang et al., 2020a).

Limonin (**Figure 1A**), a tetracyclic triterpenoid compound, is a secondary metabolite with high biological activity in plants (Fan et al., 2019). It is abundant in many traditional Chinese medicines and fruits (Fan et al., 2019). It has been recognized as one of the most beneficial and active components of medicinal foods (Gu et al., 2019). In recent years, pharmacological investigations have uncovered various bioactivities of limonin including anti-cancer (Chidambara Murthy et al., 2021), anti-inflammatory (Yang et al., 2021), anti-oxidation (Yu et al., 2005) and liver protection

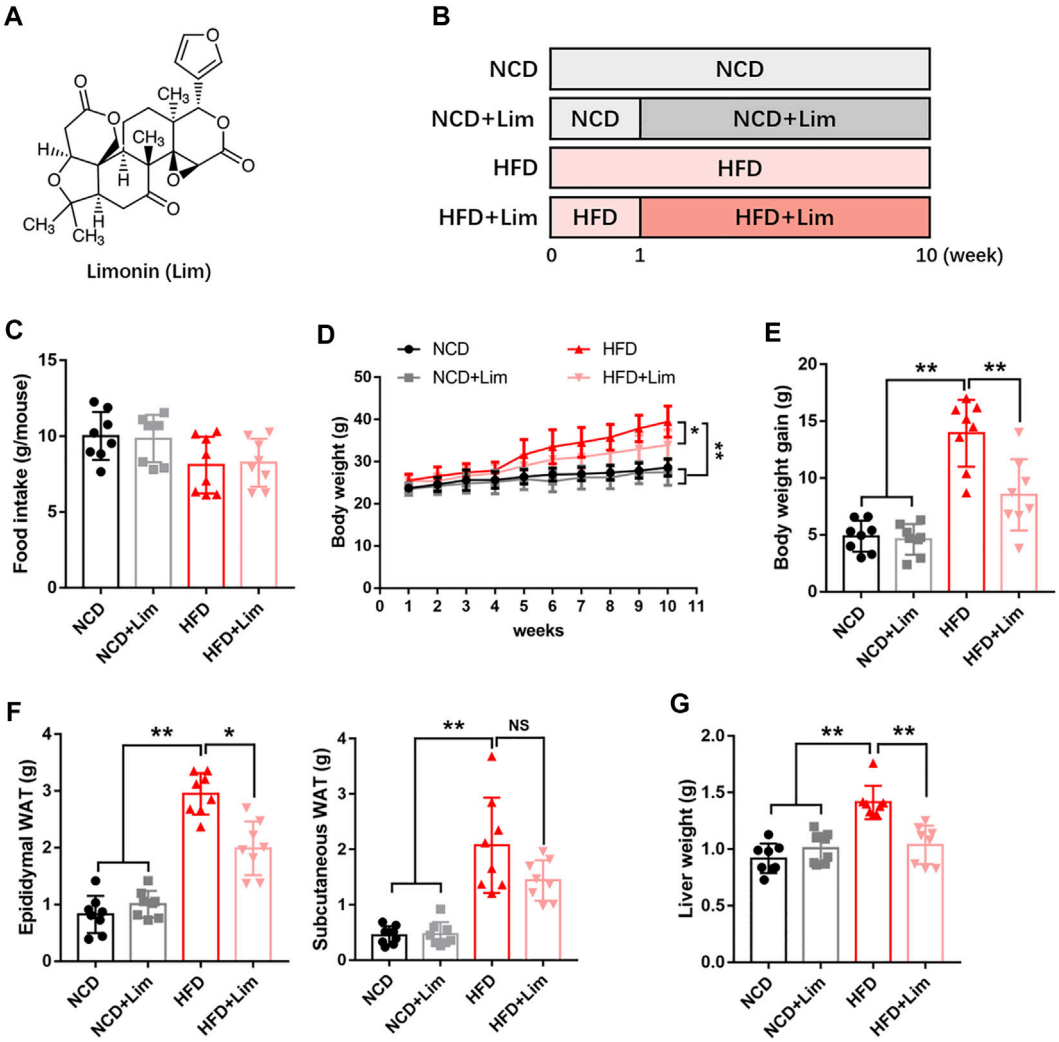

FIGURE 1 | Lim inhibits the increase of body weight, adipose weight and liver weight induced by HFD in mice. **(A)** The chemical structure of Lim. Its molecular weight is 470.53. **(B)** The schematic diagram for HFD-induced fatty liver and Lim administration. C57BL/6 mice were fed either a chow diet as NCD or HFD for 10 weeks to induce fatty liver. Mice were treated with daily oral doses of Lim (50 mg/kg) from the second week of HFD diet feeding. Water was gavaged as control. **(C)** Food intake was calculated the average food intake of each mouse from the 2nd week to the 10th week. **(D)** Body weight curve. **(E)** Body weight gain. **(F)** Weight of epididymal white adipose tissue and subcutaneous white adipose tissue. **(G)** Weight of liver. Data were expressed as the mean ± SD (n = 8). $^{*}p < 0.05$, $^{**}p < 0.01$; NS, no significance.

activity (Yang et al., 2020). Limonin reduces LDL cholesterol in HepG2 cells (Bhathena and Velasquez 2002) and regulates the expression of genes related to lipid metabolism in mice (Fan et al., 2019). However, the effect of limonin in hepatic lipid metabolism and the mechanism is still unclear.

Here, we reported that limonin inhibited hepatic lipid accumulation and fatty acid synthesis in HFD-induced mice. Further mechanistic studies revealed that limonin suppressed the transcriptional activity of SREBP1/2 by activating AMPK. In general, our study reveals that limonin may a promising therapeutic agent for the treatment of NAFLD.

MATERIALS AND METHODS

Materials

Limonin (Lim, CAS# 1,180-71-8, HPLC≥95%) was purchased from TCI (Shanghai) Development Co., Ltd., China. Compound C (#B3252) was purchased from ApexBio, United States. Antibody sources are as follows: phospho-AMPKα (#2535, Cell Signaling Technology), AMPKα (#5831, Cell Signaling Technology), phospho-ACC (#3661, Cell Signaling Technology), ACC (#3662, Cell Signaling Technology), phospho-LKB1 (#3055, Cell Signaling Technology), LKB1

(#3050, Cell Signaling Technology), phospho-CAMKK2 (#12818, Cell Signaling Technology), CAMKK2 (#16810, Cell Signaling Technology), PP2A (#2038, Cell Signaling Technology), PP2C (#3549, Cell Signaling Technology), phospho-TAK1 (#4508, Cell Signaling Technology), TAK1 (#5206, Cell Signaling Technology), SREBP1 (ab28481, Abcam), SERBP2 (ab30682, Abcam), β-actin (#3700, Cell Signaling Technology). Commercial kits used in measurement of plasma parameters are as follows: triglyceride (TG), total cholesterol (TC) assay kits were purchased from Dongou Diagnostics Co., Ltd., Zhejiang, China; alanine aminotransferase (ALT), aspartate aminotransferase (AST), alkaline phosphatase (ALP), non-esterified fatty acid (NEFA), high-density lipoprotein cholesterol (HDL-C), and low-density lipoprotein cholesterol (LDL-C) assay kits were purchased from Nanjing Jiancheng Bioengineering Institute, China.

Animal Experiments

All animal experiments were approved by the Animal Care and Use Committee of Zhejiang Chinese Medical University, where the experiments were conducted. 32 C57BL/6 male mice (eight-week-old), which were purchased from GemPharmatech Co., Ltd., Jiangsu, China (license number of animal production: SYXK 2015-0001), were housed two per cage in a temperature and humidity-controlled room with a 12:12 h light/dark cycle. After 1 week of acclimation, the mice were randomly separated into four groups: 1) NCD group: mice (n = 8) were orally administered with ultrapure water as control vehicle and fed with 10% Kcal high-fat, 7% sucrose control diet match D12492 (Research diet D12450J, Research Diet, NJ); 2) NCD + Lim group: mice (n = 8) were orally administered with limonin (Lim, 50 mg/kg/day) and fed with 10% Kcal high-fat, 7% sucrose control diet match D12492 (Research diet D12450J, Research Diet, NJ); 3) HFD group: mice (n = 8) were orally administered with ultrapure water as control vehicle and fed with 60% Kcal high-fat diet (Research diet D12492, Research Diet, NJ); 4) HFD + Lim group: mice (n = 8) were orally administered with limonin (Lim, 50 mg/kg/day) and fed with 60% Kcal high-fat diet (Research diet D12492, Research Diet, NJ). As described, the Lim administration started from the second week and the experiment lasted for 10 weeks in total (**Figure 1B**). Body weight and food intake were recorded weekly. At the end of the study, the blood samples were collected and the plasma parameters were detected using the indicated kits according to the manufacturers' instructions. The tissues were dissected, weighed, immediately frozen in liquid nitrogen and stored at −80°C.

Oral glucose tolerance tests and insulin tolerance test

OGTT and ITT were conducted at 9 weeks of the experiment. After fasting for 6 h, mice were oral D-glucose (2 g/kg) or i. p. injected with insulin (0.75 U/kg). Blood glucose levels were measured at 0, 30, 60, 90, and 120 min, which was measured by tail vein using a standard glucometer (Johnson & Johnson, United States).

Histology Examination

Mouse liver tissues were fixed in fixed in 4% v/v phosphate-buffered formaldehyde, embedded in paraffin, sectioned, and stained with hematoxylin and eosin (H&E) according to our described previously (Bai et al., 2019; Wang et al. 2020a; Wang et al. 2021a). Lipid droplets were visualized by Oil Red O (Solarbio Life Science, China) staining. The NAFLD activity score (NAS) and the intensity of Oil Red O analysis were also based on the method according to our previous researches (Wang et al., 2020a).

Cell Culture and Treatment

The mouse normal hepatic cell line AML12 (obtained from the Shanghai Bank of Cell Lines) was routinely cultured in Dulbecco's Modified Eagle's Medium (DMEM/F-12) containing 10% fetal bovine serum (FBS). Human hepatoma HepG2 cell line (obtained from the Shanghai Bank of Cell Lines) was cultured in Dulbecco's Modified Eagle's Medium (DMEM) containing 10% fetal bovine serum (FBS). To establish a hepatic lipid accumulation model using AML12 cells, we used 0.4 mM palmitic acid (PA) after starving in serum-free DMEM for 24 h.

Immunofluorescence Staining

To visualize the expression and localization of SREBP1 and SREBP2 in cells, AML12 cells were incubated with anti-SREBP1 (1:100) or anti-SREBP2 (1:100) antibody at 4°C overnight. Then the cells were stained by Alexa Fluor 488 secondary antibody for 1 h at room temperature. The fluorescence was visualized by a SUNNY RX50 fluorescence microscope. An average score of the immunofluorescence was calculated as described previously (Wang et al. 2018; Wang et al. 2019).

C. elegans Strain and Treatment

Wild-type N2 *C. elegans* and aak-2 (ok524) X mutant strains were obtained from the Caenorhabditis Genetics Center. All worms were fed on *Escherichia coli* OP50 lawn and raised at 20°C on nematode growth medium (NGM) agar plates. The yielding eggs were hatched in M9 buffer overnight at 20°C to obtain the age-synchronized L1 worms. The synchronized populations were further incubated on NGM plates which were pretreated with 100 μM Lim (dissolved in M9 buffer) for 6 days.

In vitro Lipid Accumulation

Lipid accumulation in hepatocytes or *C. elegans* was visualized by Oil Red O staining or quantified by commercial kits (TC and TG), according to the manufacturer's instructions.

ADP/ATP Ratio Measurement

Cells were treated with different concentrations of limonin dissolved in DMSO for 2 h. ADP/ATP ratio was measured by ADP/ATP Ratio Assay Kit (#ab65313, Abcam, Burlingame, CA) according to the manufacturer's instruction.

Plasmids and Transfection

AMPK-DN was cloned from pMIGR-AMPK-KD (Addgene, Cat #27296) into pcDNA-3xFlag plasmid. The fragment of AMPKγ2

TABLE 1 | The primers used in this study for real time PCR.

Description	Sense primer (5′→3′)	Antisense primer (5′→3′)
Fasn	GGAGGTGGTGATAGCCGGTAT	TGGGTAATCCATAGAGCCCAG
Scd1	TTCTTGCGATACACTCTGGTGC	CGGGATTGAATGTTCTTGTCGT
Acc1	CTCCCGATTCATAATTGGGTCTG	TCGACCTTGTTTTACTAGGTGC
Hmgcr	TGACCTTTCTAGAGCGAGTGCAT	CACGAGCTATATTTTCCCTTACTTCA
Hmgcs	AGAGAGCGATGCAGGAAACTT	AAGGATGCCCACATCTTTTGG
Gapdh	TGAGGCCGGTGCTGAGTATGT	CAGTCTTCTGGGTGGCAGTGAT

was cloned from pGEM-PRKAG2 (#HG16130-G, SinoBiological, Beijing, China) and constructed into pLKO-puro FLAG plasmid. Mutagenesis was performed using the Hieff Mut™ Site-Directed Mutagenesis Kit (YEASEN, Shanghai, China) according to the manufacturer's instruction. The transfection was performed using Lipofectamine 3000 reagent from Life Technologies (Carlsbad, CA) according to our described previously (Wang et al., 2021b).

Quantitative Reverse Transcriptase-Polymerase Chain Reaction

Quantitative real-time PCR was performed as described previously (Wang et al. 2020a; Wang et al. 2020b). In brief, total RNA from tissue or cells were isolated with TRIzol (#DP424, Tiangen Biotech Co. Ltd., Beijing, China). First-strand cDNA was synthesized from 1.5 μg of RNA using reverse transcriptase kits (ThermoFisher Scientific, Waltham, MA) according to the manufacturer's instructions. After cDNA synthesis, the expressions of indicated genes were estimated by real-time PCR using the SGExcel FastSYBR Mixture (#B532955-0005, Sangon Biotech Co., Ltd., Shanghai, China) on Roche LightCycler^{R} 480 Quantitative PCR System (Indianapolis, United States). The PCR results of GAPDH served as internal controls. The primers used for PCR are listed in **Table 1**.

Immunoblotting

Immunoblotting was performed as described previously (Wang et al., 2020a). In brief, liver tissue or cells were extracted with 1 × sodium dodecyl sulfate (SDS). A total of 25 μg protein was loaded into a 10% SDS-PAGE gel and transferred onto a polyvinylidene fluoride (PVDF) membrane. Primary antibodies were incubated overnight, and the secondary antibodies (Cell Signaling Technology, 1:3000) were added onto the membrane. Immunoreactive bands were visualized using enhanced chemiluminescence reagents (#180-501, Tanon Biotechnology, Shanghai, China). Chemiluminescence was determined using Tanon 4200SF system (Tanon Biotechnology, Shanghai, China).

Statistical Analysis

Data is presented as mean ± SD. Statistical analyses were performed using GraphPad Prism 7.0 (GraphPad Software, La Jolla California USA). Differences between the groups were analyzed using Student's t-test or one-way ANOVA followed by Dunnett's multiple comparisons test. Significance thresholds were $p < 0.05$.

RESULTS

Lim Ameliorates Metabolic Disorder in HFD Fed Mice

To explore the effect of Lim on metabolic disorder, we built up our animal model by feeding mice high fat diet (**Figure 1B**). Firstly, we took thorough examination of metabolic parameters in these mice. There was no difference in food intake between control and Lim treated groups no matter what kind of diet was fed (**Figure 1C**). We observed significant body weight loss in Lim treated mice fed with HFD, and there was no obvious difference in body weights in mice fed with chow diet with or without Lim administration (**Figures 1D,E**). Lim reduced the amount of epididymal and subcutaneous white adipose tissue in HFD fed mice (**Figure 1F**). Moreover, Lim treatment improved systematic insulin resistance and lowered serum lipids in HFD-fed mice (**Supplementary Figures S1, S2**). Of note, the increasing of liver weight induced by HFD feeding was also ameliorated by Lim treatment (**Figure 1G**).

Lim Improves Liver Function in HFD Fed Mice

Next, we focused on the effect of Lim on liver function under the condition of HFD feeding. As shown in **Figures 2A–C**, Lim significantly improved liver function in HFD fed mice revealed by decreased levels of ALP, ALT and AST in serum. The pathologic change of livers was determined by H&E staining and semi-quantitative analysis. We found that Lim obviously ameliorated hepatic steatosis and the infiltration of inflammatory cells in HFD fed mice (**Figures 2D,E**).

Lim Reduces Hepatic Lipid Accumulation in HFD Fed Mice

To further characterize the effect of Lim on hepatic lipid accumulation, we evaluated the lipid content of mouse liver by several approaches. We found that Lim treatment significantly reduced the content of total cholesterol (TC) and triglyceride (TG) in the livers of mice fed a high-fat diet (**Figures 3A,B**). The amount of hepatic neutral lipids determined by Oil Red O staining was also decreased in HFD induced mice after Lim administration (**Figures 3C,D**). Furthermore, the mRNA expression of genes associated with fatty acid synthesis (*Fasn*, *Scd1* and *Acc1*) and cholesterol synthesis (*Hmgcr* and *Hmgcs*) was

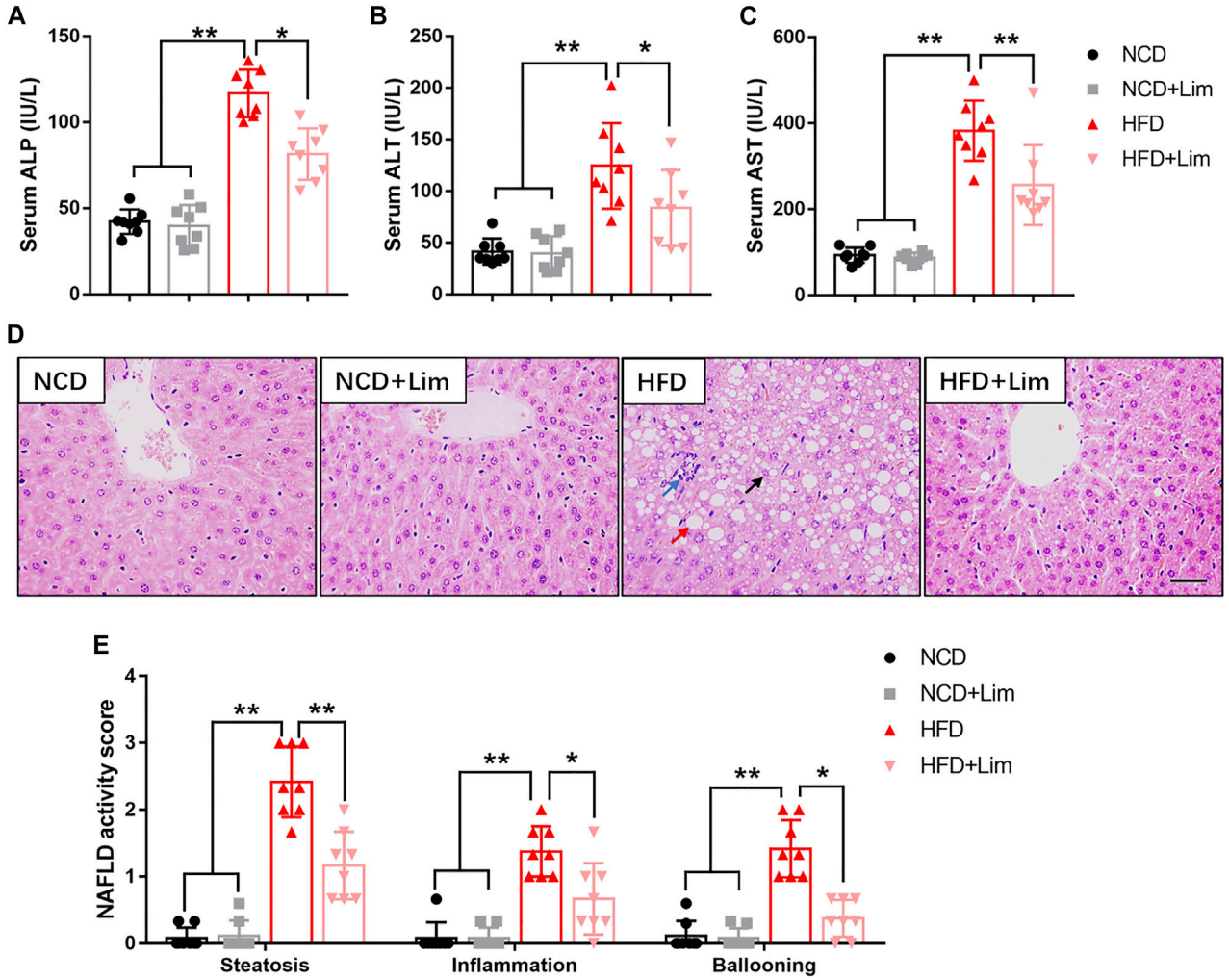

FIGURE 2 | Effects of Lim on liver function in HFD fed mice. **(A)** Serum ALP (Alkaline phosphatase) levels; **(B)** Serum ALT (Alanine Aminotransferase) levels; **(C)** Serum AST (Aspartate Aminotransferase) levels. **(D)** The representative images of H&E staining in livers from each group. Scale bar = 300 μm. Black arrow denotes macrovesicular steatosis; red arrow denotes hepatocellular ballooning; blue arrow denotes lobular inflammation. **(E)** Quantification of NAS (NAFLD activity score) based on 3 histologic features (steatosis 0-3, inflammation 0-3, hepatocellular ballooning 0–2) in H&E-stained liver sections. Data were expressed as the mean ± SD (n = 8). *$p < 0.05$, **$p < 0.01$.

down-regulated by Lim in the livers of HFD fed mice (**Figures 3E,F**).

Lim Activates AMPK *in vitro* and *in vivo*

AMPK is a master regulator to keep metabolic balance in liver tissue. Previous study reported that triterpenoids can activate AMPK (Tan et al., 2008). Lim is the first tetranortriterpenoid obtained from citrus bitter principles (Roy and Saraf 2006). Therefore, we wondered if Lim could increase AMPK activity. We found that HFD feeding inhibited AMPK phosphorylation in mouse livers, while Lim treatment greatly enhanced AMPK phosphorylation, especially in HFD mice. Meanwhile, the phosphorylation of ACC, a well-known substate of AMPK, was also increased by Lim under the condition of HFD feeding (**Figures 4A,B**). To determine if the activation of AMPK is a direct action of Lim on hepatocytes in the livers, or due to its indirect effect on whole body metabolism, we treated murine hepatic cell line AML12 with Lim in different concentrations or time. As shown in **Figures 4C,D**, Lim induced AMPK activation and ACC phosphorylation in a dose- and time-dependent manner. To mimic HFD feeding *in vitro*, we treated AML12 cells with palmitic acid (PA). Similar with the observation *in vivo*, PA challenge decreased the phosphorylation of both AMPK and ACC, while Lim treatment re-elevated both of them in PA challenged cells (**Figures 4E,F**).

Lim Ameliorates Lipid Accumulation *via* AMPK Activation

To investigate whether the activation of AMPK is required for the reductive effect of Lim on lipid accumulation, we

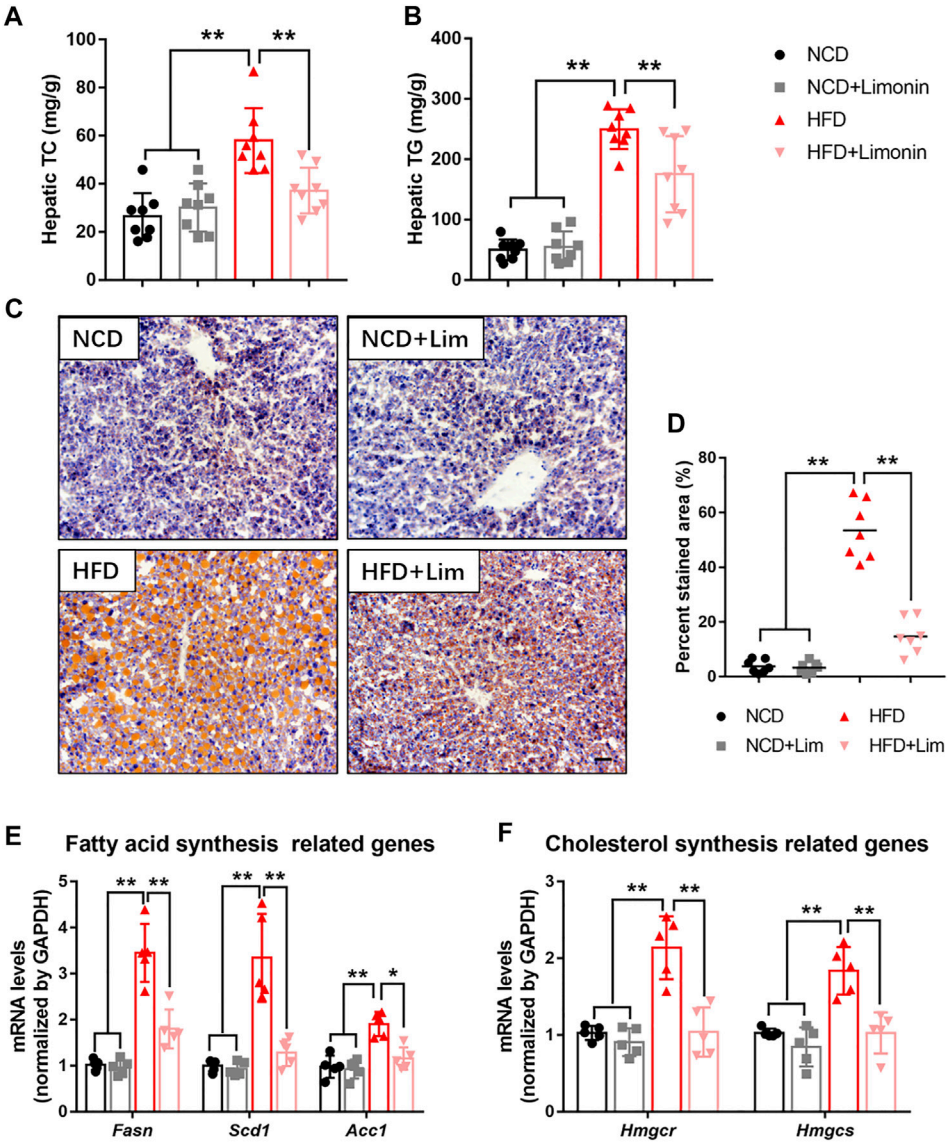

FIGURE 3 | Lim suppresses HFD-induced hepatic lipid accumulation in mice. **(A)** Hepatic TC levels. **(B)** Hepatic TG levels. **(C)** The representative images of Oil Red O staining in livers from each group. Scale bar = 300 μm. **(D)** The quantification of Oil Red O-stained areas was shown. Data were expressed as the mean ± SD (n = 8). The mRNA levels of genes related to fatty acid synthesis **(E)** and cholesterol synthesis **(F)** were determined by real-time PCR. Data were expressed as the mean ± SD (n = 5). *p < 0.05, **p < 0.01.

suppressed AMPK activity *in vitro* by Dorsomorphin (Compound C) or the expression of AMPK dominant negative plasmid. As shown in **Figure 5A** and **Supplementary Figure S3**, Lim significantly lowered PA induced lipid accumulation in AML12 cells, while Compound C almost completely abolished the effect. Similar with the result from Oil Red O staining, the measurement of TG and TC also showed that the administration of Compound C reversed Lim induced decrease of intracellular lipids (**Figure 5B**). In addition, Inhibition of AMPK activity by the expression of dominant negative AMPK plasmid also greatly reversed the repressive effect of Lim on lipid accumulation (**Figures 5C,D**).

Lim Suppresses Fat Accumulation in *Caenorhabditis elegans* Through AMPK

To further confirm AMPK activation is also necessary to Lim induced reduction of lipid accumulation *in vivo*, we used genetic model from *Caenorhabditis elegans*. Lim administration reduced the amount of lipid droplets in N2 worms determined by Oil Red O staining and TC/TG measurement. In aak-2 worms, knockout

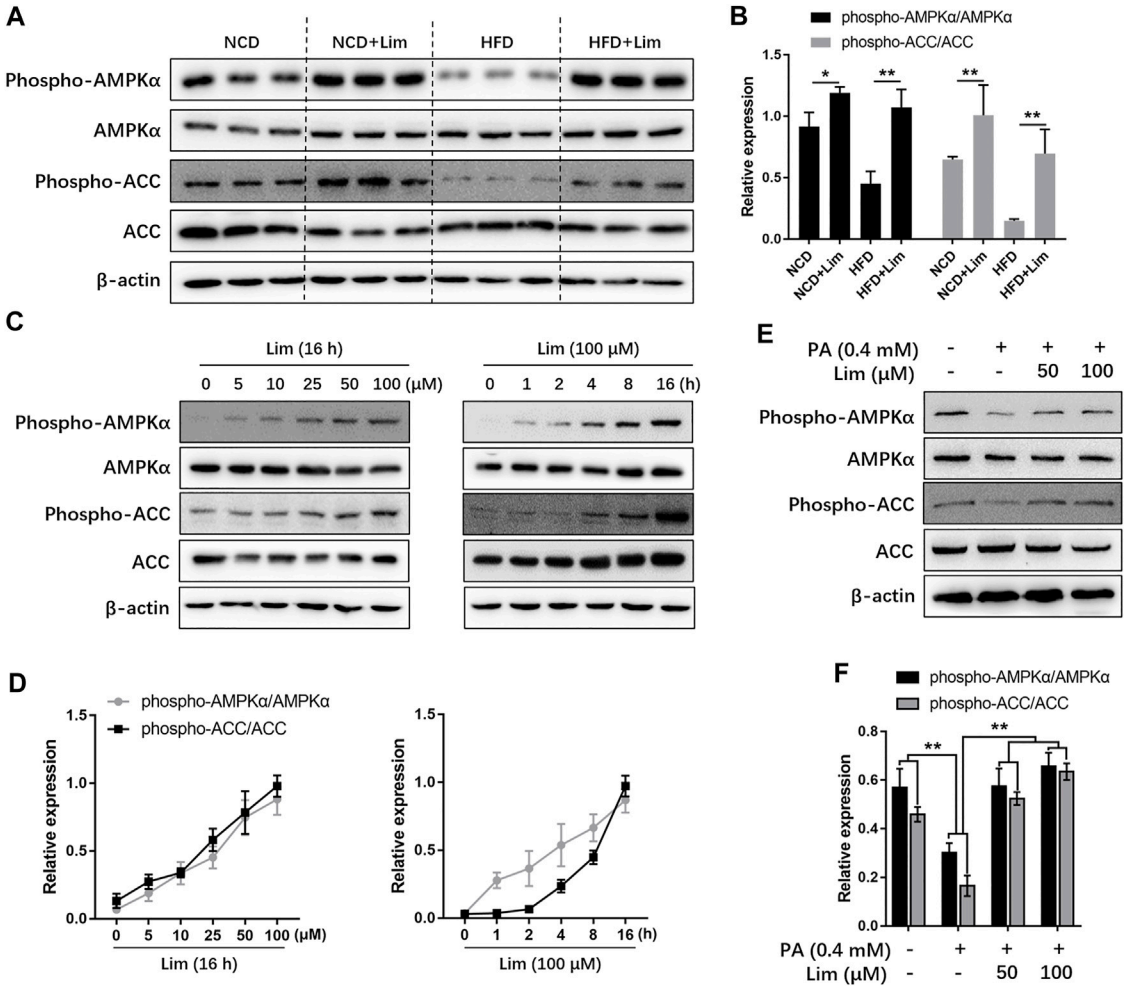

FIGURE 4 | Lim increases AMPK activity *in vitro* and *in vivo*. **(A)** The protein level of phospho-AMPK, AMPK, phospho-ACC and ACC in livers of HFD-induced mice were assessed by Western blot analysis. **(C)** Lim increased AMPK activity in a dose and time-dependent manner in AML12 cells. **(E)** The AML12 cells were treated with DMSO, 0.4 mM palmitic acid (PA), 0.4 mM PA + 50 μM Lim or 0.4 mM PA + 100 μM Lim for 16 h respectively, after starving in serum-free DMEM for 24 h. The amount of phospho-AMPK, AMPK, phospho-ACC and ACC was determined by Western blotting. **(B,D,F)** The intensity of bands for phospho-AMPK and phospho-ACC was normalized to total AMPK and ACC, respectively. Data were expressed as the mean ± SD (n = 3). *p < 0.05, **p < 0.01.

of AMPK completely abrogated Lim induced suppression of fat accumulation (**Figures 6A–C**).

Lim Activates AMPK Through Inhibition of ATP Generation

Next, we tried to find out how Lim activated AMPK. The phosphorylation of Thr172 and the binding of AMP are considered as two major ways to activate AMPK (Herzig and Shaw, 2018). There are several alternative upstream activators and negative regulators in mammals for the regulation of AMPK activity (Jian et al., 2020). We found that neither the upstream kinases, including liver kinase B1 (LKB1), calcium/calmodulin-dependent protein kinase 2 (CAMKK2), and transforming growth factor β activated kinase 1 (TAK1), nor the negative regulators such as protein phosphatase 2A (PP2A) and PP2C were significantly affected by Lim treatment (**Figure 7A**). To determine whether AMPK activation by Lim was AMP dependent, we performed the assay firstly introduced by Simon A. Hawley on *Cell Metabolism* (Hawley et al., 2010). As shown in **Figures 7B,C**, Lim induced AMPK activation and ACC phosphorylation in a dose-manner in WT but not in RG cells, suggesting Lim treatment inhibited ATP production. Indeed, Lim significantly increased ADP/ATP ratio measured by bioluminescent assay kit in parental 293T cells (**Figure 7D**).

Lim Suppresses the Transcriptional Activity of SREBP1/2 Through AMPK

Since the expression of fatty acid and cholesterol synthesis genes were down-regulated by Lim in the livers of HFD fed mice, we wondered whether Lim inhibited the expression of these genes by

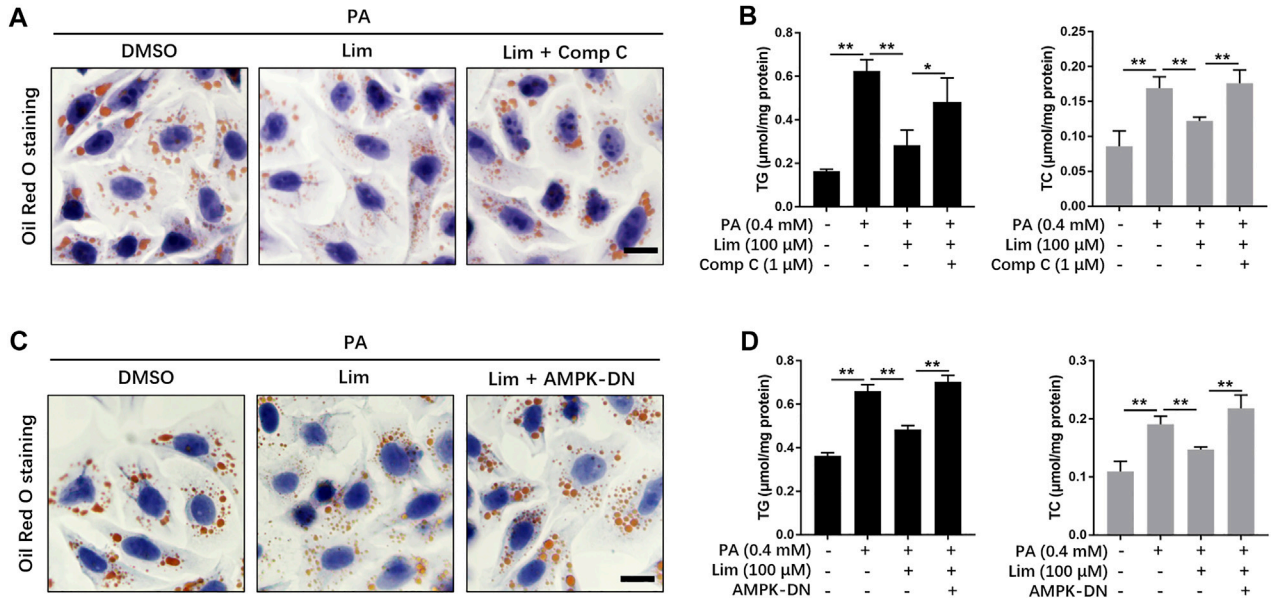

FIGURE 5 | The role of AMPK in Lim derived reduction of lipid accumulation in hepatocytes. **(A)** The AML12 cells were treated with 0.4 mM PA, 0.4 mM PA + 100 μM Lim or 0.4 mM PA + 100 μM Lim +1 μM Comp C for 16 h respectively, after starving in serum-free DMEM for 24 h. The representative images of Oil Red O staining in cells. Scale bar = 300 μm. **(B)** The AML12 cells were treated with DMSO, 0.4 mM PA, 0.4 mM PA + 100 μM Lim or 0.4 mM PA + 100 μM Lim +1 μM Comp C for 16 h respectively, after starving in serum-free DMEM for 24 h. The intracellular levels of TG and TC were determined by a colorimetric enzymatic assay. **(C,D)** Dominant negative AMPK expressing plasmid (AMPK-DN) was introduced into AML12 before treatment with PA and Lim. The lipid-lowering effect of Lim was abolished by AMPK-DN in AML12 cells treated with PA, as revealed by Oil Red O staining and the measurement of intracellular TG and TC. Data were expressed as the mean ± SD (n = 3). *p < 0.05, **p < 0.01.

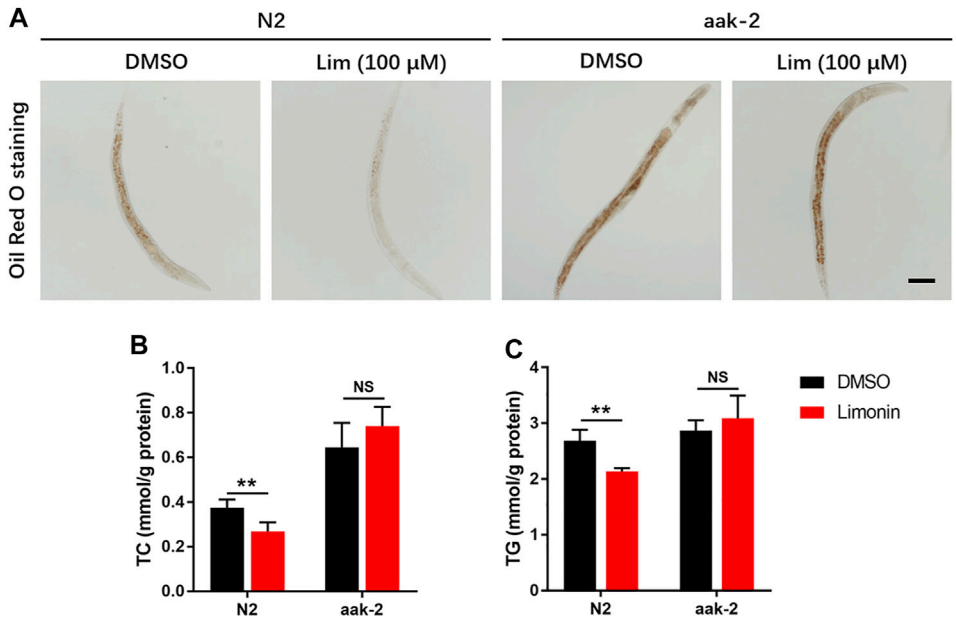

FIGURE 6 | The inhibition of fat deposition by Lim in *Caenorhabditis elegans* requires AMPK. N2 (wild-type) and aak-2 (AMPK knockout) worms were treated with or without Lim (100 μM) for 7 days. **(A)** The representative images of Oil Red O staining in worms. Scale bar = 300 μm. **(B,C)** The TC and TG levels in worms were determined by a colorimetric enzymatic assay. Data were expressed as the mean ± SD (n = 6). **p < 0.01; NS, no significance.

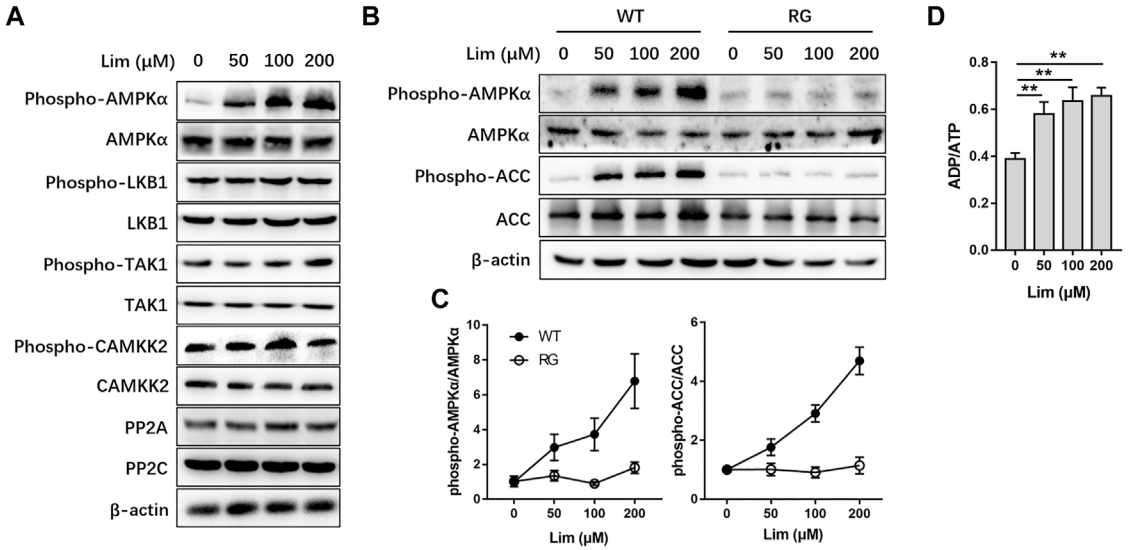

FIGURE 7 | The activation of AMPK by Lim was adenine nucleotide dependent. HepG2 cells were treated with different concentrations of Lim for 4 h. **(A)** The abundance or activation of protein kinases and phosphatases upstream of AMPK were examined by Western blotting. **(B)** HepG2 cells were transduced with wild-type (WT) or R531G (RG) AMPKγ2 before Lim treatment. The activation of AMPK and the phosphorylation of ACC were examined by Western blotting. **(C)** The intensity of bands for phospho-AMPK and phospho-ACC was normalized to total AMPK and ACC, respectively. **(D)** Lim increased the intracellular ratio of ADP and ATP in HepG2. Data were expressed as the mean ± SD (n = 3). $^{**}p < 0.01$.

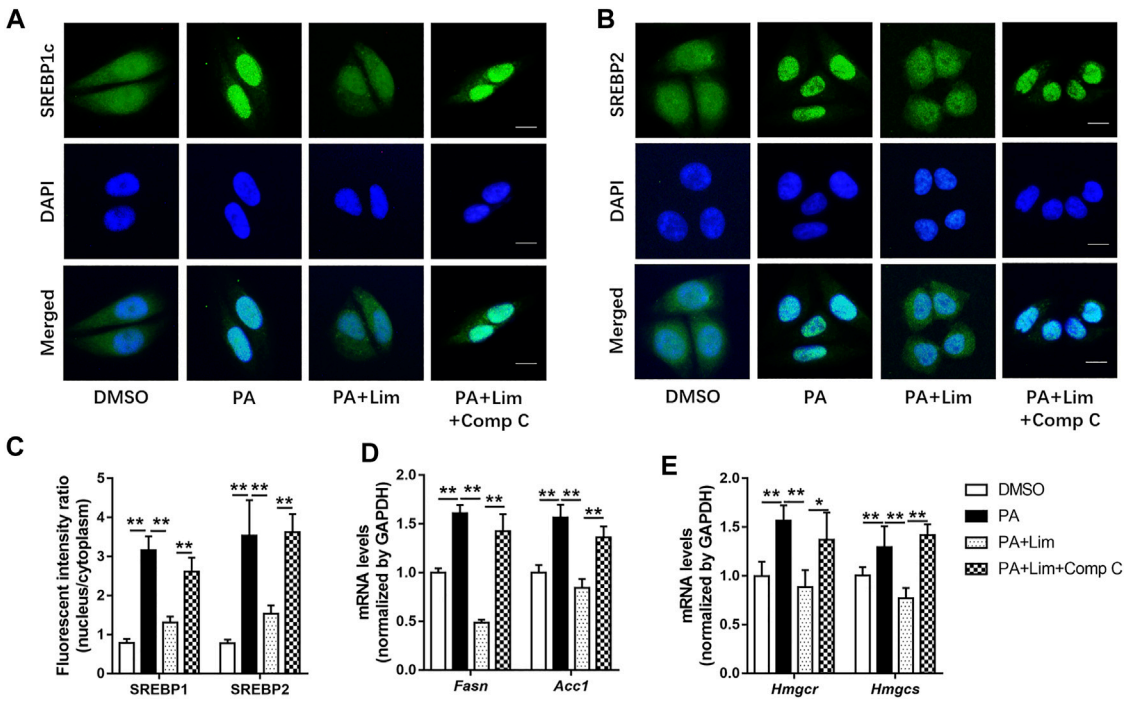

FIGURE 8 | Lim inhibits the transcriptional activity of SREBP1 and SREBP2 through AMPK in hepatocytes. The AML12 cells were treated with DMSO, 0.4 mM palmitic acid (PA), 0.4 mM PA + 100 μM Lim or 0.4 mM PA + 100 μM Lim +1 μM Comp C for 16 h respectively, after starving in serum-free DMEM for 24 h **(A,B)** The representative images of SREBP1 and SREBP2 immunofluorescent staining in cells. Scale bar = 300 μm. **(C)** Quantification of the fluorescent intensity of SREBP1 and SREBP2 in the nuclei relative to that of the cytoplasm. **(D,E)** The mRNA levels of *Fasn*, *Acc1* and *Hmgcr*, *Hmgcs* genes were evaluated using RT-PCR. Values were expressed as mean ± SD (n = 3). $^{*}p < 0.05$, $^{**}p < 0.01$.

activating AMPK. To test our hypothesis, we determined the intracellular localization of SREBP1c and SREBP2, two most crucial transcriptional factors for lipid metabolism gene expression, after PA induction. As shown in **Figures 8A,B**, PA induced nuclear translocation of SREBP1c and SREBP2, while Lim treatment decreased the gathering of these two proteins in nuclei. Inhibition of AMPK by Compound C enhanced the nuclear translocation of SREBP1c and SREBP2 in Lim treated hepatocytes (**Figures 8A–C**). In addition, we examined the expression of downstream targets of SREBP1c and SREBP2. The administration of Compound C significantly re-elevated the expression of *Fasn* and *Acc1* regulated by SREBP1c, and the expression of *Hmgcr* and *Hmgcs* regulated by SREBP2 in Lim treated AML12 cells (**Figures 8D,E**).

DISCUSSION

Here, we identify, for the first time, that limonin inhibits hepatic lipid accumulation in HFD fed mice via the activation of AMPK. Limonoids are highly oxygenated triterpenoid compounds. Limonin, nomilin and obacunone are the major limonoids in Citrus (Gualdani et al., 2016). In 2011, Eri Ono's publication stated that nomilin and obacunone can activate TGR5, a bile acid membrane receptor (Ono et al., 2011). The activation of TGR5 by bile acids increases energy expenditure and attenuates diet-induced obesity in mice (Thomas et al., 2009). Eri Ono suggested that the anti-obesity and anti-hyperglycemic effects by nomilin was through activating TGR5. Furthermore, they pointed out that limonin was not a TGR5 agonist (Ono et al., 2011). Despite some studies demonstrated the effect of limonin on reducing inflammation and oxidative stress, few reported the function of limonin in the regulation of glucose and lipid metabolism, as its incapability of activating TGR5. The current study uncovered the significant role of limonin in metabolic regulation. During our previous studies, we investigated the effects of several active compounds in the citrus aurantium on NAFLD (Bai et al., 2019; Wang et al. 2020a; Wang et al. 2021a). Using cell based system, we screened natural products with regulatory effect on AMPK activity. We found that limonin can activate AMPK *in vivo* and *in vitro*. As we known, there has been no report on the activation of AMPK by limonin so far. The key regulatory roles of AMPK on glucose and lipid homeostasis further support observation that limonin can effectively ameliorate metabolic disorders including NAFLD.

A wide variety of drugs and xenobiotics has been found to activate AMPK, for example, antidiabetic drugs like metformin, phenformin and thiazolidinediones, and natural products derived from traditional medicines or foods such as berberine, quercetin, resveratrol and epigallocatechin gallate (Hawley et al., 2010). However, the underlying mechanisms by which AMPK is activated are remain unclear in many cases. Adenine nucleotides are compartmentalized between the mitochondria and cytoplasm and their diffusion is limited, they may not be uniformly distributed within the cytoplasm. The AMPK is extremely sensitive to small changes in AMP. Subtle changes in subcellular nucleotides that may not be detectable by measuring total cellular levels would be enough to influence the activity of AMPK. The measurement of cellular contents of AMP and ADP in cell extracts will lose the information of their effects of compartmentation. Therefore, while an agent like metformin may activate AMPK without producing a detectable change in AMP, this does not prove the effect is AMP independent (Hawley et al., 2010). To determine whether or not activation of AMPK by different agents was AMP dependent, Simon A. Hawley et al. (2010) developed a test. The mutation of AMPKγ2 subunit, R531G, causes a severe loss of binding by AMP and ATP, thus generating an AMP-insensitive AMPK complex. They expressed wild-type or R531G mutant γ2 subunit in cells to replace the endogenous γ1 subunit in the assay. This method was widely adopted by later researches, and was carried out in our current study. We used oligomycin and A769662 as positive controls to validate the effectiveness of the test (**Supplementary Figure S4**). Using this system, we found that Lim activated AMPK through inhibition of cellular energy metabolism and increasing ADP: ATP ratio. However, more investigation is needed in future to elaborate whether Lim increased AMPK activity through initiating/inhibiting membrane receptor associated signal pathways, uncoupling the respiratory oxidation and ATP generation in the mitochondria, or interfering glycolysis.

At the beginning of the current study, we examined the changes of systemic metabolism in mice with or without limonin treatment. Although the remission of liver pathological changes is the focus of our attention, it is obvious that limonin has a significant impact on systemic metabolic indicators, including body weight, body fat, blood sugar, blood lipids and insulin sensitivity. These indicators are affected by diverse organs such as liver, adipose tissue, skeletal muscle as well as other factors like neuroendocrine and intestinal flora. Conversely, changes in these indicators also affect the metabolic status of liver, adipose tissue, skeletal muscle and other organs. Through cell based assays *in vitro*, we determined that limonin had a direct effect on hepatic cells. Even though, we can't rule out the possibility that limonin relieved hepatic steatosis and inflammation in mice induced by high-fat diet through its joint action on the liver and other tissues such as adipose tissue. In the body, limonin may first act on the liver, and affect the metabolism of adipose tissue through secretory factors like hepatokines, thereby improving systemic metabolism. It may also act directly on adipose tissue, lowering blood lipids, thereby alleviating hepatic steatosis. This effect superimposed with its direct effect on the liver, resulting in the overall influence we observed. These speculations warrant more investigations in future.

CONCLUSION

In summary, we found that limonin activated AMPK in hepatocytes and attenuated hepatic lipid accumulation. These findings suggest limonin as potential therapeutics for MAFLD and warrant more detailed investigation for its underlying mechanisms in future.

DATA AVAILABILITY STATEMENT

The original contributions presented in the study are included in the article/**Supplementary Material**, further inquiries can be directed to the corresponding author.

ETHICS STATEMENT

The animal study was reviewed and approved by The Animal Care and Use Committee of Zhejiang Chinese Medical University.

AUTHOR CONTRIBUTIONS

Participated in research design: FeZ and S-wW. Conducted experiments: S-wW, TL, H-fC, HS, C-yX, L-fX, and FaZ. Performed data analysis: S-wW, FeZ, and H-fC. Wrote or contributed to the writing of the manuscript: FeZ and S-wW.

FUNDING

This work was supported by National Natural Science Foundation of China (No. 81903873), Natural Science Foundation of Zhejiang Province (No. LQ19H160002), Medical and Health Technology Projects of Zhejiang Province, China (Nos. 2020PY087, 2019PY089, and 2017KY696), the Chinese medicine science foundation of Zhejiang Province, China (No. 2021ZB328), Quzhou technology projects, China (Nos. 2019K34 and 2018K20).

SUPPLEMENTARY MATERIAL

The Supplementary Material for this article can be found online at: https://www.frontiersin.org/articles/10.3389/fphar.2022.833705/full#supplementary-material

REFERENCES

Bai, Y. F., Wang, S. W., Wang, X. X., Weng, Y. Y., Fan, X. Y., Sheng, H., et al. (2019). The Flavonoid-Rich Quzhou Fructus Aurantii Extract Modulates Gut Microbiota and Prevents Obesity in High-Fat Diet-Fed Mice. *Nutr. Diabetes* 9 (1), 30. doi:10.1038/s41387-019-0097-6

Bhathena, S. J., and Velasquez, M. T. (2002). Beneficial Role of Dietary Phytoestrogens in Obesity and Diabetes. *Am. J. Clin. Nutr.* 76 (6), 1191–1201. doi:10.1093/ajcn/76.6.1191

Chidambara Murthy, K. N., Jayaprakasha, G. K., Safe, S., and Patil, B. S. (2021). Citrus Limonoids Induce Apoptosis and Inhibit the Proliferation of Pancreatic Cancer Cells. *Food Funct.* 12 (3), 1111–1120. doi:10.1039/d0fo02740e

Eslam, M., Sanyal, A. J., George, J., and International Consensus, P. (2020). MAFLD: A Consensus-Driven Proposed Nomenclature for Metabolic Associated Fatty Liver Disease. *Gastroenterology* 158 (7), 1999–e1. doi:10.1053/j.gastro.2019.11.312

Fan, S., Zhang, C., Luo, T., Wang, J., Tang, Y., Chen, Z., et al. (2019). Limonin: A Review of Its Pharmacology, Toxicity, and Pharmacokinetics. *Molecules* 24 (20). doi:10.3390/molecules24203679

Garcia, D., Hellberg, K., Chaix, A., Wallace, M., Herzig, S., Badur, M. G., et al. (2019). Genetic Liver-specific AMPK Activation Protects against Diet-Induced Obesity and NAFLD. *Cell Rep* 26 (1), 192–e6. doi:10.1016/j.celrep.2018.12.036

Garcia, D., and Shaw, R. J. (2017). AMPK: Mechanisms of Cellular Energy Sensing and Restoration of Metabolic Balance. *Mol. Cell* 66 (6), 789–800. doi:10.1016/j.molcel.2017.05.032

Gu, M., Sun, J., Qi, C., Cai, X., Goulette, T., Song, M., et al. (2019). The Gastrointestinal Fate of Limonin and its Effect on Gut Microbiota in Mice. *Food Funct.* 10 (9), 5521–5530. doi:10.1039/c9fo01274e

Gualdani, R., Cavalluzzi, M. M., Lentini, G., and Habtemariam, S. (2016). The Chemistry and Pharmacology of Citrus Limonoids. *Molecules* 21 (11), 1530. doi:10.3390/molecules21111530

Hawley, S. A., Ross, F. A., Chevtzoff, C., Green, K. A., Evans, A., Fogarty, S., et al. (2010). Use of Cells Expressing Gamma Subunit Variants to Identify Diverse Mechanisms of AMPK Activation. *Cell Metab* 11 (6), 554–565. doi:10.1016/j.cmet.2010.04.001

Heeren, J., and Scheja, L. (2021). Metabolic-associated Fatty Liver Disease and Lipoprotein Metabolism. *Mol. Metab.* 50, 101238. doi:10.1016/j.molmet.2021.101238

Herzig, S., and Shaw, R. J. (2018). AMPK: Guardian of Metabolism and Mitochondrial Homeostasis. *Nat. Rev. Mol. Cell Biol* 19 (2), 121–135. doi:10.1038/nrm.2017.95

Jian, C., Fu, J., Cheng, X., Shen, L. J., Ji, Y. X., Wang, X., et al. (2020). Low-Dose Sorafenib Acts as a Mitochondrial Uncoupler and Ameliorates Nonalcoholic Steatohepatitis. *Cell Metab* 31 (5), 892–e11. e811. doi:10.1016/j.cmet.2020.04.011

Li, Y., Xu, S., Mihaylova, M. M., Zheng, B., Hou, X., Jiang, B., et al. (2011). AMPK Phosphorylates and Inhibits SREBP Activity to Attenuate Hepatic Steatosis and Atherosclerosis in Diet-Induced Insulin-Resistant Mice. *Cell Metab* 13 (4), 376–388. doi:10.1016/j.cmet.2011.03.009

Ono, E., Inoue, J., Hashidume, T., Shimizu, M., and Sato, R. (2011). Anti-obesity and Anti-hyperglycemic Effects of the Dietary Citrus Limonoid Nomilin in Mice Fed a High-Fat Diet. *Biochem. Biophys. Res. Commun.* 410 (3), 677–681. doi:10.1016/j.bbrc.2011.06.055

Ooi, G. J., Meikle, P. J., Huynh, K., Earnest, A., Roberts, S. K., Kemp, W., et al. (2021). Hepatic Lipidomic Remodeling in Severe Obesity Manifests with Steatosis and Does Not Evolve with Non-alcoholic Steatohepatitis. *J. Hepatol.* 75 (3), 524–535. doi:10.1016/j.jhep.2021.04.013

Roy, A., and Saraf, S. (2006). Limonoids: Overview of Significant Bioactive Triterpenes Distributed in Plants Kingdom. *Biol. Pharm. Bull.* 29 (2), 191–201. doi:10.1248/bpb.29.191

Tan, M. J., Ye, J. M., Turner, N., Hohnen-Behrens, C., Ke, C. Q., Tang, C. P., et al. (2008). Antidiabetic Activities of Triterpenoids Isolated from Bitter Melon Associated with Activation of the AMPK Pathway. *Chem. Biol.* 15 (3), 263–273. doi:10.1016/j.chembiol.2008.01.013

Tang, H., Yu, R., Liu, S., Huwatibieke, B., Li, Z., and Zhang, W. (2016). Irisin Inhibits Hepatic Cholesterol Synthesis via AMPK-SREBP2 Signaling. *EBioMedicine* 6, 139–148. doi:10.1016/j.ebiom.2016.02.041

Thomas, C., Gioiello, A., Noriega, L., Strehle, A., Oury, J., Rizzo, G., et al. (2009). TGR5-mediated Bile Acid Sensing Controls Glucose Homeostasis. *Cell Metab* 10 (3), 167–177. doi:10.1016/j.cmet.2009.08.001

Wang, S. W., Bai, Y. F., Weng, Y. Y., Fan, X. Y., Huang, H., Zheng, F., et al. (2019). Cinobufacini Ameliorates Dextran Sulfate Sodium-Induced Colitis in Mice through Inhibiting M1 Macrophage Polarization. *J. Pharmacol. Exp. Ther.* 368 (3), 391–400. doi:10.1124/jpet.118.254516

Wang, S. W., Lan, T., Sheng, H., Zheng, F., Lei, M. K., Wang, L. X., et al. (2021a). Nobiletin Alleviates Non-alcoholic Steatohepatitis in MCD-Induced Mice by Regulating Macrophage Polarization. *Front. Physiol.* 12, 687744. doi:10.3389/fphys.2021.687744

Wang, S. W., Sheng, H., Bai, Y. F., Weng, Y. Y., Fan, X. Y., Lou, L. J., et al. (2020a). Neohesperidin Enhances PGC-1α-Mediated Mitochondrial Biogenesis and Alleviates Hepatic Steatosis in High Fat Diet Fed Mice. *Nutr. Diabetes* 10 (1), 27. doi:10.1038/s41387-020-00130-3

Wang, S. W., Sheng, H., Bai, Y. F., Weng, Y. Y., Fan, X. Y., Zheng, F., et al. (2021b). Inhibition of Histone Acetyltransferase by Naringenin and Hesperetin Suppresses Txnip Expression and Protects Pancreatic β Cells in Diabetic Mice. *Phytomedicine* 88, 153454. doi:10.1016/j.phymed.2020.153454

Wang, S. W., Wang, W., Sheng, H., Bai, Y. F., Weng, Y. Y., Fan, X. Y., et al. (2020b). Hesperetin, a SIRT1 Activator, Inhibits Hepatic Inflammation via AMPK/CREB Pathway. *Int. Immunopharmacol* 89 (Pt B), 107036. doi:10.1016/j.intimp.2020.107036

Wang, S. W., Xu, Y., Weng, Y. Y., Fan, X. Y., Bai, Y. F., Zheng, X. Y., et al. (2018). Astilbin Ameliorates Cisplatin-Induced Nephrotoxicity through Reducing Oxidative Stress and Inflammation. *Food Chem. Toxicol.* 114, 227–236. doi:10.1016/j.fct.2018.02.041

Yang, R., Song, C., Chen, J., Zhou, L., Jiang, X., Cao, X., et al. (2020). Limonin Ameliorates Acetaminophen-Induced Hepatotoxicity by Activating Nrf2 Antioxidative Pathway and Inhibiting NF-κB Inflammatory Response via Upregulating Sirt1. *Phytomedicine* 69, 153211. doi:10.1016/j.phymed.2020.153211

Yang, R., Yu, H., Chen, J., Zhu, J., Song, C., Zhou, L., et al. (2021). Limonin Attenuates LPS-Induced Hepatotoxicity by Inhibiting Pyroptosis via NLRP3/Gasdermin D Signaling Pathway. *J. Agric. Food Chem.* 69 (3), 982–991. doi:10.1021/acs.jafc.0c06775

Yu, J., Wang, L., Walzem, R. L., Miller, E. G., Pike, L. M., and Patil, B. S. (2005). Antioxidant Activity of Citrus Limonoids, Flavonoids, and Coumarins. *J. Agric. Food Chem.* 53 (6), 2009–2014. doi:10.1021/jf0484632

Zhao, P., Sun, X., Chaggan, C., Liao, Z., In Wong, K., He, F., et al. (2020). An AMPK-Caspase-6 axis Controls Liver Damage in Nonalcoholic Steatohepatitis. *Science* 367 (6478), 652–660. doi:10.1126/science.aay0542

Zhu, C., Tabas, I., Schwabe, R. F., and Pajvani, U. B. (2021). Maladaptive Regeneration - the Reawakening of Developmental Pathways in NASH and Fibrosis. *Nat. Rev. Gastroenterol. Hepatol.* 18 (2), 131–142. doi:10.1038/s41575-020-00365-6

Conflict of Interest: The authors declare that the research was conducted in the absence of any commercial or financial relationships that could be construed as a potential conflict of interest.

Publisher's Note: All claims expressed in this article are solely those of the authors and do not necessarily represent those of their affiliated organizations, or those of the publisher, the editors and the reviewers. Any product that may be evaluated in this article, or claim that may be made by its manufacturer, is not guaranteed or endorsed by the publisher.

frontiers in Pharmacology

ORIGINAL RESEARCH
published: 16 February 2022
doi: 10.3389/fphar.2022.843872

Combined Use of Bicyclol and Berberine Alleviates Mouse Nonalcoholic Fatty Liver Disease

*Hu Li[1†], Nan-Nan Liu[1†], Jian-Rui Li[1], Biao Dong[1], Mei-Xi Wang[1], Jia-Li Tan[1], Xue-Kai Wang[1], Jing Jiang[1], Lei Lei[1], Hong-Ying Li[1], Han Sun[1], Jian-Dong Jiang[1] and Zong-Gen Peng[1,2]**

[1]Institute of Medicinal Biotechnology, Chinese Academy of Medical Sciences and Peking Union Medical College, Beijing, China, [2]Key Laboratory of Biotechnology of Antibiotics, The National Health and Family Planning Commission (NHFPC), Institute of Medicinal Biotechnology, Chinese Academy of Medical Sciences and Peking Union Medical College, Beijing, China

Nonalcoholic fatty liver disease (NAFLD), ranging from simple steatosis to nonalcoholic steatohepatitis (NASH), is a liver disease worldwide without approved therapeutic drugs. Anti-inflammatory and hepatoprotective drug bicyclol and multi-pharmacological active drug berberine, respectively, have shown beneficial effects on NAFLD in murine nutritional models and patients, though the therapeutic mechanisms remain to be illustrated. Here, we investigated the combined effects of bicyclol and berberine on mouse steatosis induced by Western diet (WD), and NASH induced by WD/CCl_4. The combined use of these was rather safe and better reduced the levels of transaminase in serum and triglycerides and cholesterol in the liver than their respective monotherapy, accompanied with more significantly attenuating hepatic inflammation, steatosis, and ballooning in mice with steatosis and NASH. The combined therapy also significantly inhibited fibrogenesis, characterized by the decreased hepatic collagen deposition and fibrotic surface. As per mechanism, bicyclol enhanced lipolysis and β-oxidation through restoring the p62-Nrf2-CES2 signaling axis and p62-Nrf2-PPARα signaling axis, respectively, while berberine suppressed *de novo* lipogenesis through downregulating the expression of acetyl-CoA carboxylase and fatty acid synthetase, along with enrichment of lipid metabolism-related Bacteroidaceae (family) *and Bacteroides* (genus). Of note, the combined use of bicyclol and berberine did not influence each other but enhanced the overall therapeutic role in the amelioration of NAFLD. *Conclusion*: Combined use of bicyclol and berberine might be a new available strategy to treat NAFLD.

Keywords: nonalcoholic fatty liver disease, bicyclol, berberine, combination, lipid metabolism, gut microbiota

OPEN ACCESS

Edited by:
Wenji Zhang,
Guangdong Academy of Agricultural Science, China

Reviewed by:
Xujie Liu,
University of Southern California, United States
Jinan Li,
Indiana University School of Medicine, United States

****Correspondence:***
Zong-Gen Peng
pumcpzg@126.com

[†]These authors have contributed equally to this work

Specialty section:
This article was submitted to Gastrointestinal and Hepatic Pharmacology, a section of the journal Frontiers in Pharmacology

Received: *27 December 2021*
Accepted: *12 January 2022*
Published: *16 February 2022*

Citation:
Li H, Liu N-N, Li J-R, Dong B, Wang M-X, Tan J-L, Wang X-K, Jiang J, Lei L, Li H-Y, Sun H, Jiang J-D and Peng Z-G (2022) Combined Use of Bicyclol and Berberine Alleviates Mouse Nonalcoholic Fatty Liver Disease. Front. Pharmacol. 13:843872. doi: 10.3389/fphar.2022.843872

INTRODUCTION

Nonalcoholic fatty liver disease (NAFLD), a common liver disease affecting a quarter of the world's population, includes nonalcoholic fatty liver (NAFL) characterized by mere excessive lipid accumulation in the liver and nonalcoholic steatohepatitis (NASH), characterized by inflammation and/or fibrosis and even cirrhosis (Eslam et al., 2020; Huang et al., 2021). NAFLD is recently referred to as metabolic-associated fatty liver disease (MAFLD), which also includes extrahepatic complications, such as obesity, type 2 diabetes, and cardiovascular and cardiac diseases (Eslam et al., 2020; Liu et al., 2020). Abnormality of hepatic lipid metabolism, including lipogenesis, lipolysis, and fatty acid β-oxidation, links with the occurrence of progressive NAFLD. Lipogenesis is a

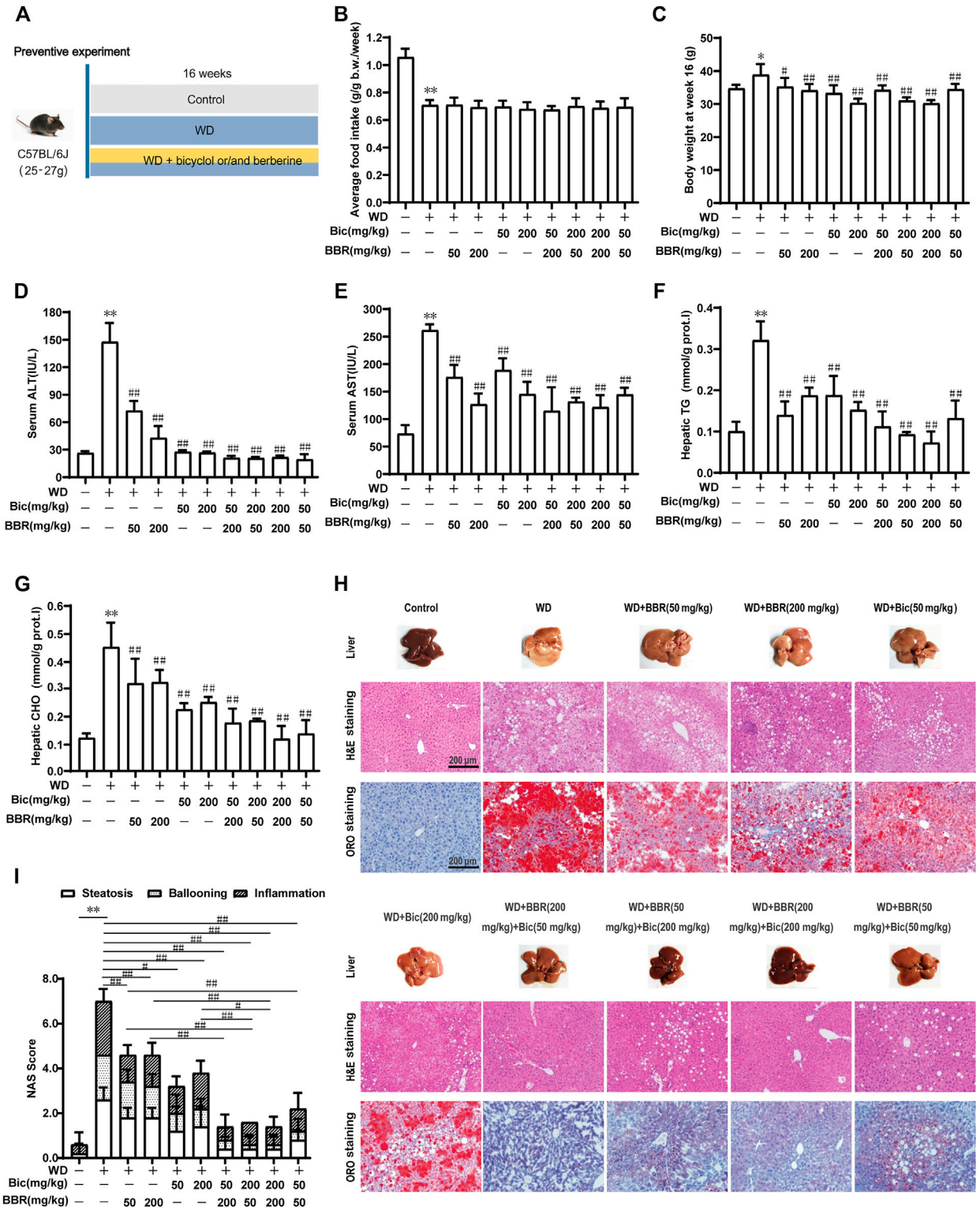

FIGURE 1 | Combination of bicyclol (Bic) and berberine (BBR) exerts better preventive effects in mice with NAFL induced by Western diet. Male C57BL/6J mice were treated by free feeding with Western diet (WD) or WD mingled with bicyclol or/and berberine **(A)**. The average food intake during the whole experiment **(B)** and body weight at week 16 **(C)** were recorded. At week 16, ALT **(D)** and AST **(E)** in serum were detected, and TG **(F)** and CHO **(G)** in the liver were measured. Liver histopathology was evaluated using H&E and ORO staining **(H)** and quantified with NAS score criteria **(I)**. Results were presented as mean ± SD. n = 5 for each group, *p < 0.05 and **p < 0.01, WD-induced model group vs. the control group; #p < 0.05 and ##p < 0.01 vs. the WD-induced model group or monotherapy group.

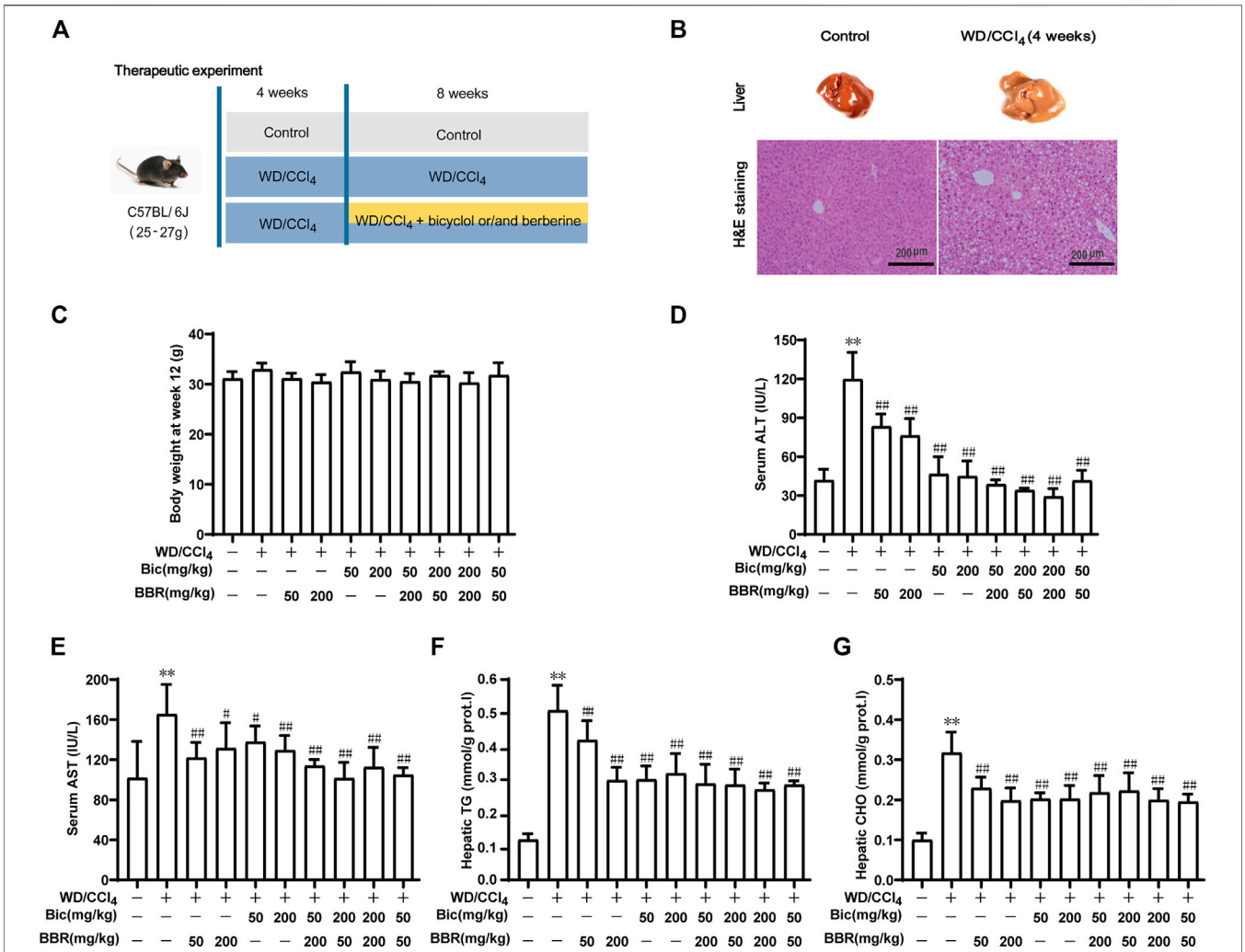

FIGURE 2 | Combination of bicyclol and berberine demonstrates better therapeutic effects on NASH in mice induced by WD/CCl_4. Male C57BL/6J mice were freely fed with Western diet plus intraperitoneal injection of 0.2 ml/kg CCl_4 (WD/CCl_4) once per week for 4 weeks **(A)**. Liver steatosis was performed with H&E staining at week 4 **(B)**. Then the mice were continuously treated with WD/CCl_4 or WD/CCl_4 plus drug for 8 weeks. The body weight **(C)** was recorded. ALT **(D)** and AST **(E)** in serum and TG **(F)** and CHO **(G)** in the liver were measured. Liver histopathology was evaluated using H&E, ORO, and Masson's trichrome staining **(H)** and quantified with NAS score criteria **(I)** and fibrotic surface **(J)**. Results were presented as mean ± SD. n = 5–9 for each group, *p < 0.05 and **p < 0.01, WD/CCl_4-induced model group vs. the control group; #p < 0.05 and ##p < 0.01 vs. the WD/CCl_4-induced model group or monotherapy group.

normal synthesis of triglycerides (TG) and fatty acids from acetyl coenzyme A (acetyl-CoA). During the *de novo* lipogenesis, acetyl-CoA is carboxylated to malonyl-CoA by the rate-limiting enzyme acetyl-CoA carboxylase (ACC) and subsequently converted by a multi-step reaction into long-chain fatty acid by fatty acid synthase (FAS) (Mashima et al., 2009; Gathercole et al., 2011), while excessive synthesis of TG is one of the main causative factors for NAFLD (Alves-Bezerra and Cohen, 2017). Conversely, lipolysis is a normal breakdown process of TG to form fatty acids and glycerol and abnormal lipolysis is another mechanism for NAFLD. Apart from classical proteins related with lipolysis, such as adipose triglyceride lipase (ATGL) and hormone-sensitive lipase (HSL), carboxylesterase 2 (CES2) is recently discovered as an efficient diglyceride, monoglyceride, and triglyceride hydrolase, which plays a causal role in the development of obesity and fatty liver diseases in human and murine (Li et al., 2016; Chalhoub et al., 2021). Hepatic mitochondrial β-oxidation is a major pathway for the catabolism of fatty acids, which is mainly regulated by peroxisome proliferator-activated receptor α (PPARα) and subsequent regulated expression of targeted genes (Wan et al., 2020). Consequently, the abnormal hepatic lipid metabolism is involved in sustained inflammation response and liver injury, further leading to the progression of NAFLD (Dong et al., 2021; Orabi et al., 2021). Apart from the aberrant hepatic lipid metabolism, gut microbiome-mediated alteration of immunity, inflammation, and metabolism are also involved in the regulation of NAFLD (He et al., 2021).

Currently, no specific drug has been approved to treat NAFLD, though several candidate drugs with different mechanisms of action have been tested in clinical trials

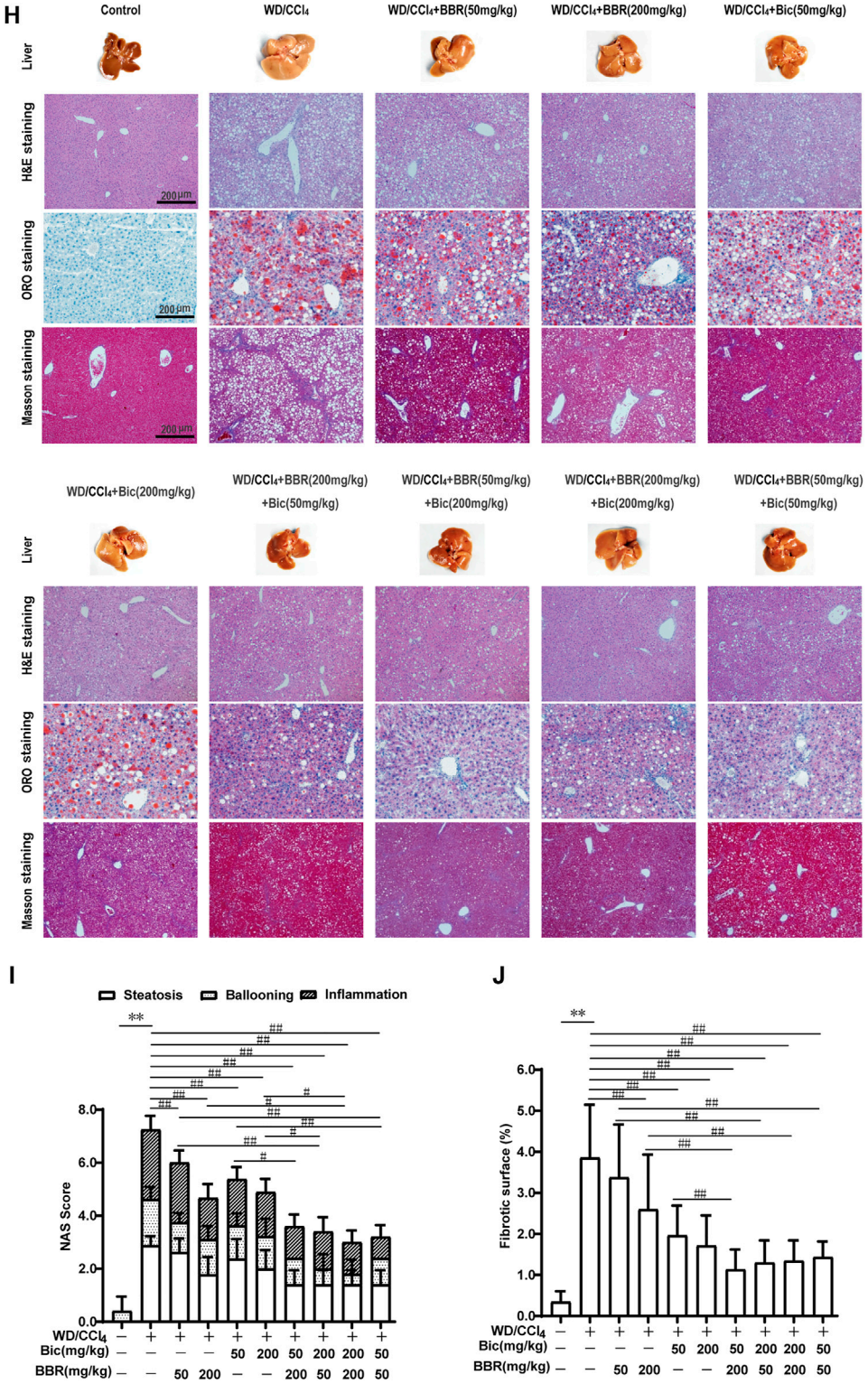

FIGURE 2 | (Continued).

(Brown et al., 2021), which target different pathophysiological pathways towards NAFLD, such as metabolic targets, inflammatory pathways, liver-gut axis, and antifibrotic targets. Because NAFLD is a multisystem disease with intricate pathological mechanisms, the therapeutic effect with a single agent is generally unsatisfactory (Huang et al., 2020; Brown et al.,

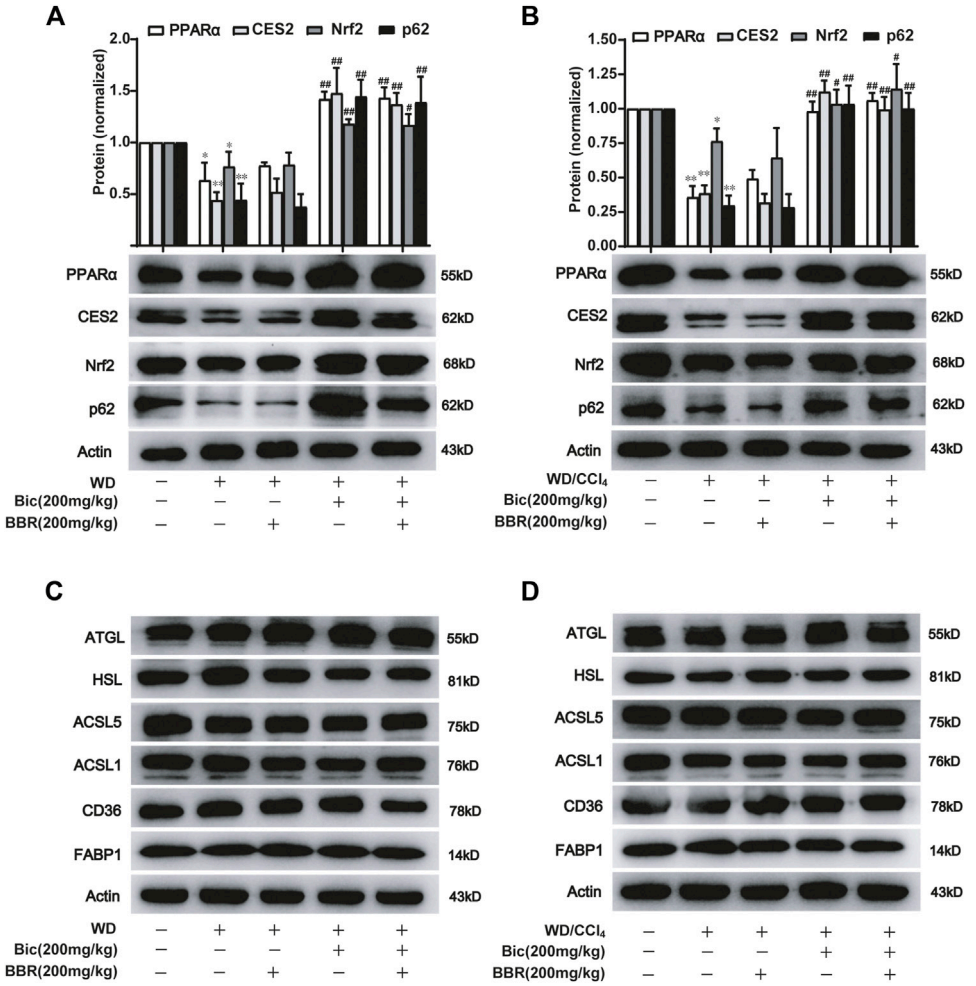

FIGURE 3 | Bicyclol with or without berberine enhances the lipolysis and β-oxidation through p62-Nrf2-CES2/PPARα axis. Male C57BL/6J mice were freely fed with WD or WD plus bicyclol and/or berberine for 16 weeks **(A,C)**, or induced with WD/CCl_4 for 4 weeks and then treated with drugs for 8 weeks **(B,D)**. The protein levels of PPARα, CES2, Nrf2, p62, CD36, FABP1, ATGL, HSL, ACSL1, and ACSL5 were detected with Western blot and quantified using a Gel-Pro analyzer. Results were presented as mean ± SD, and a representative band was shown. n = 5–9 for each group, $^{*}p < 0.05$ and $^{**}p < 0.01$, the model group vs. control group; $^{\#}p < 0.05$ and $^{\#\#}p < 0.01$ vs. the model group. PPARα, proliferator-activated receptor α; CES2, carboxylesterase 2; Nrf2, NF-E2-related factor 2; p62, ubiquitin-binding protein p62; CD36, cluster determinant 36; FABP1, fatty acid binding protein 1; ATGL, adipose triglyceride lipase; HSL, hormone-sensitive lipase; ACSL, acyl-CoA synthetase long chain family member.

2021; Zhu et al., 2021). Therefore, the combination of drugs with different mechanisms might provide potential opportunities to enhance the overall efficacy, and several clinical trials have been carried out to validate this conception (Dufour et al., 2020; Kessoku et al., 2020). Natural products were widely reported for the therapy of liver diseases (Li et al., 2019). Bicyclol, a synthetic compound that originated from the Chinese traditional herb *Schisandra chinensis*, is an approved drug for alleviating liver injuries accompanied by elevated transaminases caused by various etiologies, such as viruses, drugs, alcohol, chemicals, and immunogens (Liu, 2009; Li et al., 2018a; Li et al., 2018b). A few studies reported the therapeutic efficacy of bicyclol for NAFLD in clinic (Li et al., 2020) and in animal models (Zhao et al., 2021), though more data are needed to show its clinical benefits and the detailed mechanisms. Berberine, an approved antibacterial agent derived from a wide variety of Chinese traditional herbs, such as *Coptis chinensis* and *Berberis vulgaris* (Kong et al., 2020), has beneficial effects on NAFLD through diverse mechanisms, including the increase of insulin sensitivity, regulation of adenosine monophosphate-activated protein kinase (AMPK) pathway, improvement of mitochondrial function, and regulation of the gut microenvironment (Zhu et al., 2016; Wang et al., 2020). Therefore, considering current mono-therapeutic evidence of bicyclol and berberine and their distinguished mechanisms against NAFLD, we proposed a new potential strategy of their combined use to treat NAFLD. In this study, we demonstrated that the combination of bicyclol and berberine exerted better preventive and therapeutic effects than monotherapy for NAFLD in mice induced by Western diet (WD) or WD/CCl_4. The detailed

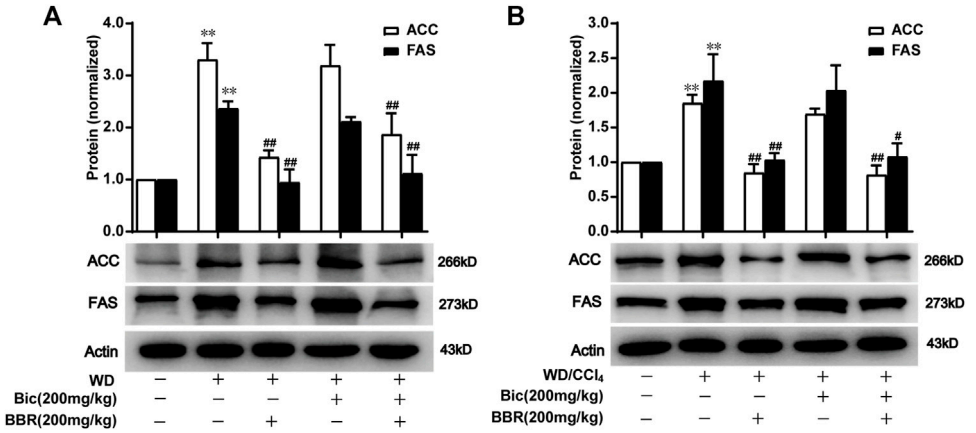

FIGURE 4 | Berberine with or without bicyclol suppresses *de novo* lipogenesis by inhibiting the protein expression of ACC and FAS. Male C57BL/6J mice were freely fed with WD or WD plus bicyclol and/or berberine for 16 weeks **(A)**, or induced with WD/CCl_4 for 4 weeks and then treated with drugs for 8 weeks **(B)**. The protein expressions of ACC and FAS were detected and quantified. Results were presented as mean ± SD, and a representative band was shown. n = 5–9 for each group, *p < 0.05 and **p < 0.01, the model group vs. control group; #p < 0.05 and ##p < 0.01 vs. the model group. ACC, acetyl-CoA carboxylase; FAS, fatty acid synthase.

mechanisms are involved in the enhancement of lipolysis and β-oxidation by bicyclol, and suppression of lipogenesis by berberine, along with its regulation of the gut microbiome. Our study provided a new strategy for the treatment of NAFLD with the combined use of bicyclol and berberine.

MATERIALS AND METHODS

Chemicals and Reagents

Bicyclol was from Beijing Union Pharmaceutical Company (Beijing, China) with a purity of over 99%. Berberine was purchased from InnoChem (Beijing, China) with a purity of over 97%. The purified low-fat, low-cholesterol diets (LFLC, LAD0011), Western diet (WD, TP26300122, contains 21.1% fat, 41% sucrose, 1.25% cholesterol), and WD mingled with low or high doses of bicyclol and berberine, and their reciprocal combination was produced by Trophic Animal Feed High-Tech Co., Ltd, China. D-fructose (Sigma, F0127), D-glucose (Sigma, G8270), and CCl_4 (Tianjin Fuchen Chemical Reagent Factory) were used in the experiments. Assay kit for alanine aminotransferase (ALT, C009-2), aspartate transaminase (AST, C010-2), triglyceride (TG, A110-1), and cholesterol (CHO, A111-1) were from Nanjing Jiancheng Biotechnology Co., Ltd, China. Oleic acid (OA, O1008); palmitic acid (PA, P0500), bovine serum albumin (BSA, B2064), and Nile Red (N3013) were from Sigma-Aldrich. Methyl thiazolyl tetrazolium (MTT, M8180), phosphate buffer solution (PBS, P1020), and trypsin (G2161) were from Beijing Solarbio Science & Technology Co., Ltd.

Animal Experiments

Male C57BL/6J mice (25–27 g) were from SPF (Beijing) Biotechnology Co., Ltd. and housed in a 12-h light/dark standard light cycle with free access to water and food. After 7 days of acclimation, mice were allocated for the preventive and therapeutic experiments. For the preventive experiment, mice were randomly divided into 10 groups, with 5 mice in each group. Mice in the drug-treated experimental group were fed with WD or WD mingled with low or high doses of bicyclol, berberine, and their reciprocal combination for 16 weeks. The low and high doses of bicyclol and/or berberine in diet were equivalently 50 and 200 mg/kg/day by gavage in mice. In parallel, high sugar drinking water with 23.1 g/L D-fructose and 18.9 g/L D-glucose were fed to the experimental group while mice in control were provided with an LFLC diet and regular drinking water. Food intake and body weight were recorded every week. In the therapeutic experiment, WD/CCl_4 (WD plus intraperitoneally injection of CCl_4 at the dose of 0.2 ml/kg in corn oil once per week) was used to induce mouse NASH. After 4 weeks of induction by WD/CCl_4, mice were divided into 10 groups (five to nine mice in each group) and fed with the corresponding diet and water as conducted in the preventive experiment for another 8 weeks. At the end of the experiments, animals were fasted for 6 h, and then blood samples were collected. For liver biochemistry and subsequent mechanism study, intralobular pieces of liver were quickly frozen in liquid nitrogen and then stored at −80°C. For histological analyses, liver slices were fixed with 4% paraformaldehyde (Servicebio, #G1101).

Biochemical Analysis

The blood samples were centrifuged at 2,500 g for 10 min, and the serum was collected. Serum levels of ALT and AST were detected using commercial assay kits. For analyses of liver biochemistry, mouse liver was homogenized, and the levels of hepatic TG and CHO were measured using assay kits according to the manufacturer's instructions.

Histological Analysis

The fixed liver tissues were conducted using hematoxylin and eosin (H&E) staining for evaluating liver inflammation, steatosis, and ballooning. The NAFLD classifications were assessed by two experts blindly according to the NAFLD activity score (NAS)

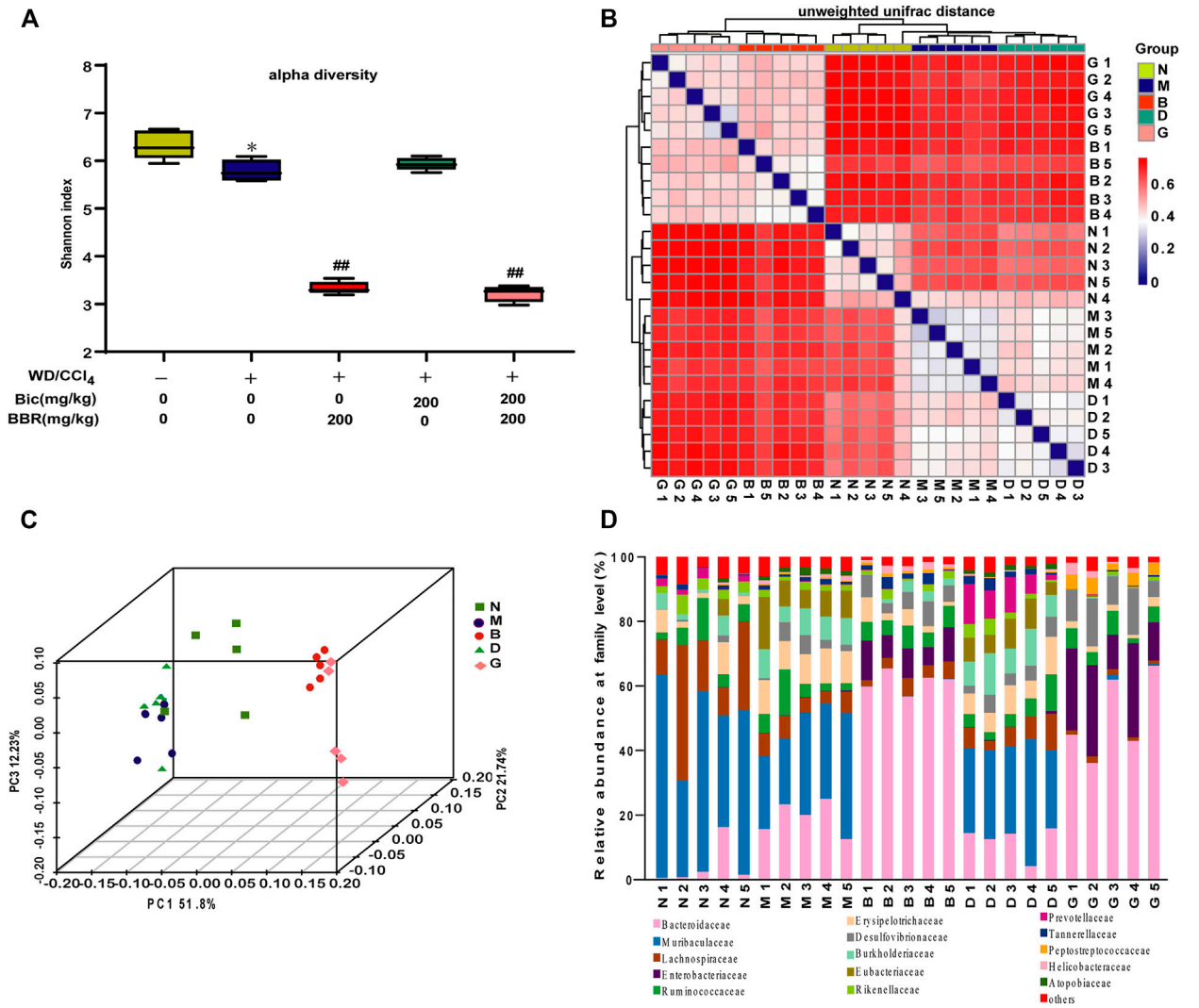

FIGURE 5 | Berberine but not bicyclol modulates the composition of gut microbiota in WD/CCl_4-induced NASH mice. A total of 25 male C57BL/6J mice fecal samples with five in each representative group were collected and analyzed using 16S rRNA gene sequencing. **(A)** The alpha diversity of each group was obtained using the Shannon index. **(B–C)** The beta diversity among samples was obtained using the unweighted UniFrac diversity distance **(B)** and PCoA **(C)** of gut microbiota. **(D–E)** The relative abundance of bacteria at family **(D)** and genus **(E)** level. **(F)** Representative histogram of the most abundant gut microbiota at the family and genus level. **(G)** Prediction of lipid metabolism-related microbiome function based on KEGG database. *p < 0.05, **p < 0.01 vs. the control group; #p < 0.05, ##p < 0.01 vs. the WD/CCl_4 group. N, Control; M, WD/CCl_4; B, WD/CCl_4+BBR(200 mg/kg); D, WD/CCl_4+Bic(200 mg/kg); G, WD/CCl_4+BBR(200 mg/kg)+Bic(200 mg/kg).

criteria, which is a composite semi-quantitative score for steatosis (0–3), lobular inflammation (0–2), hepatocellular ballooning (0–2), and fibrosis (0–4) (Kleiner et al., 2005). The presence of steatosis was further confirmed with Oil Red O (ORO) staining in frozen sections using a standard protocol. Fibrosis was qualifiedly assessed using Masson's Trichrome staining in paraffin-embedded sections, and ImageJ software was used to quantify the percentage of fibrosis surface in six fields of Masson's Trichrome staining sections of each mouse.

Cell Treatment and Cytotoxicity Assay

HepG2 cells were maintained in 5% CO_2 at 37°C and cultured in Minimum Essential Medium (Gibico, C11095500) with 10% fetal bovine serum, 100 IU/ml penicillin and 100 mg/ml streptomycin (Gibico, 15140122). HepG2 cells were plated in a 96-well plate at the concentration of $3 \times 10^4/cm^2$. The cell viability was detected with an MTT assay after 0.1 mM free fatty acid (FFA, OA:PA = 2:1) and drug treatment for 24 h, and the data were calculated as described before (Zou et al., 2021).

Nile Red Staining Assay

The cell-specific climbing slides were placed in 24-well plates and coated with rat tail collagen for 15 min. After being washed with PBS, 1×10^5 cells/well HepG2 were seeded and incubated at 37°C and 5% CO_2 for 24 h. The cells were induced with 0.1 mM FFA and simultaneously treated with 2 μM berberine, 2 μM bicyclol,

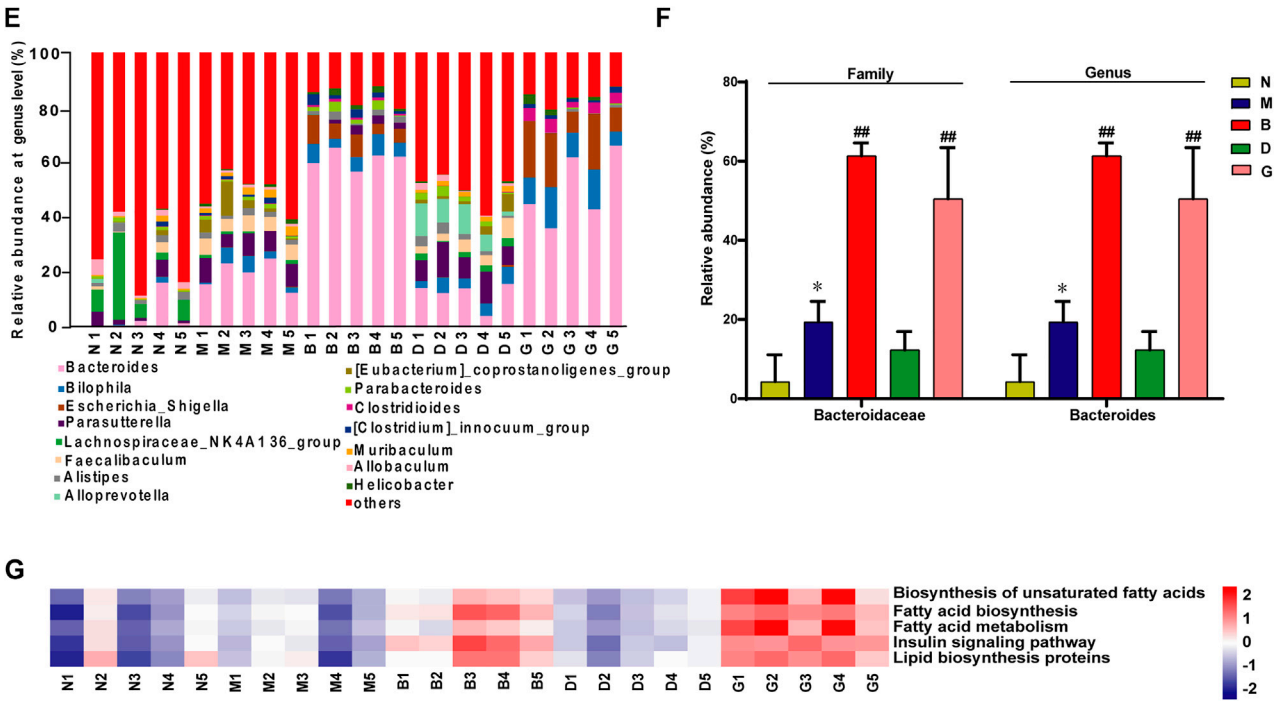

FIGURE 5 | (Continued).

or their combinations. After 24 h of treatment, the cells were washed with PBS and fixed with 3% paraformaldehyde for 10 min, followed by washing with PBS. Next, 0.5% Triton X-100 (Beyotime Biotechnology, ST795) was added for 15 min for membrane permeabilization and then washed with PBS twice. Nile Red solution at 10 μM concentration was incubated for 10 min. After being washed with PBS, the slides were sealed by mounting medium supplied with DAPI staining solution and dried in the dark. The images were acquired using Zeiss Axio observer X-cite series 120 microscope (Zeiss, Jena, Germany) at the magnification of ×63. The quantification of lipid droplets was performed using Image-Pro Plus 6.0.

Western Blot

Liver homogenates or cell lysates were prepared in a protein extraction reagent (Thermo Scientific, 78510) with protease and phosphatase inhibitor cocktail (Targetmol, C0001 and C0004). The protein concentration was determined using BCA protein assay kit (Thermo Scientific, #23225) according to the manufacturer's manual. Western blot was performed as previously described (Cheng et al., 2016; Huang et al., 2019). Briefly, 20–80 μg of proteins were separated by 10% SDS-PAGE and transferred to PVDF membranes. Membranes were blocked with 5% fat-free milk and incubated overnight at 4°C with antibodies against β-actin (CST, 3700S), CES2 (Abcam, ab215042), CES2 (Sangon Biotech, D263440), PPARα (HUABIO, EM1707-71), PPARα (Santa Cruz, sc-398394), Nrf2 (HUABIO, ER1706-41), p62 (HUABIO, EM0704), ACC (HUABIO, ET1609-77), FAS (HUABIO, R1706-8), ATGL (HUABIO, RT1058), HSL (CST, #4107), ACSL5 (HUABIO, ER60809), ACSL1 (HUABIO, ER60807), CD36 (Abcam, ab133625), and FABP1 (HUABIO, EM170403). The PVDF band was then incubated with the corresponding HRP-conjugated secondary antibody, and the signal of the target proteins was detected with ECL chemiluminescence detection kit (Vazyme, #E412) using the ChemiDoc MP imaging system (Bio-Rad). Signal intensity was scanned with Gel-Pro analyzer, and a ratio of the protein of interest to the internal control protein Actin was calculated and normalized as 1.00 for the control group.

Intestinal Microbiological Analysis

Five representative groups in the therapeutic experiment were selected to perform gut microbiological analysis, and a total of 25 mice fecal samples with five in each group were collected and subsequently analyzed using 16S rRNA gene sequencing by Oebiotech (Shanghai, China). Briefly, genomic DNA was isolated from samples using the DNeasy PowerSoil Kit (QIAGEN) and amplified using specific sequences of primers for the V3-V4 region of 16S rRNA (343F-5′ TACGGRAGGCAGCAG 3′ and 798R-5′ AGGGTATCTAATCCT 3′). The amplified products were checked by 1% agarose gel electrophoresis and purified using AMPure XP beads (Agencourt), and then amplified in another round of PCR as described above. The final amplicon was quantified using the Qubit quantification system (Life Technologies) and purified again. Equal amounts of purified amplicon were pooled for subsequent sequencing using the Illumina MiSeq System (Illumina Inc., San Diego, CA, USA). For bioinformatics analysis, the obtained raw FASTQ sequencing files were preprocessed using the QIIME software (version 1.8.0). Clean reads were subjected to primer sequence removal and clustering to generate operational taxonomic units (OTUs) using the Vsearch software (version 2.4.2)

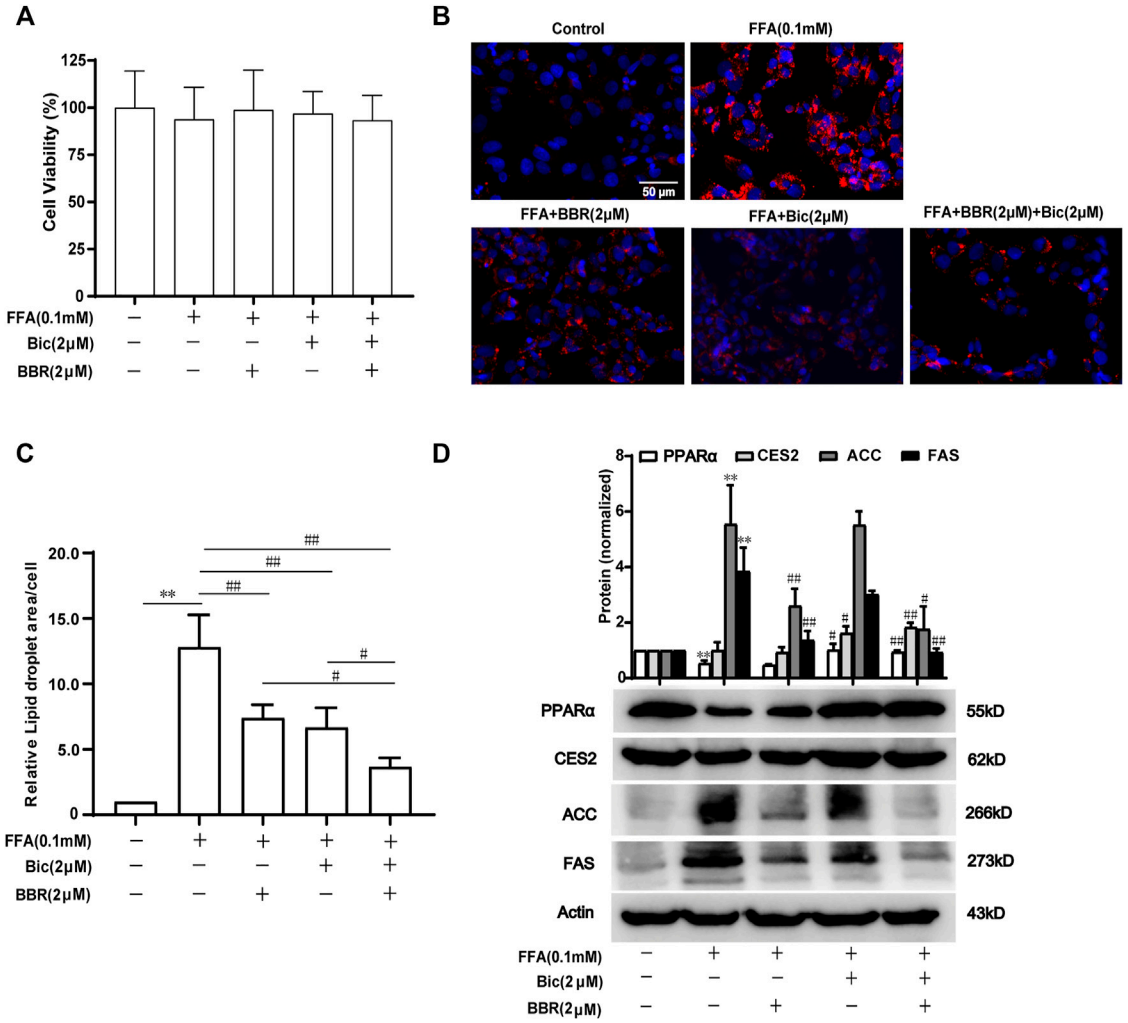

FIGURE 6 | Combined use of bicyclol and berberine decreases lipid accumulation *via* regulating lipid metabolism-related gene expression in FFA-induced HepG2 cells. HepG2 cells were induced by 0.1 mM FFA and simultaneously treated for 24 h with 2 μM berberine, 2 μM bicyclol, or their combinations. The cells were assayed with an MTT method to show the cytotoxicity **(A)**, or carried out Nile Red staining to show LDs **(B)** and the level of LDs in cells were quantified using Image-Pro Plus 6.0 **(C)**. Total proteins were extracted and detected with Western blot **(D)**. $n \geq 3$, $^{**}p < 0.01$, the model group vs. control group; $^{\#}p < 0.05$ and $^{\#\#}p < 0.01$ vs. the model group or the monotherapy group. FFA, free fatty acid; LDs, lipid droplets; PPARα, proliferator-activated receptor α; CES2, carboxylesterase 2; ACC, acetyl-CoA carboxylase; FAS, fatty acid synthase.

with 97% similarity cutoff. Based on the rarefied OTU counts, the community structure, the alpha diversity (presented as Chao index), and beta diversity [presented as unweighted UniFrac distances and principal coordinate analysis (PCoA)] were analyzed to plot the similarity or difference in the composition of the sample community. Functional inference associated with lipid metabolism was identified using Kyoto Encyclopedia of Gene and Genomes (KEGG) pathways.

Statistical Analyses

The data were presented as mean ± standard deviation (SD) and representative figures. Statistical analysis was performed using SPSS17.0 or GraphPad Prism 8 and analyzed by Student's *t*-test or analysis of variance (ANOVA) followed by Student–Newman–Keuls (SNK) post hoc tests. Kruskal–Wallis H test and Mann-Whitney *U* test were used for the nonparametric test. The value of statistical significance was set as $^{*}p < 0.05$ or $^{**}p < 0.01$.

RESULTS

Combination of Bicyclol and Berberine Exerts Better Preventive Effects in Mice With NAFL Induced by Western Diet

To analyze the combined therapeutic effect of bicyclol and berberine, we first evaluated their preventive efficacy in a murine nutritional model of NAFL. Briefly, C57BL/6J mice were treated with WD or WD mingled with low/high dose of bicyclol and/or berberine by free feeding for 16 weeks, and the

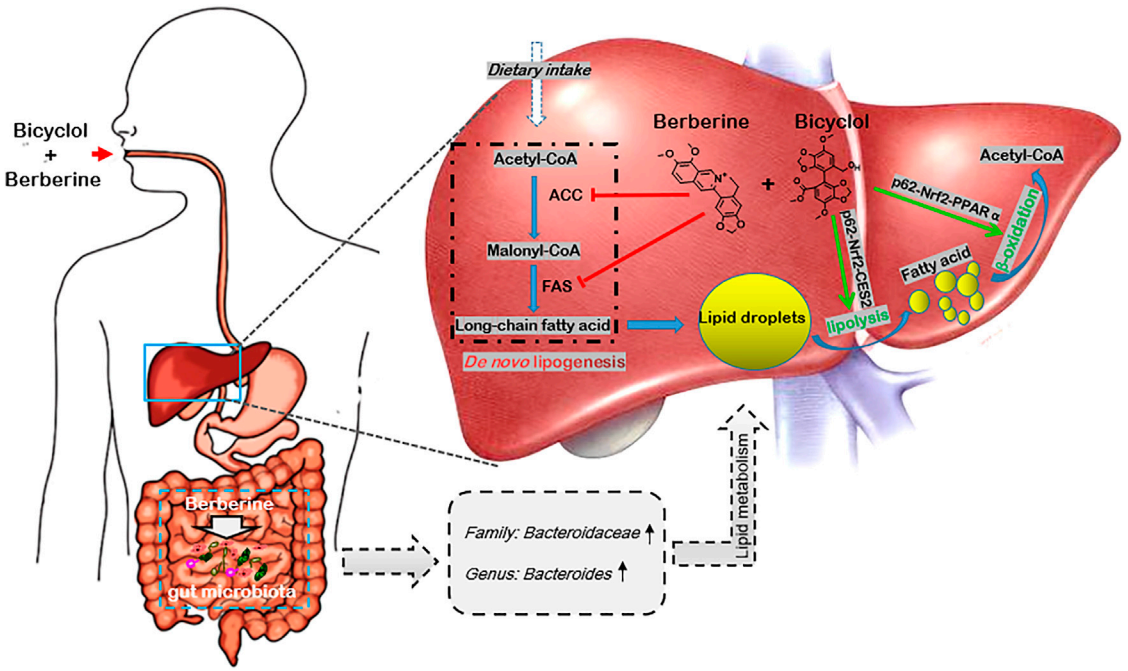

FIGURE 7 | Schematic diagram of the therapeutic mechanism of combined use of bicyclol and berberine against NAFLD. Bicyclol enhanced lipolysis through p62-Nrf2-CES2 signaling axis and improved β-oxidation through p62-Nrf2-PPARα signaling axis, while berberine suppressed the *de novo* lipogenesis by inhibiting protein expressions of ACC and FAS, along with the regulation of lipid metabolisms *via* the gut microbiota, and thus co-facilitating to ameliorate the occurrence and progress of NAFLD. The green arrow shows a stimulatory effect, the red flathead shows an inhibitory effect.

low-fat, low-cholesterol (LFLC) diet was set as normal diet control (**Figure 1A**). There were no toxic phenotypes (data not shown) and no significant difference in average food intake during the whole experiment among the WD-induced group and drug-treated groups, though the mice treated with WD decreased the food intake when compared with normal diet control (**Figure 1B**). Treatment with WD slightly increased the body weight of mice, while it was decreased after monotherapy and combination administration (**Figure 1C**). ALT and AST in serum and TG and CHO in the liver were notably ascended after WD induction (**Figures 1D–G**), suggesting that hepatic lipid accumulation induced by excessive nutrition was associated with impaired liver function. In contrast, all the biochemical indicators were decreased after bicyclol and berberine treatment, especially their combined treatment (**Figures 1D–G**). These results demonstrated that the combined use of bicyclol and berberine might possess better biochemical prevention of WD-induced liver injury and steatosis without significant toxicity.

Pathologically, treatment of WD induced a pale and rough appearance of the liver, while bicyclol or berberine mono-treatment ameliorated the liver appearance, and the combined use of these improved it more significantly at both low and high doses (**Figure 1H**, Liver). H&E and ORO staining of the livers treated with WD exhibited histopathological lesions with early liver disease, paralleled with significant hepatic inflammation, steatosis, and ballooning, while monotherapy with bicyclol or berberine significantly alleviated the histopathological lesions and the combined treatment exhibited better pharmacologic effect (**Figure 1H**, H&E and ORO staining). The effects were also confirmed by quantitation with the NAS score criterion (**Figure 1I**). Therefore, the combined use of bicyclol and berberine presented more superior preventive effects in a murine nutritional model of NAFL than individual treatment, which agrees with our putative strategy, though the dose-dependent efficacy of the two drugs was less than ideal.

Combination of Bicyclol and Berberine Demonstrates Better Therapeutic Effects on NASH Induced by Western Diet Plus CCl_4

Given the preferable preventive effect against hepatic steatosis by the combination of bicyclol and berberine, we further investigated their therapeutic effects on steatohepatitis (**Figure 2A**). C57BL/6J mice were freely fed with WD and intraperitoneally injected with 0.2 ml/kg CCl_4 once per week for 4 weeks to induce hepatic steatosis (**Figure 2B**). Then, the mice were continuously treated with WD/CCl_4 or plus low/high dose of bicyclol or/and berberine for 8 weeks. LFLC diets plus corn oil injection were conducted as normal control. There was no significant difference in body weight among the groups at week 12 (**Figure 2C**). However, ALT and AST in serum, and TG and CHO in the liver were significantly elevated by the introduction of WD/CCl_4 (**Figures 2D–G**). Bicyclol or berberine monotherapy showed efficacy to reduce these biochemical indicators, and the combined treatment of bicyclol and berberine reversed their

elevations, with an overall tendency of more excellent potency than monotherapy (**Figures 2D–G**). Histopathological results further confirmed that mice were progressed to NASH induced by WD/CCl_4, showing aberrant liver appearance, hepatic inflammation, steatosis, ballooning, and collagen deposition (**Figure 2H**). Bicyclol or berberine monotherapy showed a high beneficial effect to alleviate the pathological outcomes, and the combined therapy was more effective than monotherapy (**Figure 2H**), which was further verified by quantification of NAS score (**Figure 2I**) and fibrotic surface (**Figure 2J**). Therefore, based on the available results, combined therapy with bicyclol and berberine appears more effective than monotherapy in the treatment of NASH.

Bicyclol With or Without Berberine Enhances Lipolysis and β-Oxidation Through p62-Nrf2-CES2/PPARα Signaling Axis

Based on their respective therapeutic roles in clinic and the better improvement of NAFLD by combination of bicyclol and berberine in our animal experiments, we speculated that they might alleviate NAFLD through different mechanisms. Therefore, we first detected the expression of some potential lipid metabolism-related proteins in the high-dose and the combined groups which generally possessed the most significant pharmacologic effects (**Figure 1**, **2**). Among these potential targets, PPARα, a key nuclear receptor that promotes β-oxidation, was markedly decreased in both WD-induced steatosis mice (**Figure 3A**) and WD/CCl_4-induced NASH mice (**Figure 3B**), while bicyclol with or without berberine increased its expression. In contrast, compared with WD-induced steatosis and WD/CCl_4-induced NASH model groups, berberine alone did not change the protein expression of PPARα, and it also did not disturb the effect of bicyclol (**Figures 3A, B**), suggesting that the enhancement of PPARα-mediated β-oxidation is exclusively the mechanism of bicyclol. Similarly, CES2 was downregulated in the two model groups, while bicyclol but not berberine reversed its expression (**Figures 3A, B**). As the promoting roles for lipolysis by CES2 has been well illustrated (Li et al., 2016; Chalhoub et al., 2021), we thus speculate that bicyclol could also enhance the lipolysis process. Of note, PPARα and CES2 were downstream targets of p62-Nrf2 signaling (Zhang et al., 2012; Baker et al., 2015; Tao et al., 2021). Our results further verified the protein expressions of p62 and Nrf2 were reduced significantly in WD- and WD/CCl_4-induced model groups, while bicyclol but not berberine increased their expressions (**Figures 3A, B**). However, in WD- and WD/CCl_4-induced mouse models, the levels of free fatty acid uptake-related proteins CD36 and FABP1, lipolysis-related proteins ATGL and HSL, and β-oxidation-related proteins ACSL1 and ACSL5 were not changed significantly and were not altered by the treatment of bicyclol, berberine, and their combination (**Figures 3C, D**). Therefore, these results showed that promoting for lipolysis through inhibiting the p62-Nrf2-CES2 signaling axis and enhancing for β-oxidation through increasing p62-Nrf2-PPARα signaling axis are the mechanisms of bicyclol but not berberine to alleviate NAFLD.

Berberine With or Without Bicyclol Suppresses the *de Novo* Lipogenesis by Inhibiting Hepatic ACC and FAS Expressions

ACC catalyzes the fatty acid synthesis related carboxylation of acetyl-CoA to malonyl-CoA, and FAS catalyzes the synthesis of long-chain saturated fatty acids (Mashima et al., 2009; Gathercole et al., 2011), which are involved in *de novo* syntheses of TG and subsequent occurrence and progress of NAFLD (Alves-Bezerra and Cohen, 2017). Compared with the normal control group, ACC and FAS levels in the liver were increased after WD induction, while berberine but not bicyclol reversed the high expressions of ACC and FAS (**Figure 4A**), suggesting that WD promoted the *de novo* lipogenesis and berberine suppressed this process. Additionally, bicyclol did not disturb the inhibitory role of berberine on the expressions of ACC and FAS when combined with berberine (**Figure 4A**). Similar results were also demonstrated in the therapeutic experiment induced by WD/CCl_4 (**Figure 4B**). However, berberine did not change other lipid metabolism-related protein expression, such as CD36, FABP1, ATGL, HSL, ACSL1, and ACSL5 in WD- and WD/CCl_4-induced mice (**Figures 3C, D**). Therefore, the inhibition of *de novo* lipogenesis through downregulating the expressions of ACC and FAS might be at least one of the mechanisms for berberine to alleviate NAFLD, which is distinguished from that of bicyclol, and finally co-contribute to the enhancement of therapeutic effect against NAFLD when combined with berberine and bicyclol.

Berberine But Not Bicyclol Modulates the Composition of Gut Microbiota

Because berberine might also possess physiological functions *via* regulation of gut microbiota, to further analyze the different roles of berberine and bicyclol in the treatment of NAFLD, the NASH mice induced by WD/CCl_4 at the end of the experiment were carried out to analyze the diversity and evenness of gut microbiota. The results showed that the Shannon index was significantly lower in the WD/CCl_4 group than in the control group; berberine but not bicyclol treatment further changed the index and bicyclol also did not affect the role of berberine, as presented in the combined treatment group (**Figure 5A**). Next, compared with the model group, the unweighted UniFrac distances (**Figure 5B**) and PCoA plot (**Figure 5C**) showed a shift in the overall gut microbiota in the berberine or combination group, while the bicyclol monotherapy group showed no obvious changes, suggesting their combined alleviation for NAFLD might partially derive from the gut microbiota regulation role of berberine.

Then, the composition of microbial community was further analyzed. Results showed that WD/CCl_4 treatment led to moderate changes of community structure at the levels of bacteria family (**Figure 5D**) and genus (**Figure 5E**). Compared

with the model group, the gut microbiota changed significantly in the berberine and combination groups, while bicyclol almost did not affect the structure (**Figures 5D, E**). Bacteroidaceae (family) and *Bacteroides* (genus) were reported to be associated with beneficial effects for improving biochemical parameters and hepatic fat fraction (Lang et al., 2020; Jobira et al., 2021). In our study, among the top 15 changed gut microbiota by the treatment of berberine, the ratio of Bacteroidaceae (family) and *Bacteroides* (genus) accounts for the most abundant, and they were significantly increased after berberine but not bicyclol treatment (**Figure 5F**). The correlation of microbial community with lipid metabolism was also predicted through the KEGG databases, and berberine but not bicyclol significantly changed the abundance of lipid metabolism-related microbial community (**Figure 5G**). Overall, these results suggested that berberine might also alleviate NASH partially through regulating the lipid metabolisms *via* gut microbiota, while bicyclol almost had no effect on them and also did not disturb the effect of berberine during their combination in the NASH model.

Combined Use of Bicyclol and Berberine Decreases Lipid Accumulation *via* Regulating Lipid Metabolism-Related Gene Expression in FFA-Induced HepG2 Cells

To further verify the superior lipid-lowering effects and the mechanisms of action after combination of bicyclol and berberine, we established an FFA-induced lipid accumulation model in HepG2 cells. The MTT assay showed that 0.1 mM FFA and 2 μM bicyclol and/or berberine treatment had no obvious cytotoxicity on HepG2 cells (**Figure 6A**). Highly accumulated lipid droplets (LDs) in hepatocytes were observed by Nile Red staining after FFA induction, while the contents of LDs were dramatically reversed by berberine or bicyclol treatment, with more significant effects than their respective monotherapy after combination (**Figure 6B**). The effects were validated by the quantification of LDs (**Figure 6C**). The protein levels of PPARα and CES2 were slightly decreased by FFA induced-treatment but reversed by bicyclol with or without berberine (**Figure 6D**). In contrast, the protein expressions of ACC and FAS induced by FFA were decreased by berberine with or without bicyclol (**Figure 6D**). The results are consistent with the findings in mice models (**Figures 3**, **4**), suggesting that the combined use of bicyclol and berberine preferably alleviates lipid accumulation *via* upregulating PPARα and CES2 expressions by bicyclol and downregulating ACC and FAS expressions by berberine.

DISCUSSION

NAFLD is a multisystem disease with comprehensive causative mechanisms and therefore refers to MAFLD (Eslam et al., 2020; Liu et al., 2020). Candidate drugs underlying clinical trials with single-mechanism of action were generally unsatisfied (Brown et al., 2021). In this study, we demonstrated that combined use of bicyclol and berberine exerted better preventive effects in WD-induced mouse steatosis and also presented superior therapeutic results in WD/CCl_4-induced mouse NASH. The combination of bicyclol and berberine also showed better lipid-lowering effects in FFA-induced HepG2 cells. Mechanism study showed that bicyclol enhanced the lipolysis and β-oxidation through the p62-Nrf2-CES2/PPARα axis, while berberine suppressed the lipogenesis-related protein expressions of ACC and FAS, along with regulation of lipid metabolisms *via* gut microbiota (**Figure 7**). Importantly, co-treatment with them did not influence the pharmacologic roles of each other but enhanced the overall efficacy on NAFLD. The results validated our putative therapeutic strategy of combined use of bicyclol and berberine to treat NAFLD in the future as they have been approved, respectively, to use in clinic.

The early stage of NAFLD is mainly characterized by excessive lipid deposition in the liver, while the advanced stage of NAFLD is generally accompanied by fibrosis. In this study, we applied the Western diet (high in fat, sugar, and cholesterol) to mimic the diets in the real world, which might lead to a higher incidence of NAFLD (Lytle and Jump, 2016; Tsuchida et al., 2018). To assess the safety and preventive effect of the combined use of bicyclol and berberine, we first used a mild to moderate NAFLD mouse model induced by 16 weeks of intake of WD. Results showed that the combined use of the two drugs is rather safe, which is consistent with previous respective preclinical and clinical studies (Liu, 2009; Lan et al., 2015; Li et al., 2020). Of note, mouse body weight was slightly decreased after drug treatment compared with the WD-induced model group, though food intake was no difference. The slightly decreased body weight also predicted their pharmacological effects, which were present in the reduced indicators of lipid deposition (**Figure 1**). The combined effect in the WD/CCl_4-induced NASH mouse model is similar to that in the preventive experiment (**Figure 2**), suggesting the potential application in the preventive and therapeutic treatment of NAFLD. Overall fibrosis state most likely progresses to hepatocellular carcinoma (HCC), and the combined use of bicyclol and berberine showed efficacy on the decrease of the NAS score after induction by WD/CCl_4 for 12 weeks (**Figure 2**). Furthermore, bicyclol and berberine are, respectively, effective on HCC caused by various etiological factors (Sun et al., 2012; Xu et al., 2019). Therefore, the combined use might also be beneficial for the treatment of NAFLD-related HCC.

We previously carried out a meta-analysis study and demonstrated that bicyclol monotherapy could improve liver function and dyslipidemia in patients with NAFLD (Li et al., 2020), though the conclusion needs to be further verified with more well-designed and implemented studies, and the related mechanism study is limited. Yu et al. found that bicyclol protected against tetracycline-induced fatty liver mainly through ameliorating mitochondrial function and modulating the disturbance of PPARα-related genes (Yu et al., 2009). In contrast, Yao et al. reported that the anti-apoptosis associated with ER stress in this model might be the mechanism for bicyclol to attenuate fatty liver (Yao et al., 2016). Recently, bicyclol was reported to alleviate HFD-induced NAFLD through its anti-inflammatory mechanism (Zhao et al., 2021). Our results showed that the expression of lipolysis-related protein CES2

was decreased in WD or WD/CCl_4-induced mice, and bicyclol reversed CES2 expression to improve NAFLD, which is consistent with the fact that CES2 is reduced in high fat diet-induced obese mice, diabetic db/db mice, and NASH patients, while the liver disease was alleviated after CES2 was restored (Li et al., 2016; Xu et al., 2021). Therefore, bicyclol might be contributory to its protective roles in NAFLD *via* restoring CES2. Meanwhile, bicyclol also enhanced the PPARα-mediated β-oxidation, and this role was also verified by previous report (Yu et al., 2009). Generally, CES2 was independent of the expression of PPARα (Wen et al., 2019), while all of them could be regulated by the pleiotropic transcription factor Nrf2 (Zhang et al., 2012; Baker et al., 2015; Tao et al., 2021). Nrf2 induced the downstream PPARα expression and was regulated by its upstream increased p62 to connect with Keap1 (Zhang et al., 2012; Baker et al., 2015; Lee et al., 2020; Tao et al., 2021). In our study, p62 and Nrf2 were decreased in WD- and WD/CCl_4 treated mice and reversed by bicyclol (**Figure 3**). Altogether, the preventive and therapeutic role of bicyclol in NAFLD is related with the restoration of p62-Nrf2-CES2/PPARα signaling axis.

In contrast, the effects and mechanisms of berberine on NAFLD were well documented in various models, which were related to the increase of insulin sensitivity, regulation of the AMPK pathway, improvement of mitochondrial function, alleviation of oxidative stress, stabilization of LDLR mRNA, and regulation of gut microenvironment (Zhu et al., 2016). In this study, we verified the marked inhibition for critical fatty acid biosynthesis-related enzymes ACC and FAS in the NAFLD mouse models (**Figure 4**), which was consistent with the results in HepG2 cells directly treated with berberine (Cao et al., 2013). Encouragingly, ACC and FAS inhibitors were processed into clinical trials for treatment of patients with NAFLD (Loomba et al., 2018; Syed-Abdul et al., 2020). Consistent with the effects in animal experiments, the lipid-lowering effects and regulation for the key lipid-metabolism associated gene expressions of PPARα, CES2 by bicyclol and ACC, and FAS by berberine were verified in FFA-treated HepG2 (**Figure 6**). On the other hand, berberine possessed antimicrobial activity in clinic, and evidence indicated that the regulation for the gut microenvironment by berberine partially accounts for the improved NAFLD condition. For example, berberine increased protective bacteria like *Bifidobacteria* and decreased Gram-negative bacteria like *Escherichia coli*, which resulted in decrease of LPS release, TLR4/TNF-α activation, and insulin resistance (Liu et al., 2018). Berberine also enriched the short-chain fatty acid-producing bacteria and reduction of microbial diversity, which contribute to the treatment for high-fat diet-induced obesity in rats (Zhang et al., 2015). In this study, we also observed significant changes of gut microbiota after treatment by berberine but not bicyclol (**Figure 5**), and the most abundant microbiota are the lipid metabolism-related Bacteroidaceae (family) and *Bacteroides* (genus) in the berberine-treated groups (**Figure 5F**). We speculated that the increase of Bacteroidaceae (family) and *Bacteroides* (genus) might account for the beneficial role of berberine for NAFLD, because they were positively associated with a higher serum high-density lipoprotein (HDL) and lower levels of ALT, gamma-glutamyl-transferase (GGT), and ferritin (Lang et al., 2020) and negatively correlated with high hepatic fat fraction in patients with NAFLD (Jobira et al., 2021).

In summary, we first proposed a new available strategy of combined use of bicyclol and berberine to treat NAFLD. The better overall effect on NAFLD is related to the enhancement of lipolysis and β-oxidation by bicyclol *via* restoring the p62-Nrf2-CES2/PPARα signaling axis and suppression of lipogenesis by berberine *via* downregulating ACC and FAS, along with the enrichment of lipid metabolism-related Bacteroidaceae (family) *and Bacteroides* (genus) by berberine. Notably, the combined use of bicyclol and berberine does not influence the pharmacological roles of each other but enhances the amelioration effect for NAFLD, which predicts it to be a new available strategy to treat NAFLD.

DATA AVAILABILITY STATEMENT

The original contributions presented in the study are publicly available. This data can be found here: PRJNA795575.

ETHICS STATEMENT

The animal study was reviewed and approved by the Animal experiments were conducted following the National Guidelines for Housing and Care of Laboratory Animals. The study protocols were approved by the Institutional Animal Care and Use Committee of the Institute of Medicinal Biotechnology and Chinese Academy of Medical Sciences [SYXK (Jing)2017-0023].

AUTHOR CONTRIBUTIONS

HL and N-NL designed and performed the experiments, analyzed the data, and wrote the manuscript. Z-GP oversaw the project, designed the experiments, analyzed the data, and wrote the manuscript. Other authors participated in the experiment's performance and data analysis.

FUNDING

This work was supported by CAMS Innovation Fund for Medical Sciences (2019-I2M-1-001), National Natural Science Foundation, China (81621064), and National Mega-Project for "R&D for Innovative drugs," Ministry of Science and Technology, China (2018ZX09711001-003-010).

SUPPLEMENTARY MATERIAL

The Supplementary Material for this article can be found online at: https://www.frontiersin.org/articles/10.3389/fphar.2022.843872/full#supplementary-material

REFERENCES

Alves-Bezerra, M., and Cohen, D. E. (2017). Triglyceride Metabolism in the Liver. *Compr. Physiol.* 8, 1–8. doi:10.1002/cphy.c170012

Baker, A. A., Guo, G. L., Aleksunes, L. M., and Richardson, J. R. (2015). Isoform-Specific Regulation of Mouse Carboxylesterase Expression and Activity by Prototypical Transcriptional Activators. *J. Biochem. Mol. Toxicol.* 29, 545–551. doi:10.1002/jbt.21725

Brown, E., Hydes, T., Hamid, A., and Cuthbertson, D. J. (2021). Emerging and Established Therapeutic Approaches for Nonalcoholic Fatty Liver Disease. *Clin. Ther.* 43, 1476–1504. doi:10.1016/j.clinthera.2021.07.013

Cao, S., Zhou, Y., Xu, P., Wang, Y., Yan, J., Bin, W., et al. (2013). Berberine Metabolites Exhibit Triglyceride-Lowering Effects via Activation of AMP-Activated Protein Kinase in Hep G2 Cells. *J. Ethnopharmacol* 149, 576–582. doi:10.1016/j.jep.2013.07.025

Chalhoub, G., Kolleritsch, S., Maresch, L. K., Taschler, U., Pajed, L., Tilp, A., et al. (2021). Carboxylesterase 2 Proteins Are Efficient Diglyceride and Monoglyceride Lipases Possibly Implicated in Metabolic Disease. *J. Lipid Res.* 62, 100075. doi:10.1016/j.jlr.2021.100075

Cheng, J. J., Li, J. R., Huang, M. H., Ma, L. L., Wu, Z. Y., Jiang, C. C., et al. (2016). CD36 Is a Co-receptor for Hepatitis C Virus E1 Protein Attachment. *Sci. Rep.* 6, 21808. doi:10.1038/srep21808

Dong, X. C., Chowdhury, K., Huang, M., and Kim, H. G. (2021). Signal Transduction and Molecular Regulation in Fatty Liver Disease. *Antioxid. Redox Signal.* 35, 689–717. doi:10.1089/ars.2021.0076

Dufour, J. F., Caussy, C., and Loomba, R. (2020). Combination Therapy for Non-alcoholic Steatohepatitis: Rationale, Opportunities and Challenges. *Gut* 69, 1877–1884. doi:10.1136/gutjnl-2019-319104

Eslam, M., Sanyal, A. J., and George, J. (2020). MAFLD: A Consensus-Driven Proposed Nomenclature for Metabolic Associated Fatty Liver Disease. *Gastroenterology* 158, 1999–e1. doi:10.1053/j.gastro.2019.11.312

Gathercole, L. L., Morgan, S. A., Bujalska, I. J., Hauton, D., Stewart, P. M., and Tomlinson, J. W. (2011). Regulation of Lipogenesis by Glucocorticoids and Insulin in Human Adipose Tissue. *PLoS One* 6, e26223. doi:10.1371/journal.pone.0026223

He, L. H., Yao, D. H., Wang, L. Y., Zhang, L., and Bai, X. L. (2021). Gut Microbiome-Mediated Alteration of Immunity, Inflammation, and Metabolism Involved in the Regulation of Non-alcoholic Fatty Liver Disease. *Front. Microbiol.* 12, 761836. doi:10.3389/fmicb.2021.761836

Huang, D. Q., El-Serag, H. B., and Loomba, R. (2021). Global Epidemiology of NAFLD-Related HCC: Trends, Predictions, Risk Factors and Prevention. *Nat. Rev. Gastroenterol. Hepatol.* 18, 223–238. doi:10.1038/s41575-020-00381-6

Huang, M., Kim, H. G., Zhong, X., Dong, C., Zhang, B., Fang, Z., et al. (2020). Sestrin 3 Protects against Diet-Induced Nonalcoholic Steatohepatitis in Mice through Suppression of Transforming Growth Factor β Signal Transduction. *Hepatology* 71, 76–92. doi:10.1002/hep.30820

Huang, M. H., Li, H., Xue, R., Li, J., Wang, L., Cheng, J., et al. (2019). Up-regulation of Glycolipid Transfer Protein by Bicyclol Causes Spontaneous Restriction of Hepatitis C Virus Replication. *Acta Pharm. Sin B* 9, 769–781. doi:10.1016/j.apsb.2019.01.013

Jobira, B., Frank, D. N., Silveira, L. J., Pyle, L., Kelsey, M. M., Garcia-Reyes, Y., et al. (2021). Hepatic Steatosis Relates to Gastrointestinal Microbiota Changes in Obese Girls with Polycystic Ovary Syndrome. *PLoS One* 16, e0245219. doi:10.1371/journal.pone.0245219

Kessoku, T., Kobayashi, T., Ozaki, A., Iwaki, M., Honda, Y., Ogawa, Y., et al. (2020). Rationale and Design of a Randomised, Double-Blind, Placebo-Controlled, Parallel-Group, Investigator-Initiated Phase 2a Study to Investigate the Efficacy and Safety of Elobixibat in Combination with Cholestyramine for Non-alcoholic Fatty Liver Disease. *BMJ Open* 10, e037961. doi:10.1136/bmjopen-2020-037961

Kleiner, D. E., Brunt, E. M., Van Natta, M., Behling, C., Contos, M. J., Cummings, O. W., et al. (2005). Design and Validation of a Histological Scoring System for Nonalcoholic Fatty Liver Disease. *Hepatology* 41, 1313–1321. doi:10.1002/hep.20701

Kong, W. J., Vernieri, C., Foiani, M., and Jiang, J. D. (2020). Berberine in the Treatment of Metabolism-Related Chronic Diseases: A Drug Cloud (dCloud) Effect to Target Multifactorial Disorders. *Pharmacol. Ther.* 209, 107496. doi:10.1016/j.pharmthera.2020.107496

Lan, J., Zhao, Y., Dong, F., Yan, Z., Zheng, W., Fan, J., et al. (2015). Meta-analysis of the Effect and Safety of Berberine in the Treatment of Type 2 Diabetes Mellitus, Hyperlipemia and Hypertension. *J. Ethnopharmacol* 161, 69–81. doi:10.1016/j.jep.2014.09.049

Lang, S., Martin, A., Farowski, F., Wisplinghoff, H., Vehreschild, M. J. G. T., Liu, J., et al. (2020). High Protein Intake Is Associated with Histological Disease Activity in Patients with NAFLD. *Hepatol. Commun.* 4, 681–695. doi:10.1002/hep4.1509

Lee, D. H., Park, J. S., Lee, Y. S., Han, J., Lee, D. K., Kwon, S. W., et al. (2020). SQSTM1/p62 Activates NFE2L2/NRF2 via ULK1-Mediated Autophagic KEAP1 Degradation and Protects Mouse Liver from Lipotoxicity. *Autophagy* 16, 1949–1973. doi:10.1080/15548627.2020.1712108

Li, H., Huang, M. H., Jiang, J. D., and Peng, Z. G. (2018a). Hepatitis C: From Inflammatory Pathogenesis to Anti-inflammatory/hepatoprotective Therapy. *World J. Gastroenterol.* 24, 5297–5311. doi:10.3748/wjg.v24.i47.5297

Li, H., Li, J. R., Huang, M. H., Chen, J. H., Lv, X. Q., Zou, L. L., et al. (2018b). Bicyclol Attenuates Liver Inflammation Induced by Infection of Hepatitis C Virus via Repressing ROS-Mediated Activation of MAPK/NF-κB Signaling Pathway. *Front. Pharmacol.* 9, 1438. doi:10.3389/fphar.2018.01438

Li, H., Liu, N. N., and Peng, Z. G. (2020). Effect of Bicyclol on Blood Biomarkers of NAFLD: a Systematic Review and Meta-Analysis. *BMJ Open* 10, e039700. doi:10.1136/bmjopen-2020-039700

Li, X., Sun, R., and Liu, R. (2019). Natural Products in Licorice for the Therapy of Liver Diseases: Progress and Future Opportunities. *Pharmacol. Res.* 144, 210–226. doi:10.1016/j.phrs.2019.04.025

Li, Y., Zalzala, M., Jadhav, K., Xu, Y., Kasumov, T., Yin, L., et al. (2016). Carboxylesterase 2 Prevents Liver Steatosis by Modulating Lipolysis, Endoplasmic Reticulum Stress, and Lipogenesis and Is Regulated by Hepatocyte Nuclear Factor 4 Alpha in Mice. *Hepatology* 63, 1860–1874. doi:10.1002/hep.28472

Liu, D., Zhang, Y., Liu, Y., Hou, L., Li, S., Tian, H., et al. (2018). Berberine Modulates Gut Microbiota and Reduces Insulin Resistance via the TLR4 Signaling Pathway. *Exp. Clin. Endocrinol. Diabetes* 126, 513–520. doi:10.1055/s-0043-125066

Liu, G. T. (2009). Bicyclol: a Novel Drug for Treating Chronic Viral Hepatitis B and C. *Med. Chem.* 5, 29–43. doi:10.2174/157340609787049316

Liu, Z., Zhang, Y., Graham, S., Wang, X., Cai, D., Huang, M., et al. (2020). Causal Relationships between NAFLD, T2D and Obesity Have Implications for Disease Subphenotyping. *J. Hepatol.* 73, 263–276. doi:10.1016/j.jhep.2020.03.006

Loomba, R., Kayali, Z., Noureddin, M., Ruane, P., Lawitz, E. J., Bennett, M., et al. (2018). GS-0976 Reduces Hepatic Steatosis and Fibrosis Markers in Patients with Nonalcoholic Fatty Liver Disease. *Gastroenterology* 155, 1463–e6. doi:10.1053/j.gastro.2018.07.027

Lytle, K. A., and Jump, D. B. (2016). Is Western Diet-Induced Nonalcoholic Steatohepatitis in Ldlr-/- Mice Reversible. *PLoS One* 11, e0146942. doi:10.1371/journal.pone.0146942

Mashima, T., Seimiya, H., and Tsuruo, T. (2009). De Novo fatty-acid Synthesis and Related Pathways as Molecular Targets for Cancer Therapy. *Br. J. Cancer* 100, 1369–1372. doi:10.1038/sj.bjc.6605007

Orabi, D., Berger, N. A., and Brown, J. M. (2021). Abnormal Metabolism in the Progression of Nonalcoholic Fatty Liver Disease to Hepatocellular Carcinoma: Mechanistic Insights to Chemoprevention. *Cancers (Basel)* 13. doi:10.3390/cancers13143473

Sun, H., Yu, L., Wei, H., and Liu, G. (2012). A Novel Antihepatitis Drug, Bicyclol, Prevents Liver Carcinogenesis in Diethylnitrosamine-Initiated and Phenobarbital-Promoted Mice Tumor Model. *J. Biomed. Biotechnol.* 2012, 584728. doi:10.1155/2012/584728

Syed-Abdul, M. M., Parks, E. J., Gaballah, A. H., Bingham, K., Hammoud, G. M., Kemble, G., et al. (2020). Fatty Acid Synthase Inhibitor TVB-2640 Reduces Hepatic De Novo Lipogenesis in Males with Metabolic Abnormalities. *Hepatology* 72, 103–118. doi:10.1002/hep.31000

Tao, S., Yang, Y., Li, J., Wang, H., and Ma, Y. (2021). Bixin Attenuates High-Fat Diet-Caused Liver Steatosis and Inflammatory Injury through Nrf2/PPARα Signals. *Oxid Med. Cel Longev* 2021, 6610124. doi:10.1155/2021/6610124

Tsuchida, T., Lee, Y. A., Fujiwara, N., Ybanez, M., Allen, B., Martins, S., et al. (2018). A Simple Diet- and Chemical-Induced Murine NASH Model with Rapid Progression of Steatohepatitis, Fibrosis and Liver Cancer. *J. Hepatol.* 69, 385–395. doi:10.1016/j.jhep.2018.03.011

Wan, J., Wu, X., Chen, H., Xia, X., Song, X., Chen, S., et al. (2020). Aging-induced Aberrant RAGE/PPARα axis Promotes Hepatic Steatosis via Dysfunctional Mitochondrial β Oxidation. *Aging Cell* 19, e13238. doi:10.1111/acel.13238

Wang, Y., Zhou, X., Zhao, D., Wang, X., Gurley, E. C., Liu, R., et al. (2020). Berberine Inhibits Free Fatty Acid and LPS-Induced Inflammation via Modulating ER Stress Response in Macrophages and Hepatocytes. *PLoS One* 15, e0232630. doi:10.1371/journal.pone.0232630

Wen, X., Baker, A. A., Klaassen, C. D., Corton, J. C., Richardson, J. R., and Aleksunes, L. M. (2019). Hepatic Carboxylesterases Are Differentially Regulated in PPARα-Null Mice Treated with Perfluorooctanoic Acid. *Toxicology* 416, 15–22. doi:10.1016/j.tox.2019.01.014

Xu, J., Long, Y., Ni, L., Yuan, X., Yu, N., Wu, R., et al. (2019). Anticancer Effect of Berberine Based on Experimental Animal Models of Various Cancers: a Systematic Review and Meta-Analysis. *BMC Cancer* 19, 589. doi:10.1186/s12885-019-5791-1

Xu, Y., Pan, X., Hu, S., Zhu, Y., Cassim Bawa, F., Li, Y., et al. (2021). Hepatocyte-specific Expression of Human Carboxylesterase 2 Attenuates Nonalcoholic Steatohepatitis in Mice. *Am. J. Physiol. Gastrointest. Liver Physiol.* 320, G166–G174. doi:10.1152/ajpgi.00315.2020

Yao, X. M., Li, Y., Li, H. W., Cheng, X. Y., Lin, A. B., and Qu, J. G. (2016). Bicyclol Attenuates Tetracycline-Induced Fatty Liver Associated with Inhibition of Hepatic ER Stress and Apoptosis in Mice. *Can. J. Physiol. Pharmacol.* 94, 1–8. doi:10.1139/cjpp-2015-0074

Yu, H. Y., Wang, B. L., Zhao, J., Yao, X. M., Gu, Y., and Li, Y. (2009). Protective Effect of Bicyclol on Tetracycline-Induced Fatty Liver in Mice. *Toxicology* 261, 112–118. doi:10.1016/j.tox.2009.04.058

Zhang, X., Zhao, Y., Xu, J., Xue, Z., Zhang, M., Pang, X., et al. (2015). Modulation of Gut Microbiota by Berberine and Metformin during the Treatment of High-Fat Diet-Induced Obesity in Rats. *Sci. Rep.* 5, 14405. doi:10.1038/srep14405

Zhang, Y., Cheng, X., Aleksunes, L., and Klaassen, C. D. (2012). Transcription Factor-Mediated Regulation of Carboxylesterase Enzymes in Livers of Mice. *Drug Metab. Dispos* 40, 1191–1197. doi:10.1124/dmd.111.043877

Zhao, W., Yan, Y., Xiao, Z., Wang, M., Xu, M., Wang, Z., et al. (2021). Bicyclol Ameliorates Nonalcoholic Fatty Liver Disease in Mice via Inhibiting MAPKs and NF-Kb Signaling Pathways. *Biomed. Pharmacother.* 141, 111874. doi:10.1016/j.biopha.2021.111874

Zhu, B., Chan, S. L., Li, J., Li, K., Wu, H., Cui, K., et al. (2021). Non-alcoholic Steatohepatitis Pathogenesis, Diagnosis, and Treatment. *Front. Cardiovasc. Med.* 8, 742382. doi:10.3389/fcvm.2021.742382

Zhu, X., Bian, H., and Gao, X. (2016). The Potential Mechanisms of Berberine in the Treatment of Nonalcoholic Fatty Liver Disease. *Molecules* 21 (10), 1336. doi:10.3390/molecules21101336

Zou, L. L., Li, J. R., Li, H., Tan, J. L., Wang, M. X., Liu, N. N., et al. (2021). TGF-β Isoforms Inhibit Hepatitis C Virus Propagation in Transforming Growth Factor Beta/SMAD Protein Signalling Pathway Dependent and Independent Manners. *J. Cel Mol Med* 25, 3498–3510. doi:10.1111/jcmm.16432

Conflict of Interest: The authors declare that the research was conducted in the absence of any commercial or financial relationships that could be construed as a potential conflict of interest.

Publisher's Note: All claims expressed in this article are solely those of the authors and do not necessarily represent those of their affiliated organizations, or those of the publisher, the editors and the reviewers. Any product that may be evaluated in this article, or claim that may be made by its manufacturer, is not guaranteed or endorsed by the publisher.

frontiers in Pharmacology

ORIGINAL RESEARCH
published: 24 February 2022
doi: 10.3389/fphar.2022.857869

Engineered Bacteria EcN-MT Alleviate Liver Injury in Cadmium-Exposed Mice *via* its Probiotics Characteristics and Expressing of Metallothionein

Changwei Zou[1†], Ying Chen[1†], Hongyu Li[2], Wenyu Li[2], Jin Wei[3], Ziyan Li[1], Xinliang Wang[1], Tingtao Chen[3] and Hong Huang[1]**

[1]Key Laboratory of Poyang Lake Environment and Resource Utilization, School of Resources Environmental and Chemical Engineering, Ministry of Education, Nanchang University, Nanchang, China, [2]Queen Mary School, Nanchang University, Nanchang, China, [3]National Engineering Research Center for Bioengineering Drugs and the Technologies, Institute of Translational Medicine, Nanchang University, Nanchang, China

OPEN ACCESS

Edited by:
Menghao Huang,
Indiana University School of Medicine, United States

Reviewed by:
Jinan Li,
Indiana University School of Medicine, United States
Wenwei Lu,
Jiangan Uiversity, China

***Correspondence:**
Tingtao Chen
chentingtao1984@163.com
Hong Huang
honghuang@ncu.edu.cn

[†]These authors have contributed equally to this work and share first authorship

Specialty section:
This article was submitted to Gastrointestinal and Hepatic Pharmacology, a section of the journal Frontiers in Pharmacology

Received: 19 January 2022
Accepted: 07 February 2022
Published: 24 February 2022

Citation:
Zou C, Chen Y, Li H, Li W, Wei J, Li Z, Wang X, Chen T and Huang H (2022) Engineered Bacteria EcN-MT Alleviate Liver Injury in Cadmium-Exposed Mice via its Probiotics Characteristics and Expressing of Metallothionein. Front. Pharmacol. 13:857869. doi: 10.3389/fphar.2022.857869

Cadmium (Cd) exposure is a widespread problem in many parts of the world, but effective means to treat Cd exposure is still lacking. Hence, an engineered strain expressing metallothionein (MT) named *Escherichia coli* Nissle 1917 (EcN)-MT was constructed, and its potential in the treatment of Cd exposure was evaluated. The *in vitro* studies showed that metallothionein expressed by EcN-MT could significantly bind Cd. Further, the *in vivo* results indicated that EcN-MT strain could reduce 26.3% Cd in the liver and increase 24.7% Cd in the feces, which greatly decreased malondialdehyde (MDA) levels and increased catalase (CAT), glutathione (GSH), and superoxide dismutase (SOD) levels in liver, and reduced the expression of toll-like receptor4 (TLR4), nuclear factor-κB (NF-κB), the myeloid differentiation factor 88 (Myd88) andincreased B-cell lymphoma 2 (Bcl-2)/Bcl-2-Associated X (Bax). Moreover, high throughput sequencing results indicated that EcN-MT strain greatly enhanced the beneficial bacteria of Ruminococcaceae, Lactobacillaceae, *Akkermansia*, *Muribaculaceae*, *Lachnospiraceae*, *Dubosiella* and restored the disturbed microbial ecology to the normal level. Therefore, the high Cd binding capacity of the expressed metallothionein, together with the beneficial characteristics of the host bacteria EcN, makes EcN-MT a sound reagent for the treatment of subchronic Cd exposure-induced liver injury.

Keywords: cadmium, EcN-MT, metallothionein, inflammation, oxidative stress, intestinal microbiota

INTRODUCTION

Heavy metal pollution is the pollution caused by the entry of some biotoxic metals and metalloids and their compounds into the environment, which causes widespread concern due to its high toxicity, difficulty in being degraded, biomagnification and bioaccumulation along the food chain (Ali et al., 2019). It is reported that in China alone, contamination by cadmium (Cd), arsenic and lead has led to an annual loss of about 20 billion RMB in agricultural production and about 12 million tons of contaminated food (Clemens et al., 2013). Contaminated food and water are major sources of heavy metal exposure for non-occupational populations. Studies have shown that heavy metal exposure has toxic effects on liver, kidney, neurological, cardiovascular, and pulmonary fibrosis diseases (Hyder et al., 2013; Wang et al., 2021). In particular, Cd pollution is one of the most serious

heavy metal pollutions in China, and with the development of industry, it is expected that the risk of Cd exposure to human health will further increase in the next decade (Baba et al., 2013; Xu et al., 2021).

Currently, the two main types of methods used to treat heavy metal exposure are chelation and antioxidants. However, both therapeutic options present certain limitations. Chelating agents are generally effective only for a short period of time, and can cause liver injury when used at doses higher than 1/4 LD_{50} (Nordberg, 1984). Antioxidants mitigate the oxidative stress caused by heavy metal exposure, but have been reported unable to reduce heavy metals through chelation or excretion (Eybl et al., 2006). These limitations have prompted investigators to seek for more effective solutions involving other mechanism pathways. In addition to external therapies such as chelation and antioxidants, the body has its own removal mechanism for heavy metal exposure, namely, chelation of excess heavy metals by metallothionein. Metallothioneins (MT) are a class of low molecular weight, homocysteine proteins found in most eukaryotic organisms that bind to heavy metals primarily through cysteine thiol groups to form non-toxic chelates (Andreani et al., 2011; Shen et al., 2019). Meanwhile, MT is one of the most powerful endogenous free radical scavengers known. The researchers found that MT gene deletion exacerbated the injury caused by heavy metal exposure, further confirming its important role in the protection of the organism (Liu et al., 2002). The study also showed that exogenous MT not only helped to eliminate heavy metal Cd in aquatic animals but also reduced liver injury caused by thallium poisoning and to some extent reduced inflammation and collagen deposition, thus alleviating pulmonary fibrosis (Helal and Helal, 2009; Kilic and Kutlu, 2010; Duan et al., 2018).

Increasing evidence underscore the close association of gut microbes with numerous diseases such as cirrhosis, alcoholic fatty liver, and nonalcoholic fatty liver (Zhang et al., 2015; Schwabe and Greten, 2020). The gut microbiota is regarded as a potential therapeutic target by degrading other potentially toxic dietary products or producing nutritional metabolites (Dapito et al., 2012). Probiotics are living microorganisms that have been widely recognized for their important contribution to the regulation of intestinal microbiota (de Vrese and Schrezenmeir, 2008), and some recent reports indicated that probiotics can regulate disturbances of intestinal microbiota caused by the exposure to heavy metals (Zhai et al., 2017; Zhang et al., 2018). Among all the probiotic strains, *Escherichia coli* Nissle 1917 (EcN) has received much attention. Since its discovery in 1957, EcN has played an important role as a Gram-negative probiotics in regulating the intestinal microbiota and suppressing enteritis (Sassone-Corsi et al., 2016), due to its excellent safety profile, good tolerability, clear genetic background, availability of genetic manipulation, and excellent colonization properties (Westendorf et al., 2005; Luo et al., 2020). Moreover, with the boom of synthetic biology, EcN has been used as a engineered strain vector for the treatment of phenylketonuria in a phase I clinical study (Puurunen et al., 2021).

In this study, the MT gene was integrated into plasmid pET-28a, which was then transferred into EcN to construct the engineered bacterium EcN-MT to continuously express MT. Thus, it is expected to have the effect of one plus one more than two. The treatment effect of EcN-MT on Cd was studied using a subchronic Cd exposure mice model, which may provide a basis for its potential use in clinic.

MATERIALS AND METHODS

Strain Construction and Evaluation *in vitro*

MT genes (gene ID 856450) were inserted into the pET-28a plasmid, and then was heat stimulated into the receptor *E. coli* Nissle1917 to construct the engineered bacteria EcN-MT. Then, the growth curves (Luo et al., 2020), plasmid stability (Liu et al., 2019), acid resistance, bile salt resistance and oxidation resistance capability (Xia et al., 2020; Wang et al., 2020) were evaluated.

Finally, the binding capability of EcN-MT and EcN to Cd was tested. Briefly, EcN-MT and EcN were respectively co-incubated with 0.545 mM of $CdCl_2$ for 1 h, centrifuged at 5,000 × g for 5 min, and the supernatant was treated according to the water quality—32 elements determination—inductively coupled plasma emission spectrometry (HJ776-2015) and detected by ICP-AES for Cd content (Alexander et al., 2017).

Development and Treatment of Cadmium Exposure Model

Six-week-old Male (Sogawa et al., 2001) C57BL/6J mice (18–20 g), provided by Hunan SJA Laboratory Animal, were maintained in the specific pathogen free (SPF) laboratory animal barrier system of the Institute of Translational Medicine of Nanchang University under standard conditions (humidity 40–70%, temperature 20–26°C, 12/12 light-dark cycle) and were fed with standard mice maintain diet (Xie tong biological, CN, Cat# 101139). After 1 week of initial adaptation to the cage food and laboratory conditions, a total of 50 mice were randomly divided into groups C (n = 10, drank distilled water, gavaged with gelatin saline per day), M (n = 10, treated with 0.545 mM cadmium chloride ($CdCl_2$) (Thijssen et al., 2007; Zhai et al., 2014) (aladdin, CN, Cat#C116342), gavaged with gelatin saline per day), EcN (n = 10, treated with 0.545 mM $CdCl_2$, gavaged with 10^9 CFU EcN per day), MT (n = 10, treated with 0.545 mM $CdCl_2$, gavaged with 2 mg/kg body weight MT (Yuanye biological, CN, Cat#S12070) per day), and EcN-MT (n = 10, treated with 0.545 mM $CdCl_2$, gavaged with 10^9 CFU EcN-MT per day). After 8 weeks the mice were euthanized by a skilled technician using an intraperitoneal injection of 1% sodium pentobarbital (40 mg/kg) followed by assisted decervicalization. To further explore the mechanism of EcN-MT, 40 six-week-old male C57BL/6J mice were purchased for the experiment. Then, after 1 week of adaptive feeding, 40 mice were randomly divided into four groups: group C (n = 10, drank distilled water, gavaged with gelatin saline per day), group M (n = 10, treated with 0.545 mM cadmium chloride ($CdCl_2$) (aladdin, CN, Cat#C116342), gavaged with gelatin saline per day), group

EcN-MT ($n = 10$, treated with 0.545 mM $CdCl_2$, gavaged with 10^9 CFU EcN-MT per day), and group PDTC [treated with 0.545 mM $CdCl_2$, Intraperitoneal injection 50 mg/kg body weight Pyrrolidinedithiocarbamic acid (PDTC) (MedChemExpress, Cat#HY-18738)]. The mice were euthanized in the same manner as above at the end of the eight-week experiment.

Estimation of Cadmium in Liver Tissue and Feces

Weigh 0.1 g of mice liver tissue and feces respectively and homogenize in 1 ml of PBS. Then, the samples were digested overnight in 3 ml of concentrated nitric acid (65% (v/v)) and transferred to a Teflon digestion tube. After the first digestion at 80°C for 1 hour, 2 ml of H_2O_2 [30% (v/v)] was added and the samples were digested at 120°C until they were completely transferred into a clear colorless liquid, then filtered through a 0.22 μm hydrophilic PTFE membrane filter and diluted with MilliQ water containing 2% HCl and Indium (In) elements (50 ug/kg). The prepared samples were analyzed directly by ICP-MS and Cd calibration curves. The Cd concentrations were determined by plotting the calibration curves of ICP-MS Cd standards with known concentrations and the internal standard element In concentration.

Histology and Histopathology

The liver tissues of euthanized mice were dissected and then randomly selected, fixed with 4% paraformaldehyde and embedded in paraffin. Next, the embedded tissues were cut into 2–4 μm serial sections and after dewaxing, staining, dehydration and transparency treatment, the hematoxylin eosin-stained liver tissues could be sealed for observation under light microscope.

Then, the colon tissues of mice were randomly selected for rinsing, fixation, immersion wax embedding, dehydration, transparency, dehairing, hematoxylin eosin staining, and finally histological sections were examined by light microscopy. The histological injury was evaluated by a semiquantitative method and scored on a scale of 0–4 essentially as described previously (Cao et al., 2017).

Western Blotting

Wet protein blotting was performed as described previously (Xia et al., 2020). Briefly, 1 ml of RIPA lysis buffer and a corresponding dose of mixed protease inhibitor were added per 0.1 g of tissue to obtain the cell lysis supernatant. Then it was measured by BCA method at 592 nm for protein concentration, mixed with 5× protein loading buffer and water bath at 100°C for 5–10 min until denaturation. After that, the proteins were transferred from the polyacrylamide-SDS gels to polyvinylidene fluoride (PVDF) in TBS containing 0.1% Tween-20, 5% nonfat dry milk for 1 h. Next, the bands were incubated overnight at 4°C with anti-Bax (Cat#5174), anti-Bcl2 (Cat#5174), anti-TLR4 (Cat#19811-1-AP), anti-MyD88 (Cat#66660-1-Ig), anti-p65 (Cat#10745-1-AP), anti-p-p65 (Cat#AF 2006), anti-a-SMA (Cat#14395-1-AP), anti-Occludin (Cat#27260-1-AP), anti-β-actin (Cat#66009-1-Ig). Afterward the bands were conjugated with secondary antibodies corresponding to horseradish peroxidase, and finally the band strength was shown by chemiluminescence. Specific antibody information is shown in **Supplementary Table S1**.

Measurement of Oxidation-Related Biomarkers

According to the instructions of the kit, 0.1 g of liver tissue was weighed and added to 1 ml of the extraction solution provided in the kit, homogenized in an ice bath, centrifuged at 8,000 g for 10 min at 4°C, and the supernatant was obtained. And it was measured by enzyme standard according to the principle that malondialdehyde (MDA) (Suzhou comin Biotechnology co., Ltd., CN, Cat#MDA-1-Y) could react with thiobarbituric acid to form a red product with maximum absorbance at 532 nm, catalase (CAT) (Suzhou comin Biotechnology co., Ltd., CN, Cat#GSH-1-W) activity could be measured by reduced hydrogen peroxide at 240 nm, glutathione (GSH) (Suzhou comin Biotechnology co., Ltd., CN, Cat#GSH-1-W) could react with DTNB to form a complex with a characteristic peak at 412 nm, Superoxide dismutase (SOD) (Suzhou comin Biotechnology co., Ltd., CN, Cat#SOD-1-Y) could scavenge superoxide anion (O^{2-}) and thus reduced methanogenesis at 560 nm.

Real-Time PCR

After fast isolation of total RNA from fresh hepatocytes using Trizol, complementary first-strand cDNA synthesis was performed with the Prime Script RT Master Mix Reverse Transcription Kit (Prime Script RT Master Mix; Ta Ka Ra Biotechnology). Next, SYBR green method with ABI 7900HT fast real-time PCR system was used to detect the expression of Interleukin (IL)-1β, IL-6, and tumour necrosis factor (TNF)-α inflammatory factor markers. The primers for these analyses are listed in **Supplementary Table S2**. In the end, Real-time qPCR reactions were performed in triplicate using GAPDH as the internal reference gene, and calculated using the $2^{-\Delta\Delta Ct}$ method for analysis.

16S rRNA Gene Sequencing

According to references (Tao et al., 2020; Wang and Liu, 2020), bacterial genomic DNA was extracted and the target fragment of the 16S rRNA V4 region was amplified using bacterial universal primer 520F (5′-AYTGGGYDTAAAGNG-3′) and 802R (5′-TACNVGGGTATCTAATCC-3′). Next, amplification products were then double-ended (paired-end) sequenced against the colony DNA fragment using the Illumina platform. Then, the ASV/OTU signature sequences were obtained using the DADA2 method of analysis software for quality control. Afterward data processing was performed using QIIME v. 1.9.180 to multiplex the raw fastq data and high quality reads were obtained by quality filtering parameters (Phred quality score ≥ 20, minimum read length = 75% of nucleotides of 250). Whereafter, cluster 16 S rRNA gene sequences were then read into OTUs using UCLUST81 and the Greengenes reference database v13.882,83, and species-level

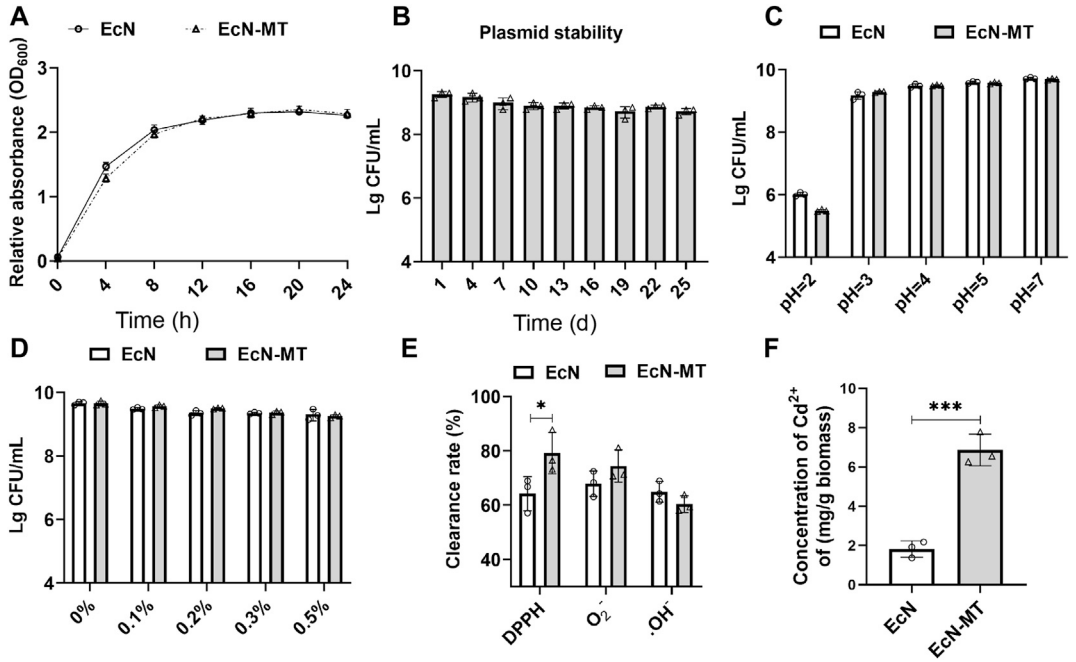

FIGURE 1 | Evaluation of the probiotic characteristics of EcN-MT. Values are presented as means ± SD ($n = 3$). **(A)** Growth curves of EcN and EcN-MT. **(B)** Plasmid stability test of EcN-MT. **(C)** The acid tolerance of EcN and EcN-MT. **(D)** The cholate tolerance of EcN and EcN-MT. **(E)** The antioxidant ability of EcN and EcN-MT. **(F)** The ability of EcN and EcN-MT to bind cadmium ions. *$p < 0.05$.

taxonomic assignments were then obtained using Megablast84 with the reference sequences of candidate OTUs from the Greengenes database. Finally, sequences were used to compare the relative abundance of OTUs in at least five samples for analyses such as species composition, alpha diversity, and beta diversity.

Statistical Analysis

The data were analyzed with Prism8 (GraphPad). Two groups of data were compared using Student's t-test. Three and multiple groups of data were analyzed using two-way ANOVA and multiple comparisons to detect statistical differences. Data for all experimental outcomes were expressed as mean plus or minus standard deviation.

RESULTS

Evaluation of Probiotic Characteristics of EcN-MT *in vitro*

Growth curve assay was used to examine the growth characteristics of EcN-MT and the results showed no difference in growth characteristics between EcN-MT and EcN strains (**Figure 1A**). Subsequently, ELISA assay was used to examine the ability of EcN-MT to express MT (**Supplementary Figure S1**). The plasmid stability of EcN-MT was then assessed and suggested that viable EcN-MT still reached 5×10^8 CFU/ml after 25 days of passaging once per day (**Figure 1B**). In addition, the resistance of EcN and EcN-MT to high concentrations of acid and bile salts was evaluated separately, and the results showed that both EcN and EcN-MT had good resistance to acid and bile salts (**Figures 1C,D**). This indicated that both EcN-MT and EcN had the ability to resist gastric acid. Finally, antioxidant properties and heavy metal binding capacity were evaluated. In the antioxidant assay, EcN and EcN-MT showed good antioxidant capacity, especially in DPPH reducing capacity, with EcN-MT scavenging capacity being superior to EcN (**Figure 1E**, $p < 0.05$). In the heavy metal binding capacity test, EcN-MT could bind the heavy metal Cd to a greater extent compared to EcN (6.536 vs. 1.822 mg/g biomass) (**Figure 1F**), suggested that EcN-MT has the potential to treat Cdexposure.

EcN-MT Treatment Ameliorates Liver Injury, Fibrosis, Oxidative Stress in the Liver of Mice

Cd-induced subchronic liver injury model was used to investigate the effect of EcN-MT on liver injury induced by Cd exposure (**Figure 2A**). The results of heavy metal Cd assay in liver tissues showed that the Cd concentration in liver tissue was significantly higher in group M compared with group C. Cd levels were slightly decreased after EcN treatment compared with the M group; in contrast, significant levels of Cd in liver tissue were reduced after MT and EcN-MT treatment (MT vs. M, $p < 0.05$; EcN-MT vs. M, $p < 0.01$) (**Figure 2B**). The results of group C were not shown in **Figure 2B** due to the very low Cd concentration in the liver tissue (mean level was only

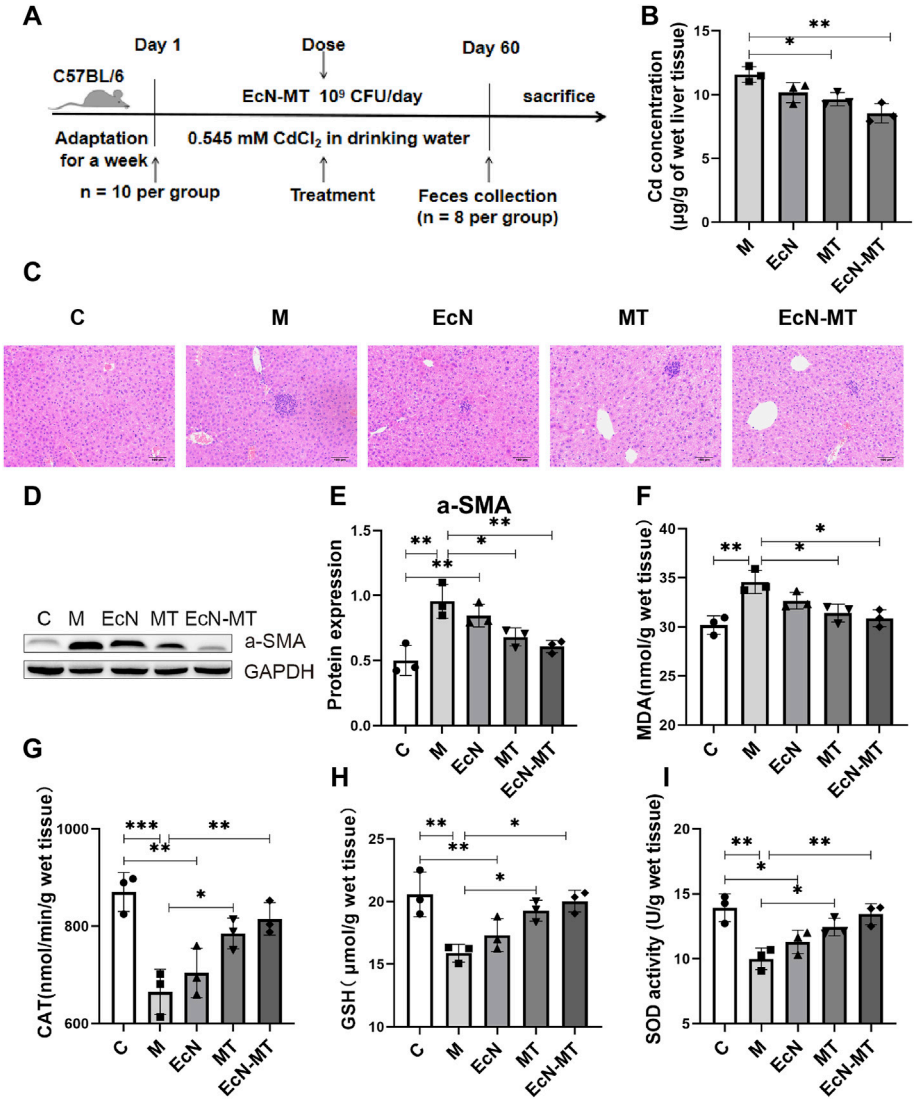

FIGURE 2 | EcN-MT treatment reduce liver injury, fibrosis, oxidative stress in the liver of mice. Values are presented as means ± SD ($n = 3$). **(A)** Treatment of EcN-MT in mice with subchronic Cd exposure. **(B)** Cd concentrations in the liver assayed by ICP-MS. **(C)** HE staining image of liver tissue (200×). **(D)** Western bloting analysis of a-SMA expression in liver tissues. **(E)** The relative expressions of a-SMA were quantified by ImageJ. GAPDH was used as an internal control. The activity of **(F)** MDA, **(G)** CAT, **(H)** GSH, **(I)** SOD. $^{*}p < 0.05$, $^{**}p < 0.01$, $^{***}p < 0.001$.

0.0242 mg/g wet weight). Then detection results of heavy metal cadmium in feces showed that MT and EcN-MT treatment, compared with group M, significantly increased the fecal Cd levels in mice (MT vs. M, $p < 0.05$; EcN-MT vs. M, $p < 0.01$) (**Supplementary Figure S2**). Next, hematoxylin-eosin (HE) staining showed that group M had a large number of eosinophil aggregates and some degree of focal necrosis of hepatocytes, while liver inflammation was reduced after treatment in EcN, MT and EcN-MT groups, with only mild cell swelling and inflammatory infiltration in the EcN-MT group presenting the most significant efficacy (**Figure 2C**). Meanwhile a-SMA protein expression results as shown in **Figure 2D** indicated that its expression level was significantly upregulated by Cd exposure, but was decreased after MT and EcN-MT treatment (MT vs. M, $p < 0.05$; EcN-MT vs. M, $p < 0.05$) (**Figure 2E**). In addition, the results of oxidative stress in the liver showed that MDA levels were significantly increased and CAT, GSH, and SOD levels were significantly decreased in the M group, while MT and EcN-MT treatments reversed these alterations (**Figures 2F–I**, $p < 0.05$).

EcN-MT Reduces Liver Inflammation and Apoptosis

To explore the potential mechanisms by which EcN-MT treatment attenuates subchronic Cd exposure-induced liver injury, key proteins of the inflammatory pathway (TLR4 signaling) and apoptotic pathway (Bcl-2 family proteins) were

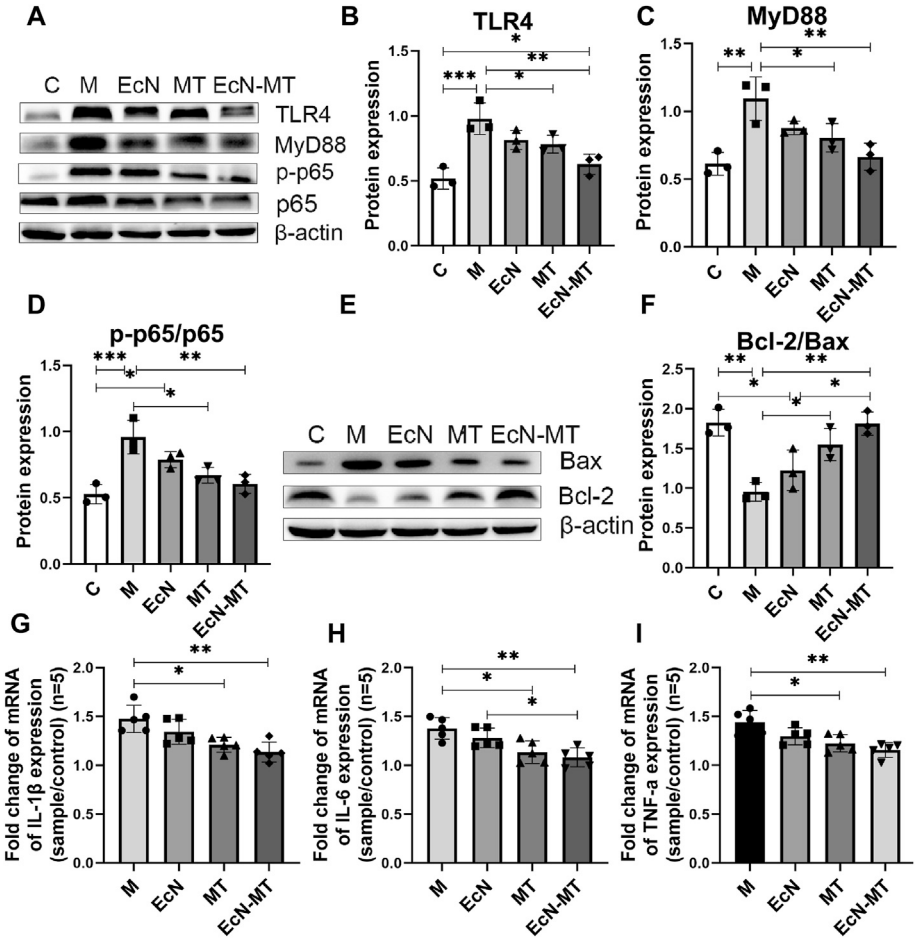

FIGURE 3 | EcN-MT reduced liver inflammation and apoptosis. Values are presented as means ± SD ($n = 3$, except q-PCR results repeated five times). **(A)** Western bloting analysis of TLR4, MyD88, p-p65, p65 expression in liver tissues. The relative expressions of **(B)** TLR4, **(C)** MyD88, **(D)** p-p65/p65 were quantified by ImageJ. β-actin was used as an internal control. **(E)** Western bloting analysis of Bax, Bcl-2 expression in liver tissues. **(F)** The relative expressions of Bcl-2/Bax were quantified by ImageJ. β-actin was used as an internal control. The relative mRNA expressions of **(G)** IL-1β, **(H)** IL-6, **(I)** TNF-α in liver tissues were detected by q-PCR. $^{*}p < 0.05$, $^{**}p < 0.01$, $^{***}p < 0.001$.

investigated. As shown in **Figures 3A–D**, oral administration of $CdCl_2$ significantly increased the expression of TLR4 (M vs. C, $p < 0.001$), MyD88 (M vs. C, $p < 0.01$), and p-p65/p65 (M vs. C, $p < 0.001$) compared with the C group. TLR4 (0.783, 0.628, respectively), MyD88 (0.805, 0.666, respectively) and p-p65/p65 (0.671, 0.605, respectively) were significantly decreased in the MT and EcN-MT groups compared with the M group, respectively. Meanwhile, Bcl-2/Bax expression was significantly reduced in the M group compared with the C group (M vs. C, 0.954 vs. 1.826), while MT and EcN-MT treatments reversed the reduction in Bcl-2/Bax expression induced by Cd exposure (MT vs. M, 1.549 vs. 0.954, EcN-MT vs. M, 1.814 vs. 0.954) (**Figures 3E,F**). In addition, the results of the relative expression of inflammatory factors revealed that the expression of IL-1β, IL-6 and TNF-α was significantly increased in the M group compared with the C group, while the relative expression of IL-1β (1.210, 1.136, respectively), IL-6 (1.135, 1.082, respectively) and TNF-α (1.226, 1.159, respectively) was significantly reduced in the livers of the MT and EcN-MT groups compared with the M group (**Figures 3G–I**; $p < 0.05$).

EcN-MT Improved Intestinal Microbiota in Subchronic Cd -Exposed Mice

High-throughput sequencing methods were used to study the effects of EcN, MT and EcN-MT on the intestinal microbiota of mice with subchronic Cd exposure. The Venn method analyze indicated that 475 common OTUs were identified from each group, and the number of unique OTUs in C, M, EcN, MT and EcN-MT groups were 654, 582, 714, 541 and 331, respectively (**Figure 4A**). The results of Shannon index of α diversity showed that compared with C group, the community diversity of M group was decreased, and EcN, MT and EcN-MT treatment alleviated the change, among which EcN-MT treatment had the most significant effect (M vs. EcN-MT, 4.835 vs. 5.948) (**Figure 4B**). And then the results of PCoA showed that the M and MT groups

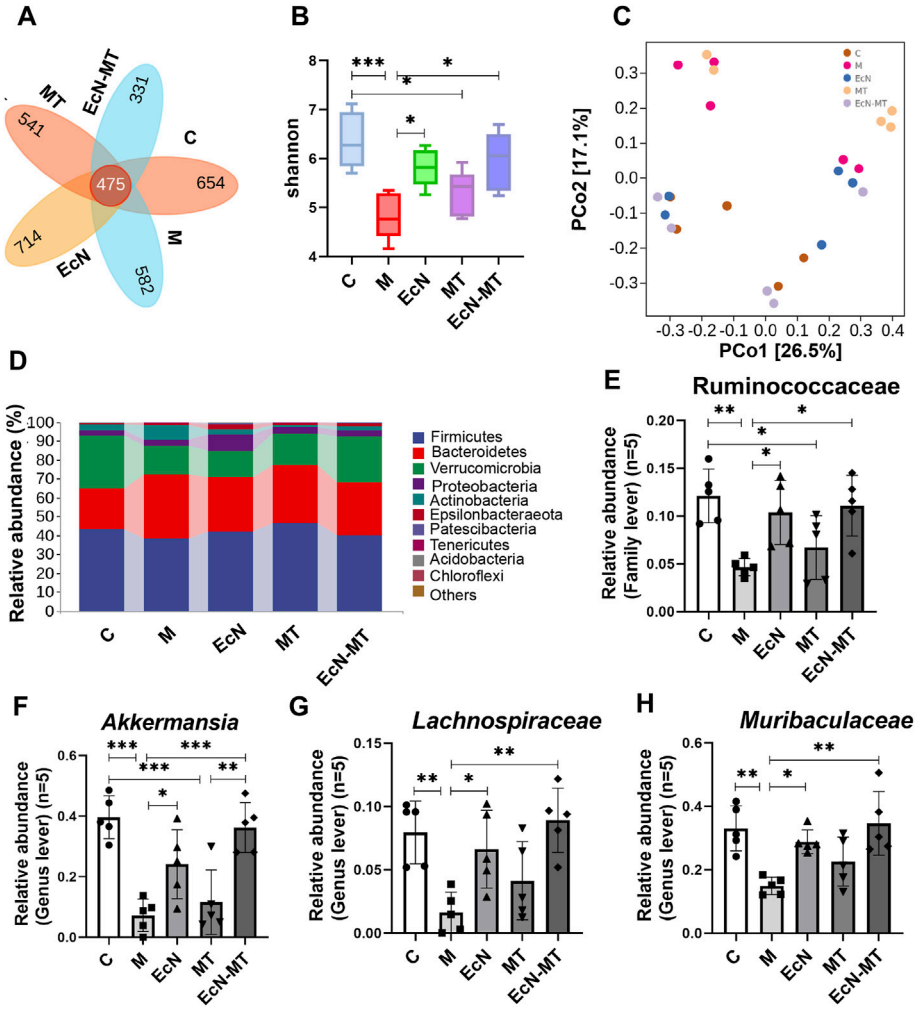

FIGURE 4 | EcN-MT improved intestinal microbiota in subchronic Cd-exposed mice. Values are presented as means ± SD ($n = 5$). **(A)** Venn map representation of OTUs. **(B)** The Shannon index. **(C)** PCoA of β diversity index. **(D)** Microbial composition at the phyla level. The relative abundance of **(E)** Ruminococcaceae, **(F)** *Akkermansia*, **(G)** *Muribaculaceae*, **(H)** *Lachnospiraceae* were analyzed. $^{*}p < 0.05$, $^{**}p < 0.01$, $^{***}p < 0.001$.

had similar sample points and were farther from the C group in the plot, indicating that the microbial diversity of the M and MT groups was significantly different from that of the C group. Meanwhile, samples from the EcN-MT and EcN groups in the plot were similar to the C group and far from the M group, indicated that the microbial diversity of the EcN and EcN-MT treatments was significantly different from that of the M group (**Figure 4C**). In addition, the results of species composition analysis at the phylum level showed a significant decrease in the thick-walled phylum and an increase in the bacillus-like phylum in the M group compared with the C group. However, the EcN and EcN-MT treatments increased the abundance of the thick-walled phylum and decreased the abundance of the anaphyla phylum compared to the M group. (**Figure 4D**). Subsequently, the data of the top 10 abundant microbial populations at family level and genus level were analyzed and the results showed that compared to C group, M group presented a significant reduction in the abundance of Ruminococcaceae at family level, *Akkermansia, Muribaculaceae, Lachnospiraceae* at genus level. After MT treatment, the abundance increased but were not significantly different, but EcN and EcN-MT treatments decreased the alteration presented in the M group (**Figures 4E–H**, $p < 0.05$).

Suppression of NF-κB Activation Reduced Hepatic Inflammation and Oxidative Stress

To further determine whether EcN-MT attenuated liver injury by inhibiting the activation of TLR4/MyD88/NF-κB signaling pathway, NF-κB inhibitor (PDTC) was used in a subchronic Cd exposure mice model. Notably, the results of heavy metal Cd assay in liver tissues showed that regarding the ability to reduce accumulated Cd in liver tissues, PDTC treatment was not as effective as EcN-MT (EcN-MT Vs PDTC, 7.925 vs. 9.547) (**Figure 5A**, $p < 0.05$). Meanwhile, the results of the determination of heavy metal Cd in feces showed that the Cd

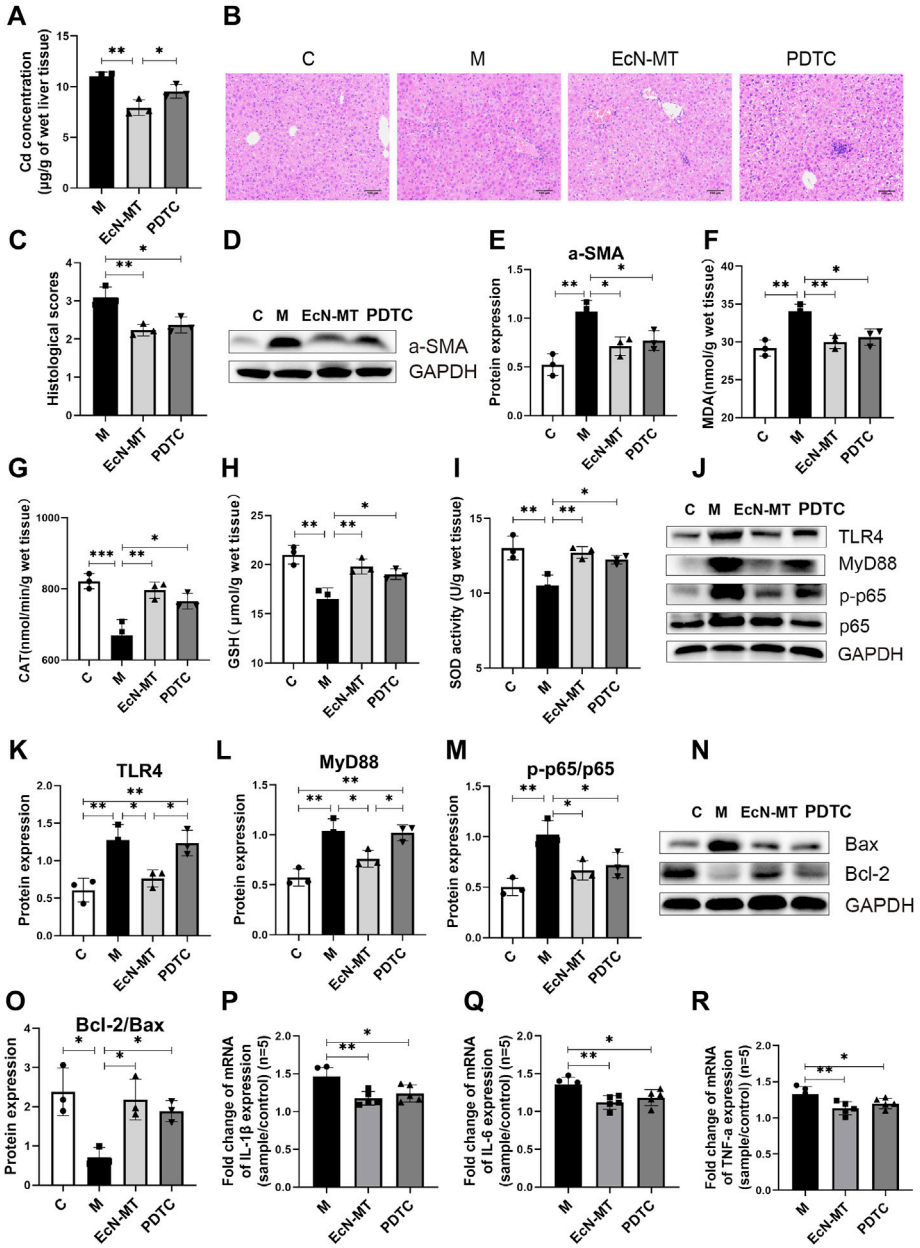

FIGURE 5 | Suppression of NF-κB activation reduced hepatic inflammation and oxidative stress. Values are presented as means ± SD ($n = 3$, except q-PCR results repeated five times). **(A)** Cd concentrations in the liver assayed by ICP-MS. **(B)** HE staining image of liver tissue (200×). **(C)** Histological score of liver injury. After 8 weeks of exposure to drinking water, the pathological changes of liver tissues stimulated by cadmium chloride (0.545 mM) were determined. **(D)** Western bloting analysis of a-SMA expression in liver tissues. **(E)** The relative expressions of a-SMA were quantified by ImageJ, expressions of a-SMA were quantified by ImageJ. GAPDH was used as an internal control. The activity of MDA; CAT; GSH; SOD, activity of **(F)** MDA; **(G)** CAT; **(H)** GSH; **(I)** SOD. **(J)** Western bloting analysis of TLR4, MyD88, p-p65, p65 expression in liver tissues. The relative expressions of **(K)** TLR4, **(L)** MyD88, **(M)** p-p65/p65 were quantified by ImageJ. GAPDH was used as an internal control. **(N)** Western bloting analysis of Bax, Bcl-2 expression in liver tissues. **(O)** The relative expressions of Bcl-2/Bax were quantified by ImageJ. GAPDH was used as an internal control. The relative mRNA expressions of **(P)** IL-1β, **(Q)** IL-6, **(R)** TNF-α in liver tissues were detected by q-PCR. $^{*}p < 0.05$, $^{**}p < 0.01$, $^{***}p < 0.001$.

content in the feces of mice increased significantly after EcN-MT treatment, however, there was no change in PDTC treatment (EcN-MT vs. PDTC, $p < 0.05$) (**Supplementary Figure S3**). Subsequent HE staining showed the same hepatocellular edema and reduced central venous congestion after PDTC and EcN-MT treatment (**Figures 5B,C**, $p < 0.05$). Similarly, PDTC treatment and EcN-MT treatment significantly reversed the upregulated a-SMA protein, increaseing MDA, decreaseing CAT, GSH and SOD induced by Cd exposure (**Figures 5D–I**, $p < 0.05$). Furthermore, the results of key protein expression assays of inflammatory pathways (TLR4/NF-κB signaling) showed that PDTC treatment did not reverse the upregulation

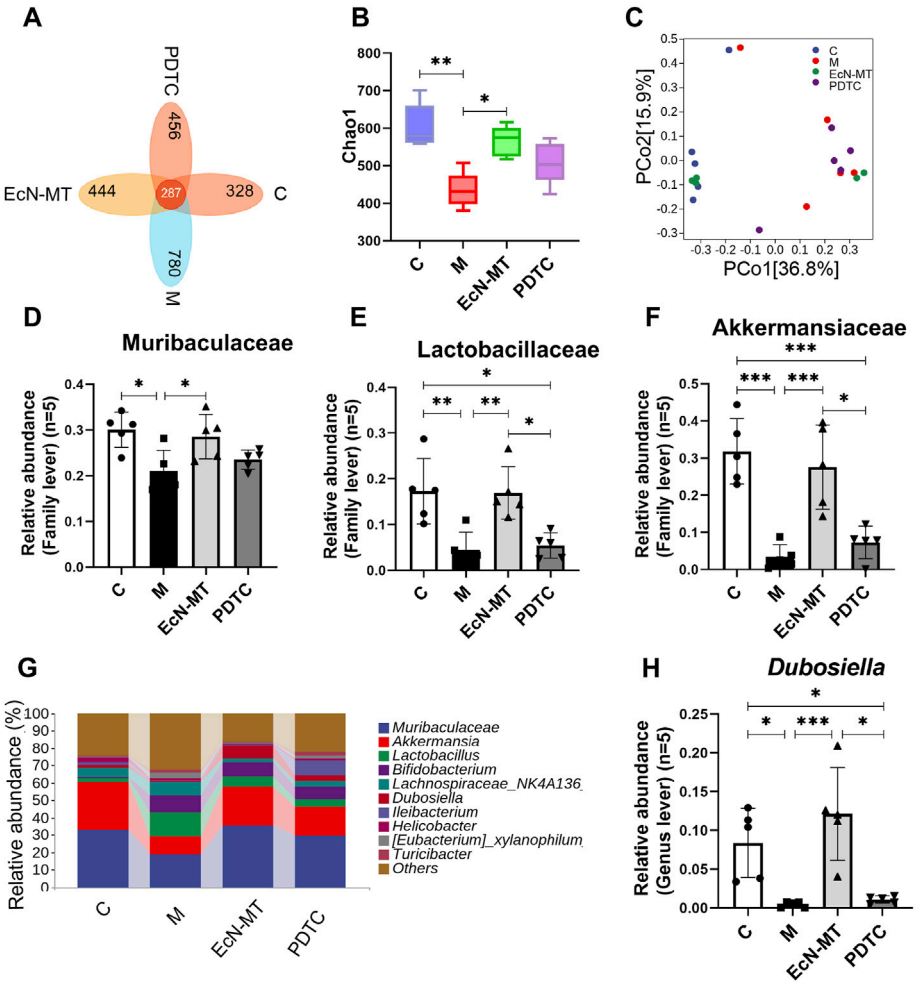

FIGURE 6 | EcN-MT rather than NF-κB inhibitors improved intestinal microbiota. Values are presented as means ± SD (n = 5). **(A)** Venn map representation of OTUs. **(B)** The Chao1 index. **(C)** PCoA of β diversity index. **(D)** Microbiota composition at the genus level. The relative abundance of **(E)** Akkermansia, **(F)** Muribaculaceae, **(G)** Lachnospiraceae **(H)** Dubosiella were analyzed. *$p < 0.05$, **$p < 0.01$, ***$p < 0.001$.

of TLR4 (EcN-MT vs. PDTC, 0.763 vs. 1.234) and MyD88 (EcN-MT vs. PDTC, 0.761 vs. 1.021) expression induced by cadmium exposure compared to the EcN-MT group whereas only p-p65/p65 expression was reduced. (**Figures 5J–M**, $p < 0.05$). Also, the results of key protein expression assays of Bcl-2 family proteins indicated that PDTC treatment as effective as EcN-MT treatment (**Figure 5N**, O, $p < 0.05$). Then, the results of inflammatory factor assay also showed that the upregulation of IL-1β, IL-6 and TNF-α expression induced by Cd exposure was significantly reduced by EcN-MT and PDTC treatment (**Figures 5P–R**, $p < 0.05$).

EcN-MT Rather Than NF-κB Inhibitors Improved Intestinal Microbiota

16S rRNA was used to study the effect of NF-κB inhibitors on the intestinal microbiota of Cd-exposed mice. Then analysis by the Venn method showed that 287 common OTUs were identified from each group, with the number of unique OTUs in C, M, EcN-MT and PDTC being 328, 780, 444 and 456, respectively (**Figure 6A**). Remarkably, the results of the chao1 index of α diversity showed no significant change in community diversity after the PDTC treatment compared to the EcN-MT treatment (**Figure 6B**, $p < 0.05$). Meanwhile, the results of PCoA showed that the sample points in the PDTC group were not far from the M group compared to the EcN-MT treatment (**Figure 6C**). Furthermore, for the composition of the top 10 family-level microbiota, PDTC treatment was not shown to upregulate the abundance of Muribaculaceae, Akkermansia, and Lactobacillaceae compared to the EcN-MT group (**Figures 6D–F**, $p < 0.05$). Similarly, analysis of the top 10 genus-level microbial populations showed that PDTC treatment did not significantly increase the relative

abundance of *Dubosiella* compared to the EcN-MT group (**Figures 6G–I**, $p < 0.05$).

DISCUSSION

Cd is known as a widespread environmental toxicant that contaminated water, food, etc., which made Cd exposure unavoidable. The liver is the main target organ for Cd accumulation and exposure (Uetani et al., 2006). Cd exposure could cause hepatic lesions, fibrosis inflammation and oxidative stress in liver tissues, which is one of the important mechanisms of Cd-induced liver injury (Saeedi et al., 2020; Xu et al., 2021). Although evidence so far have indicated that probiotic bacteria can protect against Cd-exposure hepatoexpoure (Zhai et al., 2014), the role of modified engineered bacteria in Cd-induced subchronic liver injury has rarely been reported.

Subchronic liver injury provides a more realistic simulation of human exposure to a contaminated environment, and there are limitations to the treatment of liver injury caused by subchronic Cd exposure. Therefore, in this study, we brought up a new therapeutic option for subchronic Cd exposure-induced liver injury, and carried out several experiments to verify its therapeutic functions and explore its potential mechanisms. *In vitro*, growth curve test, plasmid stability test and metallothionein expression test showed that EcN-MT was successfully constructed and had good plasmid stability and metallothionein expression ability. Then acid tolerance and bile salt tolerance tests showed that EcN-MT had the ability to tolerate gastric acid and the potential of oral administration. Subsequently, the results of antioxidant test showed that there was no significant difference between EcN-MT and EcN in OH^- radical and O_2^- radical scavenging ability. However, EcN-MT was superior to EcN in DPPH radical scavenging capacity, indicating that EcN-MT had better antioxidant capacity. In addition, the heavy metal binding test showed that the heavy metal binding capacity of EcN-MT was better than that of EcN and reached 6.7 mg/g biomass. The above experimental results indicated that EcN-MT had the potential to treat Cd exposure (**Figure 1**, **Supplementary Figure S1**).

Then, subchronic Cd exposure animal models were used to test whether EcN-MT is efficacious *in vivo*. Consistent with the previous studies (Zhai et al., 2019), Cd exposure increased hepatic Cd accumulation, while EcN-MT supplementation significantly reduced Cd levels in the liver. This may be due to the binding properties of EcN-MT to the heavy metal Cd and because the expressed MT protein can chelate with excess free heavy metal ions (Huang et al., 2020), which promoted the excretion of Cd, leading to decrease Cd levels in the liver. The results of fecal Cd assay further confirmed this conjecture. Also, HE staining results and a-SMA assay showed that EcN-MT supplementation reduced liver inflammation and a-SMA protein expression. It was shown that chronic inflammation leads to increased expression of a-SMA protein, which activated hepatic stellate cells, leading to collagen deposition and consequently fibrosis in liver tissue (Ren et al., 2019). Liver fibrosis is an intermediate step in the further development of cirrhosis (Xu et al., 2021). This suggests that EcN-MT might reduce the production of chronic inflammation in the liver, thereby reducing the production of fibrosis and thus avoiding the development of cirrhosis. In addition, the results of oxidative stress factor assay showed that Cd exposure increased MDA and decreased CAT, SOD, and GSH expression, while EcN-MT treatment reduced MDA and increased CAT, SOD, and GSH. Some studies have demonstrated that Cd exposure caused excessive production of free radicals, which were responsible for oxidative stress in the body (Mezynska et al., 2018). Excess reactive oxygen species (ROS) could lead to an increase in MDA content by β-breakage of lipoxygenated lipids. To reduce oxidative stress, the body produced antioxidant enzymes such as SOD, CAT and non-enzymatic antioxidants (GSH) to maintain the dynamic balance of free radicals in the body (Moradkhani et al., 2020). This suggested that EcN-MT could reduce hepatic oxidative stress and thus alleviate Cd -mediated hepatotoxicity (**Figure 2**, **Supplementary Figure S2**).

To further investigate the potential mechanisms of EcN-MT to avoid Cd-induced subchronic liver injury, the TLR4/NF-κB inflammatory signaling pathway and key Bcl-2 family proteins were investigated. Although *in vitro* cellular assays were not used to validate the effect of cadmium exposure on the TLR4/NF-κB signaling pathway, however, many studies have shown that TLR4/NF-κB signaling pathway is closely associated with liver injury (Dapito et al., 2012; Arab-Nozari et al., 2020). The western blotting results showed that EcN-MT treatment significantly inhibited the expression of TLR4, which in turn downregulated MyD88, an intracellular linker protein downstream of TLR4, and thus inhibited NF-κB expression. It is well known that the conventional NF-κB is a heterodimer composed of p50 and p65 subunits, of which p65 is frequently detected by Western blotting (Zhang et al., 2018). Activated p50-P65 heterodimers translocate from the cytoplasm to the nucleus, triggering inflammation, promoting oxidative stress and participating in the *trans*-activation of various genes, such as apoptosis-related genes Bax and Bcl-2 (Michio Tamatani et al., 1999). Bcl-2 and Bax are members of the Bcl-2 gene, and Bcl-2 forms an unphosphorylated complex with Bax, so that its phosphorylation releases Bax from the Bcl-2-Bax complex and thus promotes cellular apoptosis (Karna et al., 2009). Meanwhile, NF-κB could play a transcriptional regulatory role to activate the expression of inflammatory genes such as IL-1β, IL-6 and TNF-α, which ultimately caused the release of inflammatory factors (Calisto et al., 2016). The results of inflammatory factor assay showed that supplementation with EcN-MT reduced the transcriptional levels of IL-1β, IL-6 and TNF-α inflammatory factors (**Figure 3**). In addition, according to the report (Chen et al., 2020), PDTC is the most commonly used inhibitor of NF-κB. Inhibition of NF-κB activation with PDTC also reduced inflammation, oxidative stress in the liver (**Figure 5**). This further suggested that EcN-MT reduced liver injury from Cd exposure possibly by inhibiting the activation of TLR4/NF-κB signaling pathway. More importantly, EcN treatment alleviated Cd expose-induced inflammation and oxidative stress in liver tissues to some extent, but not significantly, whereas MT and EcN-MT treatments effectively reduced Cd expose-induced

inflammation and oxidative stress induced by Cd exposure. This suggested that EcN-MT suppressed the activation of TLR4/NF-κB signaling pathway mainly through expressed MT, thereby reducing liver injury.

Due to the direct anatomical link between the gut and liver and the recent rise of 16S rRNA sequencing technology, the relationship between gut microbiota and liver injury has been further explored. The results of Shannon index in α diversity and PCoA in β diversity indicated that EcN-MT appeared to promote the conversion of the intestinal microbiota of Cd-exposure mice to normal control mice. And then, the top 10 family level and genus level species composition results showed that supplementation with EcN-MT increased probiotic abundance including Ruminococcaceae at family level, *Akkermansia*, *Muribaculaceae*, *Lachnospiraceae* at genus level. Among them, Muribaculaceae belongs to the phylum Bacillus and could protect the organism through degraded dietary carbohydrates and antagonizing benzoates (Lagkouvardos et al., 2019). Likewise, Akkermania was discovered by scientists in 2004, which used intestinal mucin as an energy source to protect the intestinal tract from pathogens through competition, and the abundance of Akkermania was reduced in the intestinal microbiota of cadmium-exposed mice (Li et al., 2019). Also, recent studies have shown that Lachnospiraceae and Ruminococcaceae reduced *C. difficile* infections through the production of short-chain fatty acids that repressed pathogen proliferation and reduced intestinal inflammation (Collins et al., 2015; Guo et al., 2021). In brief, the increased abundance of intestinal probiotics leads to an increase in the production of short-chain fatty acids and an inhibition of pathogen proliferation, thereby reducing intestinal inflammation, which in turn reduces liver inflammation *via* the enterohepatic axis. This may be one of the important mechanisms by which EcN-MT treatment attenuates subchronic liver injury induced by Cd exposure (**Figure 4**). In addition, supplementation with EcN but not MT similarly ameliorated the intestinal microbiota disorder induced by Cd exposure, which suggests that EcN-MT may regulate the intestinal microbiota through the probiotic properties of the host bacterium EcN. Meanwhile, inhibition of NF-κB activation by PDTC treatment did not improve intestinal microbiome disorders (**Figure 6**), further suggesting that another mechanism of ECN-MT in the treatment of chronic Cd exposure is regulating intestinal microbiome through host bacteria EcN.

In summary, this study showed that EcN-MT treatment inhibited Cdexposure-induced liver injury by expressing MT, thereby increasing Cd excretion in the feces, reducing Cd accumulation in the liver, inhibiting TLR4/NF-κB activation, and reducing apoptosis and inflammatory factor transcription. In addition, EcN-MT treatment increased the abundance of probiotics and biodiversity through the host bacteria EcN, which transformed microorganisms ecology affected by Cd exposure to normal levels. Our experiment is the first to explore the potential role of EcN-MT in treating subchronic liver injury caused by cadmium exposure. Although this study only used mice for validation and nor other animals such as crab-eating monkeys because of economic and experimental conditions. However, the good therapeutic effect of engineered bacteria on liver injury has been proven, and with the development of synthetic biology and the further exploration of the role of probiotics in human health, it will provide a new therapeutic strategy for clinical treatment.

DATA AVAILABILITY STATEMENT

The datasets presented in this study can be found in online repositories. The names of the repository/repositories and accession number(s) can be found below: NCBI Sequence Read Archive, BioProject ID PRJNA781077.

ETHICS STATEMENT

The animal study was reviewed and approved by the Nanchang Le you Biotechnology Co., Ltd.

AUTHOR CONTRIBUTIONS

HH: conceptualization, funding acquisition, supervision, writing review, and editing. TC: conceptualization, funding acquisition, writing review, editing, and assistance with formal analysis of data. CZ: methodology, investigation, formal analysis, visualization, and experimentation all contributed. Ying Cheng: experimentation, references, original draft. HL: data formal analysis assistance. WL: reviewing. JW: reviewing. ZL: editing assistance. XW: editing assistance.

FUNDING

This study was supported by the National Natural Science Foundation of China (Grant No. 41765009), National Natural Science Foundation of China (Grant No. 82060638), Academic and Technical Leaders of Major Disciplines in Jiangxi Province (Grant No. 20194BCJ22032), and Double Thousand Plan of Jiangxi Province (High-End Talents Project of Scientific and Technological Innovation).

SUPPLEMENTARY MATERIAL

The Supplementary Material for this article can be found online at: https://www.frontiersin.org/articles/10.3389/fphar.2022.857869/full#supplementary-material

REFERENCES

Alexander, D., Ellerby, R., Hernandez, A., Wu, F., and Amarasiriwardena, D. (2017). Investigation of Simultaneous Adsorption Properties of Cd, Cu, Pb and Zn by Pristine rice Husks Using ICP-AES and LA-ICP-MS Analysis. *Microchemical J.* 135, 129–139. doi:10.1016/j.microc.2017.08.001

Ali, H., Khan, E., and Ilahi, I. (2019). Environmental Chemistry and Ecotoxicology of Hazardous Heavy Metals: Environmental Persistence, Toxicity, and Bioaccumulation. *J. Chem.* 2019, 1–14. doi:10.1155/2019/6730305

Andreani, G., Carpenè, E., Capranico, G., and Isani, G. (2011). Metallothionein cDNA Cloning, Metallothionein Expression and Heavy Metals in Scapharca Inaequivalvis along the Northern Adriatic Coast of Italy. *Ecotoxicol Environ. Saf.* 74 (3), 366–372. doi:10.1016/j.ecoenv.2010.12.008

Arab-Nozari, M., Mohammadi, E., Shokrzadeh, M., Ahangar, N., Amiri, F. T., and Shaki, F. (2020). Co-exposure to Non-toxic Levels of Cadmium and Fluoride Induces Hepatotoxicity in Rats via Triggering Mitochondrial Oxidative Damage, Apoptosis, and NF-kB Pathways. *Environ. Sci. Pollut. Res. Int.* 27 (19), 24048–24058. doi:10.1007/s11356-020-08791-4

Baba, H., Tsuneyama, K., Yazaki, M., Nagata, K., Minamisaka, T., Tsuda, T., et al. (2013). The Liver in Itai-Itai Disease (Chronic Cadmium Poisoning): Pathological Features and Metallothionein Expression. *Mod. Pathol.* 26 (9), 1228–1234. doi:10.1038/modpathol.2013.62

Calisto, K. L., Camacho, A. C., Mittestainer, F. C., Carvalho, B. M., Guadagnini, D., Carvalheira, J. B., et al. (2016). Retraction Note: Diacerhein Attenuates the Inflammatory Response and Improves Survival in a Model of Severe Sepsis. *Crit. Care* 20, 278. doi:10.1186/s13054-016-1453-8

Cao, Z., Fang, Y., Lu, Y., Tan, D., Du, C., Li, Y., et al. (2017). Melatonin Alleviates Cadmium-Induced Liver Injury by Inhibiting the TXNIP-NLRP3 Inflammasome. *J. Pineal Res.* 62 12389. doi:10.1111/jpi.12389

Chen, R., Xie, F., Zhao, J., and Yue, B. (2020). Suppressed Nuclear Factor-Kappa B Alleviates Lipopolysaccharide-Induced Acute Lung Injury through Downregulation of CXCR4 Mediated by microRNA-194. *Respir. Res.* 21 (1), 144. doi:10.1186/s12931-020-01391-3

Clemens, S., Aarts, M. G. M., Thomine, S., and Verbruggen, N. (2013). Plant Science: the Key to Preventing Slow Cadmium Poisoning. *Trends Plant Sci.* 18, 92–99. doi:10.1016/j.tplants.2012.08.003

Collins, J., Auchtung, J. M., Schaefer, L., Eaton, K. A., and Britton, R. A. (2015). Humanized Microbiota Mice as a Model of Recurrent Clostridium difficile Disease. *Microbiome* 3, 35. doi:10.1186/s40168-015-0097-2

Dapito, D. H., Mencin, A., Gwak, G. Y., Pradere, J. P., Jang, M. K., Mederacke, I., et al. (2012). Promotion of Hepatocellular Carcinoma by the Intestinal Microbiota and TLR4. *Cancer Cell* 21 (4), 504–516. doi:10.1016/j.ccr.2012.02.007

de Vrese, M., and Schrezenmeir, J. (2008). Probiotics, Prebiotics, and Synbiotics. *Adv. Biochem. Eng. Biotechnol.* 111, 1–66. doi:10.1007/10_2008_097

Duan, Y., Duan, J., Feng, Y., Huang, X., Fan, W., Wang, K., et al. (2018). Hepatoprotective Activity of Vitamin E and Metallothionein in Cadmium-Induced Liver Injury in Ctenopharyngodon idellus. *Oxid Med. Cel Longev* 2018, 9506543. doi:10.1155/2018/9506543

Eybl, V., Kotyzova, D., and Koutensky, J. (2006). Comparative Study of Natural Antioxidants - Curcumin, Resveratrol and Melatonin - in Cadmium-Induced Oxidative Damage in Mice. *Toxicology* 225 (2-3), 150–156. doi:10.1016/j.tox.2006.05.011

Guo, W., Xiang, Q., Mao, B., Tang, X., Cui, S., Li, X., et al. (2021). Protective Effects of Microbiome-Derived Inosine on Lipopolysaccharide-Induced Acute Liver Damage and Inflammation in Mice via Mediating the TLR4/NF-Kb Pathway. *J. Agric. Food Chem.* 69, 7619–7628. doi:10.1021/acs.jafc.1c01781

Helal, G. K., and Helal, O. K. (2009). Metallothionein Attenuates Carmustine-Induced Oxidative Stress and Protects against Pulmonary Fibrosis in Rats. *Arch. Toxicol.* 83 (1), 87–94. doi:10.1007/s00204-008-0325-7

Huang, X., Xiong, G., Feng, Y., Fan, W., Yang, S., Duan, J., et al. (2020). Protective Effects of Metallothionein and Vitamin E in the Trunk Kidney and Blood of Cadmium Poisoned Ctenopharyngodon idellus. *Fish. Physiol. Biochem.* 46 (3), 1053–1061. doi:10.1007/s10695-020-00771-2

Hyder, O., Chung, M., Cosgrove, D., Herman, J. M., Li, Z., Firoozmand, A., et al. (2013). Cadmium Exposure and Liver Disease Among US Adults. *J. Gastrointest. Surg.* 17 (7), 1265–1273. doi:10.1007/s11605-013-2210-9

Karna, P., Sharp, S. M., Yates, C., Prakash, S., and Aneja, R. (2009). RituEM011 Activates a Survivin-dependent Apoptotic Program in Human Non-small Cell Lung Cancer Cells. *Mol. Cancer* 8 93. doi:10.1186/1476-4598-8-93

Kiliç, G. A., and Kutlu, M. (2010). Effects of Exogenous Metallothionein against Thallium-Induced Oxidative Stress in Rat Liver. *Food Chem. Toxicol.* 48 (3), 980–987. doi:10.1016/j.fct.2010.01.013

Lagkouvardos, I., Lesker, T. R., Hitch, T. C. A., Gálvez, E. J. C., Smit, N., Neuhaus, K., et al. (2019). Sequence and Cultivation Study of Muribaculaceae Reveals Novel Species, Host Preference, and Functional Potential of This yet Undescribed Family. *Microbiome* 7 (1), 28. doi:10.1186/s40168-019-0637-2

Li, X., Brejnrod, A. D., Ernst, M., Rykær, M., Herschend, J., Olsen, N. M. C., et al. (2019). Heavy Metal Exposure Causes Changes in the Metabolic Health-Associated Gut Microbiome and Metabolites. *Environ. Int.* 126, 454–467. doi:10.1016/j.envint.2019.02.048

Liu, J., Kadiiska, M. B., Corton, J. C., Qu, W., Waalkes, M. P., Mason, R. P., et al. (2002). Acute Cadmium Exposure Induces Stress-Related Gene Expression in Wild-type and Metallothionein-I/ii-Null Mice. *Free Radic. Biol. Med.* 32 (6). 525–535. doi:10.1016/s0891-5849(01)00826-7

Liu, M., Lu, X., Khan, A., Ling, Z., Wang, P., Tang, Y., et al. (2019). Reducing Methylmercury Accumulation in Fish Using Escherichia coli with Surface-Displayed Methylmercury-Binding Peptides. *J. Hazard. Mater.* 367, 35–42. doi:10.1016/j.jhazmat.2018.12.058

Luo, X., Song, H., Yang, J., Han, B., Feng, Y., Leng, Y., et al. (2020). Encapsulation of Escherichia coli Strain Nissle 1917 in a Chitosan-Alginate Matrix by Combining Layer-By-Layer Assembly with CaCl2 Cross-Linking for an Effective Treatment of Inflammatory Bowel Diseases. *Colloids Surf. B Biointerfaces* 189, 110818. doi:10.1016/j.colsurfb.2020.110818

Mężyńska, M., Brzóska, M., Rogalska, J., and Piłat-Marcinkiewicz, B. (2018). Extract from Aronia Melanocarpa L. Berries Prevents Cadmium-Induced Oxidative Stress in the Liver: A Study in A Rat Model of Low-Level and Moderate Lifetime Human Exposure to This Toxic Metal. *Nutrients* 11 (1), 21. doi:10.3390/nu11010021

Moradkhani, S., Rezaei-Dehghanzadeh, T., and Nili-Ahmadabadi, A. (2020). & Nili-AhmadabadiRosa Persica Hydroalcoholic Extract Improves Cadmium-Hepatotoxicity by Modulating Oxidative Damage and Tumor Necrosis Factor-Alpha Status. *Environ. Sci. Pollut. Res.* 27 (25), 31259–31268. doi:10.1007/s11356-020-09450-4

Nordberg, G. F. (1984). Chelating Agents and Cadmium Toxicity: Problems and Prospects. *Environ. Health Perspect.* 54, 213–218. doi:10.1289/ehp.8454213

Puurunen, M. K., Vockley, J., Searle, S. L., Sacharow, S. J., Phillips, J. A., Denney, W. S., et al. (2021). Safety and Pharmacodynamics of an Engineered E. coli Nissle for the Treatment of Phenylketonuria: a First-In-Human Phase 1/2a Study. *Nat. Metab.* 3, 1125–1132. doi:10.1038/s42255-021-00430-7

Ren, L., Qi, K., Zhang, L., Bai, Z., Ren, C., Xu, X., et al. (2019). Glutathione Might Attenuate Cadmium-Induced Liver Oxidative Stress and Hepatic Stellate Cell Activation. *Biol. Trace Elem. Res.* 191 (2), 443–452. doi:10.1007/s12011-019-1641-x

Saeedi, B. J., Liu, K. H., Owens, J. A., Hunter-Chang, S., Camacho, M. C., Eboka, R. U., et al. (2020). Gut-Resident Lactobacilli Activate Hepatic Nrf2 and Protect against Oxidative Liver Injury. *Cell Metab* 31 (5), 956–e5. doi:10.1016/j.cmet.2020.03.006

Sassone-Corsi, M., Nuccio, S. P., Liu, H., Hernandez, D., Vu, C. T., Takahashi, A. A., et al. (2016). Microcins Mediate Competition Among Enterobacteriaceae in the Inflamed Gut. *Nature* 540 (7632), 280–283. doi:10.1038/nature20557

Schwabe, R. F., and Greten, T. F. (2020). Gut Microbiome in HCC - Mechanisms, Diagnosis and Therapy. *J. Hepatol.* 72 (2), 230–238. doi:10.1016/j.jhep.2019.08.016

Shen, X., Liu, W., Chen, Y., Guo, Y., Gao, M., Chen, W., et al. (2019). Diagnostic Significance of Metallothionein Members in Recognizing Cadmium Exposure in Various Organs under Low-Dose Exposure. *Chemosphere* 229, 32–40. doi:10.1016/j.chemosphere.2019.04.192

Sogawa, N., Sogawa, C. A., Oda, N., Fujioka, T., Onodera, K., and Furuta, H. (2001). The Effects of Ovariectomy and Female Sex Hormones on Hepatic Metallothionein-I Gene Expression after Injection of Cadmium Chloride in Mice. *Pharmacol. Res.* 44 (1), 53–57. doi:10.1006/phrs.2001.0833

Tamatani, M., Che, Y. H., Matsuzaki, H., Ogawa, S., Okado, H., Miyake, S., et al. (1999). Tumor Necrosis Factor Induces Bcl-2 and Bcl-X Expression through

NFkappaB Activation in Primary Hippocampal Neurons. *J. Biol. Chem.* 274, 8531–8538. doi:10.1074/jbc.274.13.8531

Tao, W., Zhang, G., Wang, X., Guo, M., Zeng, W., Xu, Z., et al. (2020). Analysis of the Intestinal Microbiota in COVID-19 Patients and its Correlation with the Inflammatory Factor IL-18. *Med. Microecol* 5, 100023. doi:10.1016/j.medmic.2020.100023

Thijssen, S., Cuypers, A., Maringwa, J., Smeets, K., Horemans, N., Lambrichts, I., et al. (2007). Low Cadmium Exposure Triggers a Biphasic Oxidative Stress Response in Mice Kidneys. *Toxicology* 236 (1-2), 29–41. doi:10.1016/j.tox.2007.03.022

Uetani, M., Kobayashi, E., Suwazono, Y., Honda, R., Nishijo, M., Nakagawa, H., et al. (2006). Tissue Cadmium (Cd) Concentrations of People Living in a Cd Polluted Area, Japan. *Biometals* 19 (5), 521–525. doi:10.1007/s10534-005-5619-0

Wang, L., Shang, Q., Guo, W., Wu, X., Wu, L., Wu, L., et al. (2020). Evaluation of the Hypoglycemic Effect of Probiotics via Directly Consuming Glucose in Intestines of STZ-Induced Diabetic Mice and Glucose Water-Induced Diabetic Mice. *J. Funct. Foods* 64, 103614. doi:10.1016/j.jff.2019.103614

Wang, M., Chen, Z., Song, W., Hong, D., Huang, L., and Li, Y. (2021). A Review on Cadmium Exposure in the Population and Intervention Strategies against Cadmium Toxicity. *Bull. Environ. Contam. Toxicol.* 106 (1), 65–74. doi:10.1007/s00128-020-03088-1

Wang, X. W., and Liu, Y. Y. (2020). Comparative Study of Classifiers for Human Microbiome Data. *Med. Microecol* 4, 100013. doi:10.1016/j.medmic.2020.100013

Westendorf, A. M., Gunzer, F., Deppenmeier, S., Tapadar, D., Hunger, J. K., Schmidt, M. A., et al. (2005). Intestinal Immunity of Escherichia coli NISSLE 1917: a Safe Carrier for Therapeutic Molecules. *FEMS Immunol. Med. Microbiol.* 43 (3), 373–384. doi:10.1016/j.femsim.2004.10.023

Xia, C., Cao, X., Cui, L., Liu, H., Wang, S., and Chen, T. (2020). Anti-aging Effect of the Combination of Bifidobacterium Longum and B. Animalis in a D-Galactose-Treated Mice. *J. Funct. Foods* 69, 103938. doi:10.1016/j.jff.2020.103938

Xu, Y., Mu, W., Li, J., Ba, Q., and Wang, H. (2021). Chronic Cadmium Exposure at Environmental-Relevant Level Accelerates the Development of Hepatotoxicity to Hepatocarcinogenesis. *Sci. Total Environ.* 783, 146958. doi:10.16/j.scitotenv.2021.146958

Zhai, Q., Liu, Y., Wang, C., Zhao, J., Zhang, H., Tian, F., et al. (2019). Increased Cadmium Excretion Due to Oral Administration of Lactobacillus Plantarum Strains by Regulating Enterohepatic Circulation in Mice. *J. Agric. Food Chem.* 67 (14), 3956–3965. doi:10.1021/acs.jafc.9b01004

Zhai, Q., Wang, G., Zhao, J., Liu, X., Narbad, A., Chen, Y. Q., et al. (2014). Protective Effects of Lactobacillus Plantarum CCFM8610 against Chronic Cadmium Toxicity in Mice Indicate Routes of protection besides Intestinal Sequestration. *Appl. Environ. Microbiol.* 80 (13), 4063–4071. doi:10.1128/AEM.00762-14

Zhai, Q., Yu, L., Li, T., Zhu, J., Zhang, C., Zhao, J., et al. (2017). Effect of Dietary Probiotic Supplementation on Intestinal Microbiota and Physiological Conditions of Nile tilapia (*Oreochromis niloticus*) under Waterborne Cadmium Exposure. *Antonie Van Leeuwenhoek* 110 (4), 501–513. doi:10.1007/s10482-016-0819-x

Zhang, B., Zhang, Z., Li, L., Qin, Y.-R., Liu, H., Jiang, C., et al. (2018). TSPAN15 Interacts with BTRC to Promote Oesophageal Squamous Cell Carcinoma Metastasis via Activating NF-Kb Signaling. *Nat. Commun.* 9, 1423. doi:10.1038/s41467-018-03716-9

Zhang, S., Jin, Y., Zeng, Z., Liu, Z., and Fu, Z. (2015). Subchronic Exposure of Mice to Cadmium Perturbs Their Hepatic Energy Metabolism and Gut Microbiome. *Chem. Res. Toxicol.* 28 (10), 2000–2009. doi:10.1021/acs.chemrestox.5b00237

Conflict of Interest: The authors declare that the research was conducted in the absence of any commercial or financial relationships that could be construed as a potential conflict of interest.

Publisher's Note: All claims expressed in this article are solely those of the authors and do not necessarily represent those of their affiliated organizations, or those of the publisher, the editors and the reviewers. Any product that may be evaluated in this article, or claim that may be made by its manufacturer, is not guaranteed or endorsed by the publisher.

frontiers | Frontiers in Pharmacology

ORIGINAL RESEARCH
published: 13 April 2022
doi: 10.3389/fphar.2022.841330

Thioredoxin-1 Activation by Pterostilbene Protects Against Doxorubicin-Induced Hepatotoxicity *via* Inhibiting the NLRP3 Inflammasome

Shiqing Tan[1†], *Jie Bai*[2†], *Mingxi Xu*[1], *Longying Zhang*[1*] *and Ying Wang*[1*]

[1]*The Second Affiliated Hospital, Dalian Medical University, Dalian, China,* [2]*Nutrition and Food Hygiene, Dalian Medical University, Dalian, China*

OPEN ACCESS

Edited by:
Runping Liu,
Beijing University of Chinese Medicine, China

Reviewed by:
Ahmed Esmat Abdel Moneim,
Helwan University, Egypt
Mohammad H. Abukhalil,
Al-Hussein Bin Talal University, Jordan

***Correspondence:**
Longying Zhang
563354453@qq.com
Ying Wang
wangyingwang1985@163.com

[†]*These authors have contributed equally to this work*

Specialty section:
This article was submitted to Gastrointestinal and Hepatic Pharmacology, a section of the journal Frontiers in Pharmacology

Received: *22 December 2021*
Accepted: *28 March 2022*
Published: *13 April 2022*

Citation:
Tan S, Bai J, Xu M, Zhang L and Wang Y (2022) Thioredoxin-1 Activation by Pterostilbene Protects Against Doxorubicin-Induced Hepatotoxicity via Inhibiting the NLRP3 Inflammasome. Front. Pharmacol. 13:841330. doi: 10.3389/fphar.2022.841330

Background: Doxorubicin (DOX) has been widely used in cancer treatment. However, DOX can cause a range of significant side effects, of which hepatotoxicity is a common one, and therefore limits its clinical use. Pterostilbene (PTS) has been shown to exhibit anti-oxidant and anti-inflammatory effects in the treatment of liver diseases but whether PTS could protect against hepatotoxicity in DOX-treated mice is unknown.

Methods: In our study, we use C57/BL6J mice and the HepG2 cell line. We divided the mice in 4 groups: the control, the PTS treatment, the DOX treatment, and the DOX + PTS treatment group. Liver histopathology was judged by performing hematoxylin–eosin and Masson staining. Immunohistochemistry was used to perform the expression of NLRP3. The levels of serum alanine transaminase (ALT) and aspartate transaminase (AST) were evaluated. Levels of malondialdehyde (MDA), superoxide dismutase (SOD), glutathione (GSH), and DCFH-DA staining were used to evaluate the oxidative injury. Western blot and real-time PCR were applied to evaluate the expressions of proteins and mRNA. MTT was used to evaluate DOX-induced cell injury and the protective effects of PTS. Recombinant Trx-1 was used to analyze the mechanism of PTS. A TUNEL assay was used to detect apoptosis in DOX-induced HepG2 cells and the protective effects of PTS.

Results: PTS ameliorated DOX-induced liver pathological changes and the levels of AST and ALT. PTS also decreased the level of MDA, increased the level of SOD, GSH, and the expression of Trx-1 in DOX-treated mice. PTS decreased the levels of NLRP3 and IL-1β mRNA and the expressions of their proteins in DOX-treated mice. In addition, PTS also decreased the expression of Cleaved Caspase-3 and BAX and increased the expression of BCL-2. *In vitro*, after treatment with recombinant Trx-1, ROS and NLRP3 inflammasome were both decreased. Treatment with PTS could rescue the downregulation of Trx-1, decreased the ROS level and the NLRP3 inflammasome, and protected HepG2 cells against DOX-induced apoptosis.

Conclusion: The results show that PTS exhibits protective effects against DOX-induced liver injuries *via* suppression of oxidative stress, fibrosis, NLRP3 inflammasome stimulation, and cell apoptosis which might lead to a new approach of preventing DOX-induced hepatotoxicity.

Keywords: doxorubicin, pterostilbene, Thioredoxin-1, NLRP3, hepatotoxicity

INTRODUCTION

Doxorubicin (DOX), a member of the anthracycline group of structures, is used by oncologists as a highly effective drug in the treatment of tumors (Rivankar. 2014; Yang et al., 2020). However, recent studies showed that DOX causes unanticipated side-effects such as nausea, vomiting, extravasation, severe hepatotoxicity, and cardiotoxicity which limit its use in clinical practice (Carvalho et al., 2009; Kolarovic et al., 2009). The mechanism of DOX-induced hepatotoxicity is well known and is related to the generation of reactive oxygen species (ROS) that ultimately leads to cell death (Pilco-Ferreto and Calaf, 2016; Songbo et al., 2019). Therefore, targeting oxidative stress may be a therapeutic measure to rescue and prevent DOX-induced hepatotoxicity.

Pterostilbene (3,5-dimethoxy-4′-hydroxystilbene, PTS), a natural analogue of resveratrol, is a natural component of blueberries and grapes (Estrela et al., 2013; Lange and Li, 2018). PTS has many biological activities, such as an anti-oxidative, an anti-inflammatory, an anti-cancer, an anti-diabetic one etc. (McCormack and McFadden, 2012; Gómez-Zorita et al., 2021). Previous studies have demonstrated that PTS was able to significantly attenuate astrocyte inflammation and neuronal oxidative injury after ischemia-reperfusion (Liu H. et al., 2019). Sajad A Malik et al. found that PTS was able to reverse palmitic acid induced insulin resistance in HepG2 cells by reducing oxidative stress (Malik et al., 2019). Although the anti-oxidative and anti-inflammatory effects of PTS are known, the pathways leading to these effects have not yet been worked out.

Oxidative stress results from an imbalance in the number of pro-oxidant and anti-oxidant molecules. Among anti-oxidants, thioredoxin-1 (Trx-1) and nicotinamide adenine dinucleotide phosphate (NADPH) form an important and ubiquitous redox system (Powis and Montfort, 2001; Lu and Holmgren, 2014; Perkins et al., 2014; Lu et al., 2021). Trx-1 is a sulfhydryl disulfide oxidoreductase that acts as a reducing agent for oxidized proteins (Hashemy and Holmgren, 2008). The oxidized form of Trx-1 is, in turn, reduced by NADPH (Pillay et al., 2011). Several studies have confirmed that Trx-1 exerts a protective effect in liver injuries but the mechanism is still unclear (Wang X. et al., 2019). NOD-like receptors (NLR) are multi-component assemblies that, in case they are containing the pyrin domain 3, are classified as NLRP3 proteins and as such are part of the so-called inflammasome which also comprises the adapter protein apoptosis-related speck-like protein (ASC) and pro-caspase-1 (Zhang et al., 2021). NLRP3 plays an important role in inflammatory stimulation and regulation (Chen et al., 2019). Previous studies showed that Trx-1 modulates NLRP3 inflammasome activities during atherosclerosis development (Wang et al., 2020). In this study, we will try to shed some light on the presumed PTS modulation of the Trx-1/NLRP3 signaling pathway and the PTS use as a protective agent in DOX-induced hepatotoxicity.

MATERIALS AND METHODS

Chemicals

PTS (purity >99%) was purchased from Meilunbio (Dalian, Liaoning Province, China). DOX was purchased from Sigma-Aldrich (St. Louis, MO, United States). Alanine transaminase (ALT) and aspartate transaminase (AST) were from Nanjing Jiancheng Institute of Biotechnology (Nanjing, China). Malondialdehyde (MDA), superoxide dismutase (SOD), and glutathione (GSH) kits were purchased from Solarbio (Beijing, China). Hematoxylin–eosin (H & E) and Masson staining kits were from Beyotime Biotechnology (Shanghai, China). 3-(4,5-Dimethylthiazol-2-yl)-2,5-diphenyltetrazolium bromide (MTT) was provided by Roche Diagnostics (Basel, Switzerland). TUNEL staining kits (Green) were from Beyotime Biotechnology. The bicinchoninic acid (BCA) protein assay kit was from Thermo Scientific, lysis buffer and phenylmethanesulfonylfluoride (PMSF) were obtained from Beyotime Biotechnology. Human recombinant Trx-1 was from Med Chem Express (HY-P73431).

Animals and Treatment

We used 8-week-old wild type (WT) C57/BL6J mice as experimental animals and divided the mice into four groups (with $n = 8$ for each group): a control group, a PTS treatment group, a DOX treatment group, and a DOX + PTS treatment group. The animals of the DOX group were injected a dose of 10 mg/kg intraperitoneally. This was conducted on day 1 and day 4 for a total of 2 times (20 mg/kg cumulative dose of DOX). The mice of the DOX + PTS group were injected intraperitoneally with PTS (10 mg/kg/day) every day for a total of 7 times, until one day before DOX treatment. As in the DOX treatment group, afterwards DOX was injected intraperitoneally with a dose of 10 mg/kg. This was conducted on day 1 and day 4 for a total of 2 times (20 mg/kg cumulative dose of DOX). All mice were euthanized 6 days after the initial injection of DOX (Liu D. et al., 2019). All the animal experiments were approved by the Institutional Animal Care and Use Committee of the University of Dalian Medical University (SCXK 2015-2003).

Histopathology and Immunohistochemical Staining

All the mice were sacrificed under anesthesia after our study period. The liver tissue was fixed with 4% paraformaldehyde (PFA) for more than 24 h, followed by paraffin embedding. All sections (4 μm) were subjected to a H & E and Masson staining. The liver tissues were subjected to immunohistochemical staining. For this, the sections were incubated with the primary antibody anti-NLRP3 (Wanleibio, WL02635, 1:200) at 4°C overnight and afterwards with the corresponding secondary antibody. The blots were developed using DAB. Digital images were taken at 200 × magnification and were analyzed with ImageJ software.

Measurements of MDA, SOD and GSH Levels

The levels of MDA, SOD, and GSH in DOX-treated livers were evaluated by MDA, SOD, and GSH kits (Solarbio), respectively, according to the manufacturer's instructions.

Cell Culture and Experiments

HepG2 cell were purchased from the American Type Culture Collection. Cells were cultured in DMEM supplemented with 10% fetal bovine serum and antibiotics (100 U/ml penicillin and 100 μg/ml streptomycin, Sigma) and were grown in a humidified atmosphere containing 5% CO_2 at 37°C. Hep G2 cells were treated with recombinant Trx-1 at a dose of 1 μg/ml to elucidate the presumed PTS effects (El Hadri, K., et al., 2012).

DOX-Induced Cell Injury

HepG2 cells were seeded in 96-well plates for 24 h. After 24 h, the medium was removed, 100 μL of sample solution with different concentrations of DOX (0, 1, 2, 5, 8, and 10 mM) was added for different treatment times and a period of 24 h (Song, et al., 2019b). MTT solution (5 mg/ml) was added to each well to a final concentration of 0.5 mg/ml for 4 h. After exposure, DMSO (100 μL/well) was added to dissolve the formed formazan crystals. The absorbance at 490 nm was measured with a microplate reader (Thermo, United States). Based upon these data, a suitable DOX concentration for the induction of cell injury was identified.

Cell Viability Assay

HepG2 cells were seeded in 96-well plates for 24 h and then pretreated with different concentrations of PTS (0, 5, 10, and 20 μM) for 16 h before the treatment with DOX (5 μM) for 24 h. DOX group cells were cultured without PTS pretreatment. An MTT assay was used to assess cell viability (Song S. et al., 2019).

Measurement of ROS Level in HepG2 Cells

HepG2 cells were plated in 6-well culture plates for 24 h and afterwards treated with PTS at a concentration of 10 μM for 4 h

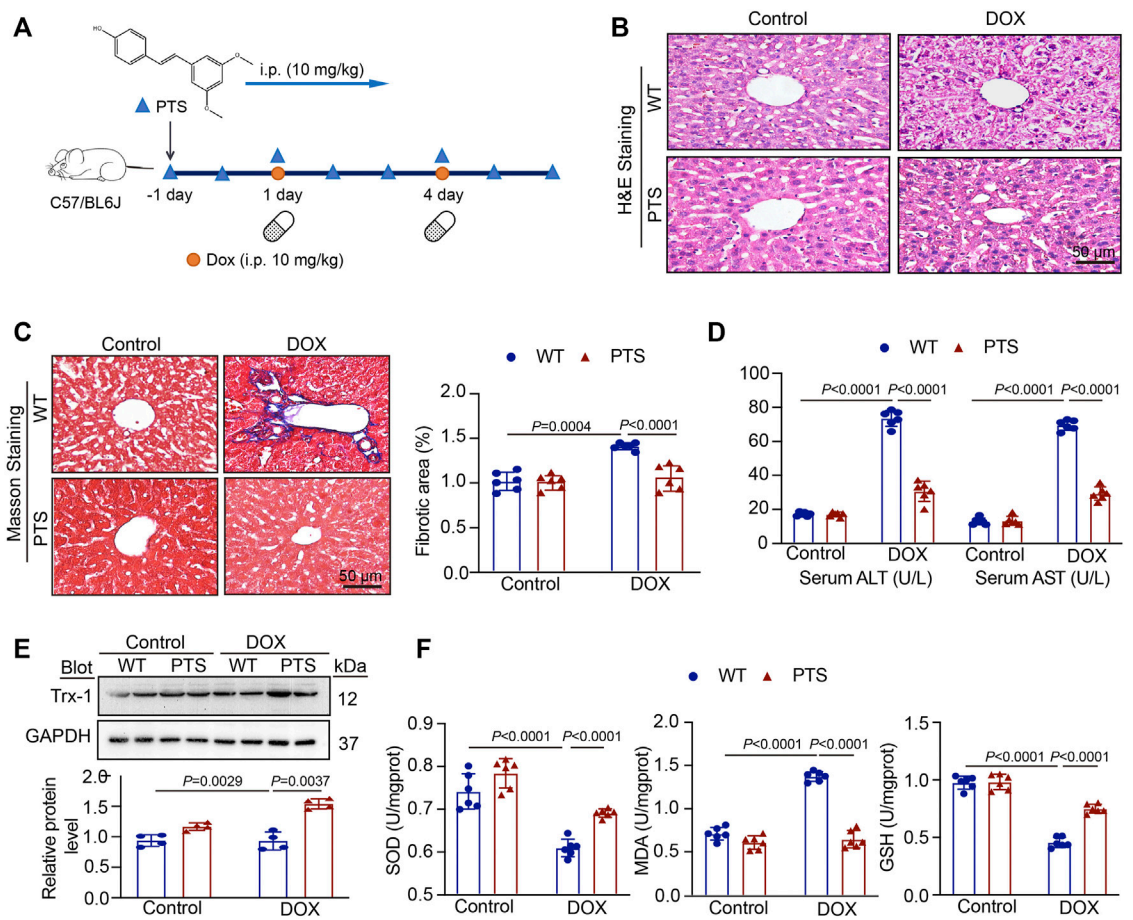

FIGURE 1 | PTS treatment prevents DOX-induced hepatotoxicity. **(A)** Diagrammatic representation of different mice treatments: PTS (10 mg/kg) was injected every day for a total of 7 times (one day before DOX treatment); DOX administration was conducted on day 1 and day 4 for a total of 2 times (20 mg/kg cumulative dose of DOX); **(B)** H & E staining of each group were analyzed (scale bar = 50μm, $n = 6$ per group); **(C)** Masson staining of each group was analyzed (left, scale bar = 50 μm), the quantification of the fibrotic area (right, $n = 6$); **(D)** The levels of serum ALT (left) and AST (right) in each group ($n = 6$ per group); **(E)** Western blot analysis of Trx-1 protein in each group (up), the quantification of Trx-1 expression (down, $n = 4$ per group); **(F)** The levels of SOD (left), MDA (middle), and GSH in each group ($n = 6$ per group).

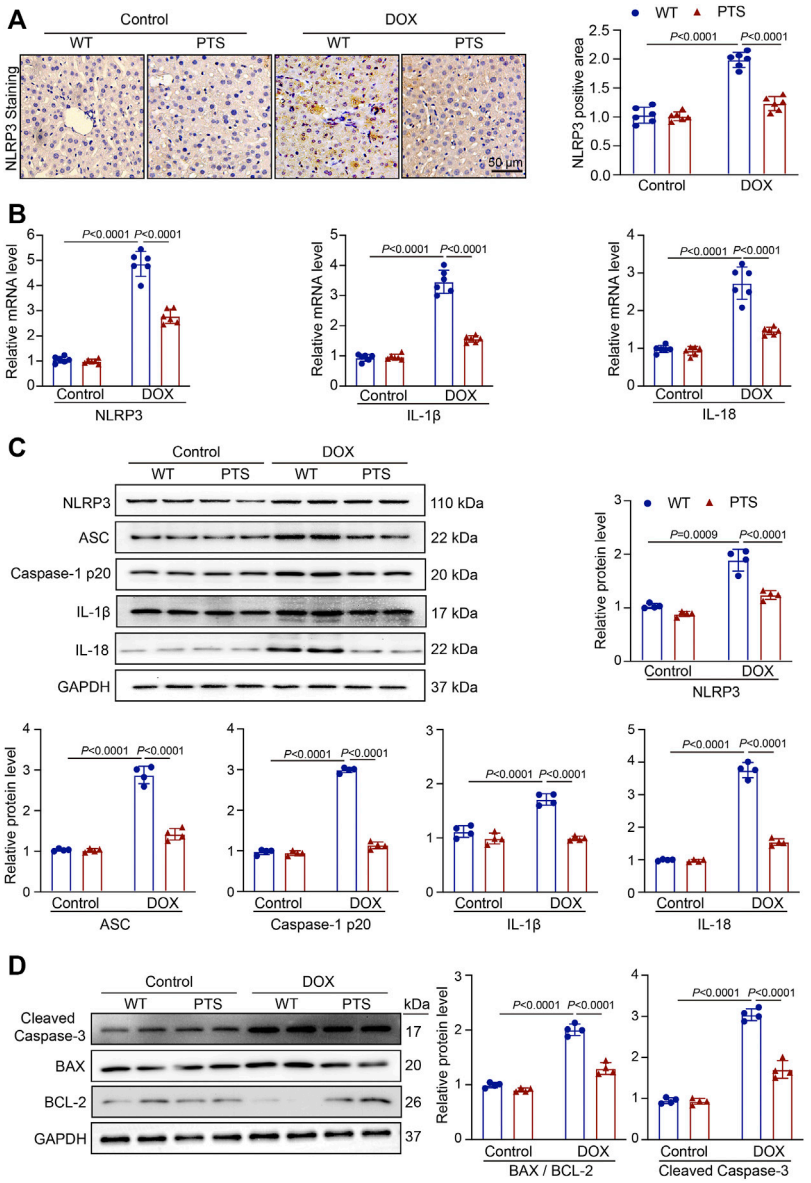

FIGURE 2 | PTS reduces reduction of NLRP3 inflammasome and apoptosis in DOX-treated mice. **(A)** WT C57/BL6J mice were pretreated with PTS (10 mg/kg) and afterwards with DOX (20 mg/kg cumulative dose) for 6 days. Immunochemistry staining of the liver sections with anti-NLRP3 (left, scale bar = 50 μm), the quantification of NLRP3 positive area in each group (right, $n = 6$); **(B)** qPCR analyses of NLRP3, IL-1β and IL-18 mRNA levels in each group ($n = 6$); **(C)** Western blot analyses of NLRP3, ASC, Caspase-1 p20, IL-1β, and IL-18 proteins and the quantification of the blots in each group ($n = 4$ per group); **(D)** Western blot analyses of Cleaved Caspase-3, BAX, and BCL-2 proteins (left) and quantification of the blots in each group (right, $n = 4$ per group).

before treatment with DOX (5 μM) for 24 h (Song S. et al., 2019). DOX group cells were cultured without PTS pretreatment and the control group was cultured in serum-free DMEM under normal conditions during the entire experiment. Cells were loaded with 10 μM DCFH-DA. After that, the cells were washed 3 times with serum-free DMEM and the images were captured by fluorescence microscopy (Olympus, Japan) with a 200 × overall magnification.

TUNEL Assay for HepG2 Apoptosis

HepG2 cell apoptosis detection was performed by using TUNEL staining (Green, Beyotime Biotechnology) and the assay was performed according to the manufacturer's instructions. For this, HepG2 cells were plated in 6-well culture plates for 24 h and afterwards treated with PTS at a concentration of 10 μM for 4 h before the treatment with DOX (5 μM) for 24 h. After that, the cells were washed 3 times with PBS and fixed with 4% PFA for 30 min after which the cells were washed 3 times with PBS. Afterwards, the cells were treated with 0.3% Triton X-100 containing PBS solution for 5 min, washed with PBS 3 times and finally the cells were incubated with the TUNEL reaction mixture for 60 min at 37°C in the dark. The cells were evaluated under a fluorescence microscope.

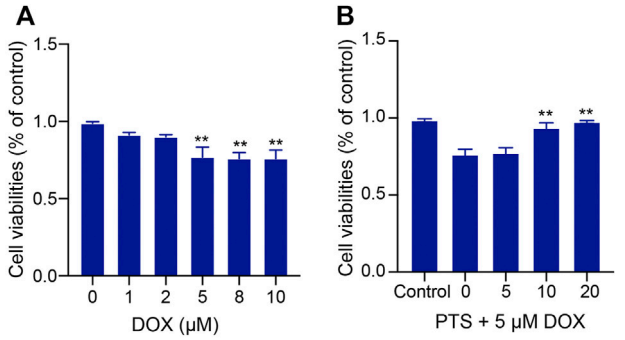

FIGURE 3 | Effect of PTS treatment on cell viability in DOX-treated HepG2 cells. **(A)**. Effects of different DOX dose (0, 1, 2, 5, 8, 10 μM) - induced hepatotoxicity on HepG2 cells ($n = 3$); **(B)** PTS effects (0, 5, 10, and 20 μM) on DOX-induced HepG2 cell viability ($n = 3$). $^{**}p < 0.01$ versus control group.

Biochemical Analysis

All mice were sacrificed under anesthesia after our study period. The serum of the animals was collected, and AST and ALT were measured by employing commercially available biochemical kits that were used according to the manufacturer's instructions.

Western Blot Assay

Total proteins were extracted from snap-frozen liver tissues or cells. We use a protein extraction kit (Keygenbio, KGP250) and centrifuge tube (Guangzhou Jet Bio-Filtration Co., Ltd.) for proteins extracting. The protein lysates (30 μg) were separated by electrophoresis in an 8–15% SDS–PAGE gel and transferred to polyvinylidene difluoride (PVDF) membranes. The blots were incubated with appropriate antibodies at 4°C overnight and then incubated with a goat anti-rabbit or mouse conjugated secondary antibody (Sino Biological Inc., 1:3000). All blots were developed using an ECL Plus chemiluminescence system. The following antibodies were used: anti-Trx-1 (CST, #2429, 1:800), anti-NLRP3 (CST, #15101, 1:800), Caspase-1 p20 (Affinity, AF5418, 1:500), IL-1β (Wanleibio, WL0227, 1:500), IL-18 (Wanleibio, WL01127, 1:1000), ASC (Wanleibio, WL02462, 1:500), BAX (CST, #14796S, 1:500), BCL-2 (CST, #3498S, 1:500) and Cleaved Caspase-3 (CST, #9664, 1:500). ImageJ software was used for densitometry analysis and GAPDH was used as an internal control.

Real-Time PCR Assay

According to the manufacturer's instructions, we used TRIzol reagent (Invitrogen, New York) to purify the total RNA from the fresh livers and cells. The first-strand cDNA (1–2 μg) was synthesized using a Superscript II kit (TAKARA, Japan). All the primers were synthesized by Sangon Biotech Company (Shanghai, China). The primer sequences were as follows: NLRP3: forward 5′-AGC CAA GAA TCC ACA GTG TAA CC-3′ and reverse 5′-AGT GTT GCC TCG CAG GTA AG-3′; IL-1β: forward 5′-TGC CAC CTT TTG ACA GTG ATG-3′ and reverse 5′-TTC TTG TGA CCC TGA GCG AC-3′; IL-18: forward 5′- GCA AAG CTT ATG ACC ATG AGA CAC AAC TG-3′ and reverse 5′-GCG AAT TCG TCG ACT TTA ACC CTG CTG TGG ACT-3′; NOX-1: forward 5′-GCT ACG CCT TCA ACA CCA AG-3′ and reverse 5′-AGT TCG TCC CCT TCT CCT GT-3′; NOX-4: forward 5′-GCA CGC TGT TGA TTT TTA TGG-3′ and reverse 5′-GCG AGG CAG GAG AGT CAG TA-3′; GAPDH: forward 5′-CAT CAA GAA GGT GGT GAA-3′ and reverse 5′-TGT TGA AGT CAG AGG AGA-3′. We used GAPDH as the internal control and normalized the resulting transcript levels to those of GAPDH gene. The results were analyzed using the ΔΔCt technique.

Statistics

All data are expressed as the mean ± SD. The statistical analyses were performed with GraphPad Prism 9 software. One-way ANOVA followed by Tukey's comparison test was used to analyze significant differences among multiple groups. Values of $p < 0.05$ were considered as being statistically significantly different.

RESULTS

Treatment with PTS Suppresses DOX-Induced Hepatotoxicity, Fibrosis and Oxidative Stress Injury in Mice

To explore the effects of PTS on DOX-induced hepatotoxicity, we pre-treated the mice with PTS (10 mg/kg) before DOX administration (**Figure 1A**). H & E staining (**Figure 1B**) revealed that the liver of control group mice displayed a normal architecture whereas apparent injuries were found in the DOX-treated group that could be restored by PTS. In addition, Masson staining revealed that administration of DOX in mice markedly increased the collagen deposition compared to the control group and that PTS remarkably reduced the DOX-induced fibrosis (**Figure 1C**). As shown in **Figure 1D**, after treatment with DOX, compared with the control group, the levels of ALT and AST were increased, respectively. The pre-treatment of PTS significantly reduced the ALT and AST levels in mice compared to the DOX-treated group. We next detected the expression of Trx-1 protein. Compared to the control group, the expression of Trx-1 was obviously decreased after DOX treatment but could be rescued by PTS (**Figure 1E**). We next evaluated the SOD, GSH, and MDA levels in DOX-treated mice. As shown in **Figure 1F**, the SOD and GSH levels were both markedly decreased after treatment with DOX compared to the control group and the MDA level in the DOX-treated group was higher than that of the control group. After PTS treatment, the level of MDA was decreased and the levels of SOD and GSH were both increased compared to the DOX-treated group. Therefore, PTS was able to prevent the increase in ROS and the decrease of Trx-1 in DOX-treated mice.

PTS Application Alleviates the Inflammation Reaction and Cell Apoptosis in DOX-Treated Mice

Oxidative stress frequently results in inflammatory reactions (Ventura et al., 2017). To further elucidate the effects of PTS,

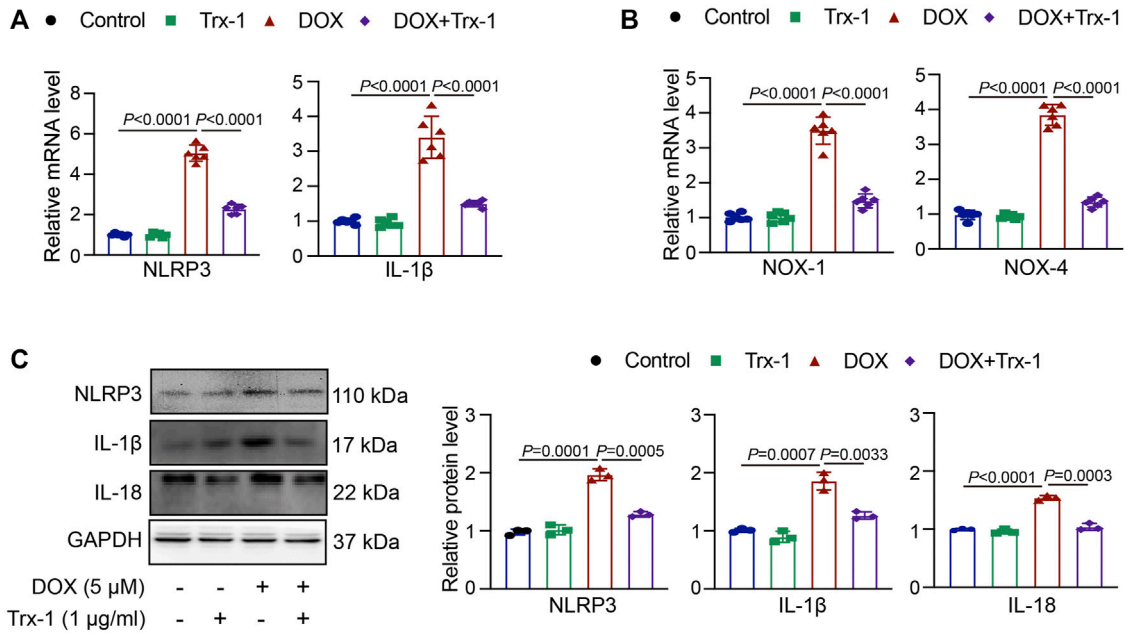

FIGURE 4 | DOX-induced damage in HepG2 cells through Trx-1/NLRP3 signaling. **(A)** HepG2 cells were pretreated with recombinant Trx-1 (1 μg/ml) for 4 h afterwards with DOX (5 μM) for 24 h qPCR analyses of NLRP3 and IL-1β mRNA levels after application of recombinant Trx-1 in DOX-treated cells (n = 6); **(B)** qPCR analyses of NOX-1 and NOX-4 mRNA levels after application of recombinant Trx-1 in DOX-treated cells (n = 6); **(C)** Western blot analyses of NLRP3, IL-1β, and IL-18 protein expressions after application of recombinant Trx-1 in DOX-treated cells (left, n = 3), the quantification of NLRP3, IL-1β, and IL-18 protein expressions (right, n = 3).

we performed immunohistochemical staining to detect the expression of NLRP3 in DOX-treated mice. As shown in **Figure 2A**, the expression of NLRP3 was upregulated in the DOX-treated group and PTS was able to alleviate the increase in NLRP3 expression. We then evaluated the levels of NLRP3, IL-1β, and IL-18 mRNA. As shown in **Figure 2B**, PTS significantly reduced the levels of NLRP3, IL-1β and IL-18 mRNA compared to those in the DOX-treated group. In addition, we evaluated the expressions of NLRP3 and its downstream proteins. Compared to the DOX-treated group, the expression of NLRP3, ASC, Caspase-1 p20, IL-1β, and IL-18 was significantly decreased after pretreatment with PTS (**Figure 2C**). In addition, we detected the expressions of Cleaved Caspase-3, BAX, and BCL-2 proteins. As shown in **Figure 2D**, the expression of Cleaved Caspase-3 and BAX were increased, and the expression of BCL-2 was significantly decreased after treatment with DOX. Compared to the DOX-treated mice, the pretreatment of PTS reduced the expression of BAX and upregulated the expression of BCL-2.

PTS Pretreatment Rescues DOX-Induced Cell Viability Inhibition

HepG2 cells were treated with different DOX doses (0, 1, 2, 5, 8, 10 μM) for 24 h. As shown in **Figure 3A**, the viability of HepG2 cells treated with 5 μM DOX for 24 h was decreased to nearly 75%, which is why we treated the cells in the following experiments with 5 μM DOX. We used PTS at concentrations of 0, 5, 10, and 20 μM to check whether PTS could protect cells against DOX-induced injury in a dose dependent manner. HepG2 cells were pretreated with different PTS concentrations for 4 h and afterwards treated with DOX (5 μM) for 24 h. Compared to the DOX-treated group, PTS at a 10 and 20 μM concentration significantly increased the viability of HepG2 cells (**Figure 3B**) so that we treated the cells in the following experiments with a PTS concentration of 10 μM.

DOX Induces Inflammation in HepG2 Cells by Reducing the Trx-1 Expression

To clarify whether the DOX-induced upregulation of NLRP3 was mediated by the reduction in Trx-1 levels, we pretreated the HepG2 cells with recombinant Trx-1 (1 μg/ml) for 4 h and afterwards with DOX (5 μM) for 24 h. Upon administration of recombinant Trx-1, the levels of both NOX-1 and NOX-4 were decreased compared to those of the DOX-treated group (**Figure 4A**). As shown in **Figure 4B**, this was also true for the NLRP3 and IL-1β mRNA levels. Similarly, the expressions of NLRP3, IL-1β, and IL-18 protein were decreased (**Figure 4C**). The results confirmed that the upregulation of Trx-1 was able to decrease the NLRP3 signal and inflammasome stimulation.

PTS inhibits DOX-induced oxidative stress in cells through increasing Trx-1 expression.

We used a DCFH-DA staining to detect the effect of PTS on DOX-treated cells. HepG2 cells were pretreated with PTS (10 μM) for 4 h and afterwards treated with DOX (5 μM)

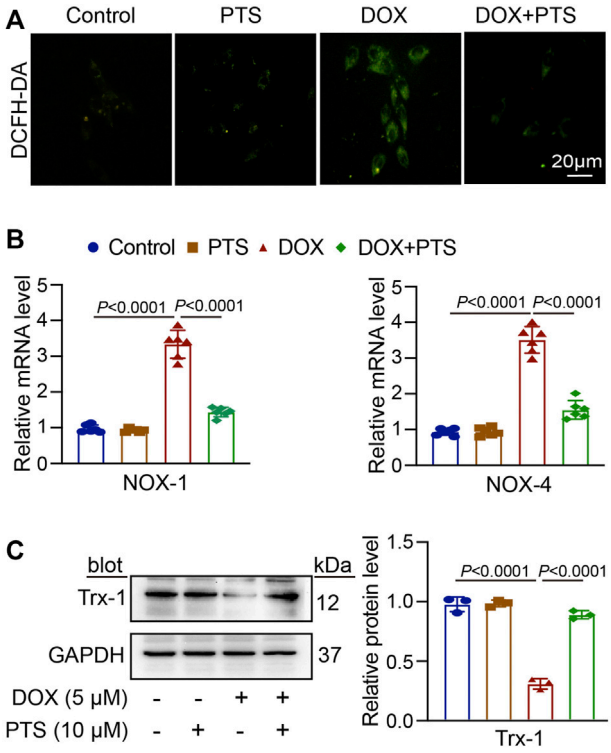

FIGURE 5 | PTS increases the expression of Trx-1 and prevents oxidative damage in DOX-treated HepG2 cells. **(A)** HepG2 cells were pretreated with PTS (10 μM) for 4 h and afterwards with DOX (5 μM) for 24 h. DCFH-DA staining of each group was analyzed to detect possible effects of PTS on the ROS level in DOX-treated HepG2 cells ($n = 3$); **(B)** PTS effects on NOX-1 and NOX-4 mRNA levels in DOX-treated HepG2 cells ($n = 6$); **(C)** PTS effects on Trx-1 protein expression in DOX-treated HepG2 cells (left, $n = 3$), quantification of Trx-1 protein expression (right, $n = 3$).

for 24 h. As shown in **Figure 5A**, treatment with DOX increased the ROS level in HepG2 cells compared to the control group. After pretreatment with PTS, the cellular ROS levels were significantly decreased compared to those in the DOX-treated group. Moreover, after treatment with DOX, the NOX-1 and NOX-4 mRNA levels were both increased compared to the control group. After pretreatment with PTS, NOX-1 and NOX-4 mRNA levels were decreased compared to those in the DOX-treated group (**Figure 5B**). We next analyzed the expression of Trx-1. As shown in **Figure 5C**, DOX induced the downregulation of Trx-1 and PTS pretreatment was able to rescue the expression of Trx-1.

PTS Relieves the Inflammatory Reaction in DOX-Treated Cells

A TUNEL assay was used to detect apoptosis in DOX-treated HepG2 cells and the protective effects of PTS. For this, HepG2 cells were pretreated with PTS (10 μM) for 4 h whereafter they were treated with DOX (5 μM) for 24 h. As shown in **Figure 6A**, DOX induced HepG2 cell apoptosis which could be reverted by pretreatment with PTS. Compared to the control group, the NLRP3 and IL-1β mRNA levels were markedly increased after DOX treatment and this effect was inhibited by PTS. Similarly, the expression of NLRP3, Caspase-1 p20, IL-1β, and IL-18 were significantly decreased after PTS treatment (**Figure 6B**).

DISCUSSION

DOX is a potent anti-cancer agent and has been widely used in chemotherapeutic treatment regimens against breast, gastric, thyroid, lung, and ovarian cancers (Pugazhendhi et al., 2018; Tacar et al., 2013). However, DOX may cause a range of significant side effects in normal tissues one of which is hepatotoxicity (Prathumsap et al., 2020; Wang et al., 2010; Prasanna et al., 2020; Ingawale et al., 2014; Pingili et al., 2019). Several studies have shown that the protective effect of anti-oxidant agents against DOX-induced hepatotoxicity is mediated *via* regulatory mechanisms related to oxidative stress and inflammation (Jeon et al., 2014; Wang R. et al., 2019). PTS is a natural stilbene derived from resveratrol that displays a higher oral bioavailability and bioactivity but is far less abundant in natural sources (Liu H. et al., 2019). The molecule exerts diverse pharmacological activities, comprising anti-oxidation and anti-inflammation effects (Song L. et al., 2019). Previous studies showed that PTS was able to prevent hepatocyte epithelial-mesenchymal transition in fructose-induced liver fibrosis through modulating the Sirt1/p53 and TGF-β/Smads signaling pathway (Song et al., 2019). We found that a mice pretreatment with PTS was able to decrease a DOX-induced fibrosis (**Figure 1C**). PTS also can reverse palmitic acid mediated insulin resistance in HepG2 cells by reducing oxidative stress (Malik et al., 2019). In addition, Dong et al. have found that PTS was able to ameliorate DOX mediated cardiotoxicity by reducing oxidative stress (Liu et al., 2020).

In our study, we applied PTS to explore the protective effects in DOX-induced hepatotoxicity. Due to previous reports, we chose a single DOX dose to induce hepatotoxicity. The DOX dose (20 mg/kg) is based on the clinical data for treating cancer patients (Chen et al., 2016). Moreover, we chose a single PTS dose (10 mg/kg) to detect the protective effects on DOX-induced hepatotoxicity (Yang et al., 2016). However, due to the fact that a single dose treatment has some limitations, future experiments will evaluate the protective effect of a repeated dosage. In this study, we could show that the serum ALT and AST levels both were decreased after PTS treatment in the DOX-treated group. PTS treatment also alleviated DOX-induced histopathological changes in mice. The results imply that PTS has protective effects by inhibiting DOX-induced hepatotoxicity, however, the mechanisms are complex.

Several groups reported that DOX-induced hepatotoxicity was resulting from ROS over-production, the imbalance between pro-oxidant and anti-oxidant molecule concentrations and inflammation over-activation (Lu and Holmgren, 2014). Trx-1 is an evolutionarily conserved protein disulfide reductase. Using two cysteines at catalytic centers 32 and 35, Trx-1 cuts the

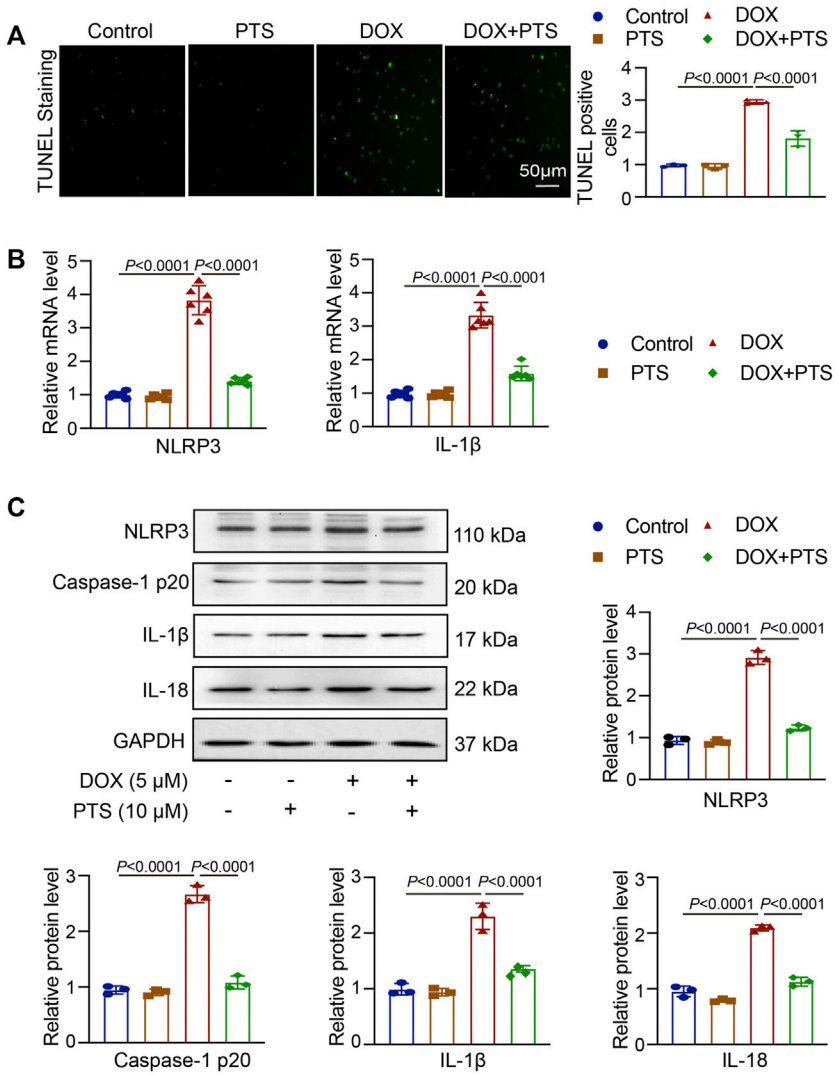

FIGURE 6 | PTS effects on NLRP3 inflammasome expression in DOX-treated HepG2 cells. **(A)** HepG2 cells were pretreated with PTS (10 μM) for 4 h and afterwards with DOX (5 μM) for 24 h. The cells were analyzed by TUNEL staining to detect apoptosis in DOX-treated HepG2 cells and the protective effects of PTS against DOX-induced apoptosis (left), relative quantification of TUNEL positive cells (right, $n = 3$); **(B)** PTS effects on NLRP3 and IL-1β mRNA levels in DOX-treated HepG2 cells ($n = 6$); **(C)** PTS effects on NLRP3, IL-1β, and IL-18 protein expression in DOX-treated HepG2 cells ($n = 3$); quantification of NLRP3, IL-1β, and IL-18 protein expressions ($n = 3$).

disulfide bonds of oxidized proteins and forms disulfide bonds in Trx-1 (Oka et al., 2020). Trx-1 has been considered as an important protective system against oxidative stress (El Hadri et al., 2012) and is also involved in controlling inflammatory responses (Ito et al., 2011). The NLRP3 inflammasome is a multi-component assembly composed of NLRP3, ASC, and Caspase-1 precursor (Zhang et al., 2021) and has been reported to be involved in the pathogenesis of liver injury (Iskusnykh et al., 2021). Trx-1 could inhibit the NLRP3 inflammasome leading to an attenuation of atherosclerosis and was able to exert protective effects (Wang et al., 2020). In our study, we found that after DOX treatment, the SOD and GSH levels were both markedly decreased, whereas the MDA level was increased, both of which were ameliorated by PTS in mice livers. We next measured the expression of Trx-1, the results showed that DOX treatment downregulated Trx-1 expression and that PTS could recuperate Trx-1 expression (**Figure 1**). Therefore, in our study, we next tested the expression of NLRP3 and its downstream proteins ASC, Caspase-1, IL-1β, and IL-18. The results showed that DOX upregulated the expression of NLRP3 inflammasome and that PTS decreased its stimulation (**Figure 2**). Consequently, inhibiting oxidative stress and inflammation reactions by influencing the Trx-1/NLRP3 signaling pathway might be the way how PTS is able to reduce the DOX-induced hepatotoxicity. Recent studies have found that Trx-1 was able to inhibit apoptosis through redox regulation and inflammation (Bai et al., 2021). We, therefore, evaluated the expression of Cleaved Caspase-3, BAX, and BCL-2 proteins

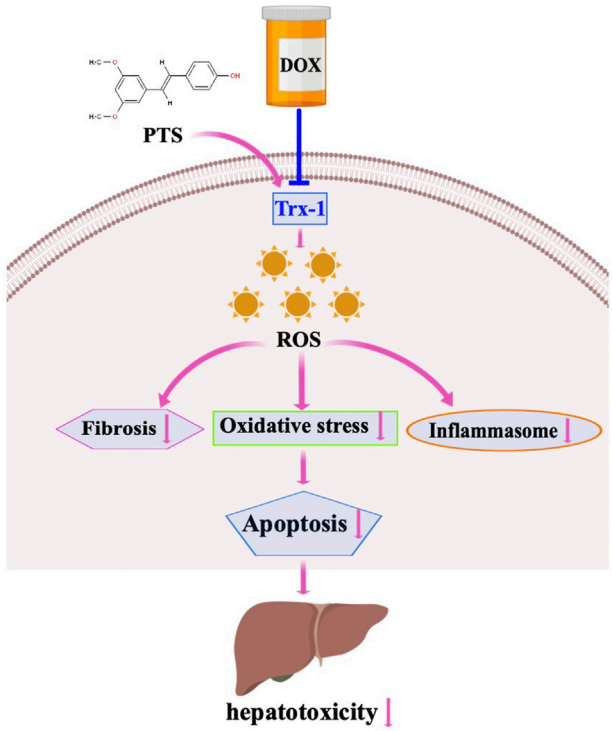

FIGURE 7 | Working model for PTS in the regulation of DOX-induced hepatotoxicity. DOX treatment induced fibrosis, oxidative stress and inflammasome stimulation which resulted in hepatotoxicity through downregulation of Trx-1. PTS is able to reduce fibrosis, oxidative stress, and inflammasome stimulation through increasing Trx-1 levels. PTS may be used as an agent to protect against DOX-induced hepatotoxicity.

and found PTS was able to protect mice against DOX-induced apoptosis. The results confirmed that PTS could increase the expression of Trx-1 leading to a decreased ROS level and a stimulation of the inflammasome which in turn inhibited apoptosis in DOX-treated mice (**Figures 1**, **2**).

To further confirm the mechanisms and the protective effects of PTS in DOX-induced liver damage, we treated HepG2 cells with recombinant Trx-1. The results suggest that the Trx-1 overexpression can significantly decrease the oxidative injury and to modulate the expression of the NLRP3 inflammasome (**Figure 3**). PTS pretreatment has similar effects to recombinant Trx-1 - they both raised the expression of Trx-1 in DOX-treated cells. The upregulation of Trx-1 led to a reduction of ROS production, inflammasome, and apoptosis (**Figures 5**, **6**). Taken Together, the protective effects of PTS in DOX-induced hepatotoxicity might be attributable to its anti-oxidative, anti-inflammatory, anti-fibrotic, and anti-apoptotic effects mediated by an increase in the expression of Trx-1 and activation of the Trx-1/NLRP3 signaling pathway (**Figure 7**). However, the detailed mechanism of PTS action in DOX-induced hepatotoxicity and its clinical application requires further studies. In conclusion, these results might point into a new direction in the therapy of this disease.

DATA AVAILABILITY STATEMENT

The original contributions presented in the study are included in the article/**Supplementary Material**, further inquiries can be directed to the corresponding authors.

ETHICS STATEMENT

The animal study was reviewed and approved by Animal experiments were conducted in accordance with the standards approved by the Institutional Animal Care and Use Committee of the University of Dalian Medical University (SCXK 2015-2003) and in accordance with the Protection of Animals Act and the National Institutes of Health Guide (NIH Publication No. 85-23) for the Care and Use of Laboratory Animals.

AUTHOR CONTRIBUTIONS

ST and JB organized and analyzed the data and made diagrams, carried out the molecular biology experiments and the experiments in vitro; MX carried out the histopathological staining and the experiments in vitro; LZ and YW drafted the article and revised the manuscript and approval of version to be published. All authors read and approved the final manuscript.

SUPPLEMENTARY MATERIAL

The Supplementary Material for this article can be found online at: https://www.frontiersin.org/articles/10.3389/fphar.2022.841330/full#supplementary-material

REFERENCES

Bai, L., Yan, F., Deng, R., Gu, R., Zhang, X., and Bai, J. (2021). Thioredoxin-1 Rescues MPP+/MPTP-Induced Ferroptosis by Increasing Glutathione Peroxidase 4. *Mol. Neurobiol.* 58 (7), 3187–3197. doi:10.1007/s12035-021-02320-1

Carvalho, C., Santos, R. X., Cardoso, S., Correia, S., Oliveira, P. J., Santos, M. S., et al. (2009). Doxorubicin: the Good, the Bad and the Ugly Effect. *Curr. Med. Chem.* 16 (25), 3267–3285. doi:10.2174/092986709788803312

Chen, X., Zhang, Y., Zhu, Z., Liu, H., Guo, H., Xiong, C., et al. (2016). Protective Effect of Berberine on Doxorubicin-induced A-cute H-epatorenal T-oxicity in R-ats. *Mol. Med. Rep.* 13 (5), 3953–3960. doi:10.3892/mmr.2016.5017

Chen, Z., Zhong, H., Wei, J., Lin, S., Zong, Z., Gong, F., et al. (2019). Inhibition of Nrf2/HO-1 Signaling Leads to Increased Activation of the NLRP3 Inflammasome in Osteoarthritis. *Arthritis Res. Ther.* 21 (1), 300. doi:10.1186/s13075-019-2085-6

El Hadri, K., Mahmood, D. F., Couchie, D., Jguirim-Souissi, I., Genze, F., Diderot, V., et al. (2012). Thioredoxin-1 Promotes Anti-inflammatory Macrophages of the M2 Phenotype and Antagonizes Atherosclerosis. *Arterioscler Thromb. Vasc. Biol.* 32 (6), 1445–1452. doi:10.1161/ATVBAHA.112.249334

Estrela, J. M., Ortega, A., Mena, S., Rodriguez, M. L., and Asensi, M. (2013). Pterostilbene: Biomedical Applications. *Crit. Rev. Clin. Lab. Sci.* 50 (3), 65–78. doi:10.3109/10408363.2013.805182

Gómez-Zorita, S., Milton-Laskíbar, I., Aguirre, L., Fernández-Quintela, A., Xiao, J., and Portillo, M. P. (2020). Effects of Pterostilbene on Diabetes, Liver Steatosis and Serum Lipids. *Cmc* 28 (2), 238–252. doi:10.2174/0929867326666191029112626

Hashemy, S. I., and Holmgren, A. (2008). Regulation of the Catalytic Activity and Structure of Human Thioredoxin 1 *via* Oxidation and S-Nitrosylation of Cysteine Residues. *J. Biol. Chem.* 283 (32), 21890–21898. doi:10.1074/jbc.M801047200

Ingawale, D. K., Mandlik, S. K., and Naik, S. R. (2014). Models of Hepatotoxicity and the Underlying Cellular, Biochemical and Immunological Mechanism(s): a Critical Discussion. *Environ. Toxicol. Pharmacol.* 37 (1), 118–133. doi:10.1016/j.etap.2013.08.015

Iskusnykh, I. Y., Kryl'skii, E. D., Brazhnikova, D. A., Popova, T. N., Shikhaliev, K. S., Shulgin, K. K., et al. (2021). Novel Antioxidant, Deethylated Ethoxyquin, Protects against Carbon Tetrachloride Induced Hepatotoxicity in Rats by Inhibiting NLRP3 Inflammasome Activation and Apoptosis. *Antioxidants* 10 (1), 122. doi:10.3390/antiox10010122

Ito, W., Kobayashi, N., Takeda, M., Ueki, S., Kayaba, H., Nakamura, H., et al. (2011). Thioredoxin in Allergic Inflammation. *Int. Arch. Allergy Immunol.* 155 (Suppl. 1), 142–146. doi:10.1159/000327501

Jeon, B. T., Kim, K. E., Heo, R. W., Shin, H. J., Yi, C. O., Hah, Y. S., et al. (2014). Myeloid-specific Deletion of SIRT1 Increases Hepatic Steatosis and Hypothalamic Inflammation in Mice Fed a High-Fat Diet. *Metab. Brain Dis.* 29 (3), 635–643. doi:10.1007/s11011-014-9542-3

Kolarovic, J., Popovic, M., Mikov, M., Mitic, R., and Gvozdenovic, L. (2009). Protective Effects of Celery Juice in Treatments with Doxorubicin. *Molecules* 14 (4), 1627–1638. doi:10.3390/molecules14041627

Lange, K. W., and Li, S. (2018). Resveratrol, Pterostilbene, and Dementia. *Biofactors* 44 (1), 83–90. doi:10.1002/biof.1396

Liu, D., Ma, Z., Xu, L., Zhang, X., Qiao, S., and Yuan, J. (2019a). PGC1α Activation by Pterostilbene Ameliorates Acute Doxorubicin Cardiotoxicity by Reducing Oxidative Stress *via* Enhancing AMPK and SIRT1 Cascades. *Aging (Albany NY)* 11 (22), 10061–10073. doi:10.18632/aging.102418

Liu, H., Wu, X., Luo, J., Wang, X., Guo, H., Feng, D., et al. (2019b). Pterostilbene Attenuates Astrocytic Inflammation and Neuronal Oxidative Injury after Ischemia-Reperfusion by Inhibiting NF-Kb Phosphorylation. *Front. Immunol.* 10, 2408. doi:10.3389/fimmu.2019.02408

Lu, J., and Holmgren, A. (2014). The Thioredoxin Antioxidant System. *Free Radic. Biol. Med.* 66, 75–87. doi:10.1016/j.freeradbiomed.2013.07.036

Lu, Y., Li, Y., Liu, Q., Tian, N., Du, P., Zhu, F., et al. (2021). MondoA-Thioredoxin-Interacting Protein Axis Maintains Regulatory T-Cell Identity and Function in Colorectal Cancer Microenvironment. *Gastroenterology* 161 (2), 575–e16. doi:10.1053/j.gastro.2021.04.041

Malik, S. A., Acharya, J. D., Mehendale, N. K., Kamat, S. S., and Ghaskadbi, S. S. (2019). Pterostilbene Reverses Palmitic Acid Mediated Insulin Resistance in HepG2 Cells by Reducing Oxidative Stress and Triglyceride Accumulation. *Free Radic. Res.* 53 (7), 815–827. doi:10.1080/10715762.2019.1635252

McCormack, D., and McFadden, D. (2012). Pterostilbene and Cancer: Current Review. *J. Surg. Res.* 173 (2), e53–61. doi:10.1016/j.jss.2011.09.054

Oka, S. I., Chin, A., Park, J. Y., Ikeda, S., Mizushima, W., Ralda, G., et al. (2020). Thioredoxin-1 Maintains Mitochondrial Function *via* Mechanistic Target of Rapamycin Signalling in the Heart. *Cardiovasc. Res.* 116 (10), 1742–1755. doi:10.1093/cvr/cvz251

Perkins, A., Poole, L. B., and Karplus, P. A. (2014). Tuning of Peroxiredoxin Catalysis for Various Physiological Roles. *Biochemistry* 53 (49), 7693–7705. doi:10.1021/bi5013222

Pilco-Ferreto, N., and Calaf, G. M. (2016). Influence of Doxorubicin on Apoptosis and Oxidative Stress in Breast Cancer Cell Lines. *Int. J. Oncol.* 49 (2), 753–762. doi:10.3892/ijo.2016.3558

Pillay, C. S., Hofmeyr, J. H., and Rohwer, J. M. (2011). The Logic of Kinetic Regulation in the Thioredoxin System. *BMC Syst. Biol.* 5, 15. doi:10.1186/1752-0509-5-15

Pingili, R. B., Pawar, A. K., Challa, S. R., Kodali, T., Koppula, S., and Toleti, V. (2019). A Comprehensive Review on Hepatoprotective and Nephroprotective Activities of Chrysin against Various Drugs and Toxic Agents. *Chem. Biol. Interact* 308, 51–60. doi:10.1016/j.cbi.2019.05.010

Powis, G., and Montfort, W. R. (2001). Properties and Biological Activities of Thioredoxins. *Annu. Rev. Pharmacol. Toxicol.* 41, 261–295. doi:10.1146/annurev.pharmtox.41.1.261

Prasanna, P. L., Renu, K., and Valsala Gopalakrishnan, A. (2020). New Molecular and Biochemical Insights of Doxorubicin-Induced Hepatotoxicity. *Life Sci.* 250, 117599. doi:10.1016/j.lfs.2020.117599

Prathumsap, N., Shinlapawittayatorn, K., Chattipakorn, S. C., and Chattipakorn, N. (2020). Effects of Doxorubicin on the Heart: From Molecular Mechanisms to Intervention Strategies. *Eur. J. Pharmacol.* 866, 172818. doi:10.1016/j.ejphar.2019.172818

Pugazhendhi, A., Edison, T. N. J. I., Velmurugan, B. K., Jacob, J. A., and Karuppusamy, I. (2018). Toxicity of Doxorubicin (Dox) to Different Experimental Organ Systems. *Life Sci.* 200, 26–30. doi:10.1016/j.lfs.2018.03.023

Rivankar, S. (2014). An Overview of Doxorubicin Formulations in Cancer Therapy. *J. Cancer Res. Ther.* 10 (4), 853–858. doi:10.4103/0973-1482.139267

Song, L., Chen, T. Y., Zhao, X. J., Xu, Q., Jiao, R. Q., Li, J. M., et al. (2019a). Pterostilbene Prevents Hepatocyte Epithelial-Mesenchymal Transition in Fructose-Induced Liver Fibrosis through Suppressing miR-34a/Sirt1/p53 and TGF-β1/Smads Signalling. *Br. J. Pharmacol.* 176 (11), 1619–1634. doi:10.1111/bph.14573

Song, S., Chu, L., Liang, H., Chen, J., Liang, J., Huang, Z., et al. (2019b). Protective Effects of Dioscin against Doxorubicin-Induced Hepatotoxicity *via* Regulation of Sirt1/FOXO1/NF-Kb Signal. *Front. Pharmacol.* 10, 1030. doi:10.3389/fphar.2019.01030

Songbo, M., Lang, H., Xinyong, C., Bin, X., Ping, Z., and Liang, S. (2019). Oxidative Stress Injury in Doxorubicin-Induced Cardiotoxicity. *Toxicol. Lett.* 307, 41–48. doi:10.1016/j.toxlet.2019.02.013

Tacar, O., Sriamornsak, P., and Dass, C. R. (2013). Doxorubicin: an Update on Anticancer Molecular Action, Toxicity and Novel Drug Delivery Systems. *J. Pharm. Pharmacol.* 65 (2), 157–170. doi:10.1111/j.2042-7158.2012.01567.x

Ventura, M. T., Casciaro, M., Gangemi, S., and Buquicchio, R. (2017). Immunosenescence in Aging: between Immune Cells Depletion and Cytokines Up-Regulation. *Clin. Mol. Allergy* 15, 21. doi:10.1186/s12948-017-0077-0

Wang, R., Dong, Z., Lan, X., Liao, Z., and Chen, M. (2019a). Sweroside Alleviated LPS-Induced Inflammation *via* SIRT1 Mediating NF-Kb and FOXO1 Signaling Pathways in RAW264.7 Cells. *Molecules* 24 (5), 872. doi:10.3390/molecules24050872

Wang, X., Zhao, H., Yan, W., Liu, Y., Yin, T., Wang, S., et al. (2019b). Thioredoxin-1 Promotes Macrophage Reverse Cholesterol Transport and Protects Liver from Steatosis. *Biochem. Biophys. Res. Commun.* 516 (4), 1103–1109. doi:10.1016/j.bbrc.2019.06.109

Wang, Y., Ji, N., Gong, X., Ni, S., Xu, L., and Zhang, H. (2020). Thioredoxin-1 Attenuates Atherosclerosis Development through Inhibiting NLRP3 Inflammasome. *Endocrine* 70 (1), 65–70. doi:10.1007/s12020-020-02389-z

Wang, Y., Wei, X., Zhang, C., Zhang, F., and Liang, W. (2010). Nanoparticle Delivery Strategies to Target Doxorubicin to Tumor Cells and Reduce Side Effects. *Ther. Deliv.* 1 (2), 273–287. doi:10.4155/tde.10.24

Yang, F., Xu, J., Fu, M., Ji, J., Chi, L., and Zhai, G. (2020). Development of Stimuli-Responsive Intelligent Polymer Micelles for the Delivery of Doxorubicin. *J. Drug Target.* 28 (10), 993–1011. doi:10.1080/1061186X.2020.1766474

Yang, Y., Wang, J., Li, Y., Fan, C., Jiang, S., Zhao, L., et al. (2016). HO-1 Signaling Activation by Pterostilbene Treatment Attenuates Mitochondrial Oxidative Damage Induced by Cerebral Ischemia Reperfusion Injury. *Mol. Neurobiol.* 53 (4), 2339–2353. doi:10.1007/s12035-015-9194-2

Zhang, J., Qiu, T., Jiang, L., Wang, N., Zhu, Y., Yan, R., et al. (2021). NLRP3 Inflammasome Blocked the Glycolytic Pathway *via* Targeting to PKLR in Arsenic-Induced Hepatic Insulin Resistance. *Ecotoxicol Environ. Saf.* 223, 112590. doi:10.1016/j.ecoenv.2021.112590

Conflict of Interest: The authors declare that the research was conducted in the absence of any commercial or financial relationships that could be construed as a potential conflict of interest.

Publisher's Note: All claims expressed in this article are solely those of the authors and do not necessarily represent those of their affiliated organizations, or those of the publisher, the editors and the reviewers. Any product that may be evaluated in this article, or claim that may be made by its manufacturer, is not guaranteed or endorsed by the publisher.

frontiers | Frontiers in Pharmacology

ORIGINAL RESEARCH
published: 02 May 2022
doi: 10.3389/fphar.2022.851342

Artemether Ameliorates Non-Alcoholic Steatohepatitis by Repressing Lipogenesis, Inflammation, and Fibrosis in Mice

Jia Xu[1], *Xiaoyun He*[1,2], *Xianghui Huang*[1], *Feng Zhang*[1], *Xinxin Ren*[1], *Charles Asakiya*[1], *Yue Li*[3]* *and Kunlun Huang*[1,2]*

[1]*Key Laboratory of Precision Nutrition and Food Quality, Key Laboratory of Functional Dairy, Ministry of Education, College of Food Science and Nutritional Engineering, China Agricultural University, Beijing, China,* [2]*Key Laboratory of Safety Assessment of Genetically Modified Organism (Food Safety), The Ministry of Agriculture and Rural Affairs, Beijing, China,* [3]*Department of Pathology, Beijing Ditan Hospital, Capital Medical University, Beijing, China*

OPEN ACCESS

Edited by:
Runping Liu,
Beijing University of Chinese Medicine, China

Reviewed by:
Wen-Chung Huang,
Chang Gung University of Science and Technology, Taiwan
Yanping Li,
Sichuan University, China
Yao Wang,
Beijing University of Chinese Medicine, China

***Correspondence:**
Yue Li
liyuedl04@126.com
Kunlun Huang
foodsafety66@cau.edu.cn

Specialty section:
This article was submitted to Gastrointestinal and Hepatic Pharmacology, a section of the journal Frontiers in Pharmacology

Received: *09 January 2022*
Accepted: *22 March 2022*
Published: *02 May 2022*

Citation:
Xu J, He X, Huang X, Zhang F, Ren X, Asakiya C, Li Y and Huang K (2022) Artemether Ameliorates Non-Alcoholic Steatohepatitis by Repressing Lipogenesis, Inflammation, and Fibrosis in Mice. Front. Pharmacol. 13:851342. doi: 10.3389/fphar.2022.851342

Background: Non-alcoholic fatty liver disease (NAFLD) is a widespread disease, but no recognized drug treatment exists. Previous studies have shown that artemether (Art) can ameliorate carbon tetrachloride (CCl_4)–induced liver fibrosis in mice. This study sets out to observe the therapeutic impact of Art on non-alcoholic steatohepatitis (NASH).

Methods: Model mice were provided with a methionine- and choline-deficient (MCD) diet for 4 weeks or a high-fat diet (HFD) for 28 weeks, respectively, and then treated with Art. RNA sequencing (RNA-Seq) analyzed gene expression changes caused by Art treatment. The molecular mechanism of the therapeutic effects of Art on NASH was studied in the mouse liver and HepG2 cells.

Results: Art treatment significantly attenuated hepatic lipid accumulation and liver damage in MCD diet– or HFD-induced NASH mice. The RNA-Seq analysis revealed lipid metabolism as a major pathway suppressed by Art administration, in addition to the regulation of inflammation pathways. Mechanistically, Art reduced lipid accumulation by repressing *de novo* lipogenesis of sterol regulatory element-binding protein-1c (SREBP-1c), acetyl-CoA carboxylase (ACC), fatty acid synthase (FASN), stearoyl-CoA desaturase (SCD1), promoting lipolysis of peroxisome proliferator–activated receptor-γ co-activator-1α (PGC1α), adipose triglyceride lipase (ATGL), and carnitine palmitoyltransferase I (CPT-1a) in NASH mouse liver and HepG2 cells. In addition, Art inhibited the secretion of pro-inflammatory factors and reduced inflammatory infiltration by effectively inhibiting M1 macrophage activation. Furthermore, Art inhibited transforming growth factor-beta 1 (TGF-β), and the SMAD signaling pathway mediates the development of liver fibrosis.

Inclusion: Art improved fat deposition by repressing *de novo* lipogenesis and promoting lipolysis *in vivo* and *in vitro*. Furthermore, Art improved inflammation and fibrosis with a significant effect. It is a prospective therapeutic agent for NASH.

Keywords: artemether, non-alcoholic steatohepatitis, inflammation, liver fibrosis, lipid metabolism, lipogenesis

INTRODUCTION

Non-alcoholic fatty liver disease (NAFLD) is a pathologic syndrome that comprises non-alcoholic fatty liver (NAFL), non-alcoholic steatohepatitis (NASH), NASH-associated cirrhosis, and hepatocellular carcinoma (HCC). NAFLD is thought to be a hepatic demonstration of metabolic disorder and is often related to metabolic risk factors, such as obesity, dyslipidemia, hypertension, and diabetes (Chalasani et al., 2020). NAFLD is becoming a major chronic liver disease worldwide, with a

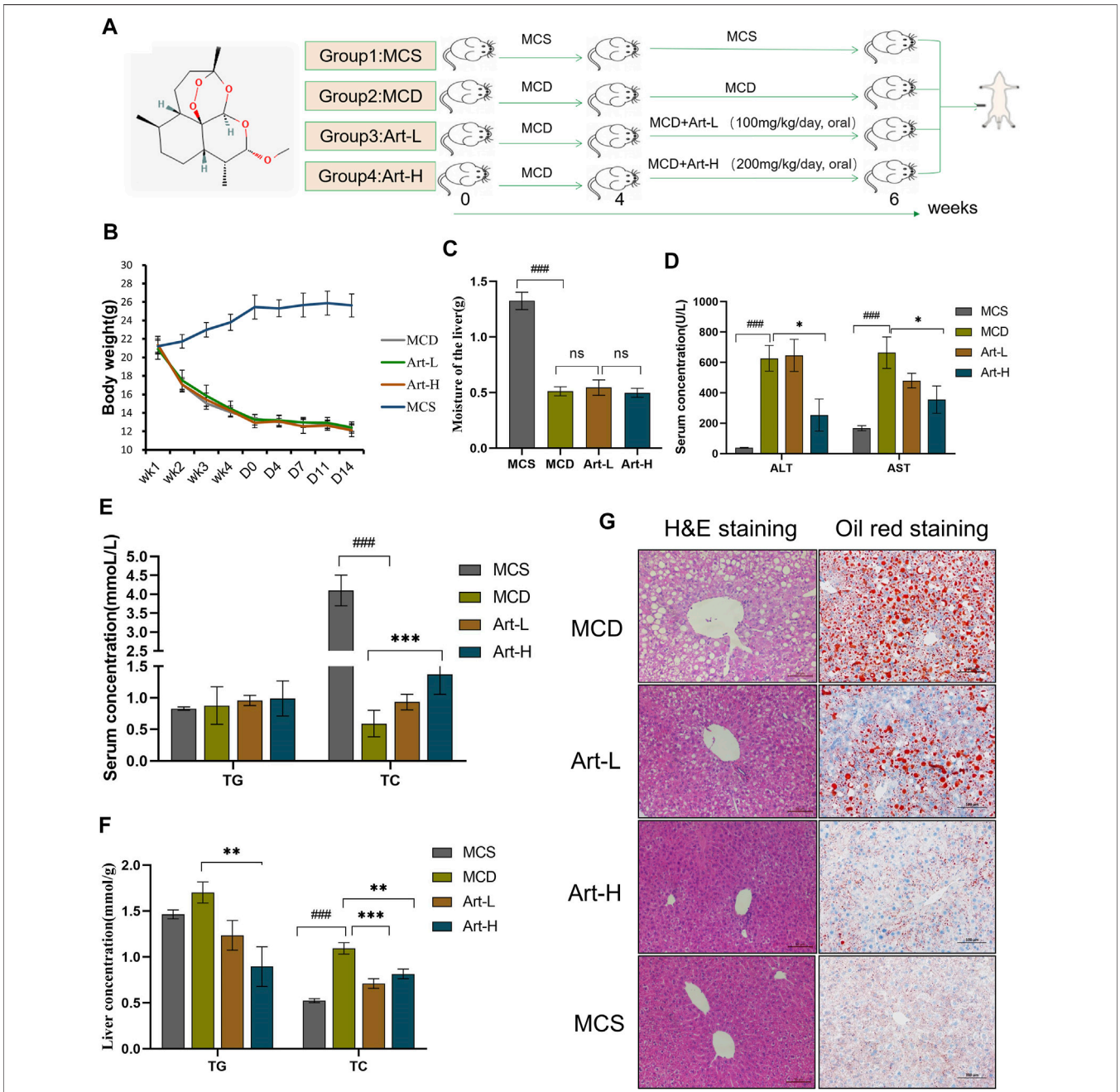

FIGURE 1 | Effect of Artemether treatment on hepatic injury and hepatic steatosis in the MCD model. **(A)** Experimental design: after 4 weeks of the MCD diet-induced NASH model, the experiment was divided into four groups: the MCD diet group (MCD); MCD diet coupled with low-dose artemether (Art-L) group: 100 mg/kg BW; MCD diet coupled with high-dose artemether (Art-H) group: 200 mg/kg BW, artemether gavage once daily for 2 weeks; and MCS control group (MCS) ($n = 6$). **(B)** Body weight change after dosing in mice. **(C)** Mouse liver weight. **(D)** Serum ALT and AST levels in mice. **(E)** Serum TG and TC concentrations in mice. **(F)** TG and TC concentrations in the liver. **(G)** From left to right, H&E staining of the liver (scale bar: 50 μM) and oil red O staining of the liver (scale bar: 50 μM). The MCS was compared with the MCD group: $^{\#}p < 0.05$, $^{\#\#}p < 0.01$, and $^{\#\#\#}p < 0.001$. MCD compared with Art-L and Art-H groups: $^{*}p < 0.05$, $^{**}p < 0.01$, and $^{***}p < 0.001$.

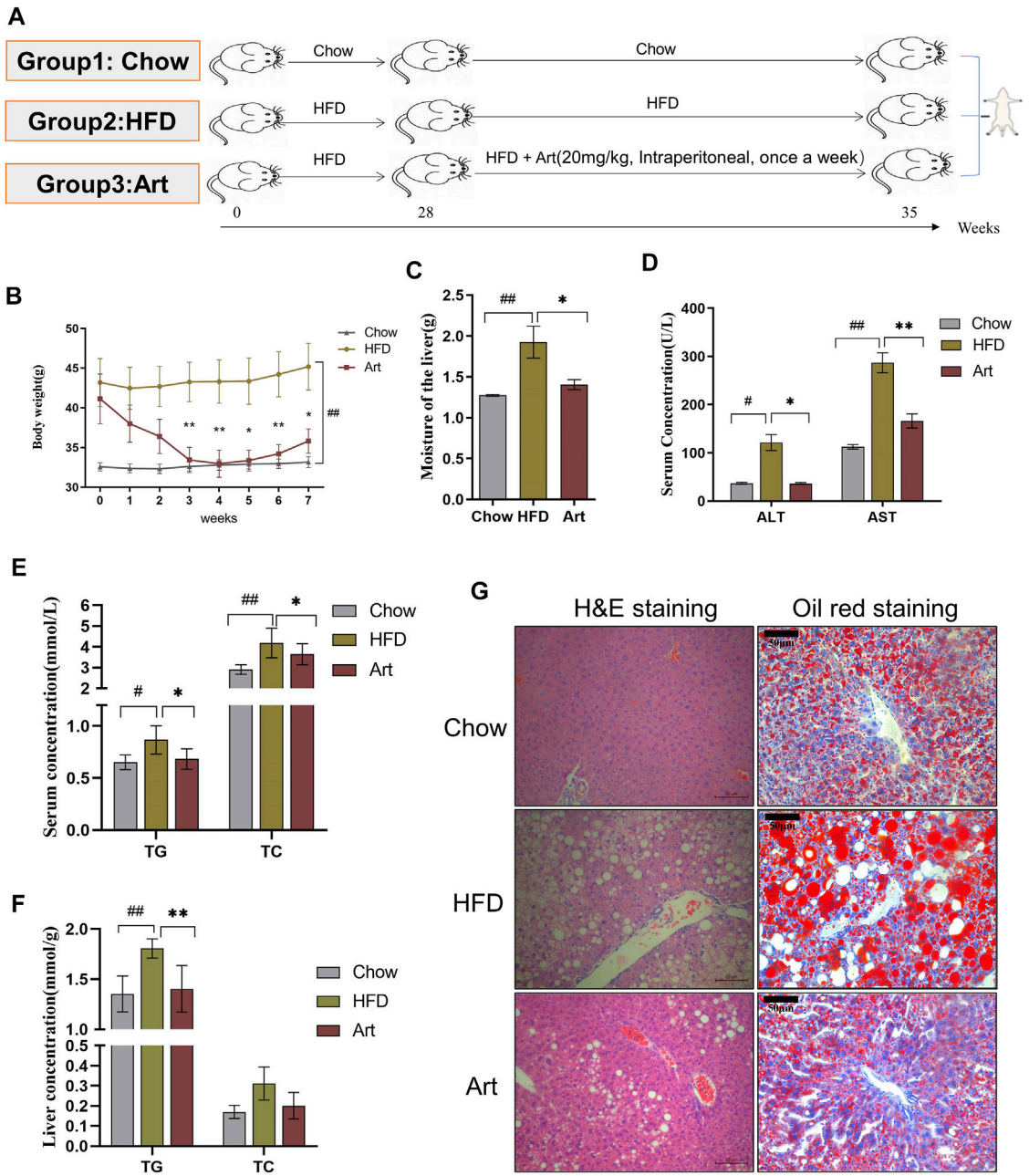

FIGURE 2 | Artemether improves hepatic steatosis and liver injury in NASH mice induced by a HFD. **(A)** Experiment design was divided into three groups: chow diet group (Chow), high-fat diet group (HFD), and high-fat diet combined with the artemether treatment group (Art): 20 mg/kg BW intraperitoneally once a week for 7 weeks ($n = 6$). **(B)** Body weight change after dosing. **(C)** Liver weight. **(D)** Serum ALT and AST levels. **(E)** Serum TG and TC levels. **(F)** TG and TC concentrations in the liver. **(G)** From left to right, H&E staining of the liver (scale bar, 50 μM) and oil red O staining of the liver (scale bar: 50 μM). The Chow group vs. the HFD group: $^{\#}p < 0.05$, $^{\#\#}p < 0.01$, and $^{\#\#\#}p < 0.001$. The Art group compared with the HFD group: $^{*}p < 0.05$, $^{**}p < 0.01$, and $^{***}p < 0.001$.

worldwide prevalence of around 25% of the adult population, and an important cause of liver transplantation for primary hepatocellular carcinoma (Paik et al., 2020; Loomba et al., 2021).

The theory of multiple hits has already been proposed in NAFLD (Loomba et al., 2021). Fatty acids are a substrate for lipotoxic substances when oversupply or elimination is impaired, causing endoplasmic reticulum stress, hepatocellular injury, and death (Pei et al., 2020). It has been shown that the main causes of hepatic fatty acid oversupply include insulin resistance (IR) (Chen et al., 2019), increased hepatic *de novo* lipogenesis (DNL) (Lambert et al., 2014), and intrahepatic lipolysis defects (e.g., decreased ATGL/CGI-58 activity and decreased hepatic mitochondrial/peroxisome beta-oxidation) (Schweiger et al., 2009). Therefore, it is important to identify the source and

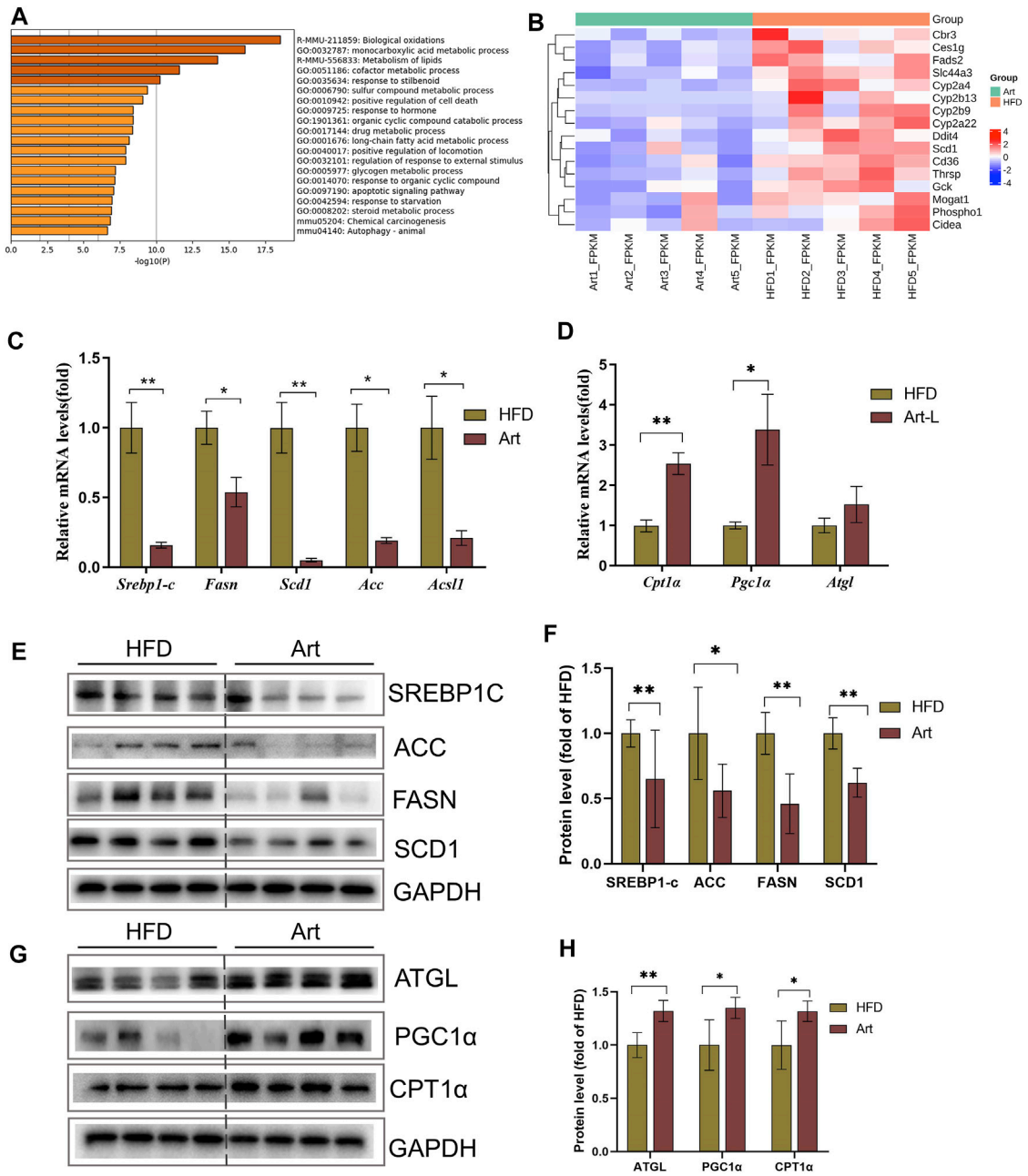

FIGURE 3 | Effect of artemether treatment on the liver lipid metabolic pathway in NASH mice induced by an HFD. **(A)** KEGG pathway enrichment of the differential gene. **(B)** Heat map of the free fatty acid metabolism-related gene. **(C,D)** Real-time PCR analysis of lipid synthesis-related genes **(C)** and lipolysis-related genes **(D)** in the liver. **(E–H)** Expression and quantification analysis of lipid synthesis-related protein **(E,F)** and lipid breakdown-related protein **(G,H)** in the liver were detected by western blot. $^{*}p < 0.05$, $^{**}p < 0.01$, and $^{***}p < 0.001$.

clearance mechanism of fatty acids in hepatocytes to understand the metabolic basis of NASH and to identify therapeutic targets. Several drugs have previously been developed to inhibit fatty acid metabolism genes, such as pioglitazone, thiazolidinediones, and Aramchol. Unfortunately, there is no currently approved drug treatment for NAFLD (Violi and Cangemi, 2010; Iruarrizaga-Lejarreta et al., 2017).

Plant extracts or natural products have been extensively studied in preventing or improving NAFLD (Li et al., 2021). Artemether is a derivative of artemisinin and has good lipid solubility (Jung et al., 2004). Artemether is currently primarily used to treat malaria and attempts to treat a variety of malignancies. Guo Y et al. (2018) found that artemether could improve the degree of hepatic steatosis, glucose homeostasis, and insulin resistance in db/db

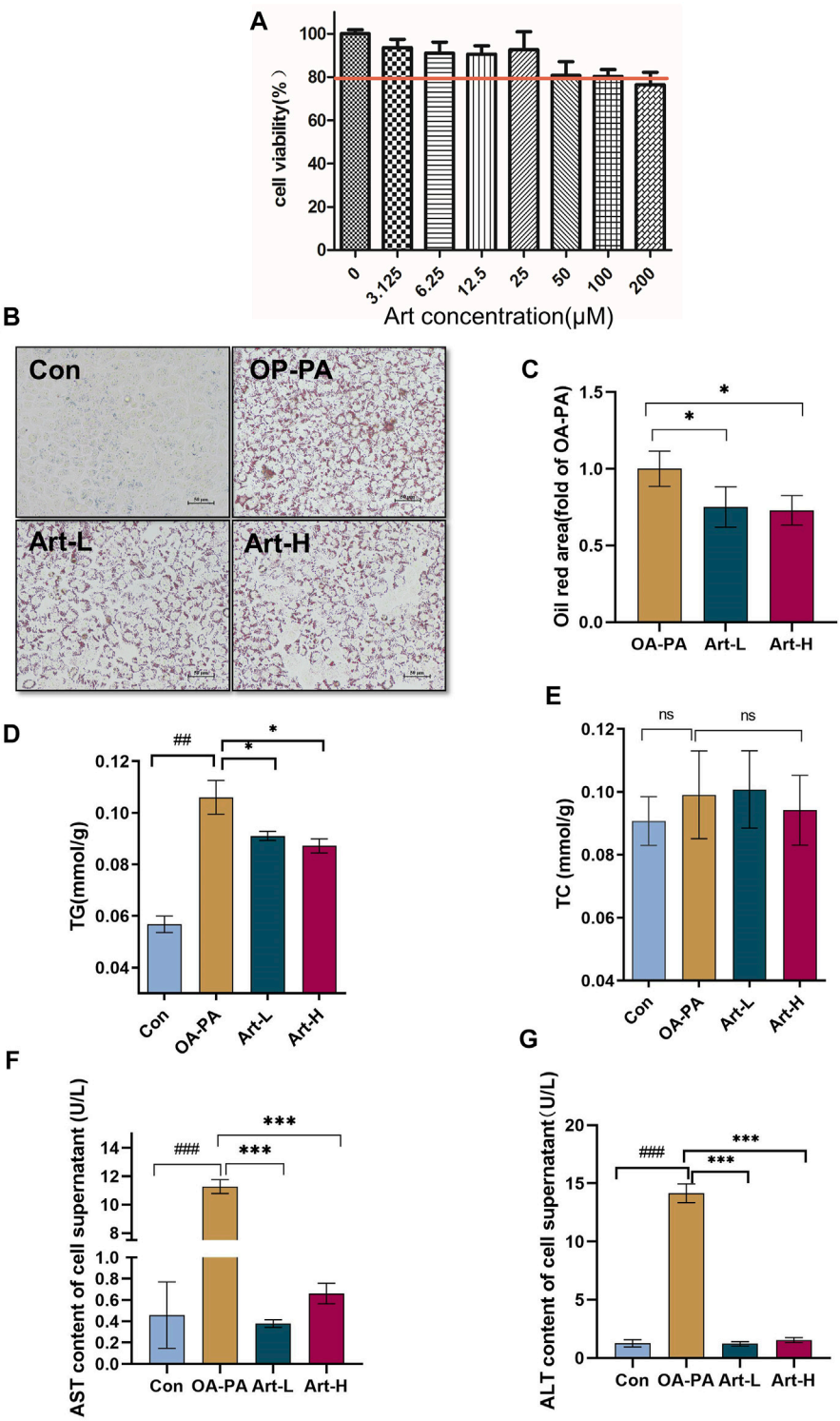

FIGURE 4 | Artemether treatment reduces lipid deposition in oleic and palmitic acid–treated cells. **(A)** Cytotoxicity effect of artemether treatment in the of HepG2 cells ($n = 6$). **(B)** Images of oil red O staining of HepG2 cells that were treated with BSA (Con), 0.5 mM FFA mixture (OA-PA), 6.25 μM Art along with 0.5 mM FFA (Art-L), and 25 μM Art along with 0.5 mM FFA mixture (Art-H). **(C)** Quantification of oil red O staining with ImageJ. **(D)** Intracellular triglyceride level. **(E)** Intracellular cholesterol level. **(F,G)** AST **(F)** and ALT **(G)** levels in the supernatant of HepG2 cells. ($n = 3$). Con vs. OA-PA: $^{\#}p < 0.05$; $^{\#\#}p < 0.01$, and $^{\#\#\#}p < 0.001$. OA-PA compared with Art-L and Art-H: $^{*}p < 0.05$, $^{**}p < 0.01$, and $^{***}p < 0.001$.

mice, but they did not observe improvement in hepatic inflammation. Wang et al. (2019) showed that artemether had a certain repressive effect on liver fibrosis induced by CCl_4 in mice, but the pathogenic mechanism of CCl_4 was different from that of diet-induced NASH-associated fibrosis. However, there has been little discussion about the ameliorated effect of artemether on NASH, and its mechanism of action is unclear.

In this study, a NASH model induced by methionine- and choline-deficient (MCD) diet or high-fat diet (HFD) in mice and a HepG2 cell model were constructed, and the molecule mechanism of artemether in the protection of NASH was clarified.

MATERIALS AND METHODS

Materials

Artemether was purchased from Solarbio, Beijing (SA8510, purity: HPLC ≥ 98%). A high-fat diet (60% of energy derived from fat) was purchased from Beijing Huafukang Co., Ltd. (H10060, Beijing, China). Methionine- and choline-deficient L-amino acid diet (MCD, 22% of calories derived from fat) and methionine- and choline-supplemented diet (MCS) were purchased from Trophic Animal Feed High-tech Co., Ltd., China (TP 3005GS and TP 3005G, Nantong, China).

Animal Experiments

The animal program was approved by the Animal Ethics Committee of China Agricultural University (approval number: KY 1700025). Animal experiments were performed in the SPF Animal Room, Beijing Agricultural Product Quality Supervision, Inspection, and Testing Center of the Ministry of Agriculture. Six-week-old male C57BL/6J mice were purchased from Beijing Vital River Laboratory Animal Technology Co., Ltd., and fed in an acclimatization period of 1 week before the experiment.

The MCD diet-induced NASH model includes the following: 1) MCS group: mice were fed with MCS diet for 6 weeks; 2) MCD group: mice were fed with MCD diet, and 0.5% carboxymethylcellulose sodium (CMC-Na^+) was given to MCS and MCD mice by oral administration; 3) Art-L and 4) Art-H group mice were fed MCD diet and orally administered with Art at 100 mg/kg or 200 mg/kg per day. MCD, Art-L, and Art-H groups maintained an MCD diet for 4 weeks and then were treated with artemether or vehicle for 2 weeks (**Figure 1A**).

The NASH model induced by HFD includes the following: 1) Normal diet group (chow): mice were fed with normal diet; 2) HFD mice group (HFD): mice were fed with HFD for 35 weeks, and DMSO was given to chow and HFD mice by intraperitoneal injection; 3) Artemether groups: mice were given HFD, and 20 mg/kg Art (dissolved in DMSO) was given by intraperitoneal injection. The HFD and artemether groups maintained an HFD for 28 weeks and were treated once a week for 7 weeks (**Figure 2A**).

Some of the livers of mice were fixed with 4% paraformaldehyde, and the rest were used for molecular and biochemical tests.

Body Composition Measurements

The whole fat and lean masses of mice were detected with the NiuMag Small Animal Body Composition Analysis and Imaging System (MesoQMR 23-060H-I, Niumag Corp., Shanghai, China), according to the reference method.

Determination of Glucose Tolerance in Mice

Fasting blood glucose was measured after 12 h fast. The glucose solution was administered intraperitoneally at 1.5 g/kg body weight, and blood glucose levels were detected at 15, 30, 60, 90, and 120 min after injection (Li et al., 2019).

Determination of Biochemical Indications in Mice

Sera of mice were collected, and a biochemistry analyzer (98640000, Indiko™ Plus Clinical Chemistry Analyzer, Thermo Fisher Scientific, California, United States) was used to determine the levels of triglycerides (TG), cholesterol (TC), alkaline phosphatase (ALP), aspartate aminotransferase (AST), and alanine aminotransferase (ALT).

RNA-Seq and Bioinformatic Analysis

TRIzol reagent (Thermo Fisher Scientific, Waltham, United States) was used to extract total RNA of HFD-fed mice liver. The mRNA library was constructed by Beijing Geek Gene Technology Co., Ltd. (Beijing, China) according to the NEBNext super RNA library preparation kit for Illumina. The main functions of differential genes were classified using the PANTHER database (HTTP://www.Un.Org). The enrichment of genes was carried out using the Metascape database (http://metascape.org/gp/index.html#/main/step1).

Cell Viability Assay

HepG2 cells (purchased from Cell Resource Center, Institute of Basic Medicine, Chinese Academy of Medical Sciences) were seeded into 96-well plates and treated with 0.5 mM free fatty acids (oleic acid: palmitic acid 2:1, molar ratios) for 24 h with or without artemether, and cell viability was detected according to the protocol of the Cell Counting Kit-8 (C0038, Beyotime, Beijing, China).

Liver Tissue and Cell Oil Red O Staining

In total, 4% paraformaldehyde-fixed liver samples were cryoprotected in 20% sucrose at 4°C overnight, and then, samples were embedded with OCT compounds in liquid nitrogen. Frozen blocks were sectioned with a cryostat (CM 1590, Leica, Wetzlar, Germany). The slides were fixed with 4% paraformaldehyde for 15 min, washed, dried, and stained with oil red dye solution (BA 4081, Baso Diagnostics, Zhuhai, China) (Rom et al., 2019). HepG2 cells were stimulated with 0.5 mM free fatty acids. Then, cells were treated with 6.25 and 25 μm artemether, respectively, for 24 h. Cells were fixed with 4% paraformaldehyde and then stained with oil red O solution (O0625, Sigma, Darmstadt, Germany), as described previously (Huang et al., 2019). The positive area of oil red O staining was quantified by ImageJ.

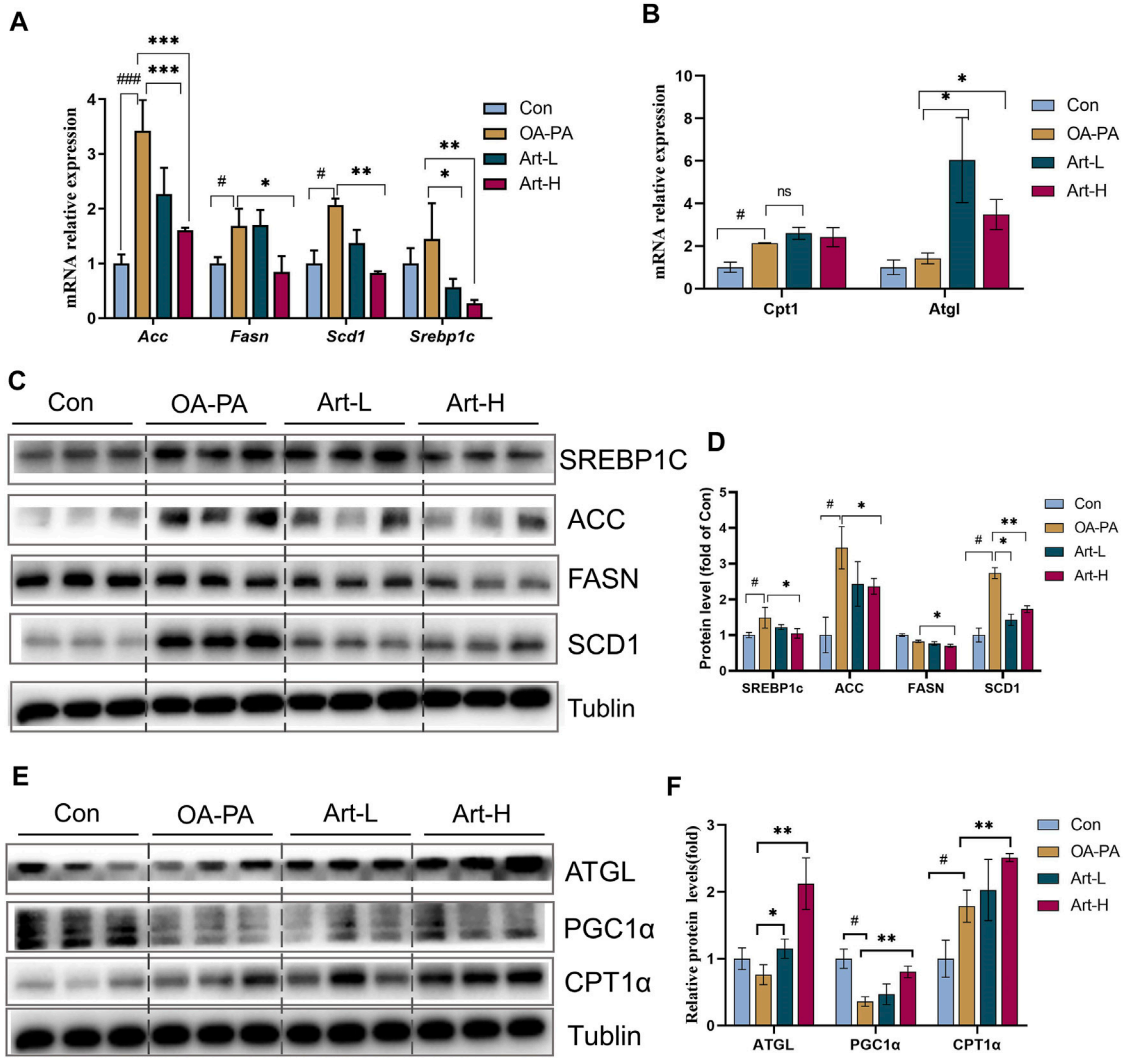

FIGURE 5 | Artemether improves lipid metabolism induced by oleic and palmitic acids in HepG2 cells. **(A,B)** Real-time PCR analysis of lipid synthesis-related genes **(A)** and lipolysis-related genes **(B)** in the HepG2 cells. **(C)** Western blot was used to detect the expression of lipid synthesis-related proteins in HepG2 cells. **(D)** Quantitative plots of the protein expression associated with lipid synthesis. **(E)** Western blot detected the expression of lipolytic protein in HepG2 cells ($n = 3$). **(F)** Quantitative plots of lipid breakdown-related protein expression. Con vs. OA-PA: $^{\#}p < 0.05$, $^{\#\#}p < 0.01$, and $^{\#\#\#}p < 0.001$. OA-PA vs. Art-L and Art-H: $^{*}p < 0.05$, $^{**}p < 0.01$, and $^{***}p < 0.001$.

Liver and Cellular Lipid Detection

The supernatant is taken after homogenization of the liver tissues; for HepG2 cells, the cell particles were collected in PBS buffer. The contents of TC and TG were determined with commercially available kits (A110-1-1 and A111-1-1, Nanjing Jiancheng Bioengineering Institute, Nanjing, China).

Western Blot Analysis

For Western blot analysis, standard SDS-PAGE blotting methods were used. Primary antibodies used in Western blot are as follows: GAPDH, β-tubulin, TLR4, and MYD88 (Beyotime, Beijing, China); ATGL and PPAR-α (Santa Cruz Biotechnology, Inc., Dallas, United States); and CPT-1, SREBP-1c, FASN, ACC, SCD1, and NF-kB (Cell Signaling Technology, Danvers, MA, United States). Chemiluminescence was visualized using an imaging system (330037, Clinx Science Instruments Co. Ltd., Shanghai, China).

Hematoxylin-Eosin, Masson, and Immunohistochemistry Staining

The fixed livers were dehydrated, embedded, sectioned, and then stained by hematoxylin-eosin (HE) and Masson's staining (BA4079A, Zhuhai Beiso Biotech Co., Ltd.), and then, sections were observed under a microscope (DM2500, Leica, Germany) (Jia et al., 2019).

Slides were incubated with 3% hydrogen peroxide buffer and 10% normal goat serum. The primary antibodies included α-SMA, F4/80, CD11C, and CD206 (Cell Signaling Technology,

Danvers, MA, United States) and TGF-β (Abcam, Waltham, United States), and secondary antibodies labeled with horseradish peroxidase were used. Detection was conducted using a horseradish peroxidase–based commercial detection system, disclosure with diaminobenzidine chromogen, and nuclear counterstaining with hematoxylin.

Real-Time Quantitative PCR

RNA was reverse-transcribed into cDNA with a One-Step gDNA Removal and cDNA Synthesis SuperMix (AT311, TransGen Biotech, Beijing, China). Real-time quantitative PCR (qPCR) was performed with a SuperReal PreMix Plus (FP 205-03, TIANGEN Biotech, Beijing, China) by using a real-time PCR system (C1000, Bio-Rad, California, United States). Gene expression levels were normalized to β-actin. Primer sequences are listed in **Supplementary Table S1**.

Statistical Analysis of Data

Statistical analyses were performed using GraphPad Prism 8 (GraphPad Software Inc., La Jolla, CA, United States). The significance of the difference between groups was calculated by Student's unpaired t-test or one-way ANOVA (Tukey's multiple comparison tests). Significant differences were considered when $p < 0.05$. Data are presented as means ± standard deviation (SD).

RESULTS

Artemether Improved Liver Injury and Lipid Deposition in the Methionine- and Choline-Deficient Diet–Induced Non-Alcoholic Steatohepatitis Model

First, we assayed the effects of artemether on MCD-induced liver injury and steatosis in NASH mice. Mice were divided into four groups, two of which were fed with MCD for 4 weeks and treated with Art-L (100 mg/kg) and Art-H (200 mg/kg) for 2 weeks, respectively (**Figure 1A**). The results showed that the body weight decreased by about 50% after 6 weeks of MCD treatment compared with that of the MCS group, whereas artemether at 100 and 200 mg/kg had no significant effect on the body weight of MCD mice (**Figure 1B**). Similarly, wet liver weight decreased by 75% in the MCD group, but no significant difference between the MCD and Art group was observed (**Figure 1C**). The serum ALT and AST of the MCD group were significantly higher than those of the MCS group, and artemether could significantly reverse this phenomenon. The reversal effect of the Art-H (200 mg/kg) group was better than that of the Art-L (100 mg/kg) group (**Figure 1D**). The serum lipid assay showed that treatment with Art-H (200 mg/kg) significantly reversed the trend of decrease in serum TC due to the MCD diet but had no effect on TG levels (**Figure 1E**).

We also observed a reversal effect of artemether on hepatic steatosis induced by the MCD diet in NASH mice. We found that treatment with Art-H (200 mg/kg) significantly reduced TG and TC levels (**Figure 1F**). In addition, H&E staining showed that numerous hepatocytes in the MCD group appeared as vacuole-like steatosis with inflammatory cell infiltration. In contrast, the number and area of fatty vacuoles and inflammatory cell infiltration in liver tissues of artemether-treated mice were decreased, and the pathological morphology of liver of MCD mice was improved in a dose-dependent mode (**Figure 1G**). Oil red O staining also demonstrated a significant increase in lipid deposition in the MCD mouse liver, and the treatment with artemether reduced lipid accumulation in a dose-dependent mode (**Figure 1G**).

Artemether Improved Hepatic Steatosis and Liver Injury in the HFD-Induced Non-Alcoholic Steatohepatitis Model

We also tested the impact of artemether on liver injury and steatosis in NASH mice induced by an HFD because MCD mice differed from human NASH in their pathogenesis. As shown in **Figure 2A**, we found that artemether could decrease the body weight of the HFD by 20% (**Figure 2B**). Compared with the Chow group, the percentage of fat in the HFD group was significantly increased by 2.05 times ($p < 0.05$), while that in the Artemether group was significantly decreased by 56.4% (**Supplementary Figure.S1A**). GTT analysis showed that treatment with artemether significantly improved glucose intolerance in mice. (**Supplementary Figures.S1B,C**). In the HFD group, the wet liver weight was significantly increased by 1.5 times compared with that of the control group ($p < 0.01$). However, artemether treatment reduced the wet liver weight by 27.1% ($p < 0.05$) (**Figure 2C**). Compared with the Chow group, the level of serum ALT and AST in the HFD group increased 3.3 times and 2.5 times, respectively. Compared with the HFD group, serum ALT decreased by 70% and AST decreased by 42% in the artemether group ($p < 0.05$) (**Figure 2D**). The analysis of TG and TC concentrations in serum showed that artemether significantly reversed the increase of the serum lipid level induced by the HFD ($p < 0.05$) (**Figure 2E**).

Similarly, we observed the anti-hepatic steatosis effect of Art in NASH mice induced by the HFD. In the HFD group, the levels of hepatic TG were increased by 1.34 times as compared with those of the control group ($p < 0.01$). However, artemether treatment reduced the hepatic TG concentration by 22.2% ($p < 0.01$). Artemether had no significant effect on hepatic TC in mice (**Figure 2F**). H&E staining showed that a large number of hepatocytes in the HFD group showed vacuolar steatosis with inflammatory infiltration, and artemether improved the pathological morphology of the liver in the HFD group. The number and area of fat vacuoles were significantly decreased, and the accumulation of inflammatory infiltration was decreased in the HFD group (**Figure 2G**). Oil red O staining confirmed that compared with the Chow group, lipid accumulation was significantly increased in the HFD group and decreased in the artemether group (**Figure 2G**). In conclusion, artemether could effectively reverse liver damage and hepatic steatosis induced by the HFD.

Artemether Influences the Lipid Metabolism Pathway in the Liver of Non-Alcoholic Steatohepatitis Mice

To explore the molecular mechanism by which artemether ameliorated liver pathological phenotypes in NASH mice, RNA-Seq was used to analyze the liver transcriptome in NASH models induced by the HFD and in Art-treated mice. Volcanic mapping of differentially expressed genes (DEGs) revealed the whole change in gene expression patterns between HFD and Artemether-treated mice. A total of 1713 DEGs were selected from Artemether-treated mice, of which 883 were elevated and 830 were decreased (**Supplementary Figures.S2A,B**). DEGs are classified by the PANTHER database, and involved molecular functions including molecular regulation, transcriptional regulation, catalysis, and translation regulation. The biological processes include metabolism and stimulation (**Supplementary Figure.S2C**). DEGs were enriched using the Metascape database, with the most prominent metabolic pathways in the first 20 pathways being monocarboxylic acid metabolism, lipid metabolism, and long-chain fatty acid metabolism. In addition, enriched pathways include inflammation, insulin response, and protein folding (**Figure 3A**). We analyzed significantly downregulated genes of the artemether group, compared with the HFD group, which were mainly enriched in lipid metabolism pathways (**Supplementary Figure.S2D**). Artemether reduced fatty acid synthesis and transport-related gene expressions, including *Cbr3*, *Ces1g*, *Fads 2*, *Slc44a3*, *Cyp2a4*, *Cyp2b13*, *Cyp2b9*, *Cyp2a22*, *Ddit4*, *Scd1*, *Cd36*, *Thrsp*, *Gck*, *Mogat 1*, *Phospho1*, and *Cieda* (**Figure.3B**).

Artemether Improved Hepatic Steatosis in Non-Alcoholic Steatohepatitis Mice by Repressing *De Novo* Lipogenesis and Promoting Lipolysis

Excessive TG storage in the liver is a dynamic imbalance between lipogenesis and lipolysis. SCD1, a key gene for *de novo* lipogenesis, was decreased in RNA-Seq assays. Therefore, we first analyzed whether artemether could improve hepatic lipid metabolism by inhibiting DNL. Interestingly, treatment with artemether significantly reduced the expression of the key genes involved in *de novo* lipogenesis, containing *Srebp-1c*, *Fasn*, *Acc*, *Scd1*, and *Ascl* (**Figure 3C**). Western blotting further confirmed that artemether decreased the protein expressions of SREBP-1C, ACC, FASN, and SCD1 in the liver tissue (**Figures 3E,F**).

Second, we considered the effects of artemether on lipolysis and fatty acid β-oxidation-related gene expressions. The results showed that artemether significantly increased the expression of fatty acid β-oxidation genes, including *Pgc1α* and *Cpt1α* (**Figure 3D**). The protein levels of ATGL, PGC-1a, and CPT-1α were also confirmed by Western blotting (**Figures 3G,H**). However, artemether had no significant effect on lipid synthesis genes (*Fasn*, *Acc*, and *Scd1*) in the MCD model and significantly increased the expression of lipolysis-related genes *Hsl*, *Mcad*, *Atgl*, and *Cpt1α*. (**Supplementary Figures S3A,B**). Therefore, artemether primarily reduced hepatic lipid deposition by increasing the expression of lipolysis genes in NASH mice induced by the MCD diet.

Artemether Reduced Oleic-Palmitic Acid–Stimulated Lipid Deposition and Cellular Damage in HepG2 Cells

Next, we observed the improved effect of artemether on hepatic lipid deposition and explored its mechanism in oleic acid (OA):palmitic acid (PA)–induced fatty liver models of HepG2 cells. CCK-8 analysis showed that the concentrations of 6.25 μmol/L and 25 μmol/L artemether had no toxic effect on HepG2 cells, so we used these concentrations as the working concentrations in the following experiments (**Figure 4A**). Art-L (6.25 μmol/L) and Art-H (25 μmol/L) significantly decreased the area of oil red O staining, respectively ($p < 0.05$) (**Figures 4B,C**). The detection of the intracellular TG concentration showed that artemether significantly reduced the intracellular TG concentration in a dose-dependent mode ($p < 0.05$) (**Figure 4D**). There was no evidence that revealed artemether influences the intracellular TC content (**Figure 4E**). Artemether significantly reduced the AST and ALT levels in the supernatant of HepG2 cells ($p < 0.001$) (**Figures 4F,G**).

Artemether Improved Lipid Metabolism of Oleic-Palmitic Acid–Stimulated HepG2 Cells by Repressing *De Novo* Lipogenesis and Promoting Lipolysis

The mechanism of artemether improving lipid metabolism was further validated in HepG2 cells. The results of mRNA analysis showed that artemether inhibited the gene transcription of *Acc*, *Fasn*, *Scd1*, and *Srebp-1* significantly (**Figure 5A**). The proteins of SREBP-1C, ACC, FASN, and SCD1 were also confirmed by Western blotting (**Figures 5C,D**). In addition, artemether significantly increased the transcription expression of *Atgl* (**Figure 5B**). At the protein level, the expressions of ATGL and PGC-1a were significantly increased by artemether treatment (**Figures 5E,F**). These results demonstrated that artemether significantly improved hepatic fatty deposition by inhibiting the expression of key enzymes of DNL and increasing lipolysis in HepG2 cells.

Artemether Reduced Hepatic Inflammation in High-Fat Diet-Induced Non-Alcoholic Steatohepatitis Mice

Liver inflammation is an important pathological feature of NASH, so we also observed the effect of artemether on liver inflammation in mice with NASH. Immunohistochemical staining of F4/80, CD11C, and CD206 showed that artemether significantly decreased liver inflammation by inhibiting M1-type macrophage activation and increasing

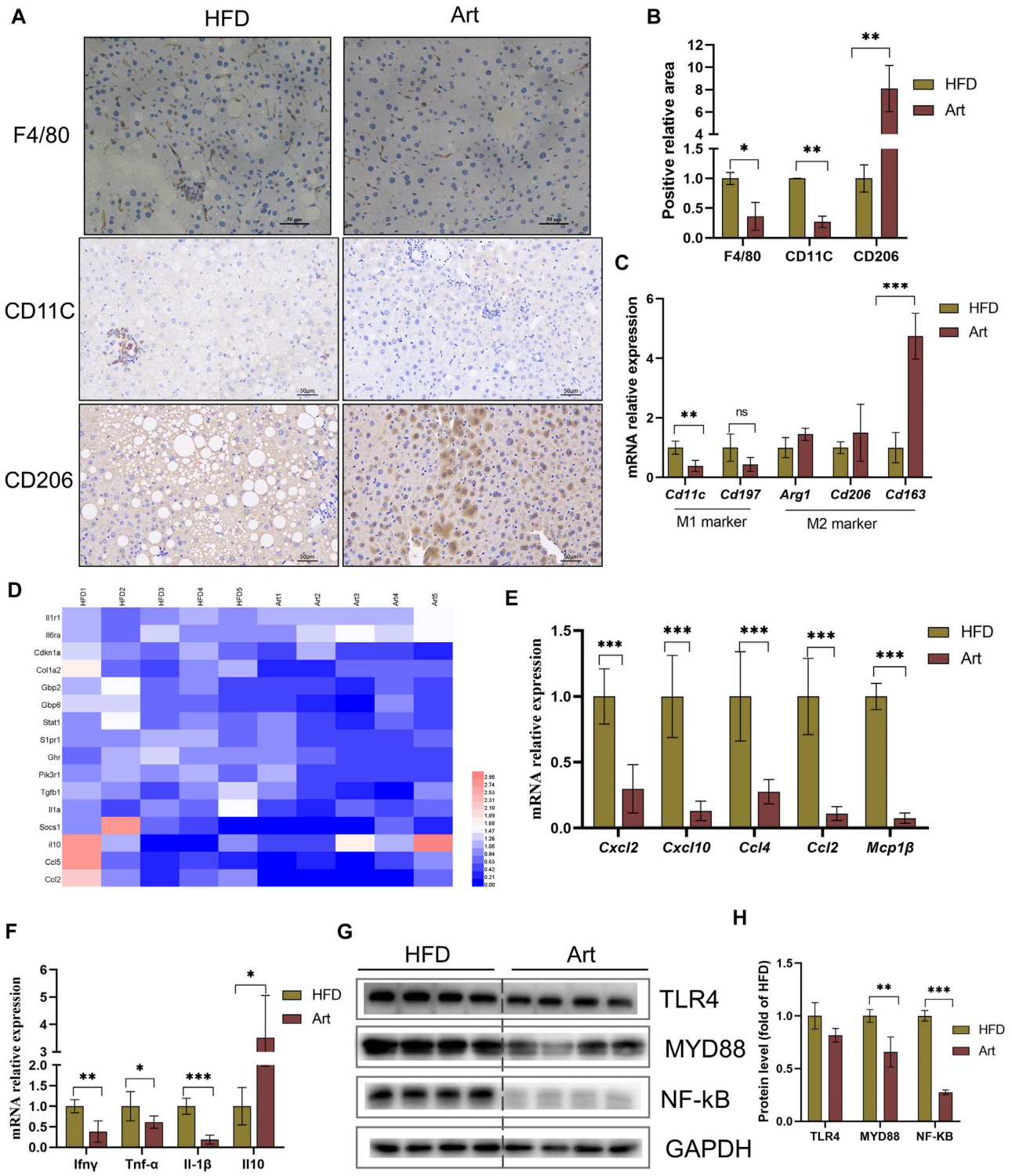

FIGURE 6 | Artemether reduced HFD-induced liver inflammation. **(A)** F4/80, CD11C, and CD206 immunohistochemistry. **(B)** Quantification of F4/80, CD11C, and CD206 staining positive areas ($n = 3$). **(C)** qRT-PCR was used to detect the expression of M1-type marker genes (*Cd11* and *Cd197*) and M2-type marker genes (*Arg1*, *Cd206*, and *Cd163*). **(D)** Heat map of liver inflammation–related differential genes between NASH and Art groups. **(E,F)** Real-time PCR analysis of chemokine-related genes **(E)** and inflammatory factor-related genes **(F)** in the liver. **(G,H)** Protein levels of TLR4, MYD88, and NF-kb in the liver. *$p < 0.05$, **$p < 0.01$, and ***$p < 0.001$.

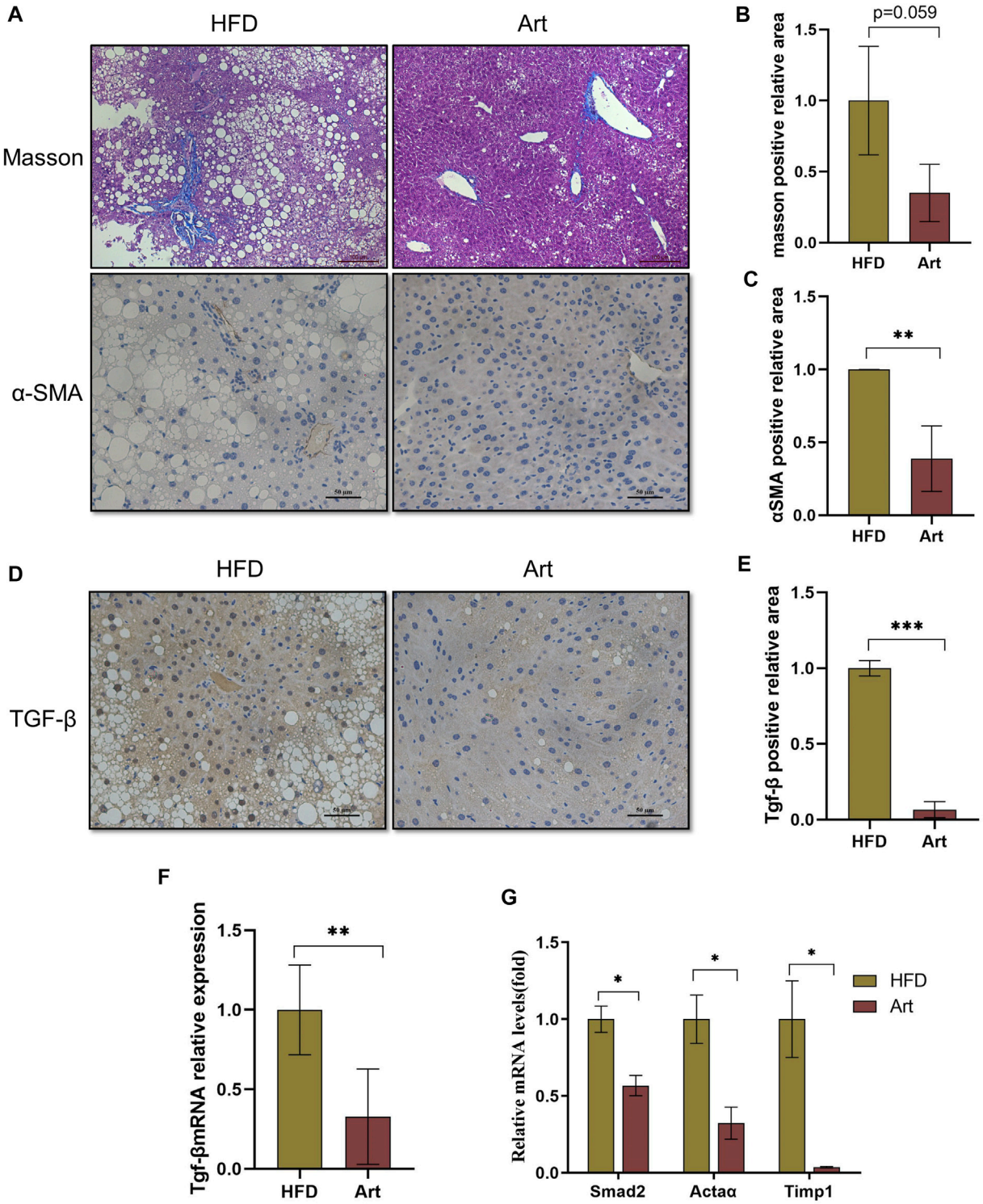

FIGURE 7 | Artemether prevented NASH-induced liver fibrosis. **(A)** From top to bottom: Masson's staining (scale bar: 50 μM) and α-SMA immunohistochemistry (scale bar: 50 μM). **(B)** Quantification of Masson's staining area. **(C)** Quantification of immunohistochemical staining for α-SMA. **(D)** TGF-β immunohistochemical staining (scale bar: 50 μM). **(E)** Quantification of TGF-β immunohistochemical staining. **(F,G)** Real-time PCR analysis of hepatic TGF-β expression **(F)** *Acta 2*, *Timp1*, and *Smad2* **(G)** in the liver. $^{*}p < 0.05$, $^{**}p < 0.01$, and $^{***}p < 0.001$.

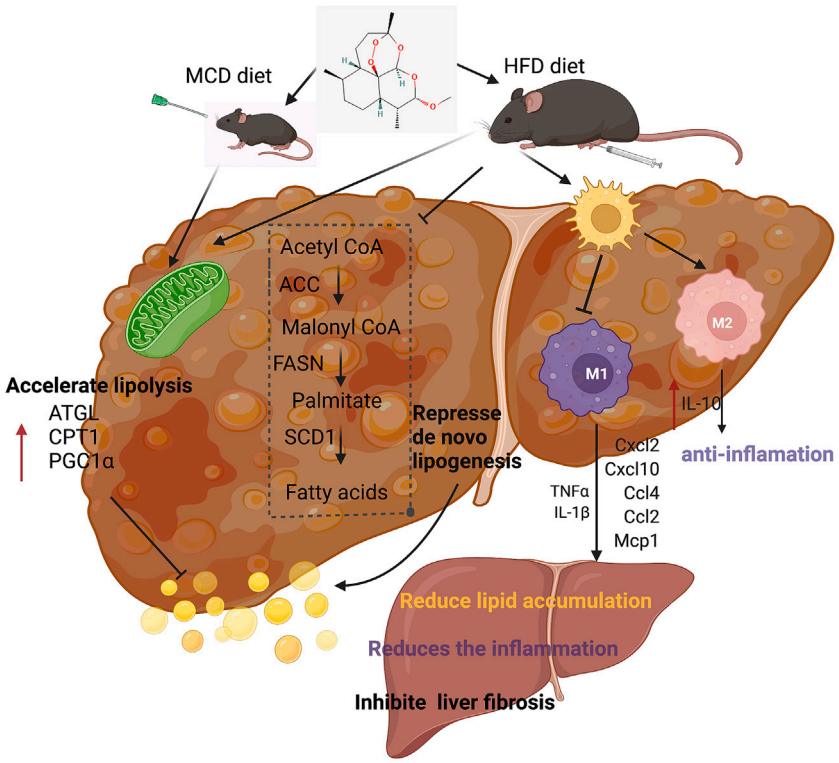

FIGURE 8 | Summary figure showing that the presumable molecular mechanism of artemether ameliorates non-alcoholic steatohepatitis.

M2-type polarization (**Figures 6A,B**). qPCR analysis showed that artemether significantly decreased *Cd11c* mRNA levels and significantly increased *Cd163* mRNA levels (**Figure 6C**). Enrichment analysis of hepatic transcriptional pathways also revealed that some of the genes downregulated by artemether treatment were closely related to the inflammatory pathway (**Figure 2B**), including interleukin-4 and interleukin-13 signaling (*Stat 1*, *Pik3r1*, *Socs1*, *Ccl2*, *Col1a2*, *Cdkn1a*, *S1pr1*, *Fos*, *Il6ra*, *Il10*, *Il1a*, and *Tgfb1*). (**Figure 6D**). qPCR analysis further confirmed that artemether significantly inhibited the expressions of chemokines (*Ccl4*, *Ccl2*, *Cxcl12*, *Cxcl10*, and *Mcp1β*) and pro-inflammatory genes (*Ifnγ*, *IL-1β*, and *TNF-α*) (**Figures 6E,F**) and significantly increased the expression of the anti-inflammatory gene (*Il10*) (**Figure 6F**). Western blotting showed that artemether decreased the levels of TLR4 and significantly decreased the levels of Myd88 and NF-κB (**Figures 6G,H**).

Artemether Ameliorated the High-Fat Diet-Induced Liver Fibrosis

Previous research has shown that artemether prevents CCl_4-induced liver fibrosis in mice (Wang et al., 2019). Does artemether improve liver fibrosis in NASH model mice? Masson staining and immunohistochemical analysis of α-smooth muscle actin (α-SMA) showed that artemether had a significant inhibitory effect on NASH-related liver fibrosis (**Figures 7A–C**). It is well known that the TGF-β/SMAD pathway mediates the development of liver fibrosis, of which TGF-β1 is the key initiator of fibrosis (Xu et al., 2016). Therefore, we examined whether artemether could reduce TGFβ-mediated liver fibrosis. These results showed artemether significantly decreased the *TGF-β* gene expression (**Figure 7F**) and protein level (**Figures 7D,G**). Finally, we tested other genes in the SMAD pathway and showed that the treatment with artemether significantly decreased fibrogenic gene expressions in the NASH mouse liver, including *smad2*, *Timp1*, and *Actaα* (**Figure 7H**).

DISCUSSION

Although NAFLD disease is becoming more prevalent worldwide, the main challenge faced by many researchers is the lack of authorized drugs specifically for the treatment of NAFLD (Paik et al., 2020). Screening and exploring novel therapeutic agents have an important social and scientific value (Peng et al., 2020). Artemether was found for the first time to improve hepatic steatosis, inflammatory infiltrates, and fibrotic progression in mice induced by HFD and MCD diet. Molecular mechanistic studies based on RNA-Seq analysis and cell models suggested that artemether plays a major role in repressing *de novo* lipogenesis, promoting lipolysis, and increasing fatty acid beta-oxidation.

Monomeric analysis of Chinese herbal drugs is considered one of the effective approaches for exploiting new drugs. In addition to the treatment of malaria, recently, investigators have examined the effects of artemether on the treatment of metabolic disorders. Artemether has improved glucose metabolism in a diabetic mouse model (Chalasani et al., 2020). Kim et al. (2016) found that *Artemisia annua* leaf extract administration in Sprague–Dawley rats with HFD-induced obesity, the major source of artemisinin, prevented the development of liver fibrosis and reduced lipid storage and inflammation in the liver. Guo Y et al. (2018) found that artemether improves glucose metabolism abnormalities in db/db mice by reducing pancreatic β-cell apoptosis and increasing insulin emission in mice. However, it did not explore the impact on liver inflammation and fibrosis in mice. This study constructed two well-known mouse models of NASH using the HFD and MCD diet. The results demonstrated that artemether consistently significantly improved the degree of hepatic steatosis, inflammatory injury, and fibrotic progression in the mouse model. In the MCD model, positive concentration-related treatment effects were also observed.

In this study, artemether could significantly inhibit the weight gain and reduce the body fat rate of NASH mice induced by the HFD, which showed a good effect on weight loss. In addition, artemether significantly improved glucose tolerance in NASH mice. The large accumulation of subcutaneous and visceral fat in obese individuals can induce insulin resistance and liver inflammation (Loomba et al., 2021), so improving obesity and weight loss is one of the important strategies for the treatment of NASH. These results reflect those of Lu et al. (2016), who also found that artemether injected subcutaneously or intravenously *via* the tail vein could effectively reduce the weight gain induced by a high-fat diet improve cold tolerance and insulin sensitivity in mice. Furthermore, the study conducted by Guo Y et al. (2018) showed that artemether significantly reduced body weight and improved insulin sensitivity in db/db mice. Subsequently, we will investigate whether artemether reduces hepatic lipid deposition by improving adipose tissue inflammation and insulin resistance.

One of the more significant findings to emerge from this study is that DNL synthesis key genes, including ACC, SREBP-1C, FASN, and SCD1, were significantly inhibited in Art-treated mice and hepatocyte models. These results further demonstrated that artemether, as a natural inhibitor of the DNL pathway, decreases hepatic lipid deposition primarily by inhibiting the DNL pathway. In this study, RNA-Seq screening in HFD-induced NASH confirmed that regulating lipid metabolism-related pathways is the primary pathway for artemether. DNL synthesis is mainly mediated by ACC, FASN, and SCD1, which play a critical role in promoting hepatic lipid deposition. Of these, ACC is an essential enzyme in the DNL process. In a phase II trial, the treatment of high-dose ACC inhibitors for 12 weeks significantly reduced hepatic steatosis in patients with NASH, but elevated serum TG levels were considered likely to be due to a compensatory increase in SREBP-1C activity (Kim et al., 2017). In our study, the expression of ACC in the liver was decreased, and the serum TG concentration was decreased in mice. SCD1 is a rate-limiting enzyme for hepatocyte lipogenesis. Aramchol, the inhibitor of SCD1, reduces hepatic steatosis in mice (Iruarrizaga-Lejarreta et al., 2017). SREBP-1c is an important transcription factor upstream of hepatic TG synthesis, which plays an important role in regulating the FASN expression and increasing lipid synthesis (Friedman et al., 2018). Our results demonstrate that treatment with artemether significantly inhibits the expression of SREBP-1C and its downstream FASN.

We also found that artemether could act as a potential drug to modulate macrophage polarization to reduce inflammatory damage in NASH. Hepatic macrophages have an obvious inflammatory phenotype that promotes disease progression in NASH through a variety of mechanisms (Tacke, 2017). The inflammatory microenvironment induces macrophages to polarize into the pro-inflammatory M1 type, increases the secretion of pro-inflammatory cytokines (TNF-α and IL-1β) and chemokines (CCL2 and CCL4), inhibits the polarization of M2-type macrophages, decreases the secretion of anti-inflammatory cytokines (IL-10), and increases the disproportionality of M1/M2-type macrophages (Li et al., 2020). In this study, artemether treatment significantly decreased the expression of the M1 macrophage marker genes (*Cd11c* and *Cd197*), pro-inflammatory factors (*TNF-α* and *IL-1β*), and chemokines (*Ccl4*, *Ccl2*, and *Mcp1*). At the same time, the expression of M2-type macrophage markers (*Arg-1* and *Cd206*) and anti-inflammatory factor (*Il-10*) were significantly increased by artemether treatment. There is scope for further progress in determining the relationship between artemether and metabolic inflammation. Guo C et al. (2018) found that the SCAP-SREBP2 complex incorporates NLRP3 inflammasome activation and cholesterol biosynthetic signaling during inflammation. We also found that artemether administration greatly decreased the cholesterol levels of liver. Further work could examine more closely the links between cholesterol and the SCAP-SREBP2 pathway by artemether administration in the NASH model.

In conclusion, our experiments showed the therapeutic effects of artemether on NASH and related disorders. Artemether effectively reduced lipid deposition by repressing *de novo* lipogenesis and promoting lipid breakdown. In addition, artemether inhibited the secretion of pro-inflammatory factors and reduced inflammatory infiltration by promoting the polarization of M2 macrophages in livers. Furthermore, artemether inhibited the TGF-β/SMAD pathway and mediates the development of liver fibrosis. Finally, our discovery provided a theoretical reference for artemether use in clinical studies (**Figure 8**).

DATA AVAILABILITY STATEMENT

The datasets presented in this study can be found in online repositories. The names of the repository/repositories and

accession number(s) can be found below: Sequence Read Archive (SRA), PRJNA803877.

ETHICS STATEMENT

The animal program was approved by the Animal Ethics Committee of China Agricultural University (approval number: KY 1700025). Animal experiments were performed in the SPF Animal Room, Beijing Agricultural Product Quality Supervision, Inspection, and Testing Center of the Ministry of Agriculture.

AUTHOR CONTRIBUTIONS

JX and CA wrote the major part of the manuscript. XyH, YL, and KH designed and funded the study. XhH and FZ carried out the animal trial. XR performed the data analyses. CA and YL revised the manuscript. All authors reviewed the manuscript.

FUNDING

This work was supported by the Science and Technology Project of Henan Province (202102310142) and the National Natural Science Foundation of China (82000555, 81500439).

ACKNOWLEDGMENTS

KH and XyH would like to acknowledge the 2115 Talent Development Program of China Agricultural University.

SUPPLEMENTARY MATERIAL

The Supplementary Material for this article can be found online at: https://www.frontiersin.org/articles/10.3389/fphar.2022.851342/full#supplementary-material

REFERENCES

Chalasani, N. P., Ramasubramanian, T. S., Bhattacharya, A., Olson, M. C., Edwards, V. D. K., Roberts, L. R., et al. (2020). A Novel Blood-Based Panel of Methylated DNA and Protein Markers for Detection of Early-Stage Hepatocellular Carcinoma. *Clin. Gastroenterol. Hepatol.* 19, 2597–2605. doi:10.1016/j.cgh.2020.08.065

Chen, Z., Yu, Y., Cai, J., and Li, H. (2019). Emerging Molecular Targets for Treatment of Nonalcoholic Fatty Liver Disease. *Trends Endocrinol. Metab.* 30, 903–914. doi:10.1016/j.tem.2019.08.006

Friedman, S. L., Neuschwander-Tetri, B. A., Rinella, M., and Sanyal, A. J. (2018). Mechanisms of NAFLD Development and Therapeutic Strategies. *Nat. Med.* 24, 908–922. doi:10.1038/s41591-018-0104-9

Guo, C., Chi, Z., Jiang, D., Xu, T., Yu, W., Wang, Z., et al. (2018a). Cholesterol Homeostatic Regulator SCAP-SREBP2 Integrates NLRP3 Inflammasome Activation and Cholesterol Biosynthetic Signaling in Macrophages. *Immunity* 49, 842. doi:10.1016/j.immuni.2018.08.021

Guo, Y., Fu, W., Xin, Y., Bai, J., Peng, H., Fu, L., et al. (2018b). Antidiabetic and Antiobesity Effects of Artemether in Db/db Mice. *Biomed. Res. Int.* 2018, 8639523. doi:10.1155/2018/8639523

Huang, Z., Wu, L. M., Zhang, J. L., Sabri, A., Wang, S. J., Qin, G. J., et al. (2019). Dual Specificity Phosphatase 12 Regulates Hepatic Lipid Metabolism through Inhibition of the Lipogenesis and Apoptosis Signal-Regulating Kinase 1 Pathways. *Hepatology* 70, 1099–1118. doi:10.1002/hep.30597

Iruarrizaga-Lejarreta, M., Varela-Rey, M., Fernández-Ramos, D., Martínez-Arranz, I., Delgado, T. C., Simon, J., et al. (2017). Role of Aramchol in Steatohepatitis and Fibrosis in Mice. *Hepatol. Commun.* 1, 911–927. doi:10.1002/hep4.1107

Jia, Q., Cao, H., Shen, D., Li, S., Yan, L., Chen, C., et al. (2019). Quercetin Protects against Atherosclerosis by Regulating the Expression of PCSK9, CD36, PPARγ, LXRα and ABCA1. *Int. J. Mol. Med.* 44, 893–902. doi:10.3892/ijmm.2019.4263

Jung, M., Lee, K., Kim, H., and Park, M. (2004). Recent Advances in Artemisinin and its Derivatives as Antimalarial and Antitumor Agents. *Curr. Med. Chem.* 11, 1265–1284. doi:10.2174/0929867043365233

Kim, K. E., Ko, K. H., Heo, R. W., Yi, C. O., Shin, H. J., Kim, J. Y., et al. (2016). Artemisia Annua Leaf Extract Attenuates Hepatic Steatosis and Inflammation in High-Fat Diet-Fed Mice. *J. Med. Food* 19, 290–299. doi:10.1089/jmf.2015.3527

Kim, C. W., Addy, C., Kusunoki, J., Anderson, N. N., Deja, S., Fu, X., et al. (2017). Acetyl CoA Carboxylase Inhibition Reduces Hepatic Steatosis but Elevates Plasma Triglycerides in Mice and Humans: A Bedside to Bench Investigation. *Cell Metab.* 26, 394. doi:10.1016/j.cmet.2017.07.009

Lambert, J. E., Ramos-Roman, M. A., Browning, J. D., and Parks, E. J. (2014). Increased De Novo Lipogenesis Is a Distinct Characteristic of Individuals with Nonalcoholic Fatty Liver Disease. *Gastroenterology* 146, 726–735. doi:10.1053/j.gastro.2013.11.049

Li, H., Zhang, C., Liu, J., Xie, W., Xu, W., Liang, F., et al. (2019). Intraperitoneal Administration of Follistatin Promotes Adipocyte browning in High-Fat Diet-Induced Obese Mice. *PLoS One* 14, e0220310. doi:10.1371/journal.pone.0220310

Li, C. L., Zhou, W. J., Ji, G., and Zhang, L. (2020). Natural Products that Target Macrophages in Treating Non-alcoholic Steatohepatitis. *World J. Gastroenterol.* 26, 2155–2165. doi:10.3748/wjg.v26.i18.2155

Li, H. Y., Gan, R. Y., Shang, A., Mao, Q. Q., Sun, Q. C., Wu, D. T., et al. (2021). Plant-Based Foods and Their Bioactive Compounds on Fatty Liver Disease: Effects, Mechanisms, and Clinical Application. *Oxid. Med. Cel Longev.* 2021, 6621644. doi:10.1155/2021/6621644

Loomba, R., Friedman, S. L., and Shulman, G. I. (2021). Mechanisms and Disease Consequences of Nonalcoholic Fatty Liver Disease. *Cell* 184, 2537–2564. doi:10.1016/j.cell.2021.04.015

Lu, P., Zhang, F. C., Qian, S. W., Li, X., Cui, Z. M., Dang, Y. J., et al. (2016). Artemisinin Derivatives Prevent Obesity by Inducing browning of WAT and Enhancing BAT Function. *Cell Res.* 26, 1169–1172. doi:10.1038/cr.2016.108

Paik, J. M., Golabi, P., Younossi, Y., Srishord, M., Mishra, A., and Younossi, Z. M. (2020). The Growing Burden of Disability Related to Nonalcoholic Fatty Liver Disease: Data from the Global Burden of Disease 2007-2017. *Hepatol. Commun.* 4, 1769–1780. doi:10.1002/hep4.1599

Pei, K., Gui, T., Kan, D., Feng, H., Jin, Y., Yang, Y., et al. (2020). An Overview of Lipid Metabolism and Nonalcoholic Fatty Liver Disease. *Biomed. Res. Int.* 2020, 4020249. doi:10.1155/2020/4020249

Peng, C., Stewart, A. G., Woodman, O. L., Ritchie, R. H., and Qin, C. X. (2020). Non-Alcoholic Steatohepatitis: A Review of its Mechanism, Models and Medical Treatments. *Front. Pharmacol.* 11, 603926. doi:10.3389/fphar.2020.603926

Rom, O., Xu, G., Guo, Y., Zhu, Y., Wang, H., Zhang, J., et al. (2019). Nitro-fatty Acids Protect against Steatosis and Fibrosis during Development of Nonalcoholic Fatty Liver Disease in Mice. *EBioMedicine* 41, 62–72. doi:10.1016/j.ebiom.2019.02.019

Schweiger, M., Lass, A., Zimmermann, R., Eichmann, T. O., and Zechner, R. (2009). Neutral Lipid Storage Disease: Genetic Disorders Caused by Mutations in Adipose Triglyceride lipase/PNPLA2 or CGI-58/ABHD5. *Am. J. Physiol. Endocrinol. Metab.* 297, E289–E296. doi:10.1152/ajpendo.00099.2009

Tacke, F. (2017). Targeting Hepatic Macrophages to Treat Liver Diseases. *J. Hepatol.* 66, 1300–1312. doi:10.1016/j.jhep.2017.02.026

Violi, F., and Cangemi, R. (2010). Pioglitazone, Vitamin E, or Placebo for Nonalcoholic Steatohepatitis. *N. Engl. J. Med.* 363, 1185–1186. doi:10.1056/NEJMc1006581

Wang, L., Zhang, Z., Li, M., Wang, F., Jia, Y., Zhang, F., et al. (2019). P53-dependent Induction of Ferroptosis Is Required for Artemether to Alleviate Carbon Tetrachloride-Induced Liver Fibrosis and Hepatic Stellate Cell Activation. *IUBMB Life* 71, 45–56. doi:10.1002/iub.1895

Xu, F., Liu, C., Zhou, D., and Zhang, L. (2016). TGF-β/SMAD Pathway and its Regulation in Hepatic Fibrosis. *J. Histochem. Cytochem.* 64, 157–167. doi:10.1369/0022155415627681

Conflict of Interest: The authors declare that the research was conducted in the absence of any commercial or financial relationships that could be construed as a potential conflict of interest.

Publisher's Note: All claims expressed in this article are solely those of the authors and do not necessarily represent those of their affiliated organizations, or those of the publisher, the editors, and the reviewers. Any product that may be evaluated in this article, or claim that may be made by its manufacturer, is not guaranteed or endorsed by the publisher.

frontiers | Frontiers in Pharmacology

ORIGINAL RESEARCH
published: 03 May 2022
doi: 10.3389/fphar.2022.863756

Scoparone Improves Nonalcoholic Steatohepatitis Through Alleviating JNK/Sab Signaling Pathway-Mediated Mitochondrial Dysfunction

Yuwei Jiang[1†], Jiaoya Xu[2†], Ping Huang[1†], Lili Yang[1], Yang Liu[1], Yiping Li[1], Jue Wang[1], Haiyan Song[1] and Peiyong Zheng[1]**

[1]Institute of Digestive Diseases, Longhua Hospital, Shanghai University of Traditional Chinese Medicine, Shanghai, China, [2]Department of Gout, Guanghua Hospital, Shanghai University of Traditional Chinese Medicine, Shanghai, China

OPEN ACCESS

Edited by:
Runping Liu,
Beijing University of Chinese Medicine, China

Reviewed by:
Atsushi Umemura,
Kyoto Prefectural University of Medicine, Japan
Lei Gao,
Southern Medical University, China

***Correspondence:**
Peiyong Zheng
zpychina@sina.com
Haiyan Song
songhy@126.com

[†]These authors have contributed equally to this work and share the first authorship

Specialty section:
This article was submitted to Gastrointestinal and Hepatic Pharmacology, a section of the journal Frontiers in Pharmacology

Received: 27 January 2022
Accepted: 18 April 2022
Published: 03 May 2022

Citation:
Jiang Y, Xu J, Huang P, Yang L, Liu Y, Li Y, Wang J, Song H and Zheng P (2022) Scoparone Improves Nonalcoholic Steatohepatitis Through Alleviating JNK/Sab Signaling Pathway-Mediated Mitochondrial Dysfunction. Front. Pharmacol. 13:863756. doi: 10.3389/fphar.2022.863756

The activated c-Jun N-terminal kinase (JNK) specifically combined with SH3 domain-binding protein 5 (Sab) may mediate damage to the mitochondrial respiratory chain. Whether mitochondrial dysfunction induced by the JNK/Sab signaling pathway plays a pivotal role in the lipotoxic injury of nonalcoholic steatohepatitis (NASH) remains a lack of evidence. Scoparone, a natural compound from Traditional Chinese Medicine herbs, has the potential for liver protection and lipid metabolism regulation. However, the effect of scoparone on NASH induced by a high-fat diet (HFD) as well as its underlying mechanism remains to be elucidated. The HepG2 and Huh7 cells with/without Sab-knockdown induced by palmitic acid (PA) were used to determine the role of JNK/Sab signaling in mitochondrial dysfunction and cellular lipotoxic injury. To observe the effect of scoparone on the lipotoxic injured hepatocytes, different dose of scoparone together with PA was mixed into the culture medium of HepG2 and AML12 cells to incubate for 24 h. In addition, male C57BL/6J mice were fed with an HFD for 22 weeks to induce the NASH model and were treated with scoparone for another 8 weeks to investigate its effect on NASH. Molecules related to JNK/Sab signaling, mitochondrial function, and lipotoxic injury were detected in *in vitro* and/or *in vivo* experiments. The results showed that PA-induced activation of JNK/Sab signaling was blocked by Sab knockdown in hepatocytes, which improved mitochondrial damage, oxidative stress, hepatosteatosis, cell viability, and apoptosis. Scoparone demonstrated a similar effect on the PA-induced hepatocytes as Sab knockdown. For the NASH mice, treatment with scoparone also downregulated the activation of JNK/Sab signaling, improved histopathological changes of liver tissues including mitochondrial number and morphology, lipid peroxide content, hepatosteatosis and inflammation obviously, as well as decreased the serum level of lipid and transaminases. Taken together, this study confirms that activation of the JNK/Sab signaling pathway-induced mitochondrial dysfunction plays a crucial role in the development of NASH. Scoparone can improve the lipotoxic liver injury partially by suppressing this signaling pathway, making it a potential therapeutic compound for NASH.

Keywords: nonalcoholic steatohepatitis, mitochondrial dysfunction, lipotoxic injury, C-jun N-terminal kinase, SH3 domain-binding protein 5, scoparone

INTRODUCTION

Nonalcoholic fatty liver disease (NAFLD) is the most common chronic liver disease worldwide, which encompasses the spectrum from simple nonalcoholic fatty liver (NAFL), to nonalcoholic steatohepatitis (NASH), and liver cirrhosis (Cotter and Rinella, 2020). NASH is the progressive form of NAFLD, characterized by the presence of inflammation with or without fibrosis in addition to hepatic steatosis (Younossi et al., 2019). Previous studies have shown that the onset of NASH is triggered by lipotoxic liver injury (Machado and Diehl, 2016). Excessive lipid accumulation promotes insulin resistance, oxidative stress, mitochondrial dysfunction, and endoplasmic reticulum stress, resulting in cell apoptosis, inflammation, and fibrosis of liver tissues (Herbert and Alexander, 2010). However, up to now, its mechanism has not been completely clarified, and there is no effective treatment available for NASH (Patel and Siddiqui, 2019).

Mitochondria produce energy for eukaryotic cells through oxidative phosphorylation and electron transport (Vinten-Johansen, 2020). Recently, mounting evidence has revealed that mitochondrial dysfunction is closely involved in NASH development (Patterson et al., 2016). Excessive accumulation of free fatty acids in the liver could exacerbate reactive oxygen species (ROS) production during oxidation, which in turn suppresses the enzyme activities within the mitochondrial respiratory chain and results in mitochondrial dysfunction, thereby affecting energy metabolism and cell damage (Genova and Lenaz, 2014; Sunny et al., 2017). The mitochondrial membrane protein SH3 domain-binding protein 5 (Sab) is a scaffold protein located on the outer mitochondrial membrane. It can interact with the key kinase Bruton's tyrosine kinase (BTK) and stress-activated protein kinase 3 (SAPK3) to regulate B cell growth and mitochondrial signal transcription (Tsukada, 1998; Wiltshire et al., 2002; Court et al., 2004). Sab activation was found up-regulated in Alzheimer's disease, neonatal cerebral ischemic injury and liver injury, etc. (Wiltshire et al., 2002; Nijboer et al., 2013). c-Jun N-terminal kinase (JNK) is a member of the mitogen-activated protein kinase (MAPK) family. Its activation played a pivotal role in lipotoxic damage (Rockenfeller et al., 2010; Ibrahim and Gores, 2012). Studies have shown that during liver injury, JNK combined with Sab, can trigger the disruption of mitochondrial electron transport chain and promote ROS release, ultimately leading to the death of hepatocytes (Takeshita et al., 2013; Win et al., 2016). However, whether JNK/Sab signaling pathway induces lipotoxic liver injury by mediating mitochondrial dysfunction in NASH still lacks evidence.

Scoparone (Scop) is a natural compound from Traditional Chinese Medicine (TCM) herbs such as Artemisia scoparia Waldst. etKit and Artemisia capillaris Thunb., with the chemical name 6,7-dimethoxycoumarin (Jin et al., 2005; Yan et al., 2011). It has the function of relieving asthma and cough, anti-myocardial injury, liver protection, anti-tumor, and so on (Nawrot-Modranka et al., 2006; Kang et al., 2013; Fang et al., 2016; Wan et al., 2018). The pharmacological activities of scoparone include anti-inflammatory, antioxidant, anti-apoptotic, anti-fibrotic, and hypolipidemic effects. In recent years, mounting evidence has shown its therapeutic potential in various liver diseases, such as acute liver injury, alcohol-induced hepatotoxicity, NAFLD, and liver fibrosis (Hui W. Y. et al., 2020). In our preliminary experiment, scoparone was found able to improve PA-induced lipid deposition and lipotoxic injury of the hepatocyte. In addition, we also find that scoparone could inhibit fatty acid-induced JNK activation.

Therefore, this study aims to clarify the contribution of JNK/Sab signaling-mediated mitochondrial dysfunction to NASH, then to explore the role of scoparone against NASH and whether the JNK/Sab signaling pathway-mediated lipotoxic injury in hepatocytes is involved in its underlying mechanism through *in vivo* and *in vitro* experiments.

MATERIALS AND METHODS

Cell Culture and Experimental Design for *in vitro* Experiment

Mouse hepatocyte AML12 and human hepatocarcinoma cell line HepG2, Huh7 were purchased from the Cell Biology Institute of Chinese Academy of Science (Shanghai, China) and cultured in DMEM with 10% FBS and 1% penicillin/streptomycin (Lonsera, Grand Island, United States) at 37°C in a humidified atmosphere containing 5% CO_2.

To induce hepatic steatosis model, cells were incubated in DMEM containing 0.5 mM palmitic acid (PA) and 1% BSA (Sigma, Steinheim, Germany) for 24 h. The cells were treated with scoparone at different doses simultaneously. The cells cultured in the DMEM with 1% BSA were used as normal control. Scoparone was purchased from Shanghai Winherb Pharmaceutical Technology Development Co., Ltd. (Batch No: 190623; Purity ≥98%), and initially dissolved in 50 mM dimethyl sulfoxide (DMSO). The final concentrations of DMSO were kept below 0.1% in all culture conditions.

Establishment of Sab Knockdown Cells

Three Sab-RNAi lentiviral vectors (sh Sab1, sh Sab2, and sh Sab3) were constructed by Genomeditech Co, Ltd (Shanghai, China) by using the vector pGMLV-SC5 RNAi-GFP. HepG2, Huh7, and AML12 cells were cultured in a 6-well plate (5×10^4 cells/well) for 24 h, and were transfected with sh Sab lentivirus with a multiplicity of infection (MOI) of 10 to establish the stable Sab knockdown cell line. Cells transfected with empty-vector lentivirus were used as a scramble. Polybrene (2 μg/ml) was used to enhance transfection efficiency. After 72 h, RNA and protein of cells were extracted to detect Sab expression level to evaluate the transfection and knockdown efficiency.

Cell Viability Assay

The cell viability was measured using the Cell Counting Kit-8 (CCK-8, Dojindo, Kumamoto, Japan). The cells were cultured in a 96-well plate (5×10^4 cells/well), and treated with 0.5 mM PA for 24 h. Then, a 110 μl CCK-8 detection reagent (CCK-8 detection solution: DMEM = 1:10) was

added and incubated for 4 h. The optical density (OD) of the cultures was detected at the absorbance of 450 nm by using Synergy H4 Hybrid Multi-Mode microplate reader (BioTeck, Winooski, United States).

DAPI and Nile Red Double Staining of Cells

The cells were fixed with 4% paraformaldehyde and then stained using Nile Red (SIGMA, Steinheim, Germany) and DAPI (MP, Biomedicals, United States). The cell image was acquired by ImageXpress Microsystem High-content imaging system (Molecular Devices, LLC. San Jose, CA, United States). The cellular imaging analysis software MetaXpress Analysis (Molecular Devices) was used to run the quantitative analysis of the lipid content in cells.

TMRM Assay and ROS Generation Determination

Tetramethyl rhodamine, methyl ester (TMRM) staining can quantify changes in mitochondrial membrane potential in living cells. It was used to monitor mitochondrial function. Cells were incubated with TMRM (Sigma, Steinheim, Germany) staining solution at 37°C for 20 min in the dark. Then TMRM was replaced with Hank's solution, and finally, cells were viewed and photographed by ImageXpress Microsystem High-content imaging system (Molecular Devices).

Intracellular reactive oxygen species (ROS) generation level was determined by using the probe 2′,7′-dichlorodihydrofluorescein diacetate (DCFH-DA) (Beyotime Biotechnology, Shanghai, China). Briefly, cells were incubated with DCFH-DA in DMEM for 20 min. After washing twice with PBS, cells were observed and photographed under a fluorescence microscope (Olympus IX71, Tokyo, Japan).

Experimental Design for *in vivo* Experiment

A total of 40 male C57BL/6J mice (6-week old) of SPF grade, were purchased from Shanghai Slack Laboratory Animal Co., Ltd. (license number SCXK (Shanghai) 2017-0005), and bred at room temperature (22°C) and relative humidity 50–70%. The mice were divided into a control group, a model group, and three scoparone intervention groups (low, medium, and high dose scoparone group), by using a completely random design according to their body weights ($n = 8$ for each group). The mice in the control group were fed a normal diet and the mice in the model group and intervention groups with a high-fat diet (HFD) (Research diet, Inc., New Brunswick, United States, D12492) for 30 weeks. From the 23rd week, mice of the low, medium, and high scoparone groups were fed with HFD supplemented with scoparone powder, at a dose of 25, 50, and 100 mg/kg body weight for 8 weeks. At the end of the experiment, the mice were fasted overnight, anesthetized, and sacrificed. The blood and liver tissues were collected for the subsequent experiments. The animal experiment procedure was approved by the Animal Experiment Ethics Committee of Longhua Hospital, Shanghai University of Traditional Chinese Medicine (No. LHERAW-190001). All animals were kept in compliance with the National Guideline for the Care and Use of Animals.

Serum Biochemical Analysis and Detection of Serum TNF-α

The mouse serum was separated at 3,000 r/15 min, and the serum alanine aminotransferase (ALT), aspartate aminotransferase (AST), triglyceride (TG)、cholesterol (TC), high-density lipoprotein cholesterol (HDL), and low-density lipoprotein cholesterol (LDL) were measured by using ROCHE cobas 8,000 modular analyzer series and corresponding reagent kits (Basel, Switzerland). The serum TNF-α was determined by using an ELISA assay (Shanghai WestTang Bio-tech Co., Ltd) according to the manufacturer's protocol.

Measurement of TG and TC Content in Liver Tissues

Mouse live tissues (40 mg) were homogenized with 360 μl alcohol, then centrifuged for 15 min at 4°C, 2,500 rpm. The supernatant was measured based on the instructions of a TG or TC assay kit (Jiancheng Institute of Bio Engineering, Inc.) using the GPOPAP enzyme method. The absorbance was measured by Synergy H4 Hybrid Reader (BioTek, United States), and calculations of TG and TC content were performed according to the formula of the kit.

Histopathology of Liver Tissues

The liver tissue was fixed with 4% paraformaldehyde, then dehydrated and embedded in paraffin and cut into 5 μm sections. The section was stained with hematoxylin-eosin (HE) solution (Yixin Biotechnology, Shanghai, China) according to a standard procedure. After mounting, the pathological changes of liver tissue were observed and photographed under a light microscope (Nikon ECLIPSE 50i, Tokyo, Japan).

TUNEL Staining of Liver Tissues

The paraffin-embedded liver tissue sections were deparaffinized, hydrated, and permeabilized. A TUNEL apoptosis detection kit (*In Situ* Cell Death Detection Kit, Roche, Indianapolis, United States) was used to label the apoptotic cells with TMR red, and nuclei were counterstained with DAPI. The images of slides were scanned and analyzed by using ImageXpress MicroSystem and MetaXpress Analysis (Molecular Devices).

The Observation of Hepatocyte Mitochondrion by Transmission Electron Microscope

The fresh liver tissues were fixed in 2% glutaraldehyde for 2 h, and the samples were then processed and photographed using HITACHI H-7650 transmission electron microscope in the

TABLE 1 | The sequences of primers used in PCR.

Gene	Sequence(5′-3′)
h β-actin	Forward: TCAAGAAAGGGTGTAACGCAATA
	Reverse: CGACAGGATGCAGAAGGAGAT
h Sab	Forward: AGTTCCGCTCTGTTCTGGTTG
	Reverse: CCTCTGGAAGTCCTGCGTG
h PGC-1α	Forward: CAAATATCTGACCACAAACGATG
	Reverse: AAGTTGTTGTTGGTTTGGCTTGTAAG
h NRF1	Forward: CCAGTTTAGTGGGTGGTAGG
	Reverse: CGGGAGCTTTCAAGACATTC
h TFAM	Forward: GTCACTGCCTCATCCACC
	Reverse: CCGCCCTATAAGCATCTT
m β-actin	Forward: GAGACCTTCAACACCCCAGC
	Reverse: ATGTCACGCACGATTTCCC
m PGC-1α	Forward: TGGCACGCAGCCCTATTC
	Reverse: GAGGATCTACTGCCTGGGGAC
m NRF1	Forward: TCCCAGAGATGCTCAAGTATTCC
	Reverse: TTAACTATGGTCCGTAATGCCTG
m TFAM	Forward: GCATCCCCTCGTCTATCAGTC
	Reverse: TGTGGAAAATCGAAGGTATGAAC
m IL-1β	Forward: GCTTCAGGCAGGCAGTATCA
	Reverse: TGCAGTTGTCTAATGGGAACG
m TNF-α	Forward: CCCTCCAGAAAAGACACCATG
	Reverse: CACCCCGAAGTTCAGTAGACAG
h mtDNA	Forward: CCACTTTCCACACAGACATCA
	Reverse: TGGTTAGGCTGGTGTTAGGG
m mtDNA	Forward: ACATCTCGATGGTATCGGGTC
	Reverse: CCTTAGGTGATTGGGTTTTGC

Science and Technology Experiment Center of Shanghai University of Traditional Chinese Medicine.

Immunohistochemistry of 4-HNE of Liver Tissues

The immunohistochemical experiment was performed to detect the level of 4-hydroxynonenal (4-HNE) in liver tissues. The paraffin-embedded liver sections were dewaxed, antigen-retrieved, and blocked, then incubated with a 4-HNE antibody (Alpha Diagnostic, Texas, United States) overnight. The secondary antibody and chromogenic reagent (Gene technology, Shanghai, China), were used to detect the positive stain. After being counterstained with hematoxylin, the section was photographed.

Real-Time Quantitative Reverse Transcription-Polymerase Chain Reaction

The total RNA from liver tissue or cells was extracted with Trizol (Invitrogen, United States) reagent, reverse-transcribed with a reverse transcription kit (Applied Biosystems, Carlsbad, CA, United States). qRT-PCR was then performed with an SYBR Green PCR Mix kit (Accurate Biology, Changsha, China) with StepOnePlus Real-Time PCR System (Applied Biosystems). The expression level relative toβ-actin was calculated with the $2^{-\Delta\Delta ct}$ method. The gene sequence was verified on the Blast website, and the primers were synthesized by Shanghai Shinegene Biotechnology. The sequence of the primers was listed in **Table 1**.

Relative Copy Number of Mitochondrial DNA

The total DNA of liver tissue or cells was extracted by using a DNA extraction kit (Tiangen Biotech, Shanghai, China). The expression level of mitochondrial DNA (mtDNA) was detected by real-time PCR. The primer sequences, which are located at the D-loop region in mitochondrial DNA, were also listed in **Table 1**.

Western Blot

The liver tissue and cell proteins were extracted with RIPA lysate (Beyotime Biotechnology), and the concentration was determined using the BCA method. The protein was separated by 10% acrylamide gel electrophoresis and transferred to the PVDF membrane (Millipore, Darmstadt, and Germany). TBST solution containing 5% skim milk (BD, Maryland, United States) was used to block the membrane for 1 h, followed by incubation with primary antibodies at 4°C overnight. Antibodies against P-JNK, JNK, P-Src, Src, P-SHP-1, SHP-1, Peroxisome proliferator-activated receptor-γ coactivator-1α (PGC-1α), and β-actin were purchased from Cell Signaling (Massachusetts, United States). Antibodies against Sab and Cleaved PARP were obtained from Proteintech (Wuhan, China) and ABclonal (Wuhan, China) respectively. The membrane was then incubated with the secondary antibodies at room temperature for 1 h and subsequently incubated with ECL luminescent substrate (Millipore, Billerica, United States). The signals were acquired using Tanon-5200 chemiluminescence image analysis system (Shanghai, China).

Statistical Analysis

The measurement data were expressed as mean ± standard deviation (SD). All data were statistically analyzed using SPSS24.0 (SPSS Inc., Chicago, IL, United States) and Graphpad Prism 8.0 software (GraphPad Software Inc., San Diego CA, United States). Student *t*-test was used to compare the means of the two groups, and One-way analysis of variance (ANOVA) followed by Tukey's post hoc comparison for three or more groups. $p < 0.05$ was considered statistically significant.

RESULTS

Sab Knockdown Suppressed PA-Induced Activation of JNK/Sab Signaling Pathway in Hepatocytes

To identify the role of JNK/Sab signaling in the NASH mechanism, the key molecule Sab was knockdown in hepatocytes to block this pathway by using RNA interference. The expression of Sab mRNA and protein in hepatocytes transfected with Sab shRNA lentivirus or scramble was

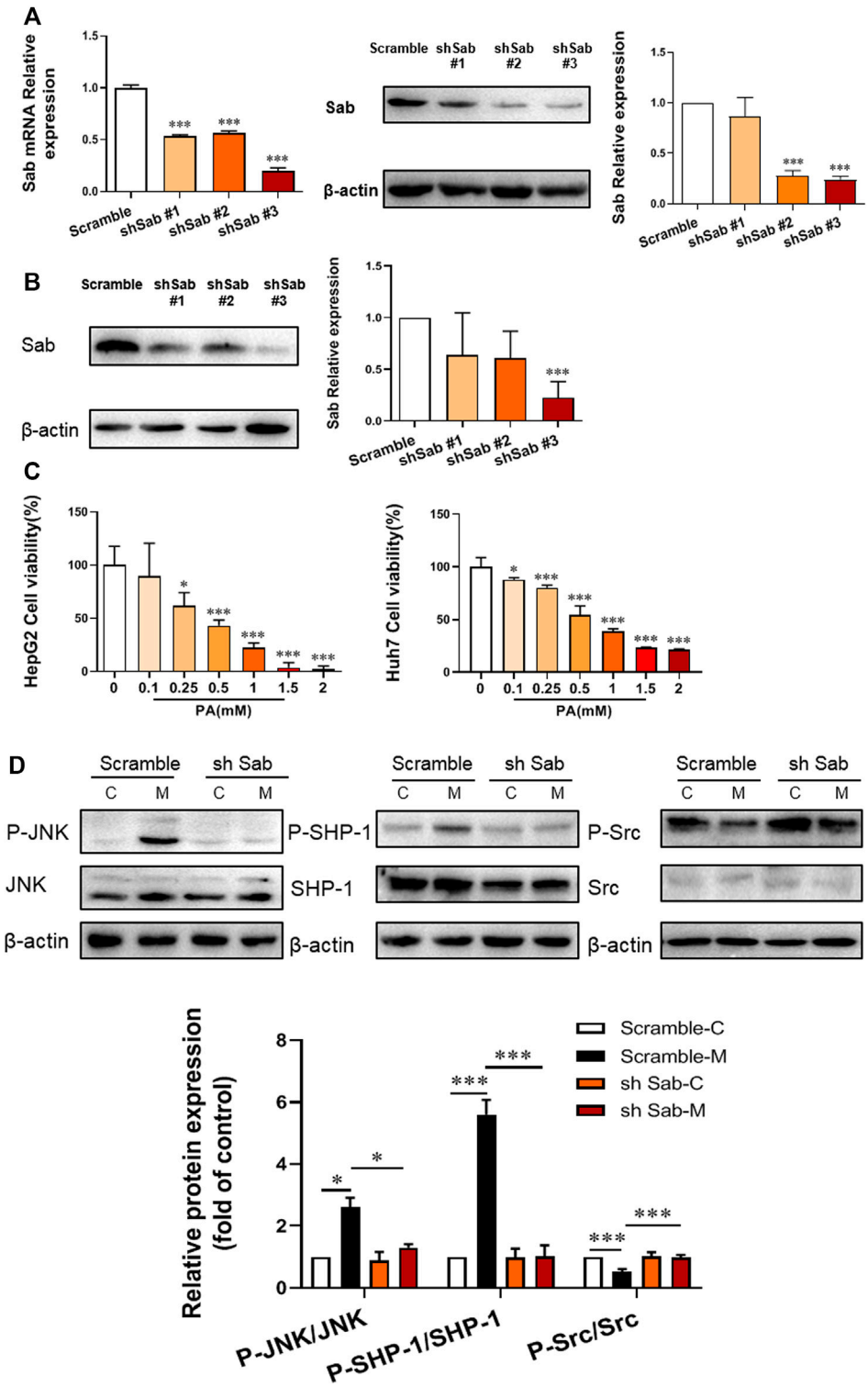

FIGURE 1 | Sab knockdown inhibited PA-induced activation of JNK/Sab signaling pathway in hepatocytes. **(A)** The mRNA and protein expression level of Sab in HepG2 cells transfected with Sab shRNA lentivirus or scramble. ***$p < 0.001$ vs. Scramble. **(B)** The protein expression level of Sab in Huh7 cells with Sab shRNA lentivirus or scramble. ***$p < 0.001$ vs. Scramble. **(C)** The effect of different concentrations of PA on cell viability. *$p < 0.05$, ***$p < 0.001$ vs. PA 0 mM group. **(D)** The expression and activation level of JNK, SHP-1, and Src protein in HepG2 cells with PA induction (Model) or without (Control). *$p < 0.05$, ***$p < 0.001$. $n = 3$.

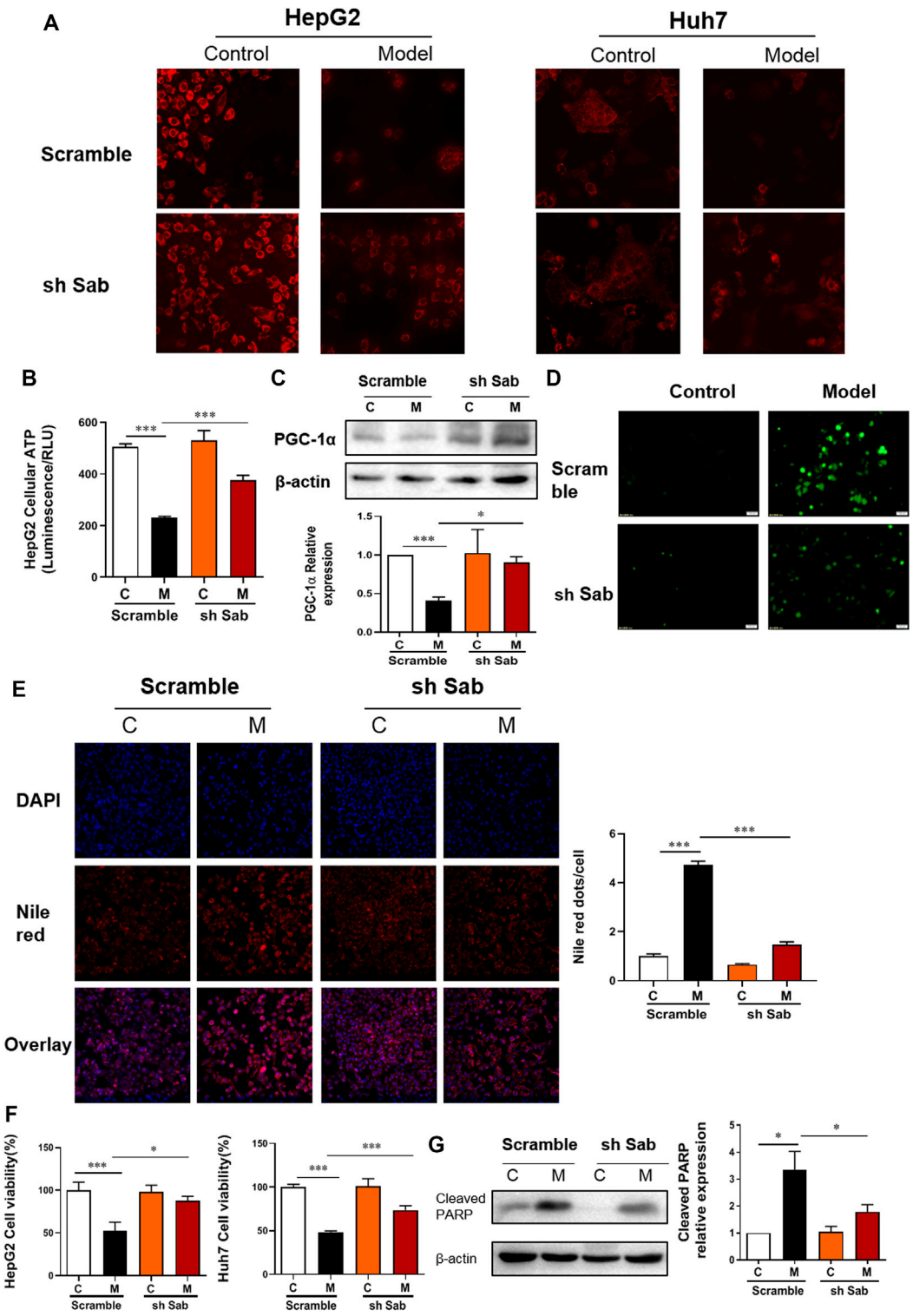

FIGURE 2 | Sab knockdown improved PA-induced mitochondrial dysfunction and lipotoxic injury of hepatocytes. **(A)** TMRM staining of HepG2 and Huh7 cells (200×). **(B)** The ATP production of HepG2 cells. **(C)** PGC-1α protein expression of HepG2 cells. **(D)** ROS level of HepG2 cells (200×). **(E)** DAPI and Nile Red double staining of HepG2 cells (200×). **(F)** The effect of Sab knockdown on HepG2 cell viability with PA induction. **(G)** The effect of Sab knockdown on Cleaved PARP level in HepG2 cells. *$p < 0.05$, ***$p < 0.001$.

detected by qRT-PCR and Western blot. **Figures 1A,B** showed that sh Sab#3 lentiviral transfection had the most obvious inhibitory effect on Sab expression, with an inhibition rate of more than 80% in both HepG2 and Huh7 cell lines and around 60% in AML12 cells (**Supplementary Figure S1A**).

To imitate the lipotoxic liver injury of NASH *in vitro*, hepatocytes were incubated with PA (0.1, 0.25, 0.5, 1, 1.5, and 2 mM) for 24 h and the corresponding cell viability was measured by CCK8 assay. The cell viability was down-regulated by PA incubation in a dose-dependent manner. The cell survival rate was around 50% with 0.5 mM PA induction in HepG2 and Huh7 cells, which was thereby selected as the dose of PA for subsequent experiments (**Figure 1C**).

Figure 1D showed that PA increased the P-JNK/JNK and P-SHP-1/SHP-1 ratios of protein expression in HepG2 cells, whereas decreased P-Src/Src ratio. Knockdown of Sab prevented the PA-induced activation of JNK/Sab signaling, demonstrated by the significantly reduced P-JNK/JNK and P-SHP-1/SHP-1 ratios, and increased P-Src/Src value.

PA-Induced Mitochondrial Dysfunction and Lipotoxic Injury of Hepatocytes Were Reversed by Suppression of the JNK/Sab Signaling Pathway

TMRM can accumulate in normal functional mitochondria and emit fluorescent signals. If the mitochondrial transmembrane potential is damaged, TMRM will diffuse, and fluorescence intensity decreases. As shown in **Figure 2A**; **Supplementary Figure S1B**, the fluorescence intensity of TMRM in PA-induced hepatocytes (Model) was significantly reduced, indicating impaired membrane potential and function of mitochondria. Whereas cells with Sab knockdown showed higher fluorescence intensity compared with scramble with PA treatment. **Figure 2B** also demonstrated the knockdown of Sab rescued mitochondrial function, as sh Sab HepG2 cells generated more ATP with PA-induction when compared with the scramble cells. As a nuclear transcription co-activator, PGC-1α can promote the transcription of target genes related to regulating mitochondrial proliferation, mitochondrial respiration chain, and β-oxidation of fatty acid (Guerrero-Beltrán et al., 2017). Western blot results showed that Sab downregulation reversed the decrease of PGC-1α level induced by PA (**Figure 2C**). **Figure 2D** showed that intracellular ROS generation increased notably in the PA-induced hepatocytes. When Sab was knocked down, the green fluorescence was significantly reduced, indicating the inhibitory effect of Sab knockdown on oxidative stress during PA-induced lipotoxic injury.

DAPI and Nile Red double staining was performed to observe cellular lipid accumulation. As shown in **Figure 2E** and **Supplementary Figure S1C**, the control HCC cells showed no obvious lipid deposition. After PA incubation for 24 h, Nile red signal was significantly enhanced, whereas the DAPI-presented cell number was reduced, and the Nile red dots normalized to cell number indicated the increased intracellular lipid content. Meanwhile, the decreased number and the presence of some irregular morphology of nuclei showed by DAPI staining also indicated cell damage with PA induction. Sab knockdown alleviated the PA-induced lipid accumulation and the decrease of cell number significantly. Similarly, the CCK8 assay also showed Sab knockdown significantly improved the viability of HepG2 cells and AML12 cells when treated with 0.5 mM PA for 24 h (**Figure 2F**, **Supplementary Figure S1D**). PARP protein can be cleaved and activated during apoptosis. Western blot results showed that PA increased the expression of cleaved PARP of scramble HepG2 cells significantly, while the Sab-knockdown cells had a lower expression, suggesting that lipid-induced apoptosis had been alleviated by inhibiting JNK/Sab signaling (**Figure 2G**).

Scoparone Reversed PA-Induced Lipotoxic Injury of Hepatocytes

To determine the concentration of scoparone to be used, the viability of HepG2 and AML12 cells incubated with scoparone at different doses was detected by CCK8 assay. Compared with control, cell viability increased with the increase of concentration and reached a peak at 25 μM. The calculated IC50 value of HepG2 cells was 350 μM and that of AML12 cells was 480 μM (**Figure 3A**). With 0.5 mM PA induction, the viability of HepG2 and AML12 cells decreased significantly. Whereas intervened by scoparone at 10 and 25μM, cell viability was improved, with the highest viability at 25 μM (**Figure 3B**). The concentration of 25 μM was far less than the IC50 value of scoparone in hepatocytes, which was thus selected to be used in subsequent experiments.

DAPI and Nile red double staining were performed on the hepatocytes in each group. Compared with the model group, the number of cells with 25 μM scoparone treatment group increased significantly and the lipid deposition decreased significantly (**Figure 3C**). Western blot results presented that scoparone could significantly reduce the expression of apoptosis indicator protein cleaved PARP in HepG2 and AML12 cells induced by PA (**Figure 3D**).

PA-Induced Mitochondrial Dysfunction Was Reversed by Scoparone

The TMRM staining found that scoparone treatment could significantly improve the attenuation of cellular mitochondrial membrane potential caused by PA (**Figure 4A**). As shown in **Figure 4B**, scoparone could also improve the PA-induced decrease of ATP production. Compared with the control group, the mtDNA copy number, the mRNA levels of PGC-1α, NRF1, and TFAM, as well as PGC-1α protein level were detected downregulated in PA-induced cells, which was improved by scoparone significantly (**Figures 4C,D**). The ROS level of cells in each group was observed under the fluorescence microscope. Compared with the model group,

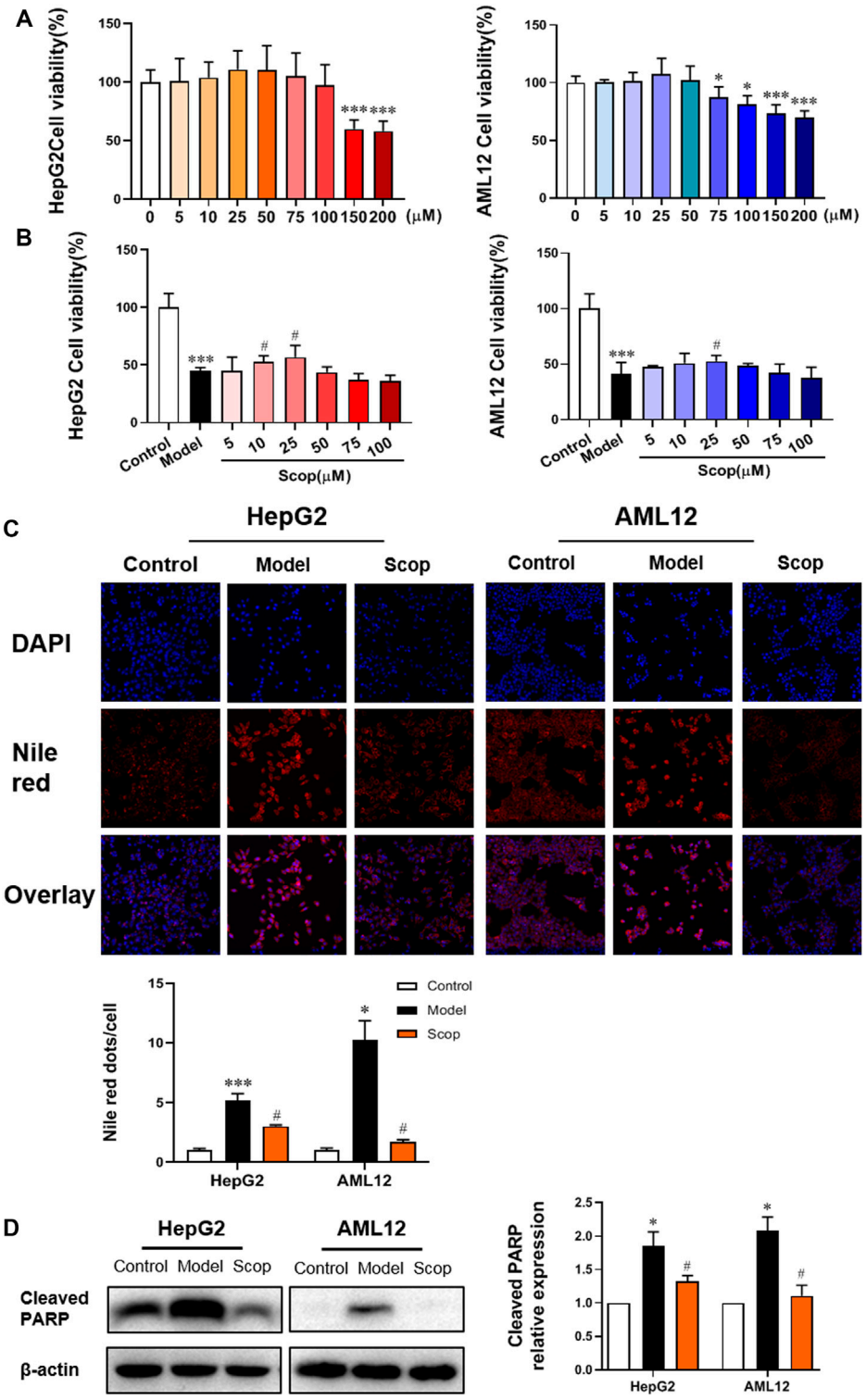

FIGURE 3 | Scoparone reversed PA-induced lipotoxic injury of hepatocytes. **(A)** The effect of different concentrations of Scoparone on the viability of HepG2 and AML12 cells. $^{*}p < 0.05$, $^{***}p < 0.001$ vs. Scop 0 μM. **(B)** The effect of different concentrations of Scoparone on the viability of HepG2 and AML12 cells with PA induction. **(C)** DAPI and Nile Red double staining of HepG2 and AML12 cells. **(D)** The effect of Scoparone on Cleaved PARP protein level in HepG2 and AML12 cells. $^{*}p < 0.05$, $^{***}p < 0.001$ vs. Control; $^{\#}p < 0.05$ vs. Model.

the ROS generation of cells in scoparone group was significantly reduced and the oxidative stress injury was improved (**Figure 4E**). Together, these results indicated that the PA-induced damage of mitochondrial function was improved by scoparone.

Scoparone Inhibited PA-Induced Activation of JNK/Sab Signaling Pathway

The protein expression of JNK/Sab signaling pathway-related molecules in HepG2 and AML12 cells were detected, which were shown in **Figure 5**. Compared with the control group, the ratio of P-JNK/JNK and P-SHP-1/SHP-1 increased, and the ratio of P-Src/Src decreased significantly. With the intervention of scoparone, compared with the model group, the ratio of P-JNK/JNK and P-SHP-1/SHP-1 decreased, and the ratio of P-Src/Src increased significantly. There was no significant difference in the expression of Sab in cells of different groups.

Scoparone Alleviated Lipotoxic Liver Injury Induced by HFD in NASH Mice

As shown in **Figure 6A**, after 30 weeks of the HFD-induction, the body weight and liver weight of mice in the model group were increased significantly compared with the control group. These

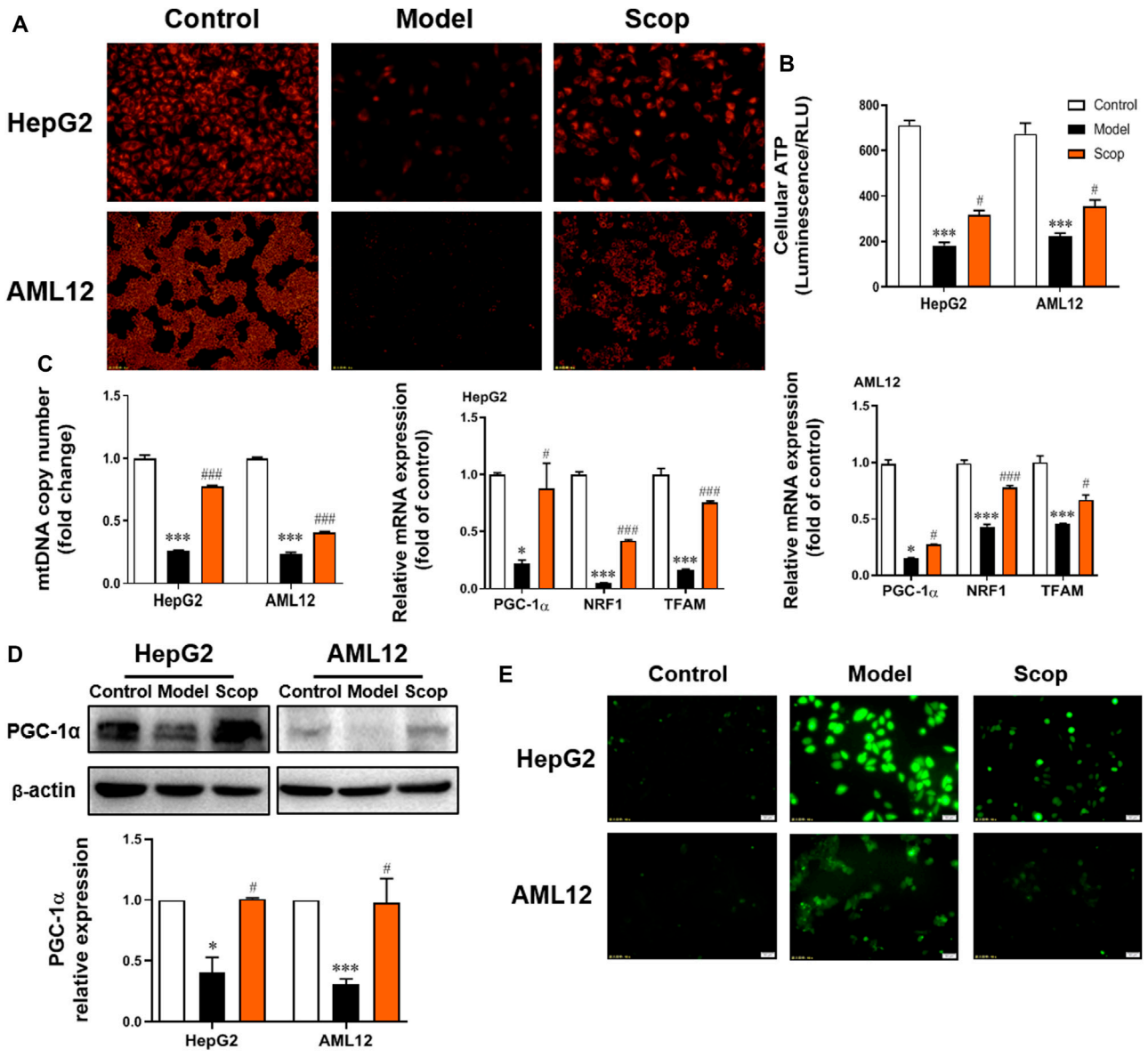

FIGURE 4 | Scoparone improved PA-induced mitochondrial dysfunction in hepatocytes. **(A)** TMRM staining (200×). **(B)** The ATP content of hepatocytes. **(C)** The mRNA level of mtDNA, PGC-1α, NRF1, TFAM in HepG2 and AML12 cells. **(D)** The effect of Scoparone on PGC-1α protein level in HepG2 and AML12 cells. **(E)** ROS staining of HepG2 and AML12 cells (200×). $^{***}p < 0.001$ vs. Control; $^{\#}p < 0.05$, $^{\#\#\#}p < 0.001$ vs. Model.

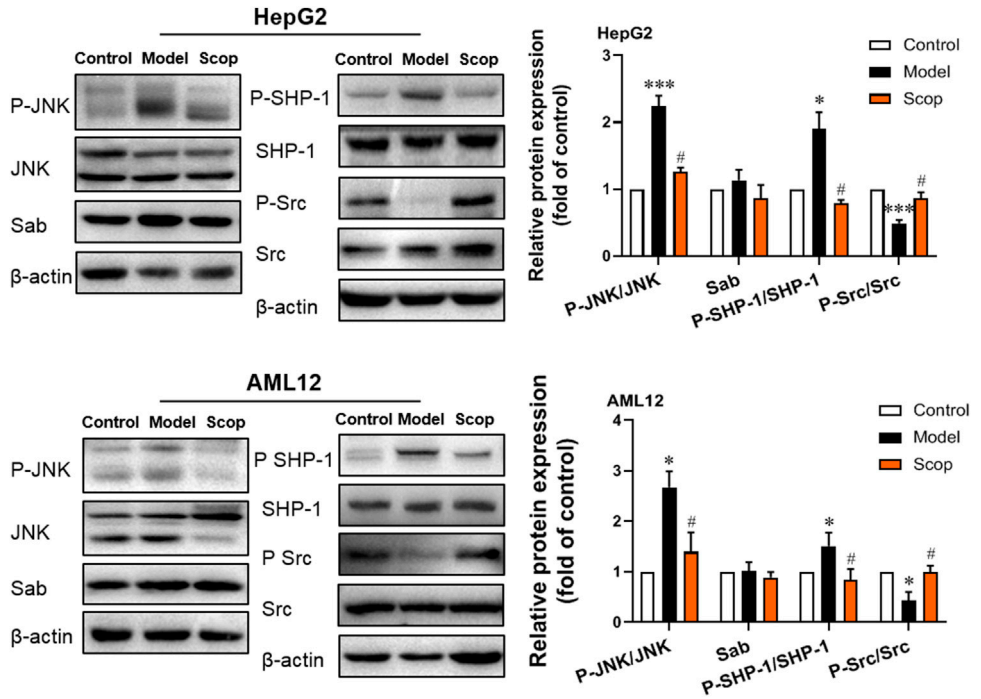

FIGURE 5 | Scoparone inhibited PA-induced activation of JNK/Sab signaling pathway in hepatocytes. The expression and activation levels of JNK, SHP-1, Src, and Sab protein in HepG2 and AML12 cells with PA induction were detected and analyzed. $^{*}p < 0.05$, $^{***}p < 0.001$ vs. Control; $^{\#}p < 0.05$ vs. Model.

were down-regulated by scoparone treatment in a dose-dependent manner. The levels of serum ALT, AST, LDH, TC, HDL, and LDL in HFD-fed mice were higher than the control group, which were also decreased by scoparone dose-dependently (**Figures 6B,C**).

The liver tissues of model mice stained with HE demonstrated the histology characteristics of NASH, with the abundant accumulation of lipid droplets in hepatocytes, scattered lobular inflammatory infiltration, and hepatocellular ballooning. The medium and high dose of scoparone improved the histopathological changes of NASH mice (**Figure 7A**). The levels of TG and TC in the liver tissues were also reduced by scoparone (**Figure 7B**), which was consistent with the impaired hepatosteatosis shown in HE staining. Moreover, the levels of serum TNF-α and mRNA expression of IL-1β, TNF-α in the liver tissues of scoparone groups were decreased as compared with NASH mice (**Figure 7C**). The Western blot results showed the Cleaved PARP protein level in the model group was significantly increased versus control, which was decreased by scoparone treatment (**Figure 7D**). **Figure 7E** showed red fluorescence in the nuclei in a large number of cells in the liver tissues of NASH model mice, whereas no obvious positive TUNEL staining in the liver tissues of control and scoparone groups. The quantified fluorescence value normalized to cell number according to DAPI counterstain revealed that the apoptotic rate of liver cells in the model group was significantly higher than that of the control and the scoparone groups.

Scoparone Alleviated Mitochondrial Dysfunction in the Hepatocytes of NASH Mice by Inhibiting JNK/Sab Signaling Pathway

Through the transmission electron microscopy images of liver tissues (**Figure 8A**), we can observe a closed cystic structure composed of the bilayer membrane of the normal mitochondria. In the slices of the model group, the mitochondrial number was significantly reduced and the mitochondria swelled when compared with control. And as indicated by the yellow arrow, the mitochondria of the model group were cavitated, which may be attributed to reduced matrix particles. While in the scoparone group, there were almost no lipid droplets and the number of mitochondria was more than that of the model group. The mRNA levels of PGC-1α, NRF1, and TFAM, and relative copy number of mtDNA were detected reduced in the liver of NASH mice, which were raised by scoparone significantly (**Figure 8B**). Mitochondrial dysfunction is generally involved in excessive ROS production, which can trigger lipid peroxidation to cause cell damage. 4-hydroxynonenal (4-HNE), a product of lipid peroxidation, is often used to indicate the ROS level. As shown in **Figure 8C**, the IHC of 4-HNE displayed an obviously higher level of oxidative stress in the liver tissues of the model group than that in the control, which was improved by scoparone treatment.

The expression levels of JNK/Sab pathway-related molecules in mice liver tissues were also measured

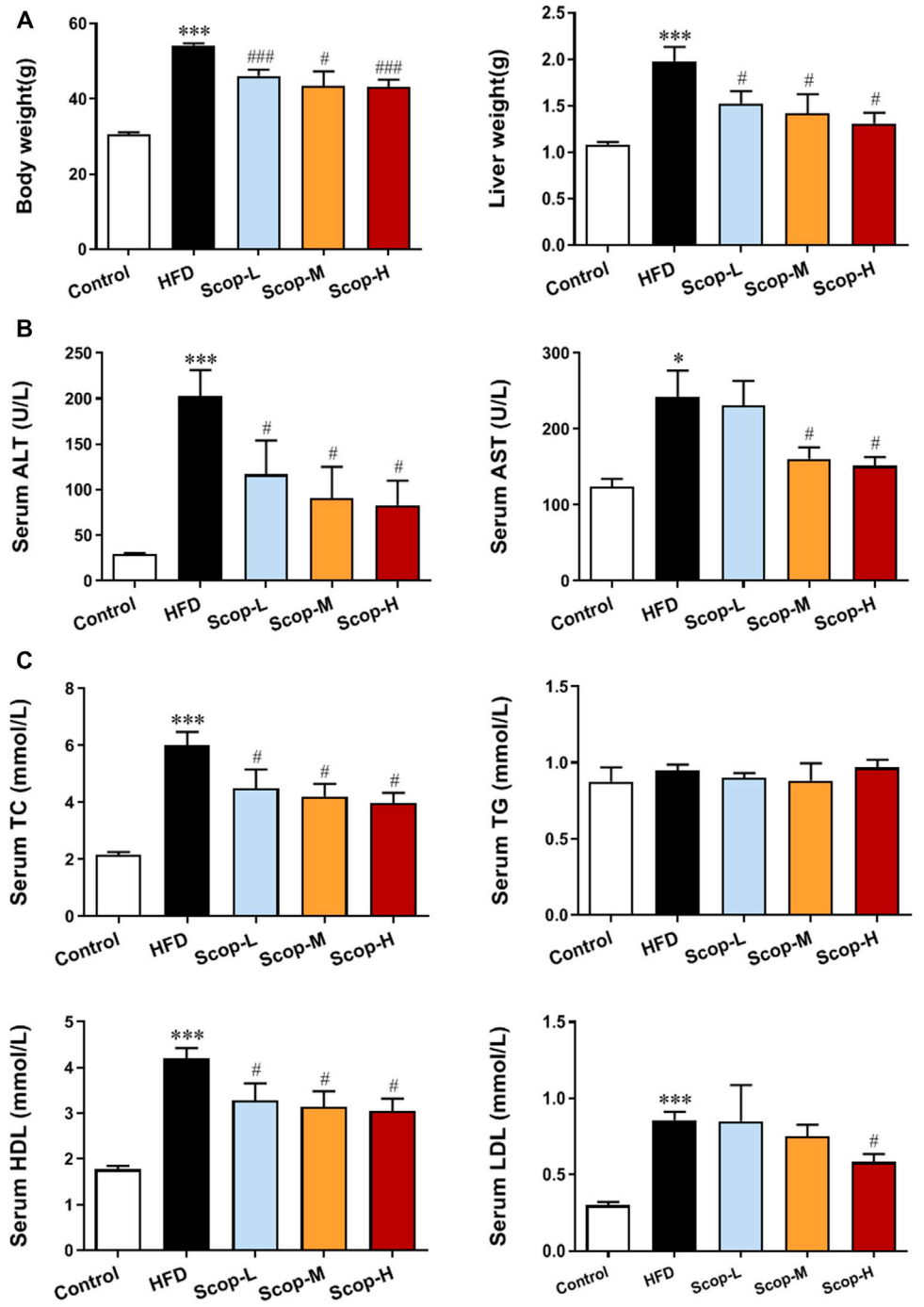

FIGURE 6 | Scoparone improved the body weight, liver weight and serum levels of lipid and aminotransferases in the HFD-induced NASH mice. **(A)** Body weight and liver weight of mice. **(B)** Serum lipid level. **(C)** Serum liver enzyme levels. $^{*}p < 0.05$, $^{***}p < 0.001$ vs. Control; $^{\#}p < 0.05$, $^{\#\#\#}p < 0.001$ vs. Model.

(**Figure 8D**). There was no difference in Sab expression as well as total JNK and Src protein among different groups. Compared with the control, P-JNK/JNK and P-SHP-1/SHP-1 ratios were significantly increased, while P-Src/Src ratio decreased in the liver tissues of NASH mice. Scoparone could reverse the changes of these protein ratios, suggesting its inhibitory effect on the activation of JNK/Sab signaling pathway in the liver of NASH mice.

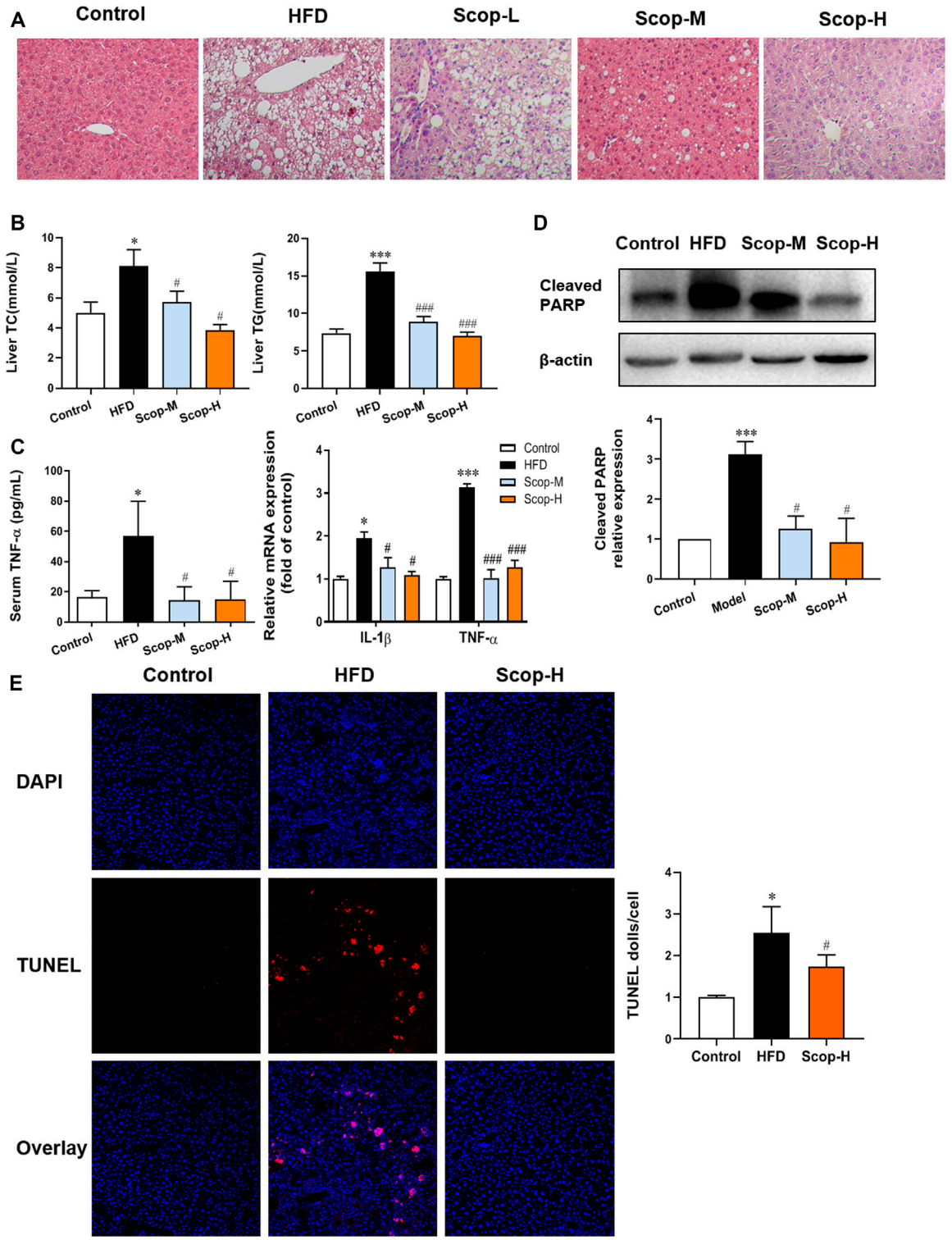

FIGURE 7 | Scoparone reduced the lipotoxic liver injury in the HFD-induced NASH mice. **(A)** HE staining of mouse liver tissues (200×). **(B)** The TG and TC content of mouse liver tissues. **(C)** Serum TNF-α level and IL-1β, TNF-α mRNA expression of liver tissues. **(D)** Cleaved PARP protein expression in mouse liver tissues. **(E)** TUNEL staining of mouse liver tissues (200×). $^{*}p < 0.05$, $^{***}p < 0.001$ vs. Control; $^{\#}p < 0.05$, $^{\#\#\#}p < 0.001$ vs. Model.

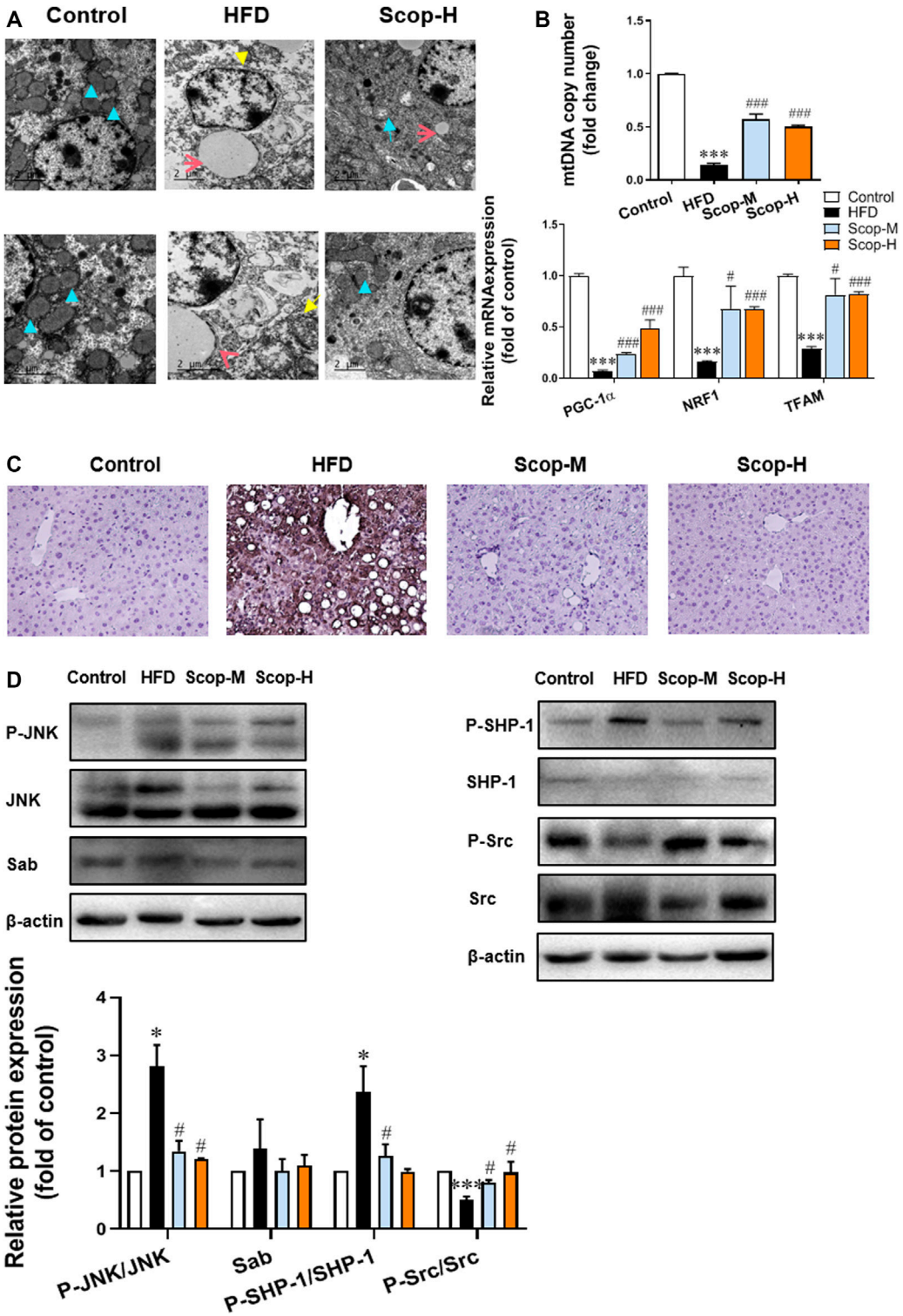

FIGURE 8 | Scoparone inhibited the JNK/Sab signaling pathway and improved mitochondrial dysfunction in the liver tissues of NASH mice. **(A)** Electron microscope images of the mouse liver tissues (blue arrow: normal mitochondria, yellow arrow: mitochondrial cavitation, red arrow: lipid droplets) (200,00×). **(B)** PGC-1α protein expression in mouse liver tissues. **(C)** IHC staining of 4-HNE in mouse liver tissues (200×). **(D)**The expression and/or activation level of JNK/Sab signaling-related protein. $^{***}p < 0.001$ vs. Control; $^{\#}p < 0.05$, $^{\#\#\#}p < 0.001$ vs. Model.

DISCUSSION

Lipotoxic liver injury refers to cell damage or even cell death attributed to the excessive accumulation of fatty acids in the liver, which is the most obvious characteristic of NASH (Machado and Diehl, 2016). Mitochondrial dysfunction induced by an overload of fatty acids is regarded as a major factor for lipotoxic liver injury of NASH (Satapati et al., 2012). Mitochondria are organelles with a biolayer membrane composed of four parts: the outer membrane, intermembrane space, inner membrane, and matrix (Vakifahmetoglu-Norberg et al., 2017). Under physiological conditions, mitochondria produce direct energy ATP and a few amounts of ROS to maintain normal cell activities (Shadel and Horvath, 2015). When the mitochondrial function was damaged, electron transfer is blocked and ATP synthesis is suppressed, leading to increased ROS generation (Cortez-Pinto et al., 1999). A high level of ROS, in turn, exacerbates mitochondrial dysfunction and energy dysmetabolism, as well as induces lipid peroxidation to cause cell damage (Kaser et al., 2005; Weltman et al., 2010). In addition, as mitochondrial membrane permeability rises when damaged, apoptosis-related factors release from the mitochondria into the cytoplasm, which could activate downstream proteins of the cysteinyl aspartate specific proteinase (Caspase) family to trigger cell apoptosis (Ma et al., 2014). Moreover, mitochondrial dysfunction can also induce inflammation, necrosis, and fibrosis of liver cells (Ding, 2010). It has been found that the severity of liver steatosis is positively relevant to the degree of mitochondrial function in NASH (Morris et al., 2011). Alleviating mitochondrial damage can reduce lipid accumulation in hepatocytes induced by high glucose (Hsu et al., 2015). And in patients with NASH, liver steatosis can be inhibited by drugs restoring the mitochondrial respiratory chain and reducing inflammation and fibrosis (Begriche et al., 2013).

In this study, the mice induced by a high-fat diet showed diffuse liver steatosis, accompanied by increased apoptosis and up-regulation of transaminase, indicating the lipotoxic liver injury in the NASH model. Of note, we found abnormal mitochondrial structure and decreased quantity in the hepatocytes and decreased PGC-1α protein expression, as well as increased lipid peroxide in the NASH mice. The *in vitro* experiment also showed PA-induced cell apoptosis and lipid accumulation, which resulted in lipotoxic damage. In addition, the decrease of mitochondrial membrane potential, ATP level, and PGC-1α protein expression, and the increase of ROS level indicated mitochondrial dysfunction in NASH mice. Consistent with previous studies, these results also proved the crucial role of lipid-induced mitochondria dysfunction in NASH progress. But the regulated mechanism remains unclear.

It has been found that sustained JNK activation plays an important role in the lipotoxic injury of NASH. JNK can be phosphorylated and activated by a variety of stress-related signals, such as saturated fatty acids, ROS, and pro-inflammatory cytokine (Gan et al., 2014). Its activation could upregulate the transcription of inflammatory cytokines and promote their release through activating the NLR family pyrin domain-containing protein 3 (NLRP3) inflammasome (Li et al., 2015). JNK can also mediate cell apoptosis by inducing activation of transcription factors like c-Jun to produce apoptotic related molecules or by directly regulating the activation of Bcl-2 family members (Han et al., 2009; Win et al., 2011). It was reported that continuous JNK activation could damage the function of the mitochondrial respiratory chain and causes mitochondrial dysfunction (Gan et al., 2014). Furthermore, previous studies have found that JNK is activated in a Sab-dependent manner in acetaminophen (APAP) and tumor necrosis factor/Galactosamine-induced acute liver injury of mice (Win et al., 2016). Under physiological conditions, the mitochondrial membrane protein Sab binds to SH2-containing protein tyrosine phosphatase (SHP-1). Whereas under stress pathological state during liver injury, continuously activated JNK specifically binds to Sab and causes its conformational change, which makes SHP-1 separate from Sab and is phosphorylated by non-receptor tyrosine kinase c-Src (Tyrosine Phosphatase c-Src, Src). SHP-1 is an important member of the protein tyrosine kinase (PTK) family and plays a role in maintaining the phosphorylation level of tyrosine (Zhang et al., 2000). Src is located both on the outer membrane and inside the mitochondrion (Gomez-Puerta and Mocsai, 2013). It regulates multiple signal transduction involving processes such as proliferation, differentiation, and apoptosis. Inhibition of Src could directly suppress the electron transport of mitochondria and promote ROS generation (Yeatman and Timothy, 2004; Sharma et al., 2016). In

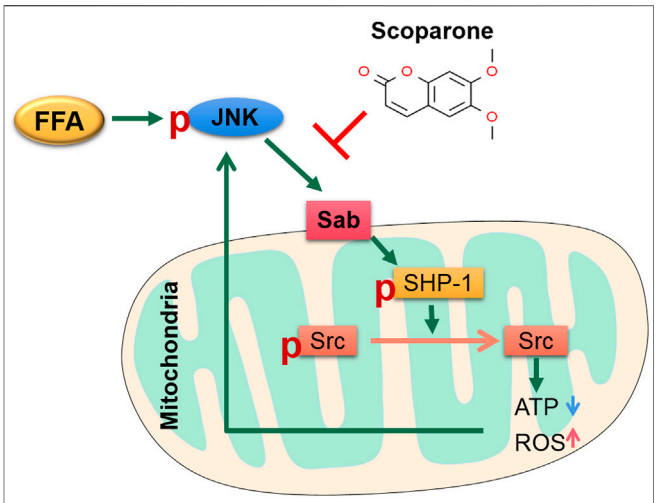

FIGURE 9 | The sketch of the mechanism of JNK/Sab signaling pathway involved in mitochondrial dysfunction in NASH and the effect of Scoparone. Stimulated by free fatty acids, JNK is activated and binds to the outer mitochondrial transmembrane protein Sab, which then releases and promotes the activation of SHP-1 in mitochondria. Phosphorylated SHP-1 could induce the inactivation of Src, which leads to damage of mitochondrial electron transport chain, thereby reducing ATP production and increasing ROS generation. The mitochondrial damage in turn stimulates JNK and thus results in sustained activation of JNK. Scoparone can reverse this process partly through inhibiting the JNK/Sab signaling.

turn, excess ROS can reduce ATP production and the activity of Src (Srikanthan et al., 2016). Activated SHP-1 by JNK/Sab is transferred to the inner mitochondrial membrane and mediates the inactivation of Src, thereby causing mitochondrial dysfunction (Win et al., 2015; Win et al., 2016).

In this study, to further clarify the role of the JNK/Sab pathway in NASH-related hepatotoxicity injury, we used the key molecule Sab knockdown cells in PA induction experiments. It was found that, compared with the scramble, Sab knockdown inhibited the activation of downstream SHP-1 while increasing Src phosphorylation level, suggesting that Sab knockdown has an inhibitory effect on this pathway. Affected by the inhibition of the JNK/Sab pathway, the mitochondrial dysfunction of Sab knockdown cells was improved than that of scramble cells induced by PA, as evidenced by the restorative upregulation of mitochondrial ATP production and mitochondrial membrane potential. And in the hepatocytes with Sab knockdown, cell viability was enhanced, whereas lipid accumulation and apoptosis were reduced, when compared with scramble cells. Interestingly, Sab knockdown also significantly reduced the phosphorylated JNK level, probably because that Sab knockdown reversed PA-induced mitochondrial dysfunction and reduced ROS level, forming a feedback inhibition to JNK. Collectively, our results indicate that JNK/Sab signaling pathway is activated after fatty acids deposit in hepatocytes of NASH mice, a mechanism that may be involved in liver mitochondrial dysfunction and liver damage (**Figure 9**).

At present, TCM is widely used in the treatment of fatty liver disease and shows curative effects. Based on the pathogenesis of NAFLD of TCM theory, we developed the compound formula Jiangzhi Granule, composed of five herbal medicine including Artemisiae Scopariae Herba, which is effective for the clinical treatment of NAFLD (Pan et al., 2013). Previous studies have shown that the compound can improve hepatic steatosis and inflammation, reduce serum transaminases, and inhibit JNK activation in liver tissue of NASH mice (Liu et al., 2014). To further explore its mechanism, pharmacological research on its components was carried out. Scoparone, one component of Artemisiae Scopariae Herba, was found effective in reducing lipid accumulation and protecting liver function. The *in vivo* experiments in our study confirmed its potential against lipotoxic liver injury in the HFD-induced NASH mice. This effect against liver injury is consistent with some previous studies. It has been found that scoparone could improve acute liver injury in mice caused by p-acetylphenol, significantly reducing histopathological changes in liver tissue and cell apoptosis (Hui Y. et al., 2020). In an *in vivo* experiment of cholestatic liver disease, scoparone inhibited liver inflammation and fibrosis, improved cholestasis, and promoted the recovery of liver injury by upregulating the expression of farnesoid X receptor/bile salt export pump (FXR/BSEP) pathway (Yuan et al., 2020). Liu X Showed that scoparone could inhibit the transforming growth factor-β (TGF-β)/Smad/Stat3 signaling pathway, therefore inhibiting the proliferation of hepatic stellate cells and significantly reducing liver fibrosis (Liu and Zhao, 2017).

Notably, Liu B et al. have shown that scoparone could improve hepatocyte inflammation, apoptosis, inflammation as well as hepatic steatosis in methionine and choline-deficient (MCD) diet-induced NASH mice, which was similar to our results in HFD-induced mice. However, in their *in vitro* experiment, scoparone was found unable to reduce the hepatosteatosis in PA-induced AML12 cells. And it was concluded that the effect of scoparone against NASH through blocking TLR-4/NF-κB signaling-mediated immune responses of macrophages (Liu et al., 2020). Different from the above study, our results demonstrated that scoparone could reverse PA-induced lipotoxic injury of hepatocytes, such as cell viability, apoptosis, and lipid accumulation in HepG2 and AML12 cells. This contradiction may be due to the different intervention conditions and the degree of cell damage in the two experiments, which may need further analysis and confirmation. However, scoparone has been shown capable of regulating lipid metabolism in some previous researches. In one study, scoparone exposure at a low, non-cytotoxic dose significantly altered metabolism in primary hepatocytes isolated from ICR male mice. Lipid changes, e.g., the levels of identified PG (19:1 (9Z)/14:0), PE (17:1 (9Z)/0:0), PE (19:1 (9Z)/0:0) were found to be upregulated in the ethanol-induced group, which were downregulated in scoparone group (Zhang et al., 2016). Moreover, scoparone could inhibit TG accumulation in the mature adipocytes. Further study revealed that scoparone negatively regulated the expression level and transcriptional activity of the key adipogenic transcription factor, PPARγ, in 3T3-L1 preadipocytes and suppressed adipogenesis (Noh et al., 2013). These studies support that scoparone could suppress the lipotoxic injury of hepatocytes directly.

In ethanol-induced HepG2 cells, it has been found that scoparone could ameliorate oxidative stress-mediated injury (Noh et al., 2011). Our results also demonstrated the level of ROS and lipid peroxide 4-HNE was downregulated by scoparone. Moreover, PA-induced reduction of mitochondrial membrane potential and ATP generation of hepatocytes, as well as the changes of mitochondrial number and morphology in the liver tissues of NASH mice were reversed by scoparone treatment, indicating the effect of scoparone in improving mitochondrial number and function. As mitochondrial dysfunction is the major contributor to ROS generation, thus the anti-oxidative stress role of scoparone might be through restoring mitochondrial function. Further study showed that scoparone treatment could reverse the PA-induced activation of JNK and SHP-1, and inactivation of Src in the experiments *in vitro* and *in vivo*, which was consistent with the results of Sab knockdown. As the aforementioned involvement of JNK/Sab signaling in mitochondrial dysfunction of hepatocytes, we consider that scoparone could ameliorate the lipotoxic liver injury in NASH partially via inhibiting the JNK/Sab pathway and improving mitochondrial dysfunction (**Figure 9**).

CONCLUSION

In summary, the accumulation of fatty acids activates JNK/Sab signaling pathway to induce mitochondrial dysfunction, promoting

ROS release and cell apoptosis, which contributes to the lipotoxic liver injury in NASH. Blocking this signaling pathway can reverse hepatic steatosis and cell damage. Moreover, we confirmed the effect of the naturally-derived compound scoparone against HFD-induced NASH. The pharmacological mechanism of scoparone involves the inhibition of JNK/Sab signaling-mediated mitochondrial dysfunction. Therefore, scoparone may serve as a potential therapeutic compound in the treatment of NASH.

DATA AVAILABILITY STATEMENT

The original contributions presented in the study are included in the article/**Supplementary Material**, further inquiries can be directed to the corresponding authors.

ETHICS STATEMENT

The study was conducted according to the guidelines of the Declaration of Helsinki and approved by the Animal Experiment Ethics Committee of Longhua Hospital Affiliated to Shanghai University of Traditional Chinese Medicine (NO. LHERAW-190001).

AUTHOR CONTRIBUTIONS

Conception and design: PZ, HS, and JX; Administrative support: PZ, LY; Collection and assembly of data: YJ, JX, PH, LY, YAL, YPL, and JW; Data analysis and interpretation: HS, YJ, and PH; Manuscript writing: YJ, HS, and PZ; Final approval of manuscript: all authors.

FUNDING

This work was supported by the National Natural Science Foundation of China (No. 81704047, 82174287, and 81704018), the Natural Science Foundation of Shanghai (No. 21ZR1463900, 20ZR1458900), and the Graduate Student Innovation Program of Shanghai University of Traditional Chinese Medicine (No. 520).

SUPPLEMENTARY MATERIAL

The Supplementary Material for this article can be found online at: https://www.frontiersin.org/articles/10.3389/fphar.2022.863756/full#supplementary-material

REFERENCES

Begriche, K., Massart, J., Robin, M. A., Bonnet, F., and Fromenty, B. (2013). Mitochondrial Adaptations and Dysfunctions in Nonalcoholic Fatty Liver Disease. *Hepatology* 58 (4), 1497–1507. doi:10.1002/hep.26226

Cortez-Pinto, H., Chatham, J., Chacko, V. P., Arnold, C., Rashid, A., and Diehl, A. M. (1999). Alterations in Liver ATP Homeostasis in Human Nonalcoholic Steatohepatitis: A Pilot Study. *JAMA* 282 (17), 1659–1664. doi:10.1001/jama.282.17.1659

Cotter, T. G., and Rinella, M. (2020). Nonalcoholic Fatty Liver Disease 2020: The State of the Disease. *Gastroenterology* 158 (7), 1851–1864. doi:10.1053/j.gastro.2020.01.052

Court, N. W., Kuo, I., Quigley, O., and Bogoyevitch, M. A. (2004). Phosphorylation of the Mitochondrial Protein Sab by Stress-Activated Protein Kinase 3. *Biochem. Biophys. Res. Commun.* 319 (1), 130–137. doi:10.1016/j.bbrc.2004.04.148

Ding, W. X. (2010). Role of Autophagy in Liver Physiology and Pathophysiology. *World J. Biol. Chem.* 1 (1), 3–12. doi:10.4331/wjbc.v1.i1.3

Fang, H., Zhang, A., Yu, J., Wang, L., Liu, C., Zhou, X., et al. (2016). Insight into the Metabolic Mechanism of Scoparone on Biomarkers for Inhibiting Yanghuang Syndrome. *Sci. Rep.* 6 (1), 37519. doi:10.1038/srep37519

Gan, L. T., Van Rooyen, D. M., Koina, M. E., Mccuskey, R. S., Teoh, N. C., and Farrell, G. C. (2014). Hepatocyte Free Cholesterol Lipotoxicity Results from JNK1-Mediated Mitochondrial Injury and Is HMGB1 and TLR4-dependent. *J. Hepatol.* 61 (6), 1376–1384. doi:10.1016/j.jhep.2014.07.024

Genova, M. L., and Lenaz, G. (2014). Functional Role of Mitochondrial Respiratory Supercomplexes. *Biochim. Biophys. Acta* 1837 (4), 427–443. doi:10.1016/j.bbabio.2013.11.002

Gomez-Puerta, J. A., and Mócsai, A. (2013). Tyrosine Kinase Inhibitors for the Treatment of Rheumatoid Arthritis. *Curr. Top. Med. Chem.* 13 (6), 760–773. doi:10.2174/15680266113139990094

Guerrero-Beltrán, C. E., Bernal-Ramírez, J., Lozano, O., Oropeza-Almazán, Y., Castillo, E. C., Garza, J. R., et al. (2017). Silica Nanoparticles Induce Cardiotoxicity Interfering with Energetic Status and Ca2+ Handling in Adult Rat Cardiomyocytes. *Am. J. Physiol. Heart Circ. Physiol.* 312 (4), H645. doi:10.1152/ajpheart.00564.2016

Han, D., Ybanez, M. D., Ahmadi, S., Yeh, K., and Kaplowitz, N. (2009). Redox Regulation of Tumor Necrosis Factor Signaling. *Antioxid. Redox Signal.* 11 (9), 2245–2263. doi:10.1089/ars.2009.2611

Hsu, W. H., Lee, B. H., and Pan, T. M. (2015). Leptin-induced Mitochondrial Fusion Mediates Hepatic Lipid Accumulation. *Int. J. Obes. (Lond)* 39 (12), 1750–1756. doi:10.1038/ijo.2015.120

Hui, W. Y., Jiing, Z., Chuan, Z. X., and Yang, Y. (2020a). Scoparone Prevents Acute Liver Injury Induced by Excessive Acetaminophen in Mice by Inhibiting the Expression of Matrilin-2. *Drugs & Clinic* 35 (07), 1301–1306. doi:10.7501/j.issn.1674-5515.2020.07.003

Hui, Y., Wang, X., Yu, Z., Fan, X., Cui, B., Zhao, T., et al. (2020b). Scoparone as a Therapeutic Drug in Liver Diseases: Pharmacology, Pharmacokinetics and Molecular Mechanisms of Action. *Pharmacol. Res.* 160, 105170. doi:10.1016/j.phrs.2020.105170

Ibrahim, S. H., and Gores, G. J. (2012). Who Pulls the Trigger: JNK Activation in Liver Lipotoxicity? *J. Hepatol.* 56 (1), 17–19. doi:10.1016/j.jhep.2011.04.017

Jin, H., Cheng, J., Hua, L. T., Long, Y. H., and He, X. X. (2005). Determination of Scoparia Lactone in Different Harvest Times and Different Parts of Herba Artemisiae and Suggestions on Resource Utilization *Pharmaceutical Journal of Chinese People' s Liberation Army* 21 (2), 155–156. doi:10.3969/j.issn.1008-9926.2005.02.026

Kang, J. W., Kim, D. W., Choi, J. S., Kim, Y. S., and Lee, S. M. (2013). Scoparone Attenuates D-Galactosamine/lipopolysaccharide-Induced Fulminant Hepatic Failure through Inhibition of Toll-like Receptor 4 Signaling in Mice. *Food Chem. Toxicol.* 57, 132–139. doi:10.1016/j.fct.2013.03.016

Kaser, S., Moschen, A., Cayon, A., Kaser, A., Crespo, J., Pons-Romero, F., et al. (2005). Adiponectin and its Receptors in Non-alcoholic Steatohepatitis. *Gut* 54 (1), 117–121. doi:10.1136/gut.2003.037010

Li, Q., Zhang, X., Wang, W., Li, L., Xu, Q., Wu, X., et al. (2015). CPT-11 Activates NLRP3 Inflammasome through JNK and NF-Kb Signalings. *Toxicol. Appl. Pharmacol.* 289 (2), 133–141. doi:10.1016/j.taap.2015.09.025

Liu, B., Deng, X., Jiang, Q., Li, G., Zhang, J., Zhang, N., et al. (2020). Scoparone Improves Hepatic Inflammation and Autophagy in Mice with Nonalcoholic Steatohepatitis by Regulating the ROS/P38/Nrf2 axis and PI3K/AKT/mTOR Pathway in Macrophages. *Biomed. Pharmacother.* 125, 109895. doi:10.1016/j.biopha.2020.109895

Liu, X., and Zhao, X. (2017). Scoparone Attenuates Hepatic Stellate Cell Activation through Inhibiting TGF-β/Smad Signaling Pathway. *Biomed. Pharmacother.* 93, 57–61. doi:10.1016/j.biopha.2017.06.006

Liu, Y., Song, H., Wang, L., Xu, H., Shu, X., Zhang, L., et al. (2014). Hepatoprotective and Antioxidant Activities of Extracts from Salvia-Nelumbinis Naturalis against Nonalcoholic Steatohepatitis Induced by Methionine- and Choline-Deficient Diet in Mice. *J. Transl. Med.* 12 (1), 315. doi:10.1186/s12967-014-0315-x

Ma, Y., Zhang, J., Zhang, Q., Chen, P., Song, J., Yu, S., et al. (2014). Adenosine Induces Apoptosis in Human Liver Cancer Cells through ROS Production and Mitochondrial Dysfunction. *Biochem. Biophys. Res. Commun.* 448 (1), 8–14. doi:10.1016/j.bbrc.2014.04.007

Machado, M. V., and Diehl, A. M. (2016). Pathogenesis of Nonalcoholic Steatohepatitis. *Gastroenterology* 150 (8), 1769–1777. doi:10.1053/j.gastro.2016.02.066

Matsushita, M., Yamadori, T., Kato, S., Takemoto, Y., Inazawa, J., Baba, Y., et al. (1998). Identification and Characterization of a Novel SH3-Domain Binding Protein, Sab, Which Preferentially Associates with Bruton's Tyrosine Kinase (Btk). *Biochem. Biophysical Res. Commun.* 245 (2), 337–343. doi:10.1006/bbrc.1998.8420

Morris, E. M., Rector, R. S., Thyfault, J. P., and Ibdah, J. A. (2011). Mitochondria and Redox Signaling in Steatohepatitis. *Antioxid. Redox Signal.* 15 (2), 485–504. doi:10.1089/ars.2010.3795

Nawrot-Modranka, J., Nawrot, E., and Graczyk, J. (2006). *In Vivo* antitumor, *In Vitro* Antibacterial Activity and Alkylating Properties of Phosphorohydrazine Derivatives of Coumarin and Chromone. *Eur. J. Med. Chem.* 41 (11), 1301–1309. doi:10.1016/j.ejmech.2006.06.004

Nijboer, C. H., Bonestroo, H. J., Zijlstra, J., Kavelaars, A., and Heijnen, C. J. (2013). Mitochondrial JNK Phosphorylation as a Novel Therapeutic Target to Inhibit Neuroinflammation and Apoptosis after Neonatal Ischemic Brain Damage. *Neurobiol. Dis.* 54, 432–444. doi:10.1016/j.nbd.2013.01.017

Noh, J. R., Kim, Y. H., Gang, G. T., Hwang, J. H., Lee, H. S., Ly, S. Y., et al. (2011). Hepatoprotective Effects of Chestnut (Castanea Crenata) Inner Shell Extract against Chronic Ethanol-Induced Oxidative Stress in C57BL/6 Mice. *Food Chem. Toxicol.* 49 (7), 1537–1543. doi:10.1016/j.fct.2011.03.045

Noh, J. R., Kim, Y. H., Hwang, J. H., Gang, G. T., Yeo, S. H., Kim, K. S., et al. (2013). Scoparone Inhibits Adipocyte Differentiation through Down-Regulation of Peroxisome Proliferators-Activated Receptor γ in 3T3-L1 Preadipocytes. *Food Chem.* 141 (2), 723–730. doi:10.1016/j.foodchem.2013.04.036

Pan, J., Wang, M., Song, H., Wang, L., and Ji, G. (2013). The Efficacy and Safety of Traditional Chinese Medicine (Jiang Zhi Granule) for Nonalcoholic Fatty Liver: A Multicenter, Randomized, Placebo-Controlled Study. *Evidence-Based Complement. Altern. Med.* 2013, 1–8. doi:10.1155/2013/965723

Patel, S. S., and Siddiqui, M. S. (2019). Current and Emerging Therapies for Non-alcoholic Fatty Liver Disease. *Drugs* 79 (1), 75–84. doi:10.1007/s40265-018-1040-1

Patterson, R. E., Kalavalapalli, S., Williams, C. M., Nautiyal, M., Mathew, J. T., Martinez, J., et al. (2016). Lipotoxicity in Steatohepatitis Occurs Despite an Increase in Tricarboxylic Acid Cycle Activity. *Am. J. Physiol. Endocrinol. Metab.* 310 (7), E484–E494. doi:10.1152/ajpendo.00492.2015

Rockenfeller, P., Ring, J., Muschett, V., Beranek, A., Buettner, S., Carmona-Gutierrez, D., et al. (2010). Fatty Acids Trigger Mitochondrion-dependent Necrosis. *Cell Cycle* 9 (14), 2836–2842. doi:10.4161/cc.9.14.12267

Satapati, S., Sunny, N. E., Kucejova, B., Fu, X., He, T. T., Méndez-Lucas, A., et al. (2012). Elevated TCA Cycle Function in the Pathology of Diet-Induced Hepatic Insulin Resistance and Fatty Liver. *J. Lipid Res.* 53 (6), 1080–1092. doi:10.1194/jlr.M023382

Shadel, G. S., and Horvath, T. L. (2015). Mitochondrial ROS Signaling in Organismal Homeostasis. *Cell* 163 (3), 560–569. doi:10.1016/j.cell.2015.10.001

Sharma, Y., Ahmad, A., Bashir, S., Elahi, A., and Khan, F. (2016). Implication of Protein Tyrosine Phosphatase SHP-1 in Cancer-Related Signaling Pathways. *Future Oncol.* 12 (10), 1287–1298. doi:10.2217/fon-2015-0057

Srikanthan, K., Shapiro, J. I., and Sodhi, K. (2016). The Role of Na/K-ATPase Signaling in Oxidative Stress Related to Obesity and Cardiovascular Disease. *Molecules* 21 (9), 1172. doi:10.3390/molecules21091172

Sunny, N. E., Bril, F., and Cusi, K. (2017). Mitochondrial Adaptation in Nonalcoholic Fatty Liver Disease: Novel Mechanisms and Treatment Strategies. *Trends Endocrinol. Metab.* 28 (4), 250–260. doi:10.1016/j.tem.2016.11.006

Takeshita, Y., Hashimoto, Y., Nawa, M., Uchino, H., and Matsuoka, M. (2013). SH3-binding Protein 5 Mediates the Neuroprotective Effect of the Secreted Bioactive Peptide Humanin by Inhibiting C-Jun NH2-terminal Kinase. *J. Biol. Chem.* 288 (34), 24691–24704. doi:10.1074/jbc.M113.469692

Tilg, H., and Moschen, A. R. M. (2010). Evolution of Inflammation in Nonalcoholic Fatty Liver Disease: the Multiple Parallel Hits Hypothesis. *Hepatology* 52 (5), 1836–1846. doi:10.1002/hep.24001

Vakifahmetoglu-Norberg, H., Ouchida, A. T., and Norberg, E. (2017). The Role of Mitochondria in Metabolism and Cell Death. *Biochem. Biophys. Res. Commun.* 482 (3), 426–431. doi:10.1016/j.bbrc.2016.11.088

Vinten-Johansen, J. (2020). Commentary: Mitochondria Are More Than Just the Cells' Powerhouse. *J. Thorac. Cardiovasc. Surg.* 160 (2), e33–e34. doi:10.1016/j.jtcvs.2019.07.029

Wan, C., Wei, Y., Ma, J., and Geng, X. (2018). Protective Effects of Scoparone against Ischemia-reperfusion-induced M-yocardial I-njury. *Mol. Med. Rep.* 18 (2), 1752–1760. doi:10.3892/mmr.2018.9123

Weltman, M. D., Farrell, G. C., Hall, P., Ingelman-Sundberg, M., and Liddle, C. (2010). Hepatic Cytochrome P450 2E1 Is Increased in Patients with Nonalcoholic Steatohepatitis. *Hepatology* 27 (1), 128–133. doi:10.1002/hep.510270121

Wiltshire, C., Matsushita, M., Tsukada, S., Gillespie, D. A., and May, G. H. (2002). A New C-Jun N-Terminal Kinase (JNK)-interacting Protein, Sab (SH3BP5), Associates with Mitochondria. *Biochem. J.* 367 (Pt 3), 577–585. doi:10.1042/BJ20020553

Win, S., Than, T. A., Han, D., Petrovic, L. M., and Kaplowitz, N. (2011). c-Jun N-Terminal Kinase (JNK)-dependent Acute Liver Injury from Acetaminophen or Tumor Necrosis Factor (TNF) Requires Mitochondrial Sab Protein Expression in Mice. *J. Biol. Chem.* 286 (40), 35071–35078. doi:10.1074/jbc.M111.276089

Win, S., Than, T. A., Le, B. H., García-Ruiz, C., Fernandez-Checa, J. C., and Kaplowitz, N. (2015). Sab (Sh3bp5) Dependence of JNK Mediated Inhibition of Mitochondrial Respiration in Palmitic Acid Induced Hepatocyte Lipotoxicity. *J. Hepatol.* 62 (6), 1367–1374. doi:10.1016/j.jhep.2015.01.032

Win, S., Than, T. A., Min, R. W., Aghajan, M., and Kaplowitz, N. (2016). c-Jun N-Terminal Kinase Mediates Mouse Liver Injury through a Novel Sab (SH3BP5)-dependent Pathway Leading to Inactivation of Intramitochondrial Src. *Hepatology* 63 (6), 1987–2003. doi:10.1002/hep.28486

Yan, Y., Wei, W. Q., and Yan, Z. (2011). Research Progress of Scoparone. *China Pharmaceuticals* 20 (19), 1–3. doi:10.3969/j.issn.1006-4931.2011.19.001

Yeatman, T. J., and Timothy, J. (2004). A Renaissance for SRC. *Nat. Rev. Cancer* 4 (6), 470–480. doi:10.1038/nrc1366

Younossi, Z. M., Stepanova, M., Anstee, Q. M., Lawitz, E. J., Wai-Sun Wong, V., Romero-Gomez, M., et al. (2019). Reduced Patient-Reported Outcome Scores Associate with Level of Fibrosis in Patients with Nonalcoholic Steatohepatitis. *Clin. Gastroenterol. Hepatol.* 17 (12), 2552–e10. e10. doi:10.1016/j.cgh.2019.02.024

Yuan, H. Y., Lang, L., Qiang, D. H., and Le, C. (2020). Effects of Scoparone on FXR/BSEP Signal Pathway and Intrahepatic Cholestasis in Rats with Common Bile Duct Ligation. *Chongqing Med.* 49 (10), 1570–1574+1584. CNKI:SUN:CQYX.0.2020-10-005

Zhang, A., Qiu, S., Sun, H., Zhang, T., Guan, Y., Han, Y., et al. (2016). Scoparone Affects Lipid Metabolism in Primary Hepatocytes Using Lipidomics. *Sci. Rep.* 6 (1), 28031. doi:10.1038/srep28031

Zhang, J., Somani, A. K., and Siminovitch, K. A. (2000). Roles of the SHP-1 Tyrosine Phosphatase in the Negative Regulation of Cell Signalling. *Semin. Immunol.* 12 (4), 361–378. doi:10.1006/smim.2000.0223

Conflict of Interest: The authors declare that the research was conducted in the absence of any commercial or financial relationships that could be construed as a potential conflict of interest.

Publisher's Note: All claims expressed in this article are solely those of the authors and do not necessarily represent those of their affiliated organizations, or those of the publisher, the editors and the reviewers. Any product that may be evaluated in this article, or claim that may be made by its manufacturer, is not guaranteed or endorsed by the publisher.

frontiers | Frontiers in Pharmacology

ORIGINAL RESEARCH
published: 14 June 2022
doi: 10.3389/fphar.2022.893336

Exploring Ganweikang Tablet as a Candidate Drug for NAFLD Through Network Pharmacology Analysis and Experimental Validation

Chuanrui Ma[1,2,3†], Xinyu Wang[4†], Jing Zhang[1,2†], Yun Zhao[1,2], Yunqing Hua[1,2], Chao Zhang[1,2], Guobin Zheng[5], Guangyan Yang[4], Jianli Guan[6], Huahuan Li[6], Meng Li[6], Lin Kang[4,7], Jiaqing Xiang[4], Guanwei Fan[1,2,3]* and Shu Yang[4,8]**

[1]First Teaching Hospital of Tianjin University of Traditional Chinese Medicine, Tianjin, China, [2]National Clinical Research Center for Chinese Medicine Acupuncture and Moxibustion, Tianjin, China, [3]State Key Laboratory of Component-based Chinese Medicine, Tianjin University of Traditional Chinese Medicine, Tianjin, China, [4]Department of Geriatrics, Shenzhen People's Hospital (The Second Clinical Medical College, Jinan University, The First Affiliated Hospital, Southern University of Science and Technology), Shenzhen, China, [5]NHC Key Laboratory of Hormones and Development, Tianjin Key Laboratory of Metabolic Diseases, Chu Hsien-I Memorial Hospital and Tianjin Institute of Endocrinology, Tianjin Medical University, Tianjin, China, [6]Henan Fusen Pharmaceutical Co., Ltd., Henan, China, [7]The Biobank of National Innovation Center for Advanced Medical Devices, Shenzhen People's Hospital, Shenzhen, China, [8]Integrated Chinese and Western Medicine Postdoctoral Research Station, Jinan University, Guangzhou, China

OPEN ACCESS

Edited by:
Wenji Zhang,
Guangdong Academy of Agricultural Science, China

Reviewed by:
Boqing Gu,
Indiana University Bloomington, United States
Xiaoyang Yu,
University of Pittsburgh, United States

***Correspondence:**
Shu Yang
yang.shu@szhospital.com
Guanwei Fan
guanwei.fan@tjutcm.edu.cn
Jiaqing Xiang
xiangjiaqing@126.com

[†]These authors have contributed equally to this work

Specialty section:
This article was submitted to Gastrointestinal and Hepatic Pharmacology, a section of the journal Frontiers in Pharmacology

Received: 10 March 2022
Accepted: 26 April 2022
Published: 14 June 2022

Citation:
Ma C, Wang X, Zhang J, Zhao Y, Hua Y, Zhang C, Zheng G, Yang G, Guan J, Li H, Li M, Kang L, Xiang J, Fan G and Yang S (2022) Exploring Ganweikang Tablet as a Candidate Drug for NAFLD Through Network Pharmacology Analysis and Experimental Validation. Front. Pharmacol. 13:893336. doi: 10.3389/fphar.2022.893336

Nonalcoholic fatty liver disease (NAFLD) is defined as liver disease in which more than 5% of hepatocytes are steatotic with little or no alcohol consumption. NAFLD includes benign nonalcoholic fatty liver (NAFL) and nonalcoholic steatohepatitis (NASH). Importantly, NASH is an advanced progression of NAFL and is characterized by steatosis, hepatocyte ballooning, lobular inflammation, and fibrosis. However, to date, no drugs specifically targeting NAFLD have been approved by the FDA. Therefore, a new drug or strategy for NAFLD treatment is necessary. However, the pathogenesis of NAFLD is complex and no single-target drugs have achieved the desired results. Noticeably, traditional Chinese medicine formulations are a complex system with multiple components, multiple targets, and synergistic effects between components. The Ganweikang tablet is a compound formula based on traditional Chinese medicine theory and clinical experience. In this study, network pharmacology analysis indicates Ganweikang tablet as a candidate for NAFLD treatment. Furthermore, we evaluated the therapeutic effects of Ganweikang tablet on the NAFL and NASH and tried to clarify the underlying molecular mechanisms in animal models and cell experiments. As expected, Ganweikang tablet was found to improve NAFL and NASH by modulating inflammation, apoptosis, and fatty acid oxidation by inhibiting NFκB, caspase-8, and activating PPARα, which not only indicates that Ganweikang tablet as a drug candidate but also provides a theoretical basis of Ganweikang tablet for the treatment of NAFL and NASH.

Keywords: network pharmacology, NAFL, hepatic steatosis, NASH, inflammation

Abbreviations: ALT, alanine transaminase; ALP, alkaline phosphatase; AST, aspartate transaminase; CCR-2, C–C chemokine receptor type-2; CASP8, caspase8; IL-1β, interleukin 1 beta; NF-κB, nuclear factor κB; and PPARα, peroxisome proliferator-activated receptor-α.

INTRODUCTION

Nonalcoholic fatty liver disease (NAFLD) is defined as liver disease in which more than 5% of hepatocytes are steatotic under the condition of little or no alcohol consumption (Sanyal et al., 2011). NAFLD commences with nonalcoholic fatty liver (NAFL) which is characterized by steatosis with minimal or no lobular inflammation. Throughout the disease, the accumulation of triacylglycerols leads to a fatty infiltration with inflammation, which evolves into a more severe stage of NAFLD, nonalcoholic steatohepatitis (NASH), characterized by ballooning hepatocyte degeneration, diffuse lobular inflammation, and fibrosis (Leoni et al., 2018). As NASH develops, it can progress further to cirrhosis and hepatocellular carcinoma (Goldner and Lavine, 2020). However, to date, no drugs for NAFLD have been approved by the FDA (Sanyal et al., 2015).

The mechanisms underlying NAFLD are mainly related to lipid-induced apoptosis and inflammation (Buzzetti et al., 2016). When the fatty acid catabolism is not sufficient to offset hepatic lipid overload, toxic fatty acid derivatives are generated, which lead to activating inflammatory vesicles, increased endoplasmic reticulum, oxidative stress, and hepatocyte death, thereby promoting the progression of steatosis to NASH (Koliaki et al., 2015). Furthermore, signals from stressed or damaged hepatocytes and activated macrophages drive resident hepatic stellate cells to activate myofibroblasts and produce excessive matrix proteins, which contribute to NASH to a severe stage (Friedman et al., 2018). Dysregulation of NF-κB activation has a significant effect on the development of hepatic steatosis and inflammation, and inhibition of NF-κB ameliorates inflammatory infiltration in the liver of NASH mice (Romics et al., 2004; Locatelli et al., 2013; Rom et al., 2020). In addition, the apoptotic markers, such as caspase-3 and caspase-8, were found to be significantly upregulated in NASH and NAFL mice; and inhibition of either can reduce apoptosis and inflammatory infiltration, which alleviates liver damage in NASH and NAFL mice (Hatting et al., 2013; Wang et al., 2017; Li et al., 2018; El-Derany and El-Demerdash, 2020). Therefore, targeting lipid metabolism and inflammation is an important strategy for NAFLD treatment. The current evidence suggests that pioglitazone, a PPARγ agonist that can improve insulin sensitivity, transaminases, steatosis, inflammation, and ballooning in patients with NASH and T2DM, showed the potential for treating NAFLD (Cusi, 2016; Rinella and Sanyal, 2016; Francque et al., 2021). However, the side effects such as heart failure, fracture, and weight gain caused by pioglitazone limit its further clinical application in the treatment of NAFLD (Morán-Salvador et al., 2011). More importantly, the pathogenesis of NAFLD is complex and no single-target drugs have achieved the desired results (Friedman et al., 2018). Noticeably, traditional Chinese medicine formulation is a complex system with multiple components, multiple targets, and synergistic effects between components, which is supported by the approach of network pharmacology (Hopkins, 2007; Ma et al., 2015). Therefore, traditional Chinese medicine formulation is a potential candidate for NAFLD treatment.

Ganweikang tablet is a compound formula based on traditional Chinese medicine theory and clinical experience, which shows beneficial effects on the liver and no serious adverse reactions have been observed to date. Lianqiao (Fructus Forsythiae), Fangfeng (Radix Saposhnikoviae divaricatae), Shanyinchaihu (Gypsophila pacifica), Mabiancao (Verbena officinalis), Huoxiang (Agastache rugosus), Baishu (Rhizoma Atractylodis macrocephalae), Huangqi (Radix Astragali), and Gancao (Radix Glycyrrhizae) are the main herbal ingredients of Ganweikang tablet. Previous studies have revealed that these herbals formulating Ganweikang tablet can attenuate inflammation (Zhou et al., 2019; Lee et al., 2021), liver injury (Hu et al., 2020), and apoptosis (Fattorusso et al., 2006; Hu et al., 2014; Adesso et al., 2018; Lee et al., 2021; Zhao et al., 2021), which indicates the potential and beneficial effects of Ganweikang tablet on NAFLD. However, whether it can alleviate NAFLD, especially the NAFL and NASH, remains unclear. Therefore, in this study, we attempt to determine the protective effect of Ganweikang tablet on NAFL and NASH and disclose the underlying mechanism through an approach of network pharmacology and animal model experiment as well as cell experiment.

METHODS

Construction of Ganweikang Tablet–Chinese Herbal–Target Genes Network

HERB (http://herb.ac.cn/), a high-throughput experimental and reference Chinese medicine database, was used for mining the target genes of herbal ingredients in Ganweikang tablet (Fang et al., 2021). Totally, 232 potential target genes of the Ganweikang tablet were predicted by HERB, and the Ganweikang herb-target genes network was constructed by Cytoscape software (Shannon et al., 2003). KEGG and WIKI enrichment analysis of Ganweikang target genes was achieved by the ENRICHR online analysis tool (maayanlab.cloud/Enrichr/) (Chen et al., 2013). The ggplot2 and ggpubr packages of R software were used for the visualization of enrichment results (Ito and Murphy, 2013; Whitehead et al., 2019), including terms, gene ratio, gene counts, and p-value.

Regents

Rabbit anti-α-SMA (Cat No. ab179467), Col4α1 (Cat No. ab6586), CD206 (Cat No. ab64693), CD68 (Cat No. ab125212), PPARα (Cat No. ab227074), and mouse anti-CD86 (Cat No. ab220188) antibodies were purchased from Abcam (Cambridge, MA). Rabbit anti-F4/80 (Cat No. #30325), NF-κB-p65 (Cat No. #8242), and phosphorylation of NF-κB-p65 (Cat No. #3033) antibodies were purchased from Cell Signaling Technology. Rabbit anti-β–actin (Cat No. AC028) was purchased from ABclonal (Wuhan, China). Mouse AST ELISA kit (Cat No. ab263882), ALT assay kit (Cat No. ab241035), ALP assay Kit (Cat

No. ab267583), gamma-glutamyl transferase (γ-GT) assay kit (Cat No. ab241029), triglyceride assay kit (Cat No. ab65336), free fatty acid assay (Cat No. ab65341), ROS detection assay (Cat No. ab139476), caspase-3 assay kit (Cat No. ab39401), and mitochondrial complex I enzyme activity microplate assay kit (Cat No. ab109721) and mitochondrial complex III activity assay kit (Cat No. ab287844) were obtained from Abcam (Cambridge, MA). Glycyrrhetinic acid (Cat No. HY-N0375), betaine (Cat No. HY-B0710), ursolic acid (Cat No. HY-N0140), and wogonin (Cat No. HY-N0400) were purchased from MedChemExpress (Shanghai, China).

In Vivo Studies With Animals

All experimental protocols for animal care and *in vivo* studies conform to the Guide for the Care and Use of Laboratory Animals published by the National Institutes of Health (NIH) (NIH Publication No. 85–23, revised 1996). The animal experiments were conducted under the ARRIVE guidelines (McGrath and Lilley, 2015; Lilley et al., 2020; Percie du Sert et al., 2020) and were approved by the Ethics Committee of the Second Clinical School of Jinan University (Shenzhen People's Hospital). Male C57BL/6J wild-type mice (8 ± 0.5 weeks old) were purchased from Gempharmatech Co., Ltd (Nanjing, Jiangsu, China). The mice were housed in the SPF unit of the Shenzhen People's Hospital Animal Centre (12-h light cycle from 8 a.m. to 8 p.m., 23 ± 1°C, 60–70% humidity) and maintained on standard rodent food with free access to water as we previously reported (Xiang et al., 2021). A maximum of 5 mice were housed in each cage bedding with corn cobs, and the mice were given a 7-days acclimatization period before the experiment. The mice were randomly divided into 12 groups and were induced into NAFL and NASH models, respectively. In detail, male C57BL/6J mice were fed a high-fat diet (HFD: 41% fat plus 0.5% cholesterol) for 8 weeks to induce the NALF model; or an MCD diet with 0% methionine and 0% choline for 1 week to induce the NASH model. In the current study, different doses of Ganweikang tablets (low dose, L, 336 mg/kg/day; medium dose, M, 672 mg/kg/day; high dose, H, 1,344 mg/kg/day) were administered in an *in vivo* experiment to detect the therapeutic effects on NAFL and NASH. Fenofibrate (Feno, 100 mg/kg) was used as the positive control drug as previously reported (Lefere et al., 2020). In the NAFL experiment, the mice were treated with normal chow (NC), high-fat diet (HFD), HFD with fenofibrate (Feno), HFD with low-dosage Ganweikang tablet (HFD + L), HFD with medium-dosage Ganweikang tablet (HFD + M), and HFD with high-dosage Ganweikang tablet (HFD + H). In the NASH experiment, the mice were treated with normal chow (NC), MCD, MCD with fenofibrate (Feno), MCD diet with low-dosage Ganweikang tablet (MCD + L), MCD with medium-dose Ganweikang tablet (MCD + M), and MCD with high-dosage Ganweikang tablet (MCD + H). At the end of the experiment, all mice were anesthetized in a CO_2 chamber with the blood and liver being collected. The blood was rested for 4 h and centrifuged (3,000 rpm/min) to obtain the serum that was used to test for γGT, AST, ALT, and ALP to evaluate liver function by the fully automatic biochemical analyzer.

Liver Histology

The liver was pathologically sectioned to assess the lesion. Formalin-fixed and paraffin-embedded liver sections were assessed by hematoxylin and eosin (H&E) for liver histology, Sirius red for fibrosis, and oil red O staining for lipid droplet accumulation. The nonalcoholic fatty liver activity score (NAS) and fibrosis stage were assessed according to the NASH CRN scoring system (Kleiner and Makhlouf, 2016). Histological scoring was performed blinded to the knowledge of the assessor of the treatment received. In addition, CD68, CD206, CD86, F4/80, Col4α1, and αSMA in the liver were detected by immunofluorescence staining to assess inflammation and fibrosis.

Quantitative Real-Time Polymerase Chain Reaction, Western Blot Assay, and ELISA Assay

The method of RNA extraction and cDNA obtained was used as we reported (Xiang et al., 2021). Briefly, qRT-PCR was performed using the ABI Step One Plus ™ Real-time PCR system (Applied Biosystem) with specific primers (**Supplementary Table S1**). The relative mRNA level of target genes was normalized using the level detected in the control group as 1. The expression of *IL-1β, TNF-α, IL-6, Mmp9, Bax, Ccl2, Ccr2, Cxcl1, IL-4, Tgf-β1, Col1α1, Col1α2, Timp-1, Bcl2, and Caspase3* mRNA was normalized by *β-actin* mRNA in the corresponding samples to reflect the transcript levels of inflammation, fibrosis, and apoptosis in the liver. Western blot was performed as we previously reported (Xiang et al., 2021). First, the collected tissue is lysed and homogenized in lysis buffer (Sigma-Aldrich; St. Louis, MO, United States), and total protein was obtained according to the classical protocol. Dilute fresh primary antibody (1:1,000) or anti-β-actin antibody (1: 5,000) and fresh HRP-conjugated anti-rabbit or mouse IgG (1: 5,000) in 1% fresh non-fat dry milk in PBS. The expression of NFκB-p65, p-NFκB-p65, caspase8, PPARα, and β-actin were determined by Western blot as we reported. The livers were cryogenically homogenized, and the TG and FFA levels in them were measured by ELISA according to the instructions.

Molecular Docking

Discovery Studio (DS) is molecular modeling software for drug discovery and protein structure analysis (Zhang et al., 2020). In this study, the DS 2019 version was used to molecularly dock the active ingredient of the Ganweikang tablet with its target protein. The structures of the active ingredients and proteins were downloaded from the NCBI database (https://www.ncbi.nlm.nih.gov/pccompound) and the Protein Data Bank (https://www.rcsb.org), respectively (Barrett et al., 2013; Karuppasamy et al., 2020). The proteins required a series of preparations before docking, including the removal of water molecules, the addition of hydrogen atoms, and the setting up of active pockets. CDocker, an algorithm that can precisely dock any number of ligands to a single protein receptor, was used for molecular docking in this study (Wu et al., 2003).

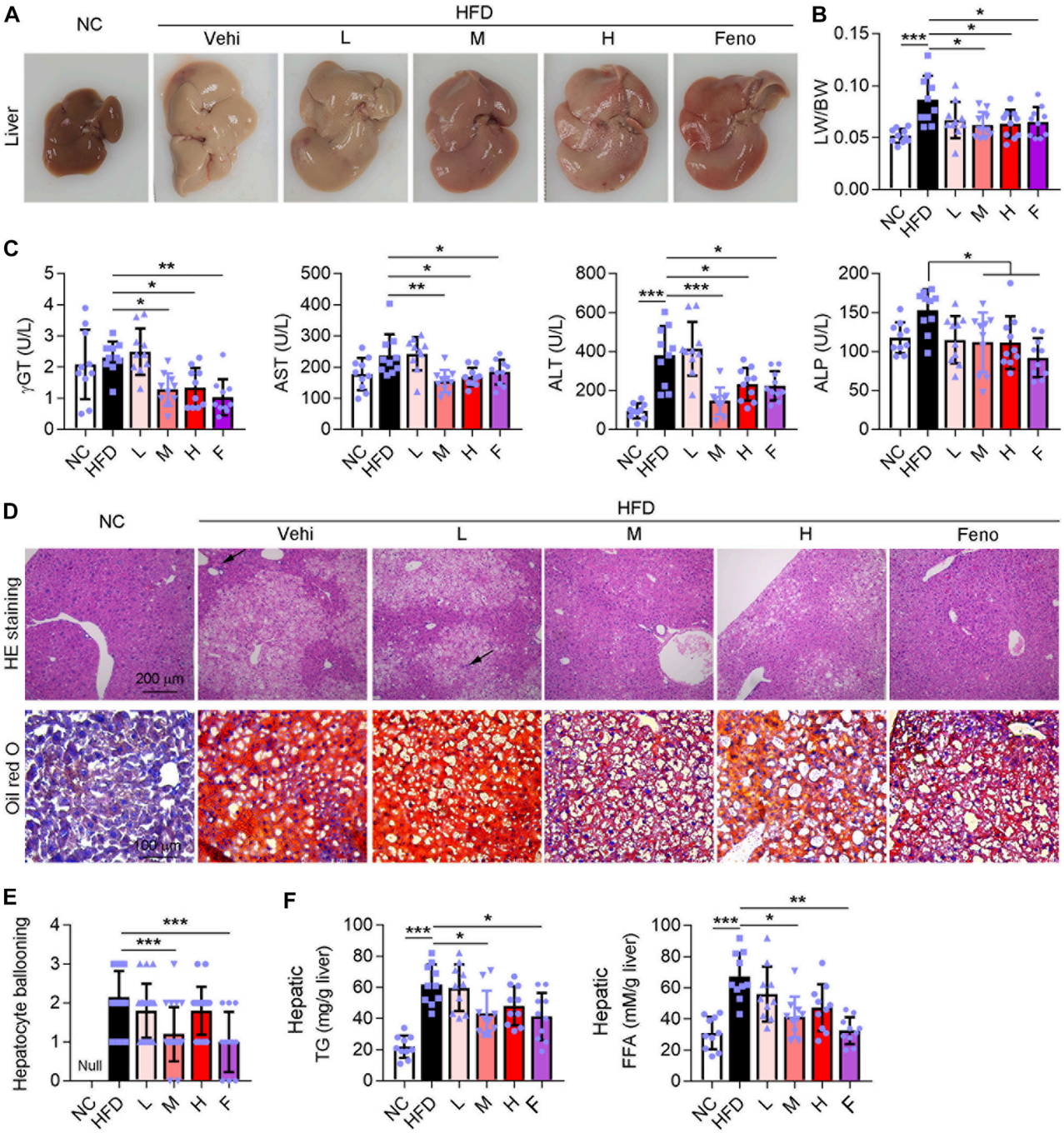

FIGURE 1 | Ganweikang tablet alleviates liver lesions in HFD-induced NAFL mice. **(A)** Representative images of mouse liver. **(B)** The ratio of liver weight (LW) to body weight (BW) in mice with different treatments as indicated in the figure, n = 10. **(C)** Serum γGT, AST, ALT, and ALP were detected using kits, n = 10. **(D)** Representative images of HE staining (up panel) and oil red O staining (down panel) of mouse liver. **(E)** Hepatocyte ballooning of mice liver, n = 10. **(F)** Hepatic TG and FFA content were determined by kit, n = 10. *p<0.05, **p<0.01, ***p<0.001, by one-way ANOVA with Bonferroni correction.

Cell Culture

HepG2 cells (a human hepatic cell line, were purchased from ATCC, Manassas, VA, United States) and were cultured in a complete DMEM medium (10% FBS, 50 μg mL^{-1} penicillin/streptomycin, and 2 mM glutamine). When cells grew to ~ 90% confluence in the culture dish, the complete DMEM medium was replaced by the serum-free medium. Cells received the treatment by glycyrrhetinic acid (GA, 20 μg/ml), ursolic acid (UA, 5 μM), betaine (bet, 5.0 mg/ml), and wogonin (wog, 10 μg/ml) in the presence or absence of LPS (1 μg/ml). After treatment, RNA and protein were extracted for the following q-RT-PCR and Western blot assay.

Data Analysis

The size of the *in vivo* study was calculated based on previous studies and pre-experiments. No outliers were identified in this study, and no data were excluded from the analysis. All data were generated from at least three independent experiments. The density of the target band and qRT-PCR target gene mRNA was normalized to β-actin in the corresponding sample to reduce variance. All values were normalized to the mean value of the experimental control group. The density of the images was quantified through ImageJ software (National Institutes of Health, Bethesda, MD, United States). The significance of differences between two or more sample means was tested by one-way ANOVA with Bonferroni correction. The declared group size is the number of independent values, and that statistical analysis was carried out using these independent values. All data are expressed as mean ± SEM. The significant difference was considered at $p < 0.05$.

Chemical Compounds Studied in This Article

Hematoxylin (PubChem CID: 442514); eosin (PubChem CID: 11048); oil red O (PubChem CID: 62330); fenofibrate (PubChem CID: 3339); glycyrrhetinic acid (PubChem CID: 73398); betaine (PubChem CID: 247); ursolic acid (PubChem CID: 64945); and wogonin (PubChem CID: 5281703).

RESULTS

Ganweikang Tablet Alleviates Hepatic Lipid Accumulation and Liver Lesion in HFD-Induced NAFL Mice

To investigate the protective effect of the Ganweikang tablet on NAFL, C57BL/6J background mice were fed HFD for a total of 16 weeks, and different doses of the Ganweikang tablet were added to the diet at the 8th week. Mice fed HFD had whiter livers and an increased liver-to-body ratio compared to that in the NC group (**Figure 1A**). Compared to the mice fed only HFD, the mice given fenofibrate and a medium or high dose of Ganweikang tablets along with HFD showed a progressive reddening of the liver and a significant decrease in the liver-to-body ratio (**Figures 1A, B**). Similarly, liver injury-related indicators, including γGT, AST, ALT, and ALP, were significantly reduced in the fenofibrate and the medium- or high-dose Ganweikang tablet group compared to the HFD group (**Figure 1C**). In addition, decreased hepatocyte ballooning and lipid droplet deposition were observed in the fenofibrate group and the Ganweikang tablet group by HE and oil red O staining (**Figures 1D, E**). Moreover, the levels of TG and FFA were significantly lower in the liver of mice that were treated with the medium dose of Ganweikang compared to the HFD group (**Figure 1F**). Altogether, these data suggest that the Ganweikang tablet protects the liver from HFD-induced lipid deposition and liver injury in HFD-induced NAFL mice.

Ganweikang Tablet Inhibits Hepatic Inflammation and Fibrosis in HFD-Induced NAFL Mice

Macrophage plays an important role in liver function. CD68 is a marker for macrophages. In addition, CD86 and CD206 are the markers of macrophage M1 and M2, respectively; the M1 phenotype is associated with an inflammatory response and the M2 phenotype with an anti-inflammatory response (Wynn and Vannella, 2016; Fan et al., 2020; Dong et al., 2016). In this study, HFD intervention increased hepatic $CD68^+$, $CD206^+$, and $CD86^+$ macrophages in mice (**Figure 2A**). Fenofibrate and medium-dose Ganweikang tablet administration reduced the number of $CD68^+$, and $CD86^+$ macrophages and increased the number of $CD206^+$ macrophages (**Figure 2A**). Moreover, we further evaluated the expression of pro-inflammatory cytokines in the liver. Notably, similar to fenofibrate, a medium dose of Ganweikang tablet significantly inhibited the HFD-induced increase in mRNA expression of *TNFα* and *Ccl2* in the liver of mice (**Figure 2B**). Meanwhile, the medium- and high-dose Ganweikang tablet intervention significantly inhibited *Ccr2* expression. Compared to the HFD group, fenofibrate slightly attenuated the *Ccr2* and *IL1β* expression but without a difference (**Figure 2B**). In addition, Ganweikang tablet slightly reduced the *IL1β* expression but without a significant difference (**Figure 2B**). Hepatic inflammation and fibrosis are accompanied by NAFL development (Brunt et al., 2015). αSMA is a marker of hepatic stellate cell activation and liver fibrosis (Xiang et al., 2020). Intervention with fenofibrate or medium dose of Ganweikang tablet significantly inhibited the expression of fibrosis-related phenotype markers, including αSMA, *Mmp9*, and *Tgf-β1* (**Figures 2A, C**). In addition, fenofibrate and Ganweikang tablet slightly reduced the *Col1α1* and *Timp-1* expression but without significant difference (**Figure 2C**). The aforementioned results suggest that Ganweikang tablet can reduce the inflammatory infiltration and fibrosis in the liver of HFD-fed NAFL mice, partially by which ameliorating the liver injury.

Ganweikang Tablet Alleviates Liver Lesion in MCD-Induced NASH Mice

NASH is a further stage of NAFL. Therefore, we further experimented to evaluate the effect of the Ganweikang tablet on NASH. Eight-week-old male mice on a C57BL/6J background were fed an MCD diet for a total of 8 weeks (NASH mice), with the fenofibrate or Ganweikang tablet intervention at the fourth week, and the serum and liver were collected at the time of mouse euthanasia. Compared to the NC group, the MCD-fed mice led to a change in the liver to whiter (**Figure 3A**), a decrease in body weight and liver weight (**Figures 3B, C**), and an increase in the liver to body ratio (**Figure 3D**), which indicated that the NASH model was successfully induced. The NASH model is accompanied by the development of lipotoxicity and extensive inflammatory infiltration as well as apoptosis in the liver. Despite no significant increase in the liver and body weight after

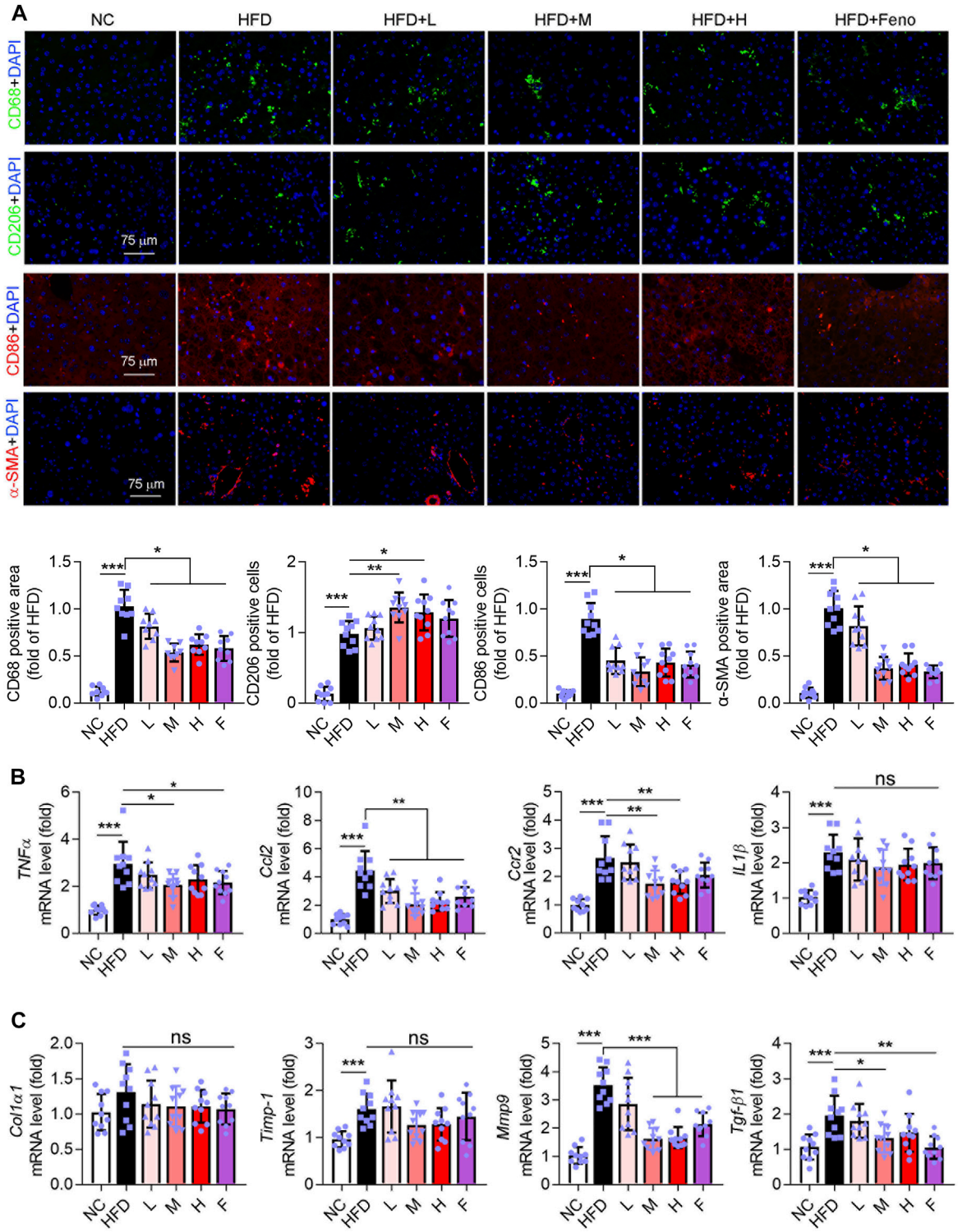

FIGURE 2 | Ganweikang tablet inhibits hepatic inflammation and fibrosis in NAFL mice. **(A)** Immunofluorescence staining for CD68 (green), CD206 (green), CD86 (red), α-SMA (red), and DAPI (blue) in liver sections from NC, HFD, HFD + L, HFD + M, HFD + H, and HFD + Feno group, followed by the quantitative analysis below. **(B)** The fold changes of *TNFα*, *Ccl2*, *Ccr2*, and *IL1β* mRNA in the liver from the indicated group (n = 10 mice examined per group). **(C)** The mRNA fold level changes of *Col1α1*, *Timp-1*, *Mmp9*, and *Tgf-β1* in the liver from the group as indicated (n = 10 mice examined per group). *p<0.05, **p<0.01, ***p<0.001, by one-way ANOVA with Bonferroni correction. ns, no significance.

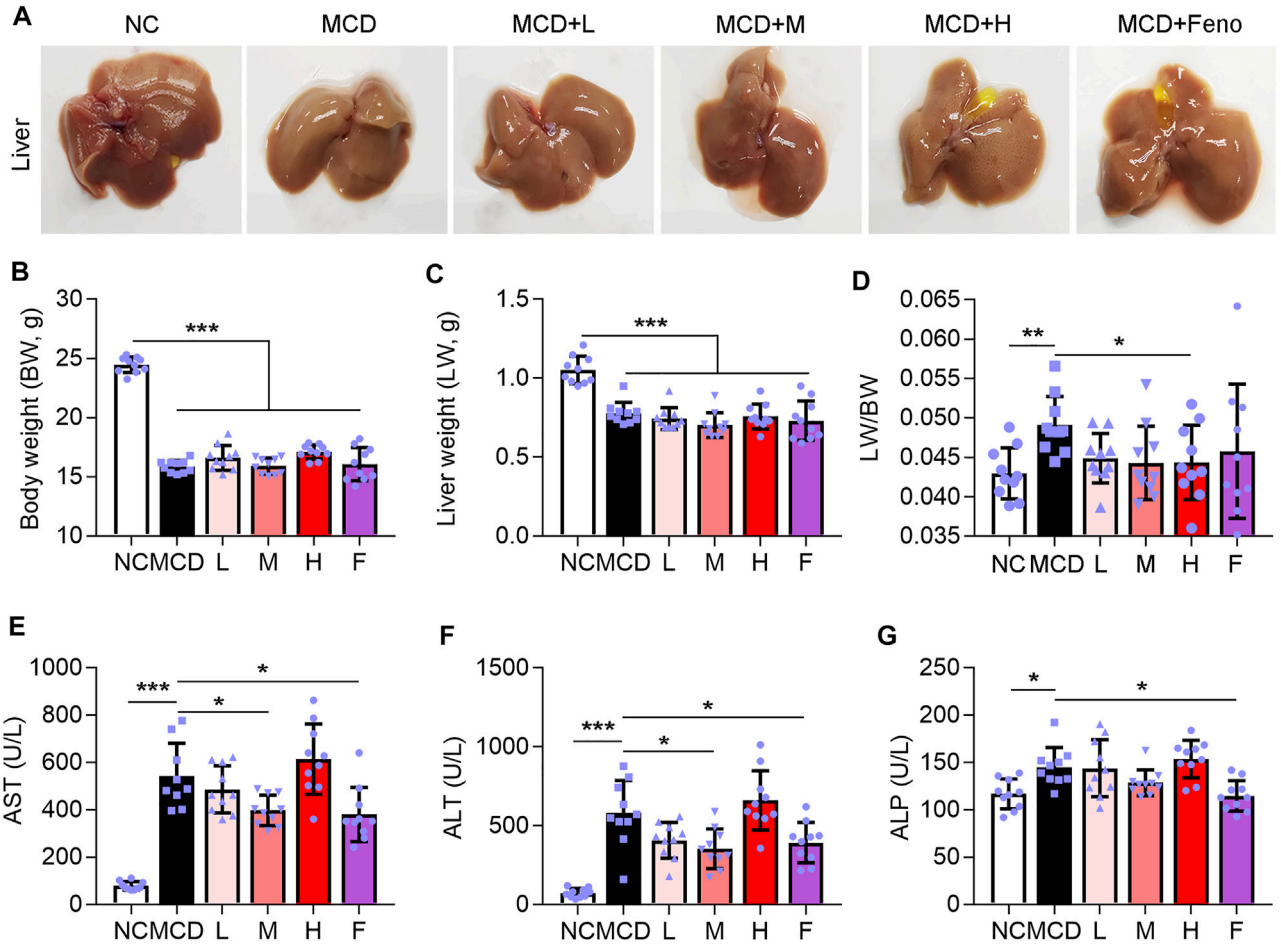

FIGURE 3 | Ganweikang tablet alleviates liver lesions in MCD-induced NASH mice. Eight-week-old male mice on a C57BL/6J background were fed an MCD diet for a total of 8 weeks, with the Ganweikang tablet intervention at the fourth week, and the serum and liver were collected at the time of mouse euthanization. **(A)** Representative images of mouse liver. **(B–D)** The body weight (BW), liver weight (LW), and the ratio of LW to BW, $n = 10$ per group. **(E–G)** Serum AST, ALT, and ALP were detected by kit, $n = 10$ per group. $^{*}p<0.05$, $^{**}p<0.01$, $^{***}p<0.001$, by one-way ANOVA with Bonferroni correction.

treatment by Ganweikang tablet or fenofibrate compared to the MCD group (**Figures 3B, C**), the features of the liver in MCD-induced NASH mice, including the whiter color and the decreased liver-to-body weight ratio, were improved by the medium-dosage Ganweikang tablet or fenofibrate administration (**Figures 3A, D**), suggesting that Ganweikang tablet administration plays a beneficial role in the NASH treatment. In addition, we detected the liver injury-related indicators ALT and AST and observed that both were significantly elevated in MCD-induced NASH mice, fortunately, which was partially reversed by fenofibrate or medium dose of Ganweikang tablet; but no differences were found in the low or high dose administration groups (**Figures 3E, F**). However, the other indicator of liver damage, ALP, was decreased only in the fenofibrate group (**Figure 3G**). Taken together, these results suggest that Ganweikang tablet intervention improves liver damage in MCD-induced NASH mice.

Ganweikang Tablet Alleviates Hepatic Steatosis in MCD-Induced NASH Mice

Hepatic steatosis is a characteristic of NASH (Manne et al., 2018). Methionine and choline are essential precursors for lecithin biosynthesis in hepatocytes and are important substrates for VLDL synthesis and secretion. When the mice are treated with an MCD diet, the synthesis and secretion of VLDL are impaired, so that endogenous TG cannot be transported out of hepatocytes and is deposited in the liver, leading to fatty degeneration of hepatocytes (Rinella and Green, 2004). In this study, we observed a large accumulation of lipid droplets in the liver of the MCD-induced NASH mice model (**Figure 4A**), accompanied by a significant increase in TG and FFA levels in the liver, which was attenuated by the administration of Ganweikang tablet or fenofibrate (**Figures 4A–C**). Moreover, HE staining showed that hepatocyte ballooning was also significantly elevated in the mice under the condition of the MCD diet (**Figure 4D**). On the other hand, the MCD diet leads to a decrease in the precursors of

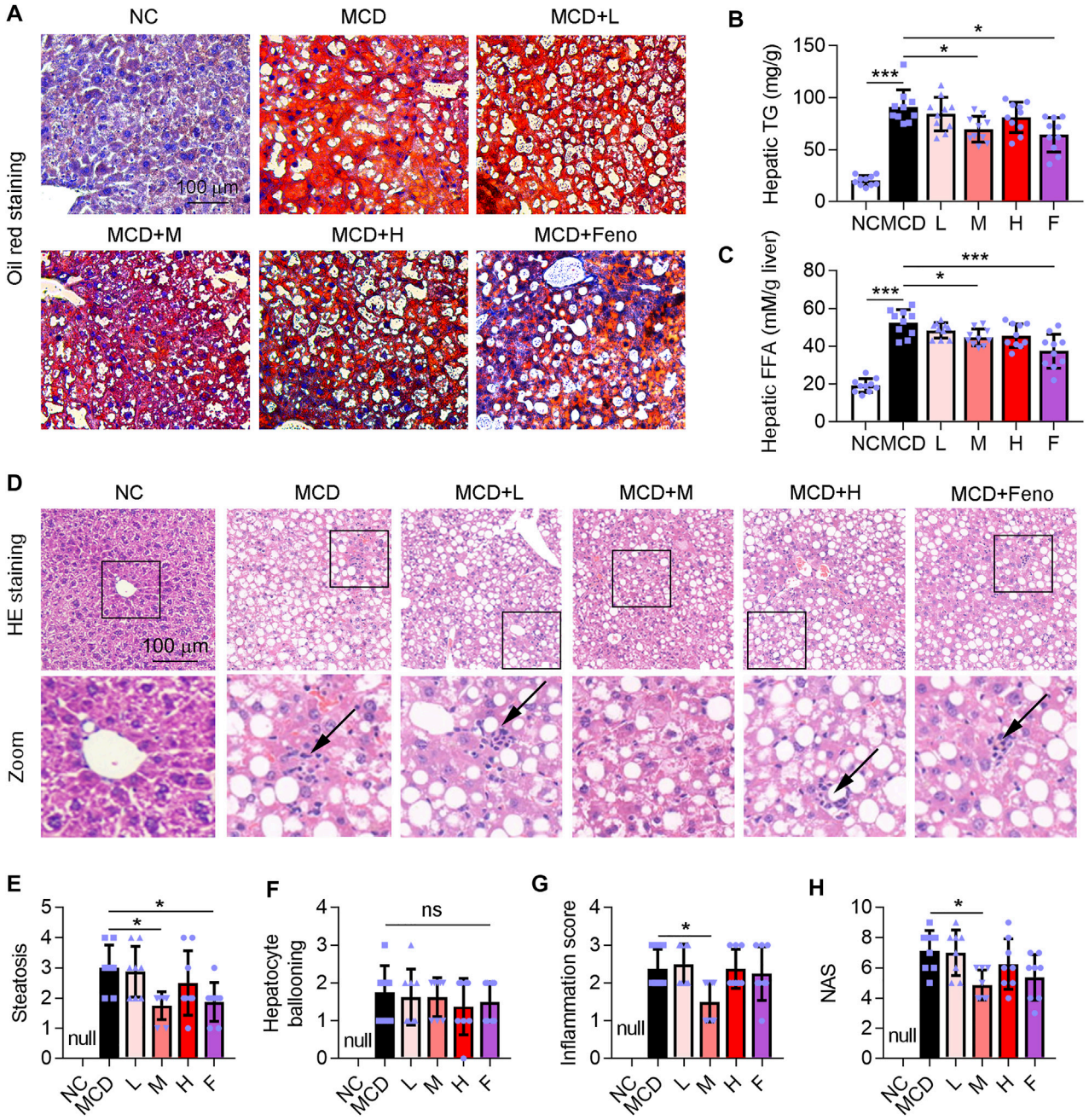

FIGURE 4 | Ganweikang tablet alleviates steatosis in the liver of MCD-fed mice. **(A)** Representative images of oil red O staining on the liver sections. **(B,C)** Hepatic TG and FFA in different groups were detected by the kit. **(D)** Representative images of HE staining on the liver sections from the indicated groups. **(E–H)** After analysis of HE staining, the changes in steatosis **(E)**, hepatocyte ballooning **(F)**, inflammation score **(G)**, and NAS **(H)** between the groups are shown in the figure. *p<0.05, ***p<0.001, by one-way ANOVA with Bonferroni correction. ns, no significance.

antioxidants, also known as reactive methyl groups, followed by the activation of oxidative stress in the liver, which causes inflammation and apoptosis of hepatocytes (Merry et al., 2016). Accordingly, the HE staining showed that hepatic inflammation was also increased in the MCD-fed mice (**Figure 4G**). Intriguingly, similar to the fenofibrate group, these features of NASH, such as high hepatic TG and FFA level, hepatic steatosis, inflammation score, and NAS, were significantly decreased in the medium-dose Ganweikang tablet administration group, while hepatocyte ballooning was slightly reduced but without significance in the medium-dose Ganweikang tablet administration group (**Figures 4B–H**). The aforementioned results indicate that the Ganweikang tablet improves lipid deposition in the liver of MCD-induced NASH mice.

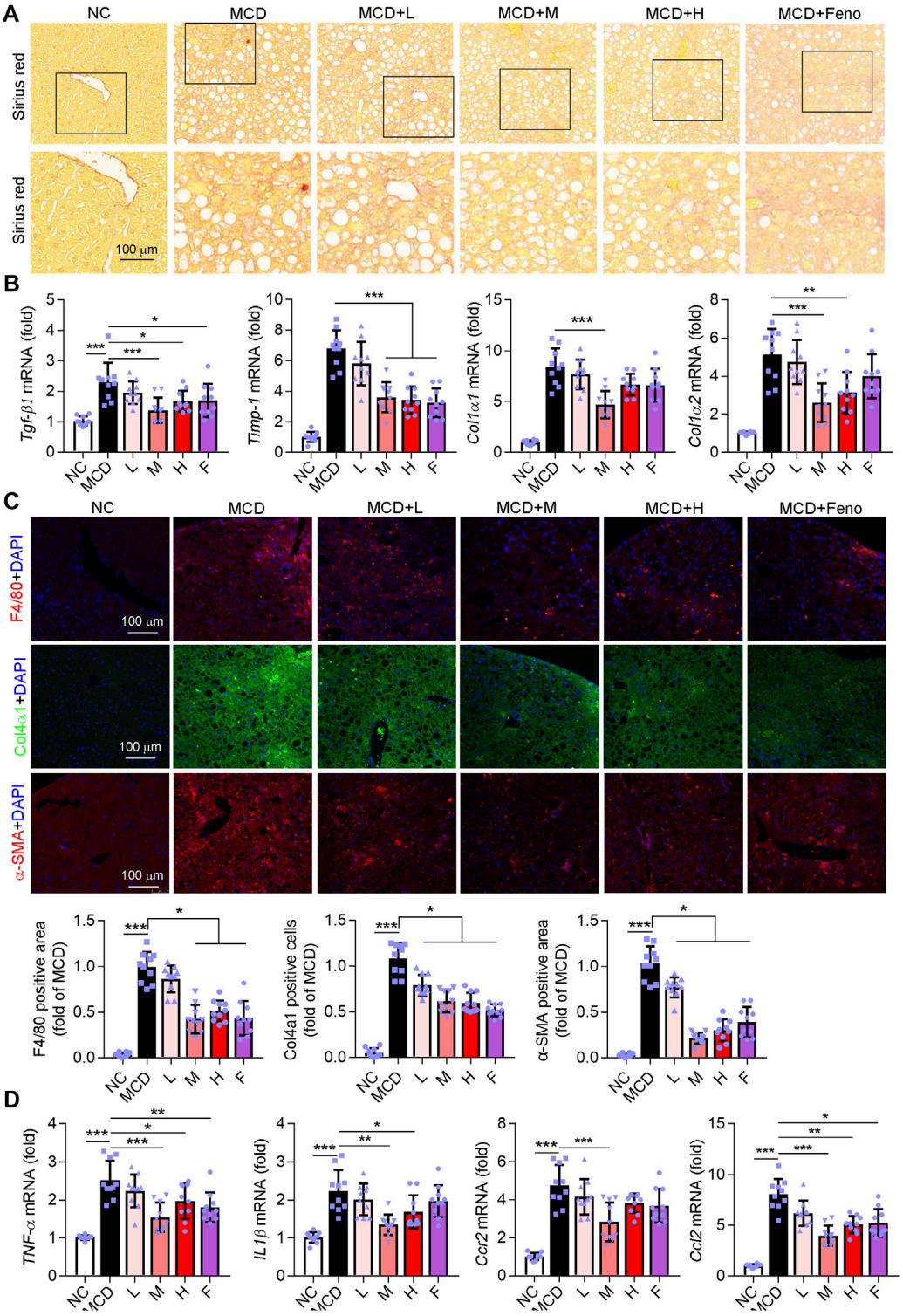

FIGURE 5 | Ganweikang tablet ameliorates fibrosis and inflammation in the liver of MCD-fed NASH mice. **(A)** Representative images of Sirius Red staining, $n = 10$. **(B)** q-RT-PCR analysis of the mRNA level of *TNFα*, *IL1β*, *Ccr2*, and *Ccl2* in the liver, $n = 10$. **(C)** Mouse liver sections were stained for F4/80, Col4α1, and α-SMA, respectively, and followed by quantitative analysis, $n = 10$. F4/80 (red), Col4α1 (green), α-SMA (red), and DAPI (blue). **(D)** q-RT-PCR analysis of the mRNA level of Tgf-β1, Timp-1, Col1α1, and Col1α2 in the liver, $n = 10$. $^{*}p<0.05$, $^{**}p<0.01$, $^{***}p<0.001$, by one-way ANOVA with Bonferroni correction.

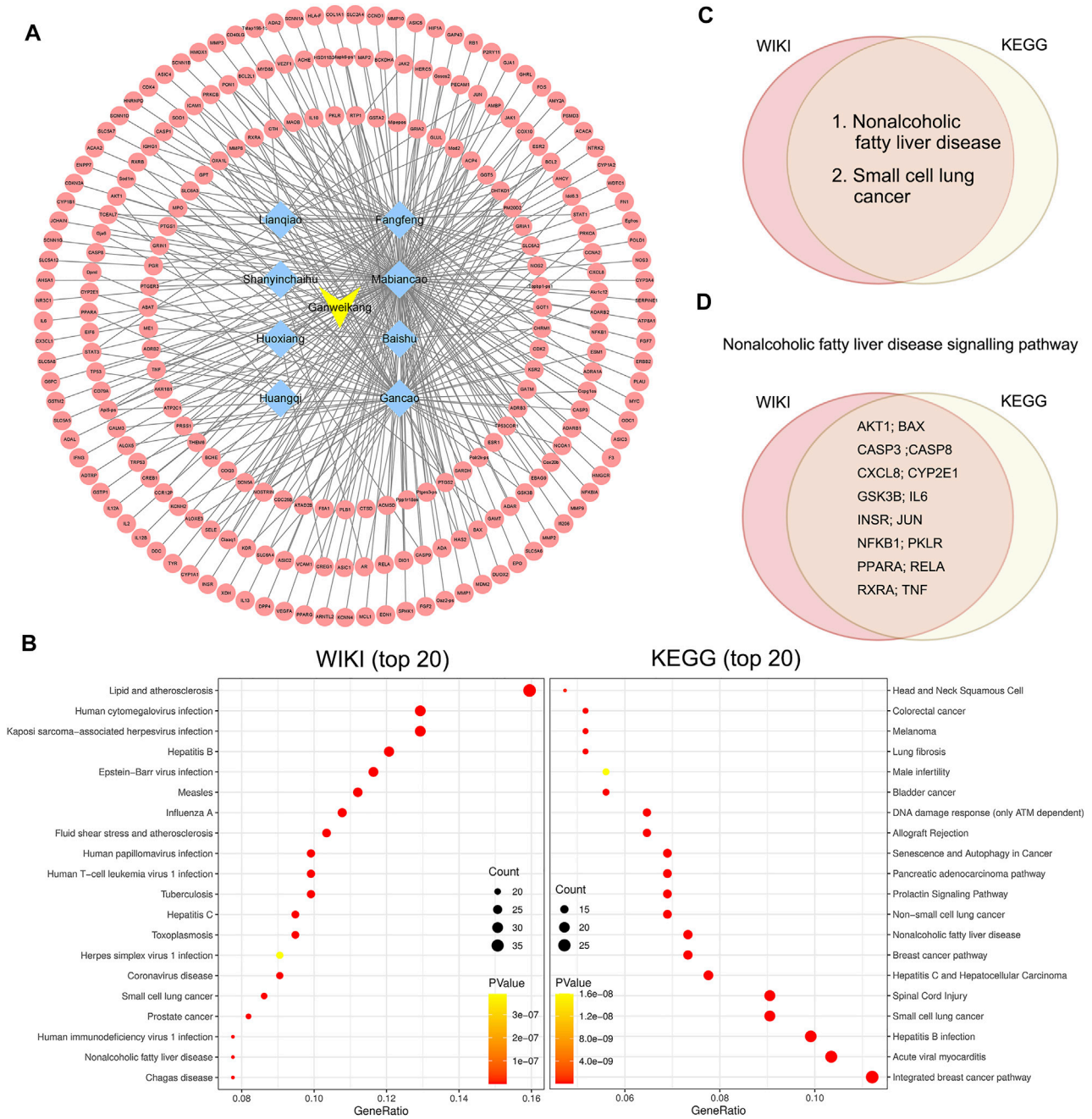

FIGURE 6 | Network pharmacology analysis on target genes and disease of the Ganweikang tablet. **(A)** Ganweikang tablet (yellow)–Chinese herbal medicine (blue)–target genes (red) network. **(B)** Enrichment analysis of Ganweikang tablet target genes in WIKI and KEGG diseases (top 20). **(C)** Venn diagram representing the intersection of Ganweikang tablet target genes in KEGG and WIKI-enriched diseases. **(D)** Venn diagram representing Ganweikang target genes that are co-owned by KEGG and WIKI in NAFLD.

Ganweikang Tablet Ameliorates Hepatic Inflammation and Fibrosis in MCD-Fed NASH Mice

Fibrosis is accompanied by NASH development. Therefore, we determined whether the Ganweikang tablet could attenuate fibrosis in the NASH mice. Intriguingly, similar to the fenofibrate group, the data of Sirius Red staining showed that the Ganweikang tablet attenuated the fibrosis (**Figure 5A**). In addition, a medium dose of Ganweikang tablet significantly reduced the increase in liver fibrosis indicators, including *TGF-β1*, *Timp-1*, *Col1α1*, and *Col1α2* in NASH mice (**Figure 5B**). Fenofibrate reduced the expression of *TGF-β1* and *Timp-1* but did not affect the *Col1α1* and *Col1α2* expression in NASH mice (**Figure 5B**). Moreover,

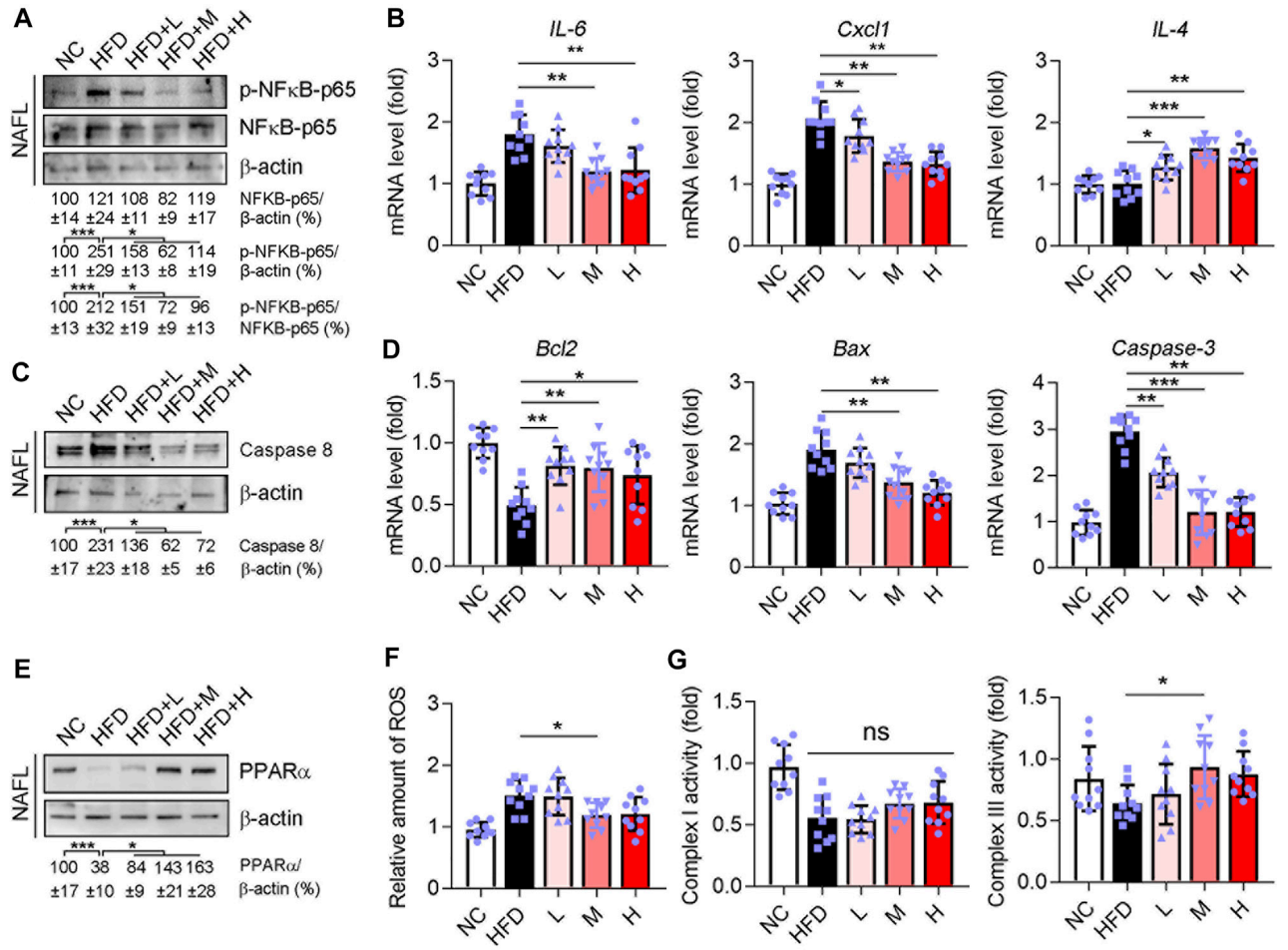

FIGURE 7 | Ganweikang tablet reduces inflammation, apoptosis, and fatty acid oxidation in the liver of NAFL mice. C57BL/6J-background mice induced into NAFL model by HFD, $n = 3$. **(A)** Western blotting demonstrates the expression of p-NFκB-p65 and NFκB-p65, $n = 3$. **(B)** Differences in mRNA fold level changes of *IL6*, *Cxcl1,* and *IL4* between the indicated groups ($n = 10$ mice examined per group). **(C)** Western blotting demonstrates the expression of Caspase8, $n = 3$. **(D)** Differences in mRNA fold level changes of *Bcl2*, *Bax,* and *Caspase3* between the indicated groups ($n = 10$ mice examined per group). **(E)** Western blotting demonstrates the expression of PPARα, $n = 3$. **(F)** Differences in the amount of ROS between the indicated groups ($n = 10$ mice examined per group). **(G)** Differences in activity between the groups for complex I and complex III ($n = 10$ mice examined per group). $^{*}p<0.05$, $^{**}p<0.01$, $^{***}p<0.001$, by one-way ANOVA with Bonferroni correction. ns, no significance.

immunofluorescent staining on the fibrosis marker, such as Col4α1 and αSMA, was markedly decreased by fenofibrate and Ganweikang tablet treatment (**Figure 5C**). These data suggest that the Ganweikang tablet can reduce liver fibrosis in NASH mice. Hepatic macrophages act as a key regulator of liver fibrosis, and excessive accumulation of macrophages markedly contributes to liver fibrosis development (Krenkel et al., 2018). According to the F4/80 (macrophage marker) immunofluorescence staining, macrophage infiltration was significantly increased in MCD-fed mice compared to NC-fed mice, which was significantly attenuated in the fenofibrate group and the medium-dose Ganweikang tablet group (**Figure 5C**). Consistent with this, the mRNA levels of inflammatory factors, such as *TNFα*, IL1β, *Ccr2,* and *Ccl2*, in the liver were significantly reduced in the medium-dose Ganweikang-treated group (**Figure 5D**). The aforementioned results suggest that the Ganweikang tablet can ameliorate inflammation and fibrosis in the liver of MCD-fed NASH mice.

Network Pharmacology Analysis Indicates Ganweikang Tablet as a Candidate for NAFLD Treatment

Furthermore, we conducted the network pharmacology analysis to determine the potential effect and molecular mechanism of Ganweikang tablet on the NAFLD. First, Ganweikang's target genes were predicted from the HERB high-throughput database (http://herb.ac.cn/) based on literature data. Ganweikang tablet consists of eight Chinese herbal ingredients, including Lianqiao, Fangfeng, Shanyinchaihu, Mabiancao, Huoxiang, Baishu, Huangqi, and Gancao, which were individually predicted by HERB, resulting in the integration of 232 potential target genes for Ganweikang tablet (**Figure 6A**). In addition, these 232 genes were analyzed for enrichment by ERICHR (https://maayanlab.cloud/Enrichr/) and showcased the top 20 disease-related signaling pathways in the KEGG and WIKI databases

(**Figure 6B**). In addition, we crossed the most significant gene enrichment in KEGG and WIKI databases and found that the targets of the Ganweikang tablet were mainly associated with NAFLD (**Figure 6C**). Furthermore, the predicted genes enriched in NAFLD in KEGG and WIKI databases were taken for intersection, and 16 genes were overlapped in KEGG and WIKI databases, including *AKT1*, *BAX*, *CASP3*, *CASP8*, *CXCL8*, *CYP2E1*, *GSK3B*, *IL6*, *INSR*, *JUN*, *NFκB1*, *PKLR*, *PPARα*, *RELA*, *RXRα*, and *TNF*α (**Figure 6D**). Taken together, network pharmacology analysis indicates that the Ganweikang tablet can serve as a candidate for NAFLD treatment and predicts the potential molecular mechanism underlying the action.

Ganweikang Tablet Attenuates the NAFL and NASH by Inhibiting Inflammation, Apoptosis and Enhancing Fatty Acid Oxidation Through Inhibiting NFκB and caspase8 and Activating PPARα

According to the network pharmacology analysis, the targeting genes of the Ganweikang tablet associated with NAFLD were mainly enriched in inflammation, apoptosis, and fatty acid oxidation. Therefore, further validation on the key targets of these signaling pathways was carried out in the liver of NAFL and NASH mice. Western blot results suggested that Ganweikang tablet significantly reduced the phosphorylation level of NF-κB in either NAFL or NASH liver (**Figure 7A** and **Supplementary Figure S1A**). Consistent with this result, the expression of the inflammatory factors *IL-6* and *Cxcl1* was significantly reduced after Ganweikang tablet treatment, while the expression of *IL-4* (anti-inflammatory cytokine) was significantly increased in either NAFL or NASH liver (**Figure 7B** and **Supplementary Figure S1B**). In the liver, caspase8, a protein that upregulates apoptosis, was reduced by intervention with the Ganweikang tablet (**Figure 7C** and **Supplementary Figure S1C**). In addition, Ganweikang tablet significantly inhibited the mRNA levels of *Bax* and *Caspase3* in NAFL and NASH mice and increased *Bcl2* mRNA level (**Figure 7D** and **Supplementary Figure S1D**). PPARα is an important target for the upregulation of fatty acid oxidation (FAO). Inhibition of PPARα in NAFLD leads to reduced FAO and mitochondrial dysfunction (Pawlak et al., 2015). In this study, the expression of PPARα was significantly reduced in NAFL and NASH mice compared to the NC group; however, Ganweikang tablet partially reversed this effect (**Figure 7E** and **Supplementary Figure S1E**), suggesting that Ganweikang tablet could increase FAO levels in the liver of NAFLD model mice. When the hepatocyte was exposed to excess FFAs for a prolonged time, oxidative stress can be activated, prompting the release of large amounts of reactive oxygen species (ROS) from the mitochondria. In line with the level of PPARα expression, the medium-dose Ganweikang tablet reduced hepatic ROS (**Figure 7F** and **Supplementary Figure S1F**), further implying that Ganweikang tablets can ameliorate oxidative stress. Mitochondria are a source of ROS and a major organelle for ROS attack. Herein, we explored the state of mitochondrial biological function by assaying the activity of mitochondrial complexes I and III. We found that Ganweikang tablets could increase the activity of mitochondrial complex III in NAFL and NASH mice (**Figure 7G** and **Supplementary Figure S1G**), which maintained normal mitochondrial function. The aforementioned results suggest that the Ganweikang tablet can reduce inflammation and apoptosis and enhance FAO by inhibiting NFκB and Caspase8 and activating PPARα, which protected the mice from NAFL and NASH suffering.

Study on the Molecular Mechanism of Ganweikang Tablet Improving NAFL and NASH *via* Network Pharmacology Combined Cell Experiment

Visualization of -Cdocker interaction energy (CIE) between the Ganweikang tablet's active ingredients that were analyzed by network pharmacology and the corresponding target genes that we have determined *in vivo* experiment is shown in **Figure 8A**. First, molecular docking simulations of the binding sites and the interaction forces of glycyrrhetinic acid (GA), CASP3 (**Figure 8B**), ursolic acid (UA), and CASP8 (**Supplementary Figure S2A**) were performed. Subsequently, Western blot analysis showed that LPS (1 μg/ml) induced an increase in protein levels of CASP3 and CASP8 in HepG2 cells, which was reversed by GA (20 μg/ml) and UA (5 μM) treatment, respectively (**Figure 8C**). In addition, CASP3 activity was enhanced by LPS, while GA treatment inhibited CASP3 activity (**Figure 8D**). Moreover, the mRNA expression levels of *BAX* and *BCL2* were increased and decreased by LPS, respectively, and GA significantly attenuated the effect of LPS on these *BAX* and *BCL2* expressions (**Figure 8E**). Next, molecular docking simulations of betaine and PPARα are shown in **Figure 8F**. In addition, the PPARα protein level was reduced by LPS while betaine (5.0 mg/ml) restored its expression (**Figure 8G**). The mRNA level of CPT1α (the downstream gene of PPARα) supported the finding that betaine treatment increased the activity of PPARα in the presence of LPS (**Figure 8H**). Molecular docking simulations of NFκB-p50 and wogonin are exhibited in **Figure 8I**. Furthermore, LPS increased NFκB-p50 expression in HepG2 cells, which was inhibited by wogonin (10 μg/ml) (**Figure 8J**). In addition, wogonin inhibited the enhanced NFκB-p65 phosphorylation caused by LPS (**Figure 8J**). Moreover, *TNFα* mRNA expression levels were increased by LPS and wogonin treatment significantly inhibited this change (**Figure 8K**). Moreover, the molecular docking prediction of GA and TNFα, UA and IL6, NFκB, and apigenin are presented in **Supplementary Figure S2**. Taken together, the aforementioned results confirmed that the active ingredient of Ganweikang that was analyzed by network pharmacology can ameliorate LPS-induced changes in apoptosis, fatty acid oxidation, and inflammatory signaling pathways, possibly by which Ganweikang tablet protects the liver from NAFL and NASH in the mice.

DISCUSSION

NAFLD, a liver disease associated with obesity, insulin resistance, type 2 diabetes mellitus, hypertension, hyperlipidemia, and metabolic syndrome, is now considered a significant driver of

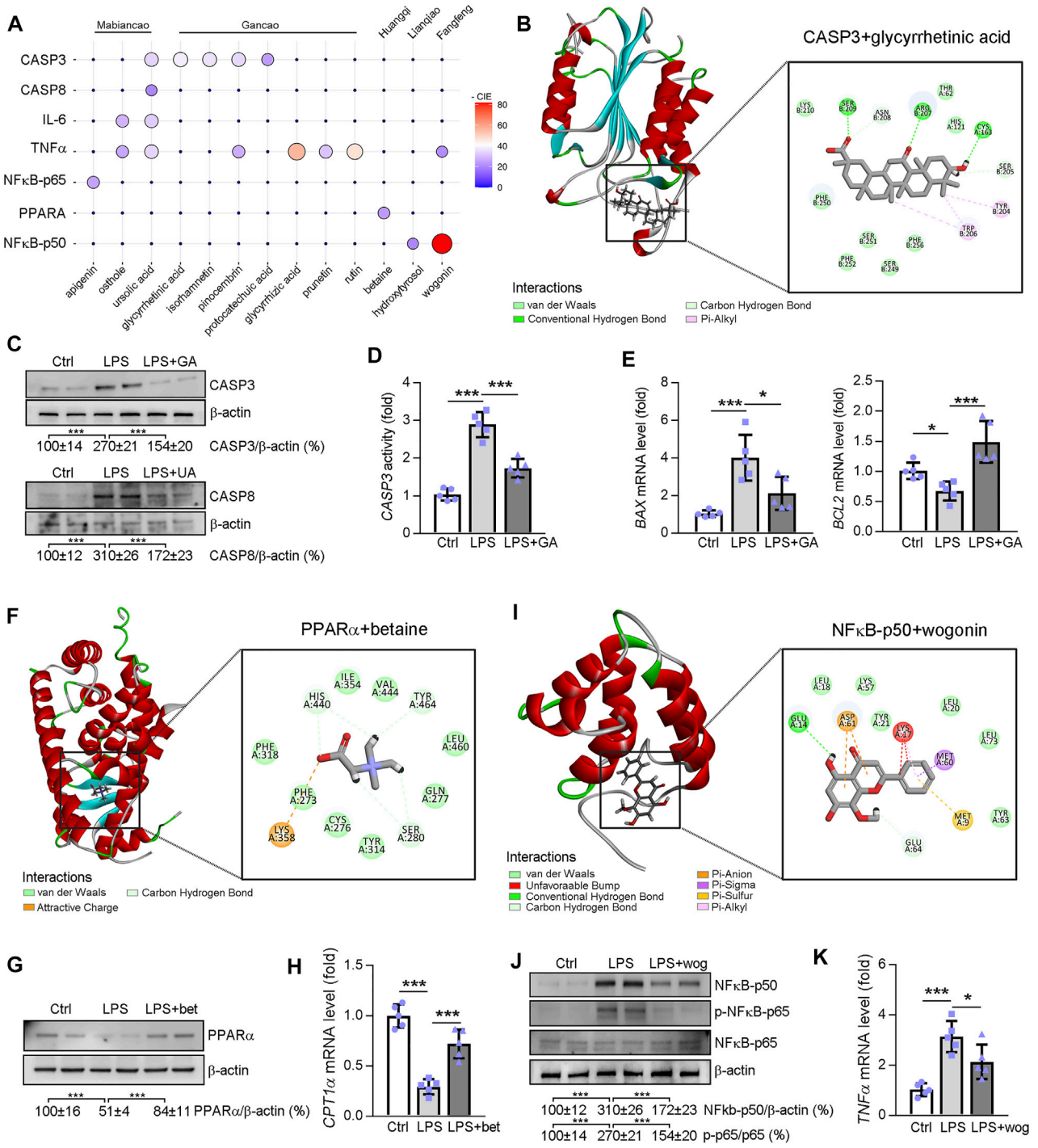

FIGURE 8 | Molecular docking between the potential molecule targets and the compound analyzed by network pharmacology. **(A)** The ggballoon plot demonstrates the degree of interaction between Ganweikang's potent small molecule compounds and the receptor proteins. The strength of the -CIE is shown by the size and color of the circles. 0 means that the relationship between the active ingredients and the proteins has not been predicted by the HERB database (http://herb.ac.cn/). **(B)** Molecular docking of glycyrrhetinic acid and CASP3. **(C)** Western blotting demonstrates the protein level of CASP3 and CASP8 in HepG2 cells after indicated treatment, $n = 3$. **(D)** Casp3 activity in HepG2 cells was determined by the commercial kit, $n = 5$. **(E)** Transcriptional expression of BAX and BCL2 in HepG2 cells after indicated treatment was determined by qRT-PCR, $n = 5$. **(F)** Molecular docking simulations of betaine and PPARα. **(G,H)** After indicated treatment, expression of PPARα and CPT1α in HepG2 cells was determined by Western blotting and qRT-PCR, $n = 5$. **(I)** Molecular docking simulations of NFκB-p50 and wogonin. **(J,K)** After indicated treatment, expression of NF-κB-p50, NF-κB-p65, p-NF-κB-p65, and TNFα in HepG2 cells was determined by Western blotting and qRT-PCR, n = 5. *p<0.05, ***p<0.001, by one-way ANOVA with Bonferroni correction.

the global burden of chronic liver disease and can carry serious sequelae (Golabi et al., 2021). There is a potential progression of NAFLD from simple steatosis (NAFL) to more severe NASH, with terminal progression to liver fibrosis, cirrhosis, and hepatocellular carcinoma, which places a heavy financial and life burden on patients (Younossi, 2019). However, to date, there are no FDA-approved drugs for the treatment of NAFLD. The pathogenesis of NAFLD is complex and no single-target drugs have achieved the desired results. Noticeably, traditional Chinese medicine has gained increasing attention for NAFLD treatment due to its multi-target and multi-pathway advantages. The underlying mechanism of action of Ganweikang tablet, a compounded traditional Chinese medicine, is not yet clear. Fortunately, network pharmacology proposed by Hopkins University in 2007 is a comprehensive discipline that integrates systems biology, information networks, computer science, and pharmacology (20), which can provide a theoretical basis for predicting the target genes and diseases potentially treated by compounded herbal medicines. In this study, we found that NAFLD is a major target disease of Ganweikang's major components, with target genes associated with inflammation, apoptosis, and fatty acid oxidation, which provide a theoretical basis for its treatment of NAFLD. Accordingly, we investigated the therapeutic effects of Ganweikang tablet on two stages of NAFLD pathogenesis through different disease models, NAFL and NASH mice, respectively. The results suggested that the Ganweikang tablet significantly reduced lipid deposition, fibrosis, and inflammation in the liver from both the NALF and NASH models.

Hepatic lipid accumulation, inflammation, and apoptosis are major contributors to NAFLD development (Friedman et al., 2018). In this study, lipid accumulation, macrophage infiltration, and collagen deposition were significantly reduced in NAFL and NASH mice after Ganweikang tablet intervention. Kupffer cells and newly recruited monocyte-derived macrophages play key roles in the regulation of inflammation, fibrosis, and fibrinolysis. Following injury, Kupfer cells recruit inflammatory blood monocytes, which differentiate into classically activated M1-type macrophages with the secretion of large amounts of pro-inflammatory cytokines and ROS (Kazankov et al., 2019). In contrast, M2-type macrophages with anti-inflammatory and repair phenotypes are associated with reduced liver injury in NAFLD (Wan et al., 2014). Our study indicates that the Ganweikang tablet can significantly promote the M2 subtypes of macrophages and reduce pro-inflammatory cytokines in the liver of mice in the NAFL model. The flow of monocytes to the liver is mainly regulated by the chemokine CCL2 and its cognate receptor CCR2 in monocytes or macrophages (Obstfeld et al., 2010). In this study, under the treatment of Ganweikang tablets, the levels of *Ccl2* and *Ccr2* in the liver of the NAFL mice were reduced, accompanied by a decrease in the expression of the pro-inflammatory factor TNF-α, which accounts for decreased macrophages infiltration and reducing inflammation in the liver of NAFL and NASH mice. In addition, fibrosis-related indicators in the liver were significantly reduced, especially in the medium-dose Ganweikang group, suggesting a protective effect on hepatic fibrosis in the NASH model.

Mechanistically, network pharmacology analysis showed that the regulated genes of Ganweikang tablet mainly enriched in the signaling pathway of fatty acid metabolism (PPARα), inflammation response (NFκB-p65), and apoptosis (Casp3 and Casp8). *PPARα* is a key gene in the regulation of fatty acid metabolism, which can affect the hepatic lipid level (Chung et al., 2018). Huangqi, as the main component of the Ganweikang tablet, can affect *PPARα* activity (Cao et al., 2021). In this study, the Ganweikang tablet increased the expression of PPARα, suggesting that the Ganweikang tablet may increase the hepatic FAO and thereby attenuating NAFL and NASH. In addition, network pharmacology predicts that *PPARα* is the target gene of betaine (the active ingredient of Huangqi). Furthermore, betaine treatment increased the protein level of PPARα and its regulated gene expression, CPT1α, in HepG2 cells in the presence of LPS. In addition, NFκB is an important factor in regulating the inflammatory signaling pathway (Cartwright and Perkins, 2016). Network pharmacology analysis indicated that NFκB is a potential target gene of Lianqiao, a component of the Ganweikang tablet. Indeed, after treatment with a Ganweikang tablet, the activity of NFκB was markedly decreased in the liver of NAFL and NASH mice. In line with the inactivation of NFκB, the inflammatory cytokines were also decreased after Ganweikang tablet treatment, which suggested that the treatment of NAFLD by Ganweikang tablet is partially through inactivating NFκB. Furthermore, network pharmacology analysis indicated that NFκB is a potential target gene of wogonin (the active ingredient of Fangfeng from the Ganweikang tablet). *In vivo*, after treatment with a Ganweikang tablet, the phosphorylation of NFκB-p65 was markedly decreased in the liver of NAFL and NASH mice. *In vitro*, wogonin treatment inhibited the expression of NFκB-p50 and phosphorylation of NFκB-p65 in HepG2 cells in the presence of LPS. Additionally, the mRNA level of *TNFα* also supported our results that wogonin decreased LPS-induced inflammation in HepG2 cells. In addition, *CASP3* and *CASP8* are apoptosis-associated key genes (Mata et al., 2010). The network pharmacology approach predicts that *CASP3* and *CASP8* are the target genes of UA and GA, two components of that Gancao and Mabiancao that are contained in the Ganweikang tablet. As expected, the markers of apoptosis were significantly reduced in the liver of NAFL and NASH mice after Ganweikang tablet treatment. In line with this, the *in vitro* experiment showed that GA treatment inhibited LPS-induced markers of apoptosis in HepG2 cells. These results showed that betaine-mediated PPARα activation, GA-mediated inactivation of CASP3, UA-mediated downregulation of CASP8, and wogonin-mediated inactivation of NFκB may be the potential mechanisms of Ganweikang tablet in the treatment of NAFLD. Altogether, Ganweikang tablet attenuated the NAFLD development by attenuating the hepatic lipid accumulation, inflammation, and apoptosis through the different herbal components, suggesting that Ganweikang tablet can ameliorate the disease by a multi-target effect. Moreover, *in vivo* experiments revealed that medium-dose Ganweikang tablet (672 mg/kg/day) significantly improved liver injury in NAFLD mice, in some respects, which showed a better effect than that of low- and high-dose treatments. Commonly, the lower dose of the drug was safer than the high dose in the treatment of NAFLD. Meanwhile, given the comparable effect between medium- and high-dose Ganweikang tablets, we suggested that the medium dose of Ganweikang tablet was better. Therefore, the

optimal dose for Ganweikang tablet administration was considered at 672 mg/kg/day in this study.

CONCLUSION

In summary, we have observed that Ganweikang tablet can improve liver lesions in a mouse model of NAFL and NASH by modulating inflammation, apoptosis, and fatty acid oxidation through inhibiting NFκB, inactivating caspase3/8, and activating PPARα, which indicates Ganweikang tablet not only as a drug candidate but also provides a theoretical basis of Ganweikang tablet in the treatment of NAFLD.

DATA AVAILABILITY STATEMENT

The original contributions presented in the study are included in the article/**Supplementary Material**; further inquiries can be directed to the corresponding authors.

ETHICS STATEMENT

The animal study was reviewed and approved by the Ethics Committee of the Second Clinical School of Jinan University (Shenzhen People's Hospital).

AUTHOR CONTRIBUTIONS

JX performed *in vivo* experiments; GY and YZ completed molecular biological experiments and biochemical assays; XW performed the network pharmacology analysis. CZ, GZ, GF, YZ, YH, and LK edited the manuscript; JG, HL, and ML offer the drug for animal study; SY and CM designed experiments, interpreted results, and wrote the manuscript.

FUNDING

All sources of funding received for the research being submitted. This work was supported by grants from the National Natural Science Foundation of China (NSFC) (82000824, 82003747); the China Postdoctoral Science Foundation (2020M683179); the Natural Science Foundation of Tianjin Grants (20JCQNJC00260, 19JCQNJC12600, and 20JCZXJC00150); the Extension Project of First Teaching Hospital of Tianjin University of Traditional Chinese Medicine (ZD202101).

SUPPLEMENTARY MATERIAL

The Supplementary Material for this article can be found online at: https://www.frontiersin.org/articles/10.3389/fphar.2022.893336/full#supplementary-material

REFERENCES

Adesso, S., Russo, R., Quaroni, A., Autore, G., and Marzocco, S. (2018). Astragalus Membranaceus Extract Attenuates Inflammation and Oxidative Stress in Intestinal Epithelial Cells via NF-Kb Activation and Nrf2 Response. *Int. J. Mol. Sci.* 19 (3). doi:10.3390/ijms19030800

Barrett, T., Wilhite, S. E., Ledoux, P., Evangelista, C., Kim, I. F., Tomashevsky, M., et al. (2013). NCBI GEO: Archive for Functional Genomics Data Sets-Uupdate. *Nucleic Acids Res.* 41 (Database issue), D991–D995. doi:10.1093/nar/gks1193

Brunt, E. M., Wong, V. W., Nobili, V., Day, C. P., Sookoian, S., Maher, J. J., et al. (2015). Nonalcoholic Fatty Liver Disease. *Nat. Rev. Dis. Prim.* 1, 15080. doi:10.1038/nrdp.2015.80

Buzzetti, E., Pinzani, M., and Tsochatzis, E. A. (2016). The Multiple-Hit Pathogenesis of Non-alcoholic Fatty Liver Disease (NAFLD). *Metabolism* 65 (8), 1038–1048. doi:10.1016/j.metabol.2015.12.012

Cao, Y., Liu, Y., Zhang, T., Pan, J., Lei, W., and Zhang, B. (2021). Comparison and Analysis on the Existing Single-Herbal Strategies against Viral Myocarditis. *Genet. Res. (Camb)* 2021, 9952620. doi:10.1155/2021/9952620

Cartwright, T., and Perkins, N. D. (2016). NFKB1: a Suppressor of Inflammation, Ageing and Cancer. *Febs J.* 283 (10), 1812–1822. doi:10.1111/febs.13627

Chen, E. Y., Tan, C. M., Kou, Y., Duan, Q., Wang, Z., Meirelles, G. V., et al. (2013). Enrichr: Interactive and Collaborative HTML5 Gene List Enrichment Analysis Tool. *BMC Bioinforma.* 14, 128. doi:10.1186/1471-2105-14-128

Chung, K. W., Lee, E. K., Lee, M. K., Oh, G. T., Yu, B. P., and Chung, H. Y. (2018). Impairment of PPARα and the Fatty Acid Oxidation Pathway Aggravates Renal Fibrosis during Aging. *J. Am. Soc. Nephrol.* 29 (4), 1223–1237. doi:10.1681/ASN.2017070802

Cusi, K. (2016). Treatment of Patients with Type 2 Diabetes and Non-alcoholic Fatty Liver Disease: Current Approaches and Future Directions. *Diabetologia* 59 (6), 1112–1120. doi:10.1007/s00125-016-3952-1

Dong, P., Ma, L., Liu, L., Zhao, G., Zhang, S., Dong, L., et al. (2016). CD86$^+$/CD206$^+$, Diametrically Polarized Tumor-Associated Macrophages, Predict Hepatocellular Carcinoma Patient Prognosis. *Int. J. Mol. Sci.* 17 (3), 320. doi:10.3390/ijms17030320

El-Derany, M. O., and El-Demerdash, E. (2020). Pyrvinium Pamoate Attenuates Non-alcoholic Steatohepatitis: Insight on hedgehog/Gli and Wnt/β-Catenin Signaling Crosstalk. *Biochem. Pharmacol.* 177, 113942. doi:10.1016/j.bcp.2020.113942

Fan, M., Chen, S., Weng, Y., Li, X., Jiang, Y., Wang, X., et al. (2020). Ciprofloxacin Promotes Polarization of CD86+CD206- M-acrophages to S-uppress L-iver C-ancer. *Oncol. Rep.* 44 (1), 91–102. doi:10.3892/or.2020.7602

Fang, S., Dong, L., Liu, L., Guo, J., Zhao, L., Zhang, J., et al. (2021). HERB: a High-Throughput Experiment- and Reference-Guided Database of Traditional Chinese Medicine. *Nucleic Acids Res.* 49 (D1), D1197–d1206. doi:10.1093/nar/gkaa1063

Fattorusso, R., Frutos, S., Sun, X., Sucher, N. J., and Pellecchia, M. (2006). Traditional Chinese Medicines with Caspase-Inhibitory Activity. *Phytomedicine* 13 (1-2), 16–22. doi:10.1016/j.phymed.2005.03.004

Francque, S., Szabo, G., Abdelmalek, M. F., Byrne, C. D., Cusi, K., Dufour, J. F., et al. (2021). Nonalcoholic Steatohepatitis: the Role of Peroxisome Proliferator-Activated Receptors. *Nat. Rev. Gastroenterol. Hepatol.* 18 (1), 24–39. doi:10.1038/s41575-020-00366-5

Friedman, S. L., Neuschwander-Tetri, B. A., Rinella, M., and Sanyal, A. J. (2018). Mechanisms of NAFLD Development and Therapeutic Strategies. *Nat. Med.* 24 (7), 908–922. doi:10.1038/s41591-018-0104-9

Golabi, P., Paik, J. M., AlQahtani, S., Younossi, Y., Tuncer, G., and Younossi, Z. M. (2021). Burden of Non-alcoholic Fatty Liver Disease in Asia, the Middle East and North Africa: Data from Global Burden of Disease 2009-2019. *J. Hepatol.* 75 (4), 795–809. doi:10.1016/j.jhep.2021.05.022

Goldner, D., and Lavine, J. E. Nonalcoholic Fatty Liver Disease in Children: Unique Considerations and Challenges. *Gastroenterology*. 2020;158(7):1967-e1.doi:10.1053/j.gastro.2020.01.048

Hatting, M., Zhao, G., Schumacher, F., Sellge, G., Al Masaoudi, M., Gaβler, N., et al. (2013). Hepatocyte Caspase-8 Is an Essential Modulator of Steatohepatitis in Rodents. *Hepatology* 57 (6), 2189–2201. doi:10.1002/hep.26271

Hopkins, A. L. (2007). Network Pharmacology. *Nat. Biotechnol.* 25 (10), 1110–1111. doi:10.1038/nbt1007-1110

Hu, N., Guo, C., Dai, X., Wang, C., Gong, L., Yu, L., et al. (2020). Forsythiae Fructuse Water Extract Attenuates Liver Fibrosis via TLR4/MyD88/NF-Kb and

TGF-B/smads Signaling Pathways. *J. Ethnopharmacol.* 262, 113275. doi:10.1016/j.jep.2020.113275

Hu, W. X., Xiang, Q., Wen, Z., He, D., Wu, X. M., and Hu, G. Z. (2014). Neuroprotective Effect of Atractylodes Macrocephalaon Polysaccharides *In Vitro* on Neuronal Apoptosis Induced by Hypoxia. *Mol. Med. Rep.* 9 (6), 2573–2581. doi:10.3892/mmr.2014.2105

Ito, K., and Murphy, D. (2013). Application of Ggplot2 to Pharmacometric Graphics. *CPT Pharmacometrics Syst. Pharmacol.* 2 (10), e79. doi:10.1038/psp.2013.56

Karuppasamy, M. P., Venkateswaran, S., and Subbiah, P. (2020). PDB-2-PBv3.0: An Updated Protein Block Database. *J. Bioinform Comput. Biol.* 18 (2), 2050009. doi:10.1142/S0219720020500092

Kazankov, K., Jørgensen, S. M. D., Thomsen, K. L., Møller, H. J., Vilstrup, H., George, J., et al. (2019). The Role of Macrophages in Nonalcoholic Fatty Liver Disease and Nonalcoholic Steatohepatitis. *Nat. Rev. Gastroenterol. Hepatol.* 16 (3), 145–159. doi:10.1038/s41575-018-0082-x

Kleiner, D. E., and Makhlouf, H. R. (2016). Histology of Nonalcoholic Fatty Liver Disease and Nonalcoholic Steatohepatitis in Adults and Children. *Clin. Liver Dis.* 20 (2), 293–312. doi:10.1016/j.cld.2015.10.011

Koliaki, C., Szendroedi, J., Kaul, K., Jelenik, T., Nowotny, P., Jankowiak, F., et al. (2015). Adaptation of Hepatic Mitochondrial Function in Humans with Non-alcoholic Fatty Liver Is Lost in Steatohepatitis. *Cell Metab.* 21 (5), 739–746. doi:10.1016/j.cmet.2015.04.004

Krenkel, O., Puengel, T., Govaere, O., Abdallah, A. T., Mossanen, J. C., Kohlhepp, M., et al. (2018). Therapeutic Inhibition of Inflammatory Monocyte Recruitment Reduces Steatohepatitis and Liver Fibrosis. *Hepatology* 67 (4), 1270–1283. doi:10.1002/hep.29544

Lee, D. G., Nam, B. R., Huh, J. W., and Lee, D. S. (2021). Isoliquiritigenin Reduces LPS-Induced Inflammation by Preventing Mitochondrial Fission in BV-2 Microglial Cells. *Inflammation* 44 (2), 714–724. doi:10.1007/s10753-020-01370-2

Lefere, S., Puengel, T., Hundertmark, J., Penners, C., Frank, A. K., Guillot, A., et al. (2020). Differential Effects of Selective- and Pan-PPAR Agonists on Experimental Steatohepatitis and Hepatic Macrophages☆. *J. Hepatol.* 73 (4), 757–770. doi:10.1016/j.jhep.2020.04.025

Leoni, S., Tovoli, F., Napoli, L., Serio, I., Ferri, S., and Bolondi, L. (2018). Current Guidelines for the Management of Non-alcoholic Fatty Liver Disease: A Systematic Review with Comparative Analysis. *World J. Gastroenterol.* 24 (30), 3361–3373. doi:10.3748/wjg.v24.i30.3361

Li, R., Li, J., Huang, Y., Li, H., Yan, S., Lin, J., et al. (2018). Polydatin Attenuates Diet-Induced Nonalcoholic Steatohepatitis and Fibrosis in Mice. *Int. J. Biol. Sci.* 14 (11), 1411–1425. doi:10.7150/ijbs.26086

Lilley, E., Stanford, S. C., Kendall, D. E., Alexander, S. P. H., Cirino, G., Docherty, J. R., et al. (2020). ARRIVE 2.0 and the British Journal of Pharmacology: Updated Guidance for 2020. *Br. J. Pharmacol.* 177 (16), 3611–3616. doi:10.1111/bph.15178

Locatelli, I., Sutti, S., Vacchiano, M., Bozzola, C., and Albano, E. (2013). NF-κB1 Deficiency Stimulates the Progression of Non-alcoholic Steatohepatitis (NASH) in Mice by Promoting NKT-Cell-Mediated Responses. *Clin. Sci. (Lond)* 124 (4), 279–287. doi:10.1042/CS20120289

Ma, Y. M., Zhang, X. Z., Su, Z. Z., Li, N., Cao, L., Ding, G., et al. (2015). Insight into the Molecular Mechanism of a Herbal Injection by Integrating Network Pharmacology and *In Vitro*. *J. Ethnopharmacol.* 173, 91–99. doi:10.1016/j.jep.2015.07.016

Manne, V., Handa, P., and Kowdley, K. V. (2018). Pathophysiology of Nonalcoholic Fatty Liver Disease/Nonalcoholic Steatohepatitis. *Clin. Liver Dis.* 22 (1), 23–37. doi:10.1016/j.cld.2017.08.007

Mata, J. F., Silveira, V. S., Mateo, E. C., Cortez, M. A., Queiroz, R. G., Yunes, J. A., et al. (2010). Low mRNA Expression of the Apoptosis-Related Genes CASP3, CASP8, and FAS Is Associated with Low Induction Treatment Response in Childhood Acute Lymphoblastic Leukemia (ALL). *Pediatr. Blood Cancer* 55 (1), 100–107. doi:10.1002/pbc.22463

McGrath, J. C., and Lilley, E. (2015). Implementing Guidelines on Reporting Research Using Animals (ARRIVE etc.): New Requirements for Publication in BJP. *Br. J. Pharmacol.* 172 (13), 3189–3193. doi:10.1111/bph.12955

Merry, T. L., Tran, M., Dodd, G. T., Mangiafico, S. P., Wiede, F., Kaur, S., et al. (2016). Erratum to: Hepatocyte Glutathione Peroxidase-1 Deficiency Improves Hepatic Glucose Metabolism and Decreases Steatohepatitis in Mice. *Diabetologia* 59 (12), 2729–2644. doi:10.1007/s00125-016-4124-z

Morán-Salvador, E., López-Parra, M., García-Alonso, V., Titos, E., Martínez-Clemente, M., González-Périz, A., et al. (2011). Role for PPARγ in Obesity-Induced Hepatic Steatosis as Determined by Hepatocyte- and Macrophage-specific Conditional Knockouts. *Faseb J.* 25 (8), 2538–2550. doi:10.1096/fj.10-173716

Obstfeld, A. E., Sugaru, E., Thearle, M., Francisco, A. M., Gayet, C., Ginsberg, H. N., et al. (2010). C-C Chemokine Receptor 2 (CCR2) Regulates the Hepatic Recruitment of Myeloid Cells that Promote Obesity-Induced Hepatic Steatosis. *Diabetes* 59 (4), 916–925. doi:10.2337/db09-1403

Pawlak, M., Lefebvre, P., and Staels, B. (2015). Molecular Mechanism of PPARα Action and its Impact on Lipid Metabolism, Inflammation and Fibrosis in Non-alcoholic Fatty Liver Disease. *J. Hepatol.* 62 (3), 720–733. doi:10.1016/j.jhep.2014.10.039

Percie du Sert, N., Hurst, V., Ahluwalia, A., Alam, S., Avey, M. T., Baker, M., et al. (2020). The ARRIVE Guidelines 2.0: Updated Guidelines for Reporting Animal Research. *J. Cereb. Blood Flow. Metab.* 40 (7), 1777–1769.doi:10.1177/0271678X20943823

Rinella, M. E., and Green, R. M. (2004). The Methionine-Choline Deficient Dietary Model of Steatohepatitis Does Not Exhibit Insulin Resistance. *J. Hepatol.* 40 (1), 47–51. doi:10.1016/j.jhep.2003.09.020

Rinella, M. E., and Sanyal, A. J. (2016). Management of NAFLD: a Stage-Based Approach. *Nat. Rev. Gastroenterol. Hepatol.* 13 (4), 196–205. doi:10.1038/nrgastro.2016.3

Rom, O., Liu, Y., Liu, Z., Zhao, Y., Wu, J., Ghrayeb, A., et al. (2020). Glycine-based Treatment Ameliorates NAFLD by Modulating Fatty Acid Oxidation, Glutathione Synthesis, and the Gut Microbiome. *Sci. Transl. Med.* 12 (572). doi:10.1126/scitranslmed.aaz2841

Romics, L., Jr., Kodys, K., Dolganiuc, A., Graham, L., Velayudham, A., Mandrekar, P., et al. (2004). Diverse Regulation of NF-kappaB and Peroxisome Proliferator-Activated Receptors in Murine Nonalcoholic Fatty Liver. *Hepatology* 40 (2), 376–385. doi:10.1002/hep.20304

Sanyal, A. J., Brunt, E. M., Kleiner, D. E., Kowdley, K. V., Chalasani, N., Lavine, J. E., et al. (2011). Endpoints and Clinical Trial Design for Nonalcoholic Steatohepatitis. *Hepatology* 54 (1), 344–353. doi:10.1002/hep.24376

Sanyal, A. J., Friedman, S. L., McCullough, A. J., and Dimick-Santos, L. (2015). Challenges and Opportunities in Drug and Biomarker Development for Nonalcoholic Steatohepatitis: Findings and Recommendations from an American Association for the Study of Liver Diseases-U.S. Food and Drug Administration Joint Workshop. *Hepatology* 61 (4), 1392–1405. doi:10.1002/hep.27678

Shannon, P., Markiel, A., Ozier, O., Baliga, N. S., Wang, J. T., Ramage, D., et al. (2003). Cytoscape: a Software Environment for Integrated Models of Biomolecular Interaction Networks. *Genome Res.* 13 (11), 2498–2504. doi:10.1101/gr.1239303

Wan, J., Benkdane, M., Teixeira-Clerc, F., Bonnafous, S., Louvet, A., Lafdil, F., et al. (2014). M2 Kupffer Cells Promote M1 Kupffer Cell Apoptosis: a Protective Mechanism against Alcoholic and Nonalcoholic Fatty Liver Disease. *Hepatology* 59 (1), 130–142. doi:10.1002/hep.26607

Wang, P. X., Ji, Y. X., Zhang, X. J., Zhao, L. P., Yan, Z. Z., Zhang, P., et al. (2017). Targeting CASP8 and FADD-like Apoptosis Regulator Ameliorates Nonalcoholic Steatohepatitis in Mice and Nonhuman Primates. *Nat. Med.* 23 (4), 439–449. doi:10.1038/nm.4290

Whitehead, M. J., McCanney, G. A., Willison, H. J., and Barnett, S. C. (2019). MyelinJ: an ImageJ Macro for High Throughput Analysis of Myelinating Cultures. *Bioinformatics* 35 (21), 4528–4530. doi:10.1093/bioinformatics/btz403

Wu, G., Robertson, D. H., Brooks, C. L., 3rd, and Vieth, M. (2003). Detailed Analysis of Grid-Based Molecular Docking: A Case Study of CDOCKER-A CHARMm-Based MD Docking Algorithm. *J. Comput. Chem.* 24 (13), 1549–1562. doi:10.1002/jcc.10306

Wynn, T. A., and Vannella, K. M. (2016). Macrophages in Tissue Repair, Regeneration, and Fibrosis. *Immunity* 44 (3), 450–462. doi:10.1016/j.immuni.2016.02.015

Xiang, D., Zou, J., Zhu, X., Chen, X., Luo, J., Kong, L., et al. (2020). Physalin D Attenuates Hepatic Stellate Cell Activation and Liver Fibrosis by Blocking TGF-

β/Smad and YAP Signaling. *Phytomedicine* 78, 153294. doi:10.1016/j.phymed.2020.153294

Xiang, J., Yang, G., Ma, C., Wei, L., Wu, H., Zhang, W., et al. (2021). Tectorigenin Alleviates Intrahepatic Cholestasis by Inhibiting Hepatic Inflammation and Bile Accumulation via Activation of PPARγ. *Br. J. Pharmacol.* 178 (12), 2443–2460. doi:10.1111/bph.15429

Younossi, Z. M. (2019). Non-alcoholic Fatty Liver Disease - A Global Public Health Perspective. *J. Hepatol.* 70 (3), 531–544. doi:10.1016/j.jhep.2018.10.033

Zhang, L., Shi, X., Huang, Z., Mao, J., Mei, W., Ding, L., et al. (2020). Network Pharmacology Approach to Uncover the Mechanism Governing the Effect of Radix Achyranthis Bidentatae on Osteoarthritis. *BMC Complement. Med. Ther.* 20 (1), 121. doi:10.1186/s12906-020-02909-4

Zhao, Y., Sun, X., Lin, J., Zhang, T., Liu, S., and Yan, Z. (2021). Panaxynol Induces Fibroblast-like Synovial Cell Apoptosis, Inhibits Proliferation and Invasion through TLR4/NF-Kb Pathway to Alleviate Rheumatoid Arthritis. *Int. Immunopharmacol.* 101 (Pt A), 108321. doi:10.1016/j.intimp.2021.108321

Zhou, Y., Tao, H., Wang, A., Zhong, Z., Wu, X., Wang, M., et al. (2019). Chinese Herb Pair Paeoniae Radix Alba and Atractylodis Macrocephalae Rhizoma Suppresses LPS-Induced Inflammatory Response through Inhibiting MAPK and NF-Kb Pathway. *Chin. Med.* 14, 2. doi:10.1186/s13020-019-0224-2

Conflict of Interest: Author JG, HL, and ML were employed by the company Henan Fusen Pharmaceutical Co., Ltd.

The remaining authors declare that the research was conducted in the absence of any commercial or financial relationships that could be construed as a potential conflict of interest.

frontiers | Frontiers in Pharmacology

ORIGINAL RESEARCH
published: 05 July 2022
doi: 10.3389/fphar.2022.909280

Nootkatone, a Sesquiterpene Ketone From *Alpiniae oxyphyllae* Fructus, Ameliorates Metabolic-Associated Fatty Liver by Regulating AMPK and MAPK Signaling

Zhang Yong[1†], Huang Zibao[2†], Zhou Zhi[3†], Ma Ning[3], Wang Ruiqi[2], Chen Mimi[2], He Xiaowen[4], Dong Lin[2], Xia Zhixuan[1], Liu Qiang[1], Lu Weiying[3] and Zhang Xiaopo[2]**

[1]Department of Pharmacology, Hainan Medical University, Haikou, China, [2]Key Laboratory of Tropical Translational Medicine of the Ministry of Education, Hainan Key Laboratory for Research and Development of Tropical Herbs, School of Pharmaceutical Science, Hainan Medical University, Haikou, China, [3]Reproductive Medical Center, Hainan Women and Children's Medical Center, Haikou, China, [4]Public Research Laboratory, Hainan Medical University, Haikou, China

Metabolic-associated fatty liver disease (MAFLD) is becoming more common due to lifestyle changes. A long-term high-fat and high-glucose diet induces glycolipid metabolism disorders in the liver, which results in the development of MAFLD. To date, there is no specific clinically useful therapeutics for this disease. Natural products or synthetic compounds were screened and investigated to find effective agents for treating MAFLD. In this study, nootkatone (Nok), a natural sesquiterpene ketone isolated from *Alpiniae oxyphyllae* fructus, was explored for its potential to treat MAFLD, and underlying mechanisms were studied. Our results show that Nok dramatically ameliorated the disordered lipid and glucose metabolism in MAFLD mice, decreased fat accumulation in hepatic tissue, and improved liver injury. Inflammation, metabolic disorder, and oxidative stress were ameliorated in liver tissue based on RNA-seq transcriptome comparison between a Nok-treated group and an MAFLD model group. Furthermore, Nok significantly activated AMPK activity and inhibited MAPK activity, especially the p38 and JNK signaling pathways, *in vivo* based on western blot analysis. The pharmaceutical effects and potential signaling pathways impacted by Nok were also investigated in L02 cells. Nok significantly promoted the consumption of glucose and decreased the deposition of triglycerides *in vitro*. The p-AMPKα level was notably upregulated by Nok, indicating dramatic AMPK activation. In addition, Nok decreased the levels of p-ERK1/2, p-p38, and p-JNK. Nok also inhibited the activation of MAPK signaling and, thus, alleviated MAFLD development. Our results suggest that Nok may be useful in treating MAFLD. Nok may ameliorate MAFLD by regulating glycolipid metabolism disorders by activating AMPK and inhibiting MAPK activity. Collectively, this study suggests that Nok is an effective compound for the treatment of MAFLD.

Keywords: MAFLD (metabolic-associated fatty liver disease), nootkatone, AMPK, MAPK, *Alpiniae oxyphyllae* Fructus

OPEN ACCESS

Edited by:
Menghao Huang,
Indiana University school of medicine, United States

Reviewed by:
Jinan Li,
Indiana University School of Medicine, United States
Jagannath Misra,
Indiana University, Purdue University Indianapolis, United States
Xiaojiaoyang Li,
Beijing University of Chinese Medicine, China

****Correspondence:***
Zhang Xiaopo
z_xp1412@163.com
Lu Weiying
2490206511@qq.com

[†]These authors have contributed equally to this work

Specialty section:
This article was submitted to Gastrointestinal and Hepatic Pharmacology, a section of the journal Frontiers in Pharmacology

Received: *31 March 2022*
Accepted: *27 May 2022*
Published: *05 July 2022*

Citation:
Yong Z, Zibao H, Zhi Z, Ning M, Ruiqi W, Mimi C, Xiaowen H, Lin D, Zhixuan X, Qiang L, Weiying L and Xiaopo Z (2022) Nootkatone, a Sesquiterpene Ketone From Alpiniae oxyphyllae Fructus, Ameliorates Metabolic-Associated Fatty Liver by Regulating AMPK and MAPK Signaling. Front. Pharmacol. 13:909280. doi: 10.3389/fphar.2022.909280

INTRODUCTION

With changing lifestyles, the incidence of nonalcoholic fatty liver disease (NAFLD) has increased. NAFLD has been newly termed metabolic-associated fatty liver disease (MAFLD) to exclude ethanol consumption and other liver disease factors in diagnosis (Eslam, Sanyal et al., 2020). MAFLD is the most common liver-related disease in the world and usually includes simple fatty liver, fatty liver hepatitis, liver fibrosis, alcoholic fatty liver, and even cirrhosis during development (Friedman, Neuschwander-Tetri et al., 2018; Eslam, Sanyal et al., 2020). MAFLD is becoming a great threat to human health, and the medical burden on society will increase with the increasing incidence (Younossi, Anstee et al., 2018). Multiple parallel hits produced in the liver from lipid accumulation, lipid toxicity from overaccumulation, oxidative stress and inflammation from lipid metabolic disorders, endoplasmic reticulum stress, mitochondrial damage, and insulin resistance are acknowledged as the main drivers of MAFLD pathogenesis (Younossi, Anstee et al., 2018; Eslam, Sanyal et al., 2020; Huang M, Kim H et al., 2020). Although there are many studies of MAFLD, the exact pathogenesis remains unclear, and there is no specific drug for treating MAFLD in the clinic (Kuchay, Choudhary et al., 2020). Finding effective and safe therapeutic agents from natural or synthetic resources for MAFLD is a common goal worldwide.

Glycolipid metabolism disorder in hepatocytes is considered a key development risk factor for MAFLD. Regulating hepatocyte glucose and lipid metabolism is beneficial to MAFLD and can inhibit the development of MAFLD. AMP-activated protein kinase (AMPK), the key enzyme regulating cellular glucose and lipid metabolism, is considered a cell energy sensor (Trefts and Shaw 2021). Targeting AMPK activation has been widely shown to correct glycolipid metabolism disorders and is useful for MAFLD treatment (Smith, Marcinko et al., 2016). The effects of AMPK activation in promoting glucose and lipid metabolic decomposition, inhibiting lipid synthesis and gluconeogenesis, and especially promoting a metabolic switch from fat synthesis to fat oxidation (Trefts and Shaw 2021) have been widely studied and reported. AMPK agonists are potential candidates for treating MAFLD.

Mitogen-activated protein kinase (MAPK) is also a very important kinase regulating a multitude of hepatic metabolic processes. There are three major MAPK subgroups in the mammalian liver, including extracellular signal-regulated kinases 1 and 2 (ERK1/2), c-Jun N-terminal kinases 1, 2, and 3 (JNK1/2/3), and p38α/β/δ/γ (p38) (Zeng, Tang et al., 2014; Lawan and Bennett 2017). MAPK is usually activated by disorders of glucose and lipid metabolism, oxidative stress, inflammation, and other factors associated with MAFLD (Lawan and Bennett 2017). Inhibiting the MAPK signaling pathway could improve MAFLD by regulating glucose and lipid metabolism and exhibiting anti-inflammatory, antioxidant, and other effects (Lawan, Zhang et al., 2015; Hwang, Wang et al., 2020). Many anti-MAFLD potential compounds, such as betaine (Ge, Yu et al., 2016), liraglutide (Zhang, Yang et al., 2013), and chlorogenic acid (Yan, Gao et al., 2018), inhibit MAPK activity. Suppressing MAPK signaling is a potentially effective therapeutic strategy for MAFLD treatment.

Nootkatone (Nok), 5,6-dimethyl-8-isopropyl-dicyclic-(4,4,0)-dec-1-ene-3-one, with a molecular formula of $C_{15}H_{22}O$, is a sesquiterpene ketone that naturally exists in *Alpiniae oxyphyllae* fructus, grapefruit, and citrus (Wang, Wang et al., 2018). *Alpiniae oxyphyllae* is a famous traditional Chinese medicine and Li Medicine, rich in Hainan Province of China. *Alpiniae oxyphyllae* has many effects in traditional Chinese medicine, including warming the spleen, stopping diarrhea, reducing salivation, warming the kidney, reducing urine, and solidifying essence (Li, Du et al., 2021). Previous studies have reported that Nok reduced weight gain (Murase, Misawa et al., 2010), increased the sensitivity of the non-small-cell cancer cell Line A549 to doxorubicin (Moon, Ryu et al., 2019), protected against chronic kidney injury (Li, Tan et al., 2016; Chen, Lin et al., 2021), and showed anti-anxiety and anti-depression effects (Yan, Li et al., 2021). To date, there have been no reports about its anti-MAFLD activity or potential mechanisms, which attracted our interest in this study.

MATERIALS AND METHODS

Extraction and Isolation of Nok

Fructus (1.0 kg) from *Alpiniae oxyphyllae* was extracted using petroleum ether under reduced pressure (30 g) and further separated by a silica gel column eluted with a petroleum ether-ethyl acetate (1:0-0:1) gradient to afford six fractions (Fra. A-F). Fra. E was then isolated by Sephadex LH-20 to give Nok (20 mg). The purity of Nok was determined by HPLC. The methods were as follows. Column: Thermo HyPURITY C18, 4.6 × 150 mm, 3.0 μm; UV detector wavelength: 238 nm; mobile phase flow rate: 1.0 ml/min; sample: prepared in methanol; mobile phase: A, acetonitrile; B, 0.1% phosphoric acid in water; gradient elution conditions: A, 50%–60%, 15 min. To obtain a sufficient amount of the compound, 10 g of Nok was purchased from Chengdu Biopurify Phytochemicals Ltd., and its purity was also determined by HPLC.

Animals and Treatments

A total of 32 male mice (age, 5 weeks; weight 19–21 g) were purchased from Gempharmatech Co., Ltd. (Jiang Su, China). Mice were fed in the animal research center of Hainan Medical University (HMU). Our study was approved by the ethics committee of HMU. The environmental surroundings were maintained at an indoor temperature of 25 ± 0.5°C with a 12-h light–dark cycle and free access to water and food.

After adaptive feeding for 3 days, the mice were stochastically divided, 8 mice each, into 4 experimental groups: normal, MAFLD model, 25 mg kg^{-1} Nok and 50 mg kg^{-1} Nok. The normal group was fed a basal control diet. The MAFLD model group was fed a 60% high-fat diet (60% fat, HFD). For the Nok test groups, mice were fed an HFD in addition to 25 mg $kg^{-1}\cdot d^{-1}$ or 50 mg $kg^{-1}\cdot d^{-1}$ Nok, i. g.; Nok was dissolved in vegetable oil. The same volume of vegetable oil was given to the normal group

and MAFLD model group mice. Fasting blood glucose levels and body weights were tested weekly during the experimental period. After 12 weeks of drug intervention, blood samples were taken after 8 h of fasting, and serum samples were obtained by centrifugation for further testing. Then, the mice were killed by CO_2, and the liver tissues were used for other experiments.

Oral Glucose Tolerance Test

During the 11–12 weeks of administration, the OGTT was performed as follows. The blood glucose level of each mouse was tested after 8 h of fasting overnight, and the data were defined as an initial blood glucose value of 0 min. Each mouse was orally gavaged with 50% glucose solution, and the volume was calculated according to 0.02 g/10 g. We then detected blood glucose levels using a glucose meter (Roche, ACCU-CHEK) 30, 60, 120, and 180 min after oral glucose administration.

Serum Biochemical Analysis

After 12 weeks of drug administration, blood was taken, and the serum was isolated by centrifugation at 3,000 rpm at 15°C for 15 min. Then, serum lipids, such as triglyceride (TG), low-density lipoprotein cholesterol (LDL-c), high-density lipoprotein cholesterol (HDL-c), and total cholesterol (TC), were tested by appropriate kits (Nanjing Jiancheng Bioengineering Institute). The hepatic function indices in serum, such as alanine aminotransferase (ALT) and aspartate aminotransferase (AST), were also measured using kits (Nanjing Jiancheng Bioengineering Institute). The serum IL-1β, TNFα, IL-6, and IL-18 levels were assayed by corresponding ELISA kits from Nanjing Jiancheng Bioengineering Institute.

Liver Histopathological Analysis

After 12 weeks of drug administration, liver tissue was isolated from the same part of the mouse liver and drenched in a 10% formalin tissue fixator for 48 h. After sufficient tissue fixation, liver samples were embedded in paraffin, sectioned (4 μm), stained with hematoxylin and eosin (H&E), and imaged. Oil Red O staining was also performed on liver tissues to detect lipid deposition. Scores of hepatic tissue steatosis based on H&E staining were used to evaluate the pathological changes, and 5 grades were defined as follows: 0%–5% of parenchyma-involved steatosis was scored as zero, 5%–25% was scored as one, 25%–50% was scored as two, 50%–75% was scored as three, and over 75% was scored as four. Oil Red O staining was quantified by the red area coefficient.

RNA-Seq Assay

Three mouse hepatic tissues were isolated from the normal, MAFLD model, and Nok (50 mg kg^{-1}) treatment groups. Total RNA was extracted, and quality was assessed by integrity. Relevant sample processing, sequencing, and data analysis methods were described in our previous research (Yong, Ruiqi et al., 2021).

Cell Culture and Treatment

L02 hepatocytes were used in this study, and the culture medium was DMEM supplemented with 10% fetal bovine serum (FBS) and 1% penicillin–streptomycin solution. After two generations of stable passage of L02 cells, the cell suspension was prepared and seeded into the plates and cultured for approximately 24 h. Nok and metformin (Met) dissolved in dimethylsulfoxide (DMSO) were added and treated with or without PO (200 μM PA-BSA and 400 μM OA-BSA) coincubation for another 24 h. For blocking experiments, L02 cells were cultured and seeded as above, and before drug treatment, the cells were pretreated with a AMPK inhibitor Compound C (CC, dissolved in DMSO) at 10 μM or a JNK agonist anisomycin (AN, dissolved in DMSO) at 1 μM for 1 h. Following pretreatment, PO and drugs were added to the corresponding wells and cocultured with the cells for 24 h. Then, total cellular protein was extracted after treatment and detected by western blotting.

Cytotoxicity Assay

The cytotoxicity of Nok to L02 cells was evaluated by the MTT method. Cell culture and treatment were performed as above, and 5 replicates were performed for each drug treatment. The highest treatment concentration of Nok was 400 μM. A similar volume of DMSO (volume ratio as 0.1%) was added to the control group. After 24 h of drug treatment, the culture medium of each well was removed, and 50 μl MTT solution was added to the cells. Then, the plates were incubated at 37°C for 4 h. The level of formazan was detected at OD 490 nm with a microplate reader to assess cell viability. The DMSO treatment group was normalized to 100% cell viability, and the others are shown as percentages of the DMSO treatment group.

Glucose Consumption Assay

Cell culture and treatment were performed as above, and 5 replicates were performed for each drug treatment. The glucose consumption was calculated by subtracting the glucose level present in media from cells cultured for 24 h with drug or equal volume DMSO (volume ratio as 0.1%) treatment from the glucose level in plates containing only culture medium. After drug treatment, the glucose concentration in the supernatant of each cell culture well was measured by a glucose detection kit (Beijing Strong Biotechnologies, Inc.), and the glucose consumption level of each treatment group was calculated as above.

Intracellular TG Assay

Cell culture was performed as described above. L02 cells were inoculated in a cell culture plate at a density of $1.0*10^5$ cells/ml, and four replicates were performed for each drug treatment. Then, 600 μM PO (200 μM PA-BSA and 400 μM OA-BSA) was added to induce a cell model of intracellular TG accumulation. The normal control group was supplemented with 10% BSA solution. After incubation with PO or BSA for 24 h, equal volumes of DMSO (volume ratio of 0.1%) to 40 μM Nok, or Nok or Met at the indicated concentrations were added to the cell culture wells for another 24 h of incubation. The cells were collected, the intracellular TG content was determined by a cellular TG assay kit (Applygen Technologies Inc.), and the intracellular TG level was normalized to the protein concentration. With the same treatment, the oil red O

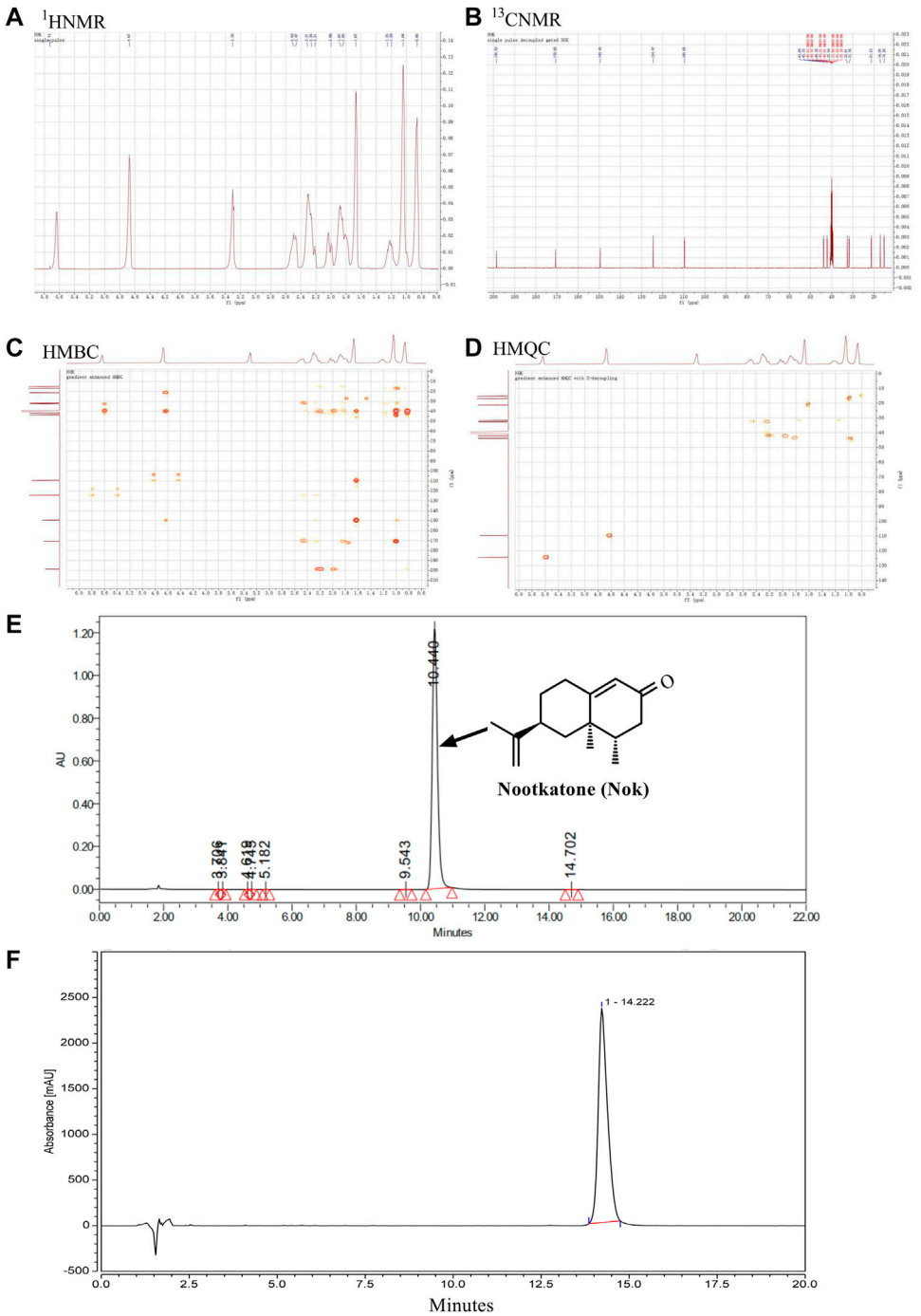

FIGURE 1 | Isolation and structural characterization of nootkatone. **(A)** The structure and ^{1}H-NMR spectrum of Nok **(B)** ^{13}C-NMR spectrum of Nok; **(C)** HMQC spectrum of Nok **(D)** HMBC spectrum of Nok. **(E)** HPLC of Nok from *Alpiniae oxyphyllae* Fructus. **(F)** HPLC of Nok from Chengdu Biopurify Phytochemicals Ltd.

staining was done to evaluate the intracellular lipid accumulation induced by PO.

Intracellular ATP Assay

With the same treatment conditions as intracellular TG assay, the intracellular ATP in L02 cells was detected by ATP assay kits.

Western Blots

The L02 cells and liver tissue samples were prepared as described above, and total protein was extracted. Western blotting was used to detect the target proteins of each sample, such as phospho-ERK1/2 (p-ERK1/2) (AM071, Beyotime), ERK1/2 (AF1051, Beyotime), phospho-p38

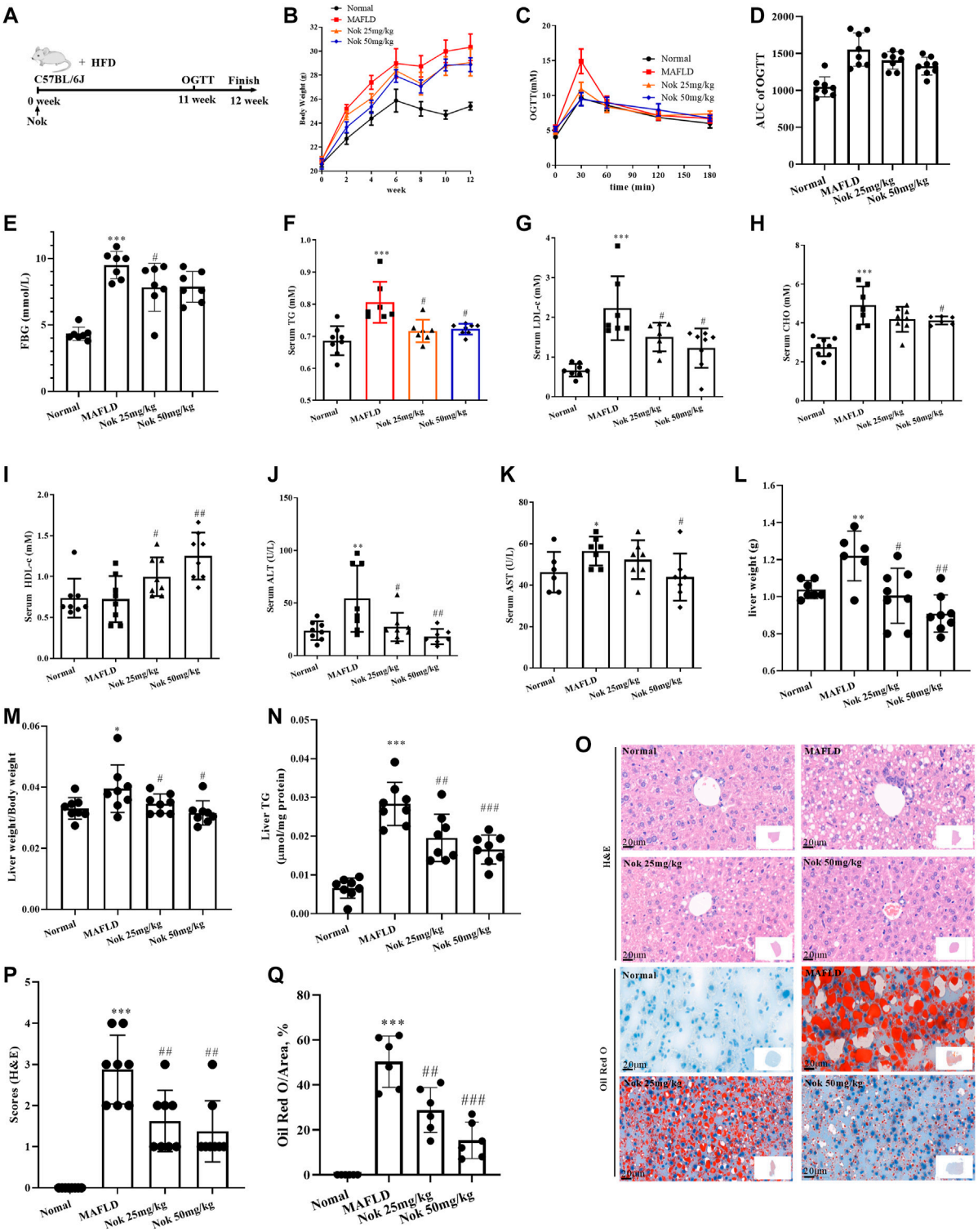

FIGURE 2 | Nootkatone ameliorated metabolic-associated fatty liver. Mice fed a high-fat diet were administered Nok at doses of 25 mg kg^{-1} and 50 mg kg^{-1} daily for 12 weeks **(A)**. Changes in body weight **(B)**, OGTT test results at 11–12 weeks **(C)** and OGTT AUC **(D)**, FBG **(E)**, serum lipid **(F–I)**, liver function **(K–L)**, liver index (liver weight/body weight, **(M)**, liver TG **(N)**, and liver histopathological examination including H&E and Oil Red staining **(O)**, grading **(P)** and quantity by red area coefficient **(Q)** were measured. All data points represent the means ± SD (n = 8 per group); *$p < 0.05$, **$p < 0.01$, ***$p < 0.001$ vs. normal group mice; #$p < 0.05$, ##$p < 0.01$, ###$p < 0.001$ vs. MAFLD group mice.

MAPK (Thr180) (p-p38) (AF5884, Beyotime), p38 MAPK (p38) (AF7668, Beyotime), phospho-JNK1/2 (Thr183/Tyr185) (p-JNK) (AF5860, Beyotime), JNK (AJ518, Beyotime), GAPDH (AF1186, Beyotime), phospho-AMPKα (Thr172) (p-AMPKα) (2535T, CST), AMPKα (t-AMPK) (2532S, CST), phospho-ACC (Ser79) (p-ACC) (3661S, CST), and ACC (t-ACC) (3676T, CST). The target protein bands of western blots were analyzed and quantified. The levels of p-AMPKα, p-ACC p-ERK1/2, p-p38 and p-JNK were normalized to those of AMPKα, ACC, ERK1/2, p38 and JNK, respectively, and are presented as the fold change compared to the control treatment.

Quantitative PCR Analysis

Total RNA was extracted from liver tissues, and quantitative PCR (qPCR) assays were performed with SYBR Green PCR master mix (rr42lr, Takara, Beijing, China) in an ABI Prism 7,900 high-throughput real-time PCR system. The forward (F) and reverse (R) primer sequences were as follows: Il-1β (F, 5′cgacaaaatacctgtggcct3'; R, 5′ttctttgggtattgcttggg3′), IL-6 (R, 5′tagtcc ttcctaccccaatttcc3'; R, 5′ttggtccttagccactccttc3′), TNFα (F, 5′ccctcacactcagatcatcttct3'; R, 5′gctacgacgtgggctacag3′), IL-18 (F, 5′catgccatggctgctgaaccagtagaaga3'; R, 5′cgggatcc aatagc tagtcttcgttttg3′) and β-actin (F, 5′ggatgcagaaggagattactgc3'; R, 5′ccaccg atccacagagta3′).

Statistical Analysis

For *in vitro* experiments, our values are displayed as the mean ± SD with three independent repetitions. For *the in vivo* experiments, our results are also presented as the mean ± SD. There were 8 mice in each group. GraphPad Prism 5.0 software was used to process and analyze data. The differences among the studied groups were assessed by *t* test or one-way ANOVA, and $p < 0.05$ was considered statistically significant.

RESULTS

Extraction and Identification of Nok

Nok was identified by analyzing NMR data. The ^{1}H-NMR (400 MHz, DMSO-d_6) spectrum displayed signals of δ_H: 5.64 (1H, brs), 4.67 (2H, brs), 1.66 (3H, brs), 1.04 (3H, s), 0.87 (3H, d, J = 7.2 Hz) (**Figure 1A**), which were attributed to two double bonds and three methyl groups. In the ^{13}C-NMR spectrum (100 MHz, DMSO-d_6), fifteen carbon signals were observed (**Figure 2B**). These carbon signals were δ_C: 198.6, 170.1, 149.5, 124.5, 109.7, 43.8, 42.1, 40.5, 40.4, 39.9, 32.6, 31.7, 21.2, 17.0, and 15.2 (**Figure 2B**). These NMR data were identical to Nok and were further confirmed by analyzing 2D HMQC and HMBC NMR spectra (**Figures 1C,D**). In the HMQC spectrum, correlations between hydrogen and carbons were observed to assign the CH, CH_2, and CH_3 in Nok. In the HMBC spectrum, long-range correlations between hydrogen and carbons were carefully analyzed for connecting different structural units together to confirm the structure of Nok. The purity of Nok from our extraction and a commercial source were greater than 99% based on HPLC (**Figures 1E,F**).

Nok Ameliorates MAFLD Effects

The timeline and design of the animal experiments are shown in **Figure 2A**. The body weight (**Figure 2B**), OGTT and AUC (**Figures 2C,D**), levels of fasting blood glucose (**Figure 2E**), serum TG (**Figure 2F**), LDL-c (**Figure 2G**) and CHO (**Figure 2H**) of the MAFLD model group mice were prominently higher than those of the normal control group, and HDL-c was decreased (**Figure 2I**), indicating significant glucose and lipid metabolism disorders. At the same time, the liver weight (Figure 2L), liver index (Figure 2M) and liver TG (Figure 2N) of mice in the MAFLD group were also significantly increased, and liver function (**Figures 2G–K**) and liver glucose tolerance (**Figures 2C,D**) were impaired. The H&E and oil red staining (Figure 2O) results showed that the model group displayed significant fatty liver characteristics, including bullae steatosis, inflammation and lipid accumulation. Meanwhile, the steatosis score (Figure 2P) and oil red O-positive area (Figure 2Q) were significantly higher than those of the normal group, suggesting that the model mice had significant metabolism-associated fatty liver disease. In the Nok-treated group, body weight (**Figure 2B**), fasting glucose (**Figure 2E**), and blood lipid levels (**Figures 2F–H**) were significantly reduced, serum HDL-c levels (**Figure 2I**) and glucose tolerance conditions (**Figures 2C,D**) were significantly improved, and liver function was recovered (**Figures 2G–K**). The liver weight (Figure 2L), liver index (Figure 2M) and liver TG (Figure 2N) were significantly decreased. Histopathological changes were significantly ameliorated in the Nok treatment group mice compared with the MAFLD model group (Figure 2O–Q). This abnormality in the MAFLD model was dose-dependently improved by Nok treatment (**Figure 2B**-Q). Collectively, these results suggested that Nok had the capability to improve MAFLD.

RNA-Seq Assay of the Effects of Nok on MAFLD Treatment

RNA-seq of liver tissue was performed to investigate the mechanisms underlying Nok's effects on MAFLD. In the normal group, the MAFLD model group, and the Nok (50 mg kg^{-1}·d^{-1}) treatment group, 3 mouse liver tissues from each group were isolated, and total RNA was extracted. In the MAFLD group, compared with the normal group, there were 773 upregulated genes and 433 downregulated genes (**Figure 3C**). In the Nok (50 mg kg^{-1})-treated group, compared with the normal group mice, there were 893 upregulated genes and 1,153 downregulated genes (**Figure 3A**), and compared to the MAFLD model group mice, there were 837 upregulated genes and 1,896 downregulated genes (**Figure 3B**). All changes were based on an FDR<0.05 and fold change>1.5. These three groups of differentially expressed genes are depicted in the Venn diagram in **Figure 3D**; 242 genes are common to all three comparisons, including 119 upregulated genes and 123 downregulated genes in the Nok group (**Figures 3D,E**). These genes were visualized by a heatmap (**Figure 3E**). Gene ontology (GO) enrichment was analyzed by the clusterProfiler R package and sangerbox, and GO terms with padj less than 0.05 were considered significantly differentially enriched. The biological processes (BP), cellular

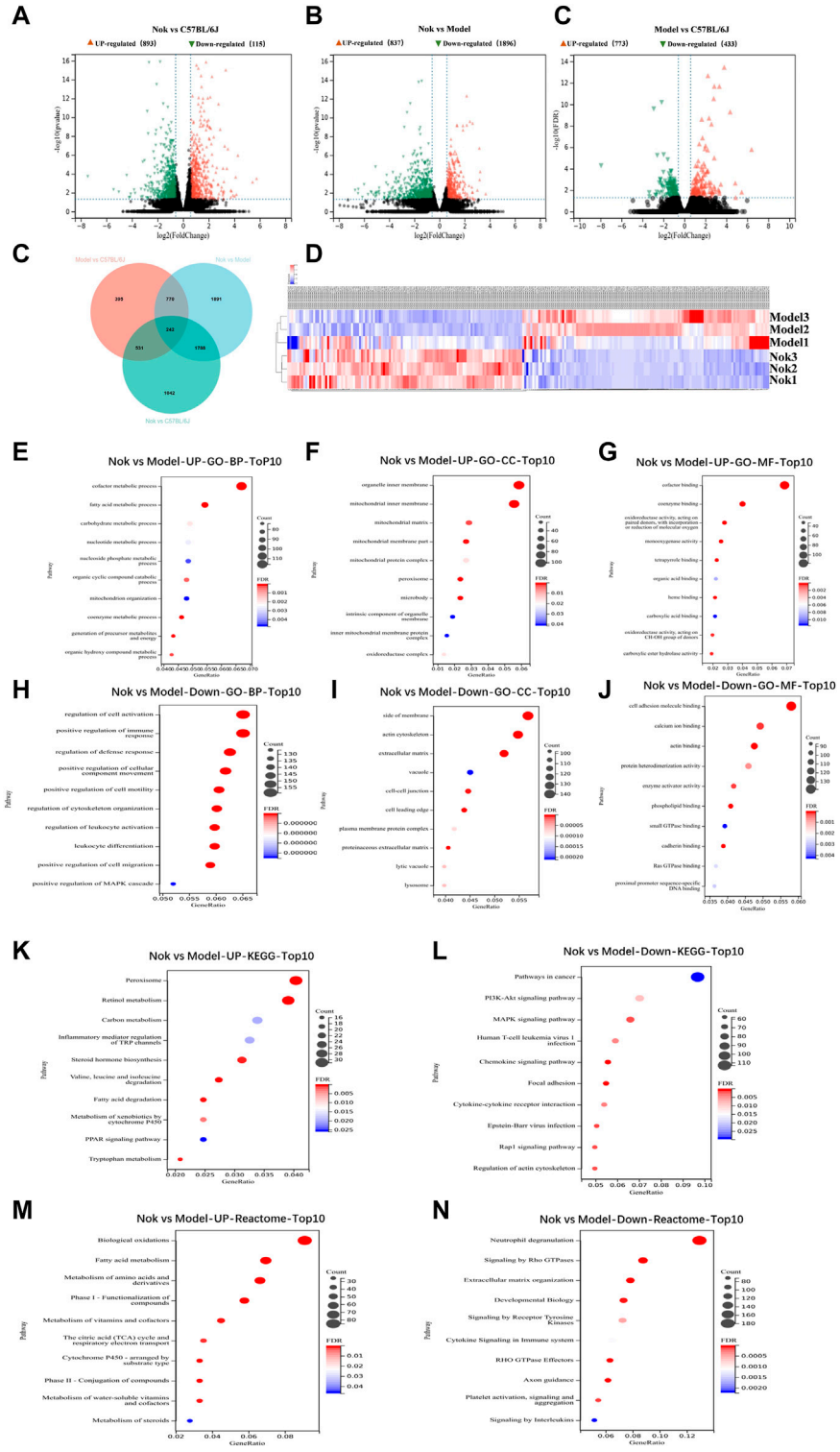

FIGURE 3 | Analysis of hepatic transcriptome**.** RNA-seq assay of mouse hepatocytes between the Nok treatment group (n = 3) and MAFLD model group (n = 3). Volcano plots show the differentially expressed genes in **(A)** Nok-treated vs. normal mice, **(B)** Nok-treated vs. MAFLD mice, and **(C)** MAFLD vs. normal mice show fold changes ($|\log_2$ (fold change)$|>0.58$ and adjusted p value padj≤ 0.05). **(D)** Venn diagram showing the intersections among differentially expressed genes in different group-to-group comparisons. **(E)** Heatmap showing the differentially expressed genes between Nok-treated and MAFLD model mice. **(F–K)** Gene Ontology (GO) analysis showing the main changes in gene functions between Nok-treated and MAFLD model mice. **(L–M)** Kyoto Encyclopedia of Genes and Genomes (KEGG) showing enriched differentially expressed genes belonging to different pathways between Nok-treated and MAFLD model mice. **(N–O)** The Reactcomes of the main changes of gene functions between Nok treated and MAFLD model mice.

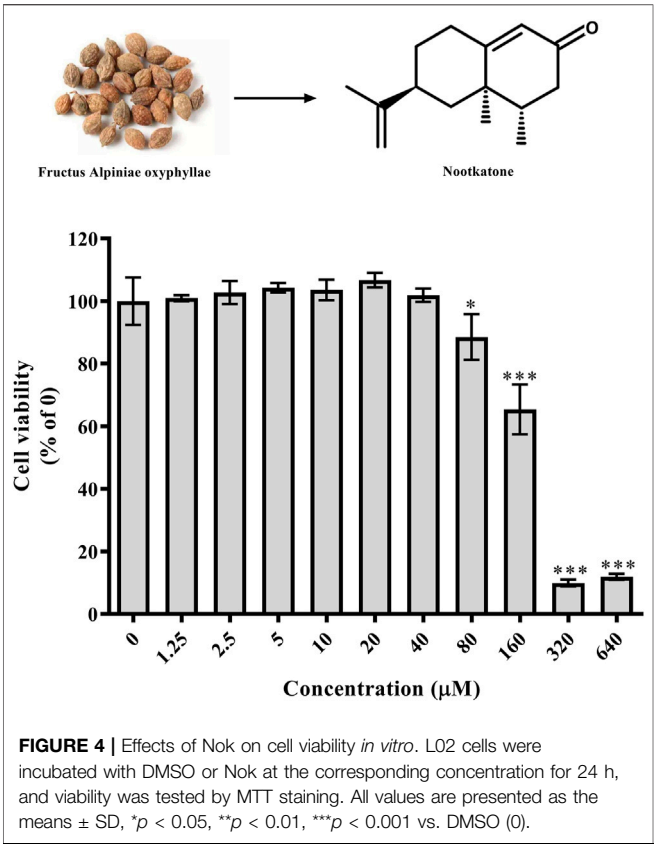

FIGURE 4 | Effects of Nok on cell viability *in vitro*. L02 cells were incubated with DMSO or Nok at the corresponding concentration for 24 h, and viability was tested by MTT staining. All values are presented as the means ± SD, $^{*}p < 0.05$, $^{**}p < 0.01$, $^{***}p < 0.001$ vs. DMSO (0).

components (CC), and molecular functions (MF) of significantly upregulated genes in the Nok treatment group compared to the MAFLD model group mice are shown in **Figures 3F–H**. These were mainly related to influencing metabolic processes, fatty acid metabolic processes and carbohydrate metabolic processes in BP and were mainly associated with the organelle inner membrane, mitochondrial matrix, mitochondrial membrane, and mitochondrial protein complex in CC and cofactor binding and coenzyme binding in MF (**Figures 3F–H**). The biological processes (BP), cellular components (CC), and molecular functions (MF) of significantly downregulated genes in the Nok treatment group compared to the MAFLD model group mice are shown in **Figures 3I–K**. These genes were mainly associated with positive regulation of the immune response, defense response, cell motility, leukocyte activation, and MAPK cascade in BP and were also correlated with side of membrane, actin cytoskeleton, extracellular matrix, vacuole, cell–cell junction, cell leading edge, plasma membrane protein components in CC and cell adhesion molecule binding, actin binding, protein heterodimerization activity, enzyme activator activity, phospholipid binding, calcium ion binding, and small GTPase binding in MF (**Figures 3I–K**). These results suggested that Nok might act on the immune system and that its pharmacological effects might be related to inflammation. The clusterProfiler R package was applied to assay the differential expression gene enrichments in KEGG pathways for the Nok treatment group compared to the MAFLD model group mice. The upregulated gene enrichment results showed that Nok could significantly promote peroxisome, retinol metabolism, carbon metabolism, steroid hormone biosynthesis, and fatty acid degradation signaling pathways (Figure 3L). The downregulated gene enrichment pathways suggested that Nok could significantly inhibit the PI3K-AKT, MAPK, chemokine, and Rap1 signaling pathways (Figure 3M). The reactome assay also showed that Nok may regulate biological oxidation, fatty acid metabolism and inflammation in the liver (Figure 3N–O).

Nok Cytotoxicity in L02 Cells

As shown in **Figure 4**, Nok showed no cytotoxicity at a concentration of 40 μM in L02 cells. However, the viability of L02 cells was significantly reduced at 80 μM (**Figure 4**, $p < 0.05$ vs. DMSO).

Nok Regulates Hepatocyte Glucose and Lipid Metabolism by AMPK Activation *In Vitro* and *In Vivo*

As shown in **Figures 5A, 5** μM Nok significantly increased glucose consumption (**Figure 5A**, p ˂ 0.05 vs. DMSO), and the glucose consumption-promoting activity of 40 μM Nok was similar to that of metformin at 2 mM (**Figure 5A**). Moreover, Nok exhibited a remarkable dose-dependent increase in glucose consumption in L02 cells (**Figure 5A**, p ˂ 0.05, p ˂ 0.01 or p ˂ 0.001 vs. DMSO). Western blot analysis showed that Nok activated AMPK (**Figure 5B**) and dose-dependently increased the levels of p-AMPKα (Thr172) and p-ACC (Ser79) in L02 cells (**Figures 5B–D**, p ˂ 0.05 or p ˂ 0.01 or p ˂ 0.001 vs. DMSO). We further investigated the effects of Nok on lipid metabolism through a PO-induced hepatocyte lipid accumulation model *in vitro*. As shown in **Figure 5E**, the levels of intracellular TG in L02 cells were dramatically increased by incubation with 0.6 mM PO (0.2 mM PA-BSA and 0.4 mM OA-BSA) for 24 h (**Figure 5E**, p ˂ 0.001 vs. DMSO+10% BSA), but they were dose-dependently reduced by the addition of Nok (**Figure 5E**, p ˂ 0.01 or p ˂ 0.001 vs. PO + DMSO). The oil red O staining results showed that more lipid accumulation was observed in L02 cells induced by PO (**Figure 5F**), but Nok treatment limited this accumulation (**Figure 5F**). These phenomena showed that Nok could regulate glycolipid metabolism in L02 cells (**Figures 5E,F**). Because AMPK plays a key role in the regulation of intracellular energy metabolism and glycolipid metabolism, we tested the effects of Nok on AMPK signal pathway activation in L02 cells undergoing PO treatment. Nok could also activate the AMPK signaling pathway (**Figure 5G**), and dose-dependently increased the levels of p-AMPKα (Thr172) and p-ACC (Ser79) in L02 cells treated with PO (**Figures 5H,I**). Nok also decreased the production of ATP in L02 cells with PO incubation (**Figure 5J**). Moreover, AMPK activation was abolished by pretreatment with Compound C (CC), an AMPK inhibitor (**Figure 5K**-M). The AMPK activation of Nok was also observed by western blots of liver tissues (Figure 5N–P). These results suggest that the effects of Nok on hepatocyte glucose and lipid metabolism regulation may be dependent on AMPK activation (**Figure 5**).

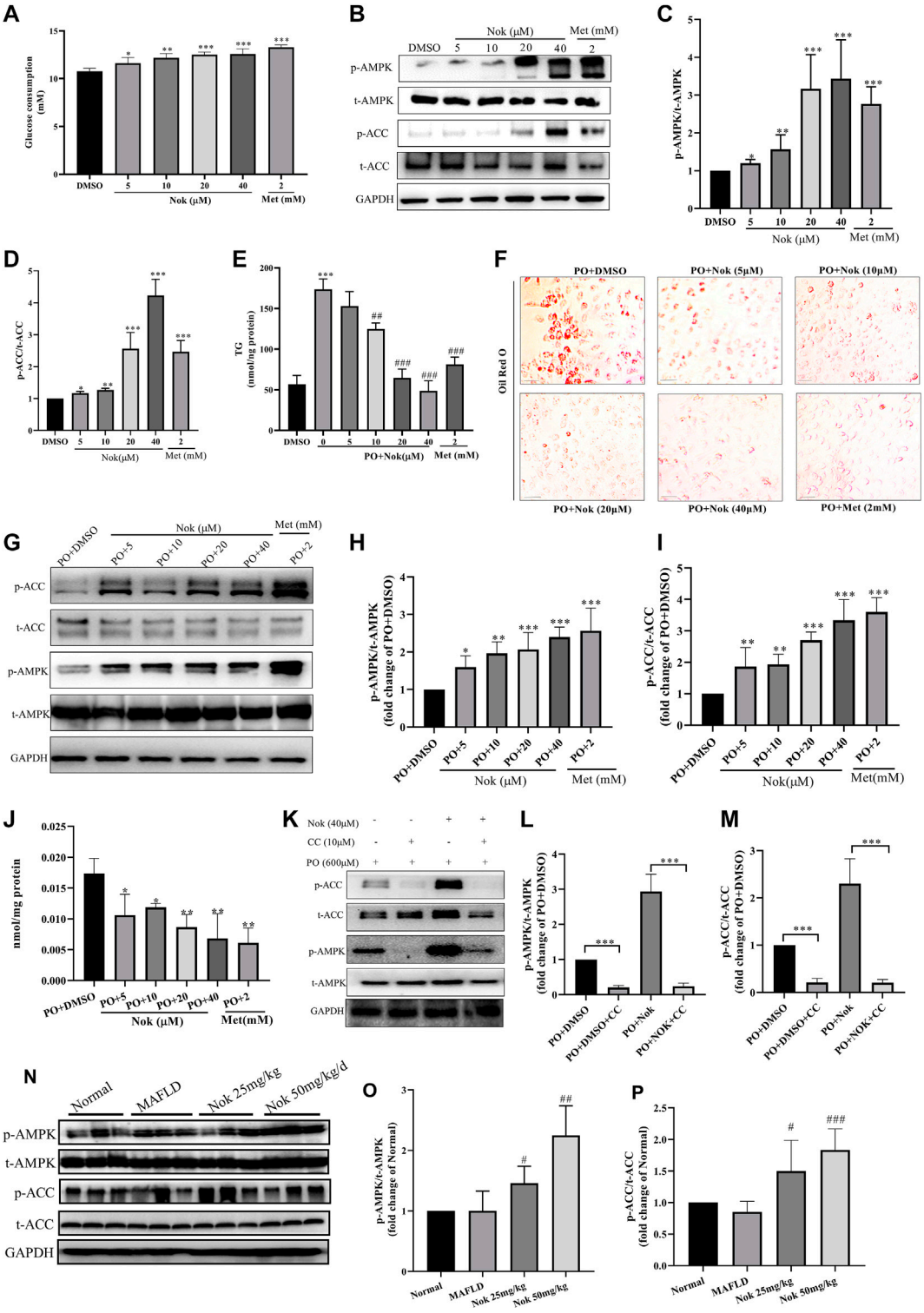

FIGURE 5 | The effects of Nok on glucose and lipid metabolism and AMPK activation *in vitro* and *in vivo*. **(A)** Glucose consumption; values are the means ± SD, n = 5, $^{*}p < 0.05$, $^{**}p < 0.01$ or $^{***}p < 0.001$ vs. DMSO. **(B)** Western blots were performed to analyze the levels of p-AMPK, AMPK, p-ACC and ACC in L02 cells. Examples of representative blots as above and fold changes of p-AMPK/T-AMPK **(C)** and p-ACC/T-ACC **(D)** are shown by semiquantitative analyses. Values are the means ± SD from three separate experiments, $^{*}p < 0.05$, $^{**}p < 0.01$, $^{***}p < 0.001$ vs. DMSO. **(E)** Intracellular TG detection in L02 cells treated with Nok and undergoing PO induction. Values are the means ± SD, n = 4, $^{***}p < 0.001$ vs. PO + DMSO, $^{\#\#}p < 0.01$ or $^{\#\#\#}p < 0.001$ vs. PO + DMSO. (O) Oil Red O staining detection in L02 cells treated with Nok and undergoing PO induction, and the representative image as above. **(G)** Western blots were performed to analyze the phosphorylated and total

(*Continued*)

FIGURE 5 | protein levels of AMPK and ACC in L02 cells with Nok treatment and PO induction, and representative western blot images are shown above. The fold changes in p-AMPK/T-AMPK **(H)** and p-ACC/T-ACC **(I)** are shown by semiquantitative analyses. The values are the means ± SD from three separate experiments, $^{*}p < 0.05$, $^{**}p < 0.01$, $^{***}p < 0.001$ vs. PO + DMSO. **(J)** Intracellular ATP detection in L02 cells treated with Nok and undergoing PO induction. Values are the means ± SD, n = 3, $^{*}p < 0.05$, $^{**}p < 0.01$ vs. PO + DMSO. **(K)** Inhibitory effect of Compound C (CC) on Nok activation of AMPK. Representative western blot images are shown, and fold changes in p-AMPK/T-AMPK **(L)** and p-ACC/T-ACC **(M)** are shown by semiquantitative analyses. Values are the means ± SD from three separate experiments, $^{***}p < 0.001$. After 12 weeks of Nok treatment of C57BL/6J mice with a HFD, total protein was extracted from the livers. The p-AMPK, t-AMPK, p-ACC, t-ACC and GAPDH levels in liver tissues were determined by western blotting. Representative blots for each group are presented in **(N)**, and fold changes in p-AMPK/t-AMPK **(O)** and p-ACC/t-ACC **(P)** are depicted above. Values are the means ± SD (n = 6 per group); $\#p < 0.05$, $\#\#p < 0.01$, $\#\#\#p < 0.001$ vs. MAFLD group mice.

Nok Inhibits MAPK Signaling in Hepatocytes

The MAPK signaling pathway is closely related to a variety of cellular biological processes, such as cell growth, differentiation, apoptosis, necrosis and inflammation. Excessive MAPK signaling pathway activation is commonly detected in many metabolic diseases, including MAFLD. Elevated MAPK signaling involved in the development of MAFLD and has been widely confirmed and reported. Our RNA-seq results also demonstrated that Nok might affect the MAPK signaling pathway in the liver. Our animal and cellular experiments showed that Nok inhibited MAPK pathways in hepatocytes by western blots of *in vitro* and *in vivo* samples, as shown in **Figure 6**. We first detected the main MAPK signaling pathway protein kinases, including ERK1/2, p-ERK1/2, p38, p-p38, JNK, and p-JNK, in L02 cells by western blotting. The results showed that Nok significantly downregulated the p-ERK1/2, p-p38, and p-JNK levels (**Figure 6A**) and showed no effect on the total MAPK protein kinase level, especially when the Nok concentration reached 40 μM (**Figures 6A–D**). Moreover, inhibition of the p38 and JNK signaling pathways was more potent and evident at only 10 μM (**Figures 6A–D**). The levels of p-p38 and p-JNK in the 10 μM Nok treatment group were 0.61 ± 0.040-fold and 0.37 ± 0.02-fold lower than those in the DMSO treatment group (**Figures 6C,D**). When the treatment concentration increased to 40 μM, the p38 and JNK signaling pathways were very significantly suppressed, and the levels decreased to 0.25 ± 0.04-fold and 0.14 ± 0.03-fold compared to DMSO (**Figures 6C,D**). We further detected the effects of Nok on MAPK signaling in L02 cells treated with PO and identified inhibition of MAPK signaling and downregulated levels of p-ERK1/2, p-P38 and p-JNK, as previously detected in L02 cells directly treated with Nok (**Figures 6E–H**). Moreover, its inhibition of MAPK signaling pathway activation was abolished by pretreatment with anisomycin, a JNK agonist (Figure 6M–O). We further detected the effects of Nok on MAPK signaling pathways *in vivo*. In NAFLD mouse liver tissues, the MAPK signaling pathways were significantly activated based on western blot analysis. The levels of p-p38 and p-JNK were potently upregulated in MAFLD model mice, but the phosphorylated levels of these primary MAPK signal pathway kinases were decreased in Nok-treated mice at doses of 25 mg kg^{-1} and 50 mg·kg-1 (**Figure 6I**-L).

Anti-Inflammatory Effects of Nok

Inflammation is one of the major risk factors for the development of MAFLD. MAPK signaling pathways, especially the p38 and JNK signaling pathways, regulate the production of inflammatory cytokines. The serum levels of IL-1β, IL-18, TNFα and IL-6 are the major inflammatory cytokines that were tested in this study. The levels of all these cytokines were significantly higher in MAFLD model mice than in normal animals (**Figures 7A–D**), and they were significantly decreased by Nok treatment, especially at a 50 mg kg^{-1} dose (**Figures 7A–D**). We also detected the mRNA levels of IL-1β, IL-18, TNFα and IL-6 in the liver, and Nok decreased the transcription levels of these genes (**Figures 7E–H**). Therefore, Nok possessed potent anti-inflammatory capability *in vivo*, which might be associated with its inhibition of MAPK signaling.

DISCUSSION

Metabolic-associated fatty liver disease is a new description that differs from NAFLD, in that alcohol consumption and other liver disease factors are no longer considered (Eslam, Sanyal et al., 2020). The pathophysiological changes of MAFLD include a variety of interrelated pathological processes, such as glucose and lipid metabolism disorders, insulin resistance, lipid toxicity, inflammation, liver injury, and liver fibrosis (Lin, Huang et al., 2020; Zhong, Huang et al., 2020). MAFLD has become the most common chronic liver disease worldwide, with a prevalence of 24%, and the prevalence increases to 70–80% in obese and diabetic patients (Ciardullo and Perseghin 2021). The widespread prevalence of MAFLD has placed a huge financial burden on the healthcare system in China and around the world. With the increasing number of MAFLD patients and the lack of effective treatments, the development of effective drugs for the clinical prevention and treatment of MAFLD is greatly desired. Nok is mainly extracted from *Alpiniae Oxyphyllae* Fructus, a famous traditional Chinese medicine rich in Hainan Province. This traditional medicine has been reported to have many biological activities, including antioxidant stress, anti-inflammation, and anti-apoptosis activities (Murase, Misawa et al., 2010). In this work, we focused on the efficacy and potential mechanisms of Nok in preventing MAFLD *in vitro* and *in vivo*.

Our *in vivo* results showed that Nok significantly reversed the body weight, liver weight and liver index increases in MAFLD mice, ameliorated glucose and lipid metabolism disorders, and improved liver function and glucose tolerance damage compared to MAFLD mice. The *in vitro* results showed that Nok significantly promoted glucose consumption and decreased intracellular TG accumulation in L02 cells. We further demonstrated that this activity might contribute to its

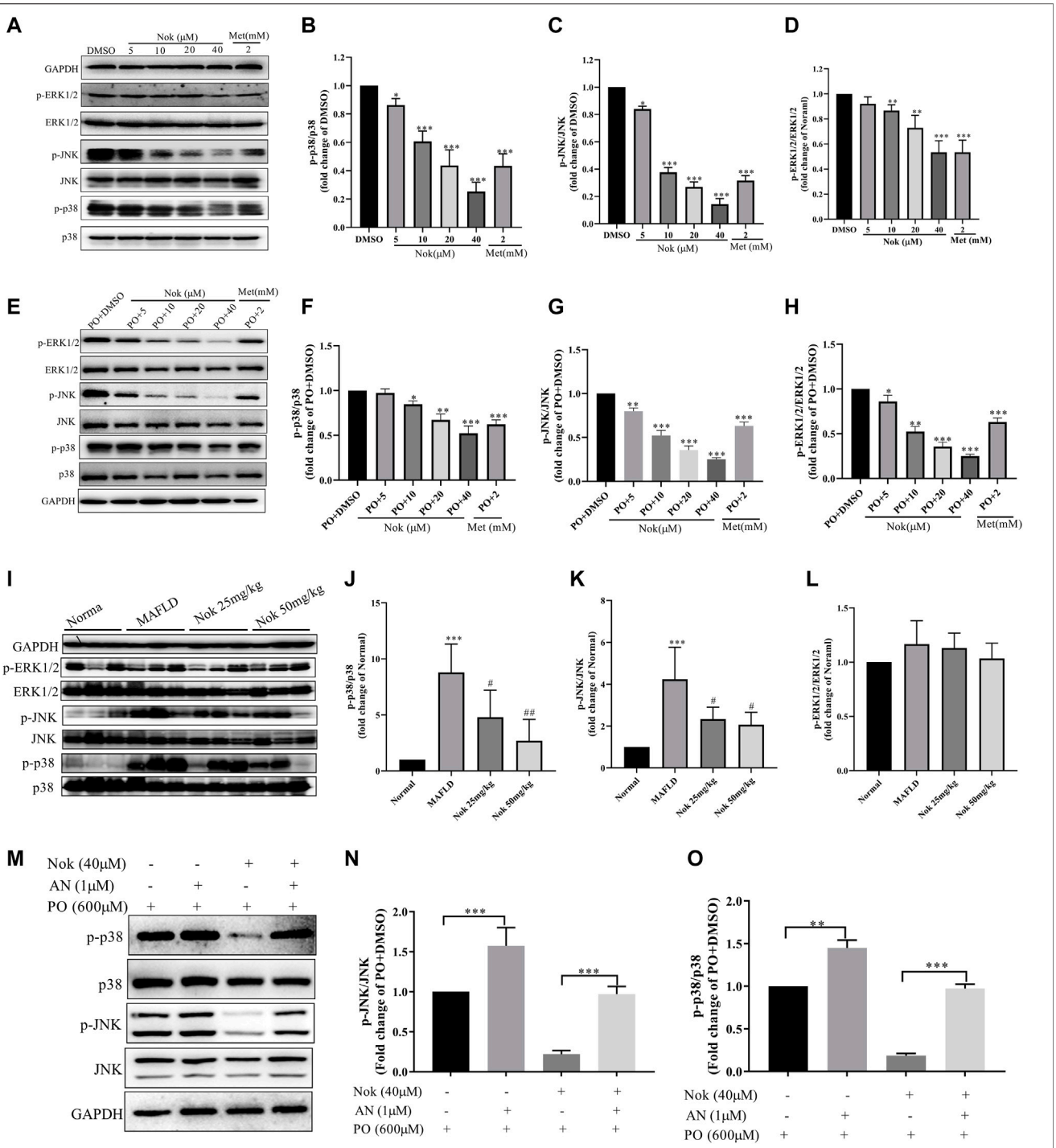

FIGURE 6 | Nok inhibited MAPK signaling pathways *in vitro* and *in vivo*. Total protein was extracted from the L02 cells after Nok treatment for 24 h. The levels of p-ERK1/2, ERK1/2, p-p38, p38, p-JNK, JNK and GAPDH were determined by western blotting. Representative blots for each sample are presented in **(A)**, and fold changes in p-p38/p38 **(B)**, p-JNK/JNK **(C)** and p-ERK1/2/ERK1/2 **(D)** are shown by semiquantitative analyses. Values are the means ± SD from 3 separate experiments, $^{*}p < 0.05$, $^{**}p < 0.01$, $^{***}p < 0.001$ vs. DMSO. **(E)** Western blots were performed to analyze the phosphorylated and total protein levels of p38, JNK and ERK1/2 in L02 cells with Nok treatment and undergoing PO induction, and representative western blot images are shown as above. The fold changes in p-p38/p38 **(F)**, p-JNK/JNK **(G)** and p-ERK1/2/ERK1/2 **(H)** are shown by semiquantitative analyses. The values are the means ± SD from three separate experiments, $^{*}p < 0.05$, $^{**}p < 0.01$, $^{***}p < 0.001$ vs. PO + DMSO. After 12 weeks of Nok treatment of C57BL/6J mice with a HFD, total protein was obtained from the mouse livers. The levels of p-ERK1/2, ERK1/2, p-p38, p38, p-JNK, JNK and GAPDH were tested by western blotting. Representative blots for each group are presented in **(I)**. Fold changes in p-p38/p38**(J)**, p-JNK/JNK **(K)** and p-ERK1/2/ERK1/2 **(L)** were determined by semiquantitative analyses, and the values are expressed as the means ± SD (n = 6 per group). $^{*}p < 0.05$, $^{**}p < 0.01$, $^{***}p < 0.001$ vs. Normal group mice $\#p < 0.05$, $\#\#p < 0.01$, $\#\#\#p < 0.001$ vs. MAFLD model mice. **(M)** Inhibitory effect of anisomycin (AN, a JNK agonist) on Nok inhibition of MAPK pathways, especially the JNK pathway. Representative western blot images are shown in (M), and fold changes in p-JNK/JNK **(N)** and p-p38/p38 **(O)** are shown by semiquantitative analyses, $^{*}p < 0.05$, $^{**}p < 0.01$, $^{***}p < 0.001$.

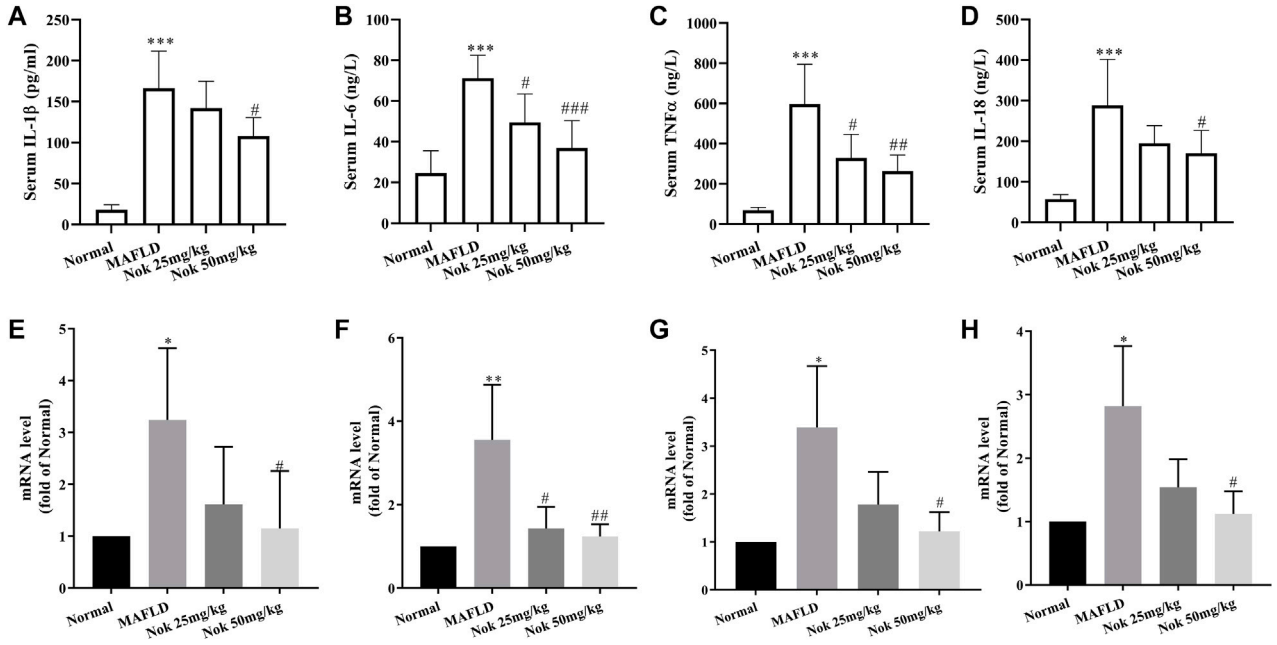

FIGURE 7 | Anti-inflammatory effects of Nok. After 12 weeks of daily administration of Nok to C57BL/6J mice fed a HFD, the serum IL-1β **(A)**, IL-6 **(B)**, TNFα **(C)**, and IL-18 **(D)** levels were tested. At the same time, we detected the mRNA levels of IL-1β **(E)**, IL-6 **(F)**, TNFα **(G)**, and IL-18 **(H)** in livers. Values are the means ± SD (n = 6 per group). *$p < 0.05$, **$p < 0.01$, ***$p < 0.001$ vs. C57BL/6J normal mice. #$p < 0.05$, ##$p < 0.01$, ###$p < 0.001$ vs. the MAFLD model mice.

regulatory effects on the AMPK and MAPK signaling pathways both *in vitro* and *in vivo*.

AMPK is a core kinase that regulates cellular energy metabolism and balance and is also closely related to the regulation of glycolipid metabolism, which is also a target for MAFLD. AMPK activation in the liver is beneficial for glucose consumption, lipid oxidative decomposition, and body energy provision. Many AMPK agonists, such as mangiferin (Yong, Ruiqi et al., 2021), berberine (Zhu, Bian et al., 2019), and metformin (Zamani-Garmsiri, Hashemnia et al., 2021), are considered potential drugs for MAFLD treatment. The results of this study are the first to demonstrate that Nok can improve MAFLD based on activation of hepatic AMPK *in vitro* and *in vivo*.

MAPK signaling pathways participate in a multitude of processes that control and are associated with MAFLD development (Jiao, Feng et al., 2013; Lawan and Bennett 2017). The MAPK signaling pathway involves three primary pathways: ERK1/2, p38 and JNK (Lawan and Bennett 2017). The ERK1/2 signaling pathway is usually involved in the proliferation and differentiation of cells, and the p38 and JNK signaling pathways are mainly involved in the cell stress response and apoptosis (Balmanno and Cook 2009; Lawan and Bennett 2017). Many studies have reported that hepatic metabolic dysfunction might cause JNK activation and promote MAFLD development (Yan, Gao et al., 2017; Cai, Zhang et al., 2018). Moreover, the expression level of p-p38 MAPK in the MAFLD model group induced by a high-fat diet was higher than that in the normal group, and the activated p38 MAPK signaling pathway promoted the development of MAFLD by leading to insulin resistance (Zeng, Tang et al., 2014). Meanwhile, inhibiting p38 MAPK activity could ameliorate MAFLD progression in a rodent animal model (Zeng, Tang et al., 2014; Lawan and Bennett 2017; Deng, Tang et al., 2018). As extensively reported, the MAPK signaling pathway mediates the production of inflammation, oxidative stress and glycolipid metabolism disorders induced by many factors, such as hyperglycemia and hyperlipidemia, during the development of MAFLD. Many compounds, such as berberine (Li, Geng et al., 2014), bergamot polyphenols (Musolino, Gliozzi et al., 2020), baicalin (Fang, Sun et al., 2019), and isoliquiritigenin (Kim, Kim et al., 2010), can ameliorate MAFLD progression by inhibiting MAPK activity. In our study, we confirmed that Nok inhibited MAPK activity *in vivo* and *in vitro*. This is the first report that Nok showed a potential role and efficacy in treating MAFLD by inhibiting MAPK activation. Interestingly, the inhibition of p38 and JNK activity by Nok was more obvious than the inhibition of ERK1/2 signaling.

Our study also showed that Nok could improve hepatic tissue glucose tolerance and liver function in HFD-induced MAFLD mice. Impaired hepatic glucose tolerance is another cause of MAFLD development, especially in type 2 diabetic or obese patients. Improving hepatic tissue glucose tolerance can significantly ameliorate the progression of MAFLD, and it is currently a common method for the clinical treatment of MAFLD. In addition, the protective effect of Nok on liver function was also observed. Collectively, these results suggested that Nok could be beneficial for preventing and treating MAFLD.

CONCLUSION

In this study, we isolated Nok from *Alpiniae Oxyphyllae* Fructus and analyzed its structure and purity. Our study is the first to show that NOK an ameliorate MAFLD *in vitro* and *in vivo*. Our data showed that Nok significantly improved the body weight and liver weight/index elevation, corrected glycolipid metabolism disorder, ameliorated glucose tolerance, decreased hepatic lipid accumulation and steatosis, and protected the liver function in HFD-induced MAFLD mice *in vivo*. Nok increased hepatocyte glucose metabolism and decreased FFA-induced intracellular TG *in vitro*. We further demonstrated that the protective mechanisms of Nok against MAFLD might be associated with AMPK signaling pathway activation and MAPK signaling pathway inhibition *in vivo* and *in vitro*. In summary, we first clarified and reported that Nok, a sesquiterpene ketone from *Alpiniae oxyphyllae* Fructus, could ameliorate MAFLD, and we provide a scientific basis for its clinical application in MAFLD treatment or prevention in the future.

DATA AVAILABILITY STATEMENT

The datasets presented in this study can be found in online repositories. The names of the repository/repositories and accession number(s) can be found at: https://www.ncbi.nlm.nih.gov/sra/PRJNA825669.

ETHICS STATEMENT

The animal study was reviewed and approved by the medical ethics committee of Hainan Medical University. Written informed consent was obtained from the owners for the participation of their animals in this study.

AUTHOR CONTRIBUTIONS

ZY and ZZ designed this study, completed the data analysis, drafted all figures, and wrote of the manuscript; WR, HZ, and CM performed the experiment and data collection; and MN, HX, DL, XZ, and LQ revised the manuscript. All authors read and agree with the final manuscript. ZX and LW designed, supervised, and guided this study and revised the final manuscript.

FUNDING

This work was financially supported by the Hainan provincial Nature Science Foundation of China (822RC694), Hainan provincial KRDP (ZDYF2022SHFZ037 and ZDYF2022SHFZ074), the NSFC (82060778 and 81760628), and Project Supported by the Hainan Province Clinical Medical Center and the Excellent Talent Team of Hainan Province (No. QRCBT202121).

REFERENCES

Balmanno, K., and Cook, S. J. (2009). Tumour Cell Survival Signalling by the ERK1/2 Pathway. *Cell Death Differ.* 16 (3), 368–377. doi:10.1038/cdd.2008.148

Cai, J., Zhang, X. J., and Li, H. (2018). Role of Innate Immune Signaling in Non-alcoholic Fatty Liver Disease. *Trends Endocrinol. Metab.* 29 (10), 712–722. doi:10.1016/j.tem.2018.08.003

Chen, C. M., Lin, C. Y., Chung, Y. P., Liu, C. H., Huang, K. T., Guan, S. S., et al. (2021). Protective Effects of Nootkatone on Renal Inflammation, Apoptosis, and Fibrosis in a Unilateral Ureteral Obstructive Mouse Model. *Nutrients* 13 (11), 3921. doi:10.3390/nu13113921

Ciardullo, S., and Perseghin, G. (2021). Prevalence of NAFLD, MAFLD and Associated Advanced Fibrosis in the Contemporary United States Population. *Liver Int.* 41 (6), 1290–1293. doi:10.1111/liv.14828

Deng, Y., Tang, K., Chen, R., Liu, Y., Nie, H., Wang, H., et al. (2018). Effects of Shugan-Jianpi Recipe on the Expression of the P38 MAPK/NF-κB Signaling Pathway in the Hepatocytes of NAFLD Rats. *Med. (Basel)* 5 (3), 106. doi:10.3390/medicines5030106

Eslam, M., Sanyal, A. J., George, J., Sanyal, A., Neuschwander-Tetri, B., Tiribelli, C., et al. (2020). MAFLD: a Consensus-Driven Proposed Nomenclature for Metabolic Associated Fatty Liver Disease. *Gastroenterology* 158 (7), 1999–2014. e1991. doi:10.1053/j.gastro.2019.11.312

Fang, P., Sun, Y., Gu, X., Shi, M., Bo, P., Zhang, Z., et al. (2019). Baicalin Ameliorates Hepatic Insulin Resistance and Gluconeogenic Activity through Inhibition of P38 MAPK/PGC-1α Pathway. *Phytomedicine* 64, 153074. doi:10.1016/j.phymed.2019.153074

Friedman, S. L., Neuschwander-Tetri, B. A., Rinella, M., and Sanyal, A. J. (2018). Mechanisms of NAFLD Development and Therapeutic Strategies. *Nat. Med.* 24 (7), 908–922. doi:10.1038/s41591-018-0104-9

Ge, C. X., Yu, R., Xu, M. X., Li, P. Q., Fan, C. Y., Li, J. M., et al. (2016). Betaine Prevented Fructose-Induced NAFLD by Regulating LXRα/PPARα Pathway and Alleviating ER Stress in Rats. *Eur. J. Pharmacol.* 770, 154–164. doi:10.1016/j.ejphar.2015.11.043

Huang, M., Kim, H. G., Zhong, X., Dong, C., Zhang, B., Fang, Z., et al. (2020). Sestrin 3 Protects against Diet-Induced Nonalcoholic Steatohepatitis in Mice through Suppression of Transforming Growth Factor β Signal Transduction. *Hepatology* 71 (1), 76–92. doi:10.1002/hep.30820

Hwang, S., Wang, X., Rodrigues, R. M., Ma, J., He, Y., Seo, W., et al. (2020). Protective and Detrimental Roles of P38α Mitogen-Activated Protein Kinase in Different Stages of Nonalcoholic Fatty Liver Disease. *Hepatology* 72 (3), 873–891. doi:10.1002/hep.31390

Jiao, P., Feng, B., Li, Y., He, Q., and Xu, H. (2013). Hepatic ERK Activity Plays a Role in Energy Metabolism. *Mol. Cell Endocrinol.* 375 (1), 157–166. doi:10.1016/j.mce.2013.05.021

Kim, Y. M., Kim, T. H., Kim, Y. W., Yang, Y. M., Ryu, D. H., Hwang, S. J., et al. (2010). Inhibition of Liver X Receptor-α-dependent Hepatic Steatosis by Isoliquiritigenin, a Licorice Antioxidant Flavonoid, as Mediated by JNK1 Inhibition. *Free Radic. Biol. Med.* 49 (11), 1722–1734. doi:10.1016/j.freeradbiomed.2010.09.001

Kuchay, M. S., Choudhary, N. S., and Mishra, S. K. (2020). Pathophysiological Mechanisms Underlying MAFLD. *Diabetes Metab. Syndr.* 14 (6), 1875–1887. doi:10.1016/j.dsx.2020.09.026

Lawan, A., and Bennett, A. M. (2017). Mitogen-activated Protein Kinase Regulation in Hepatic Metabolism. *Trends Endocrinol. Metab.* 28 (12), 868–878. doi:10.1016/j.tem.2017.10.007

Lawan, A., Zhang, L., Gatzke, F., Min, K., Jurczak, M. J., Al-Mutairi, M., et al. (2015). Hepatic Mitogen-Activated Protein Kinase Phosphatase 1 Selectively Regulates Glucose Metabolism and Energy Homeostasis. *Mol. Cell Biol.* 35 (1), 26–40. doi:10.1128/MCB.00503-14

Li, Z., Geng, Y.-N., Jiang, J.-D., and Kong, W.-J. (2014). Antioxidant and Anti-inflammatory Activities of Berberine in the Treatment of Diabetes Mellitus. *Evidence-Based Complementary Altern. Med.*, 2014, 289264. doi:10.1155/2014/289264

Li, Y. H., Tan, Y. F., Cai, H. D., and Zhang, J. Q. (2016). Metabonomic Study of the Fruits of Alpinia Oxyphylla as an Effective Treatment for Chronic Renal Injury in Rats. *J. Pharm. Biomed. Anal.* 124, 236–245. doi:10.1016/j.jpba.2016.02.035

Li, J., Du, Q., Li, N., Du, S., and Sun, Z. (2021). Alpiniae Oxyphyllae Fructus and Alzheimer's Disease: An Update and Current Perspective on This Traditional Chinese Medicine. *Biomed. Pharmacother.* 135, 111167. doi:10.1016/j.biopha.2020.111167

Lin, S., Huang, J., Wang, M., Kumar, R., Liu, Y., Liu, S., et al. (2020). Comparison of MAFLD and NAFLD Diagnostic Criteria in Real World. *Liver Int.* 40 (9), 2082–2089. doi:10.1111/liv.14548

Moon, J. Y., Ryu, J.-Y., and Cho, S. K. (2019). Nootkatone, an AMPK Activator Derived from Grapefruit, Inhibits KRAS Downstream Pathway and Sensitizes Non-small-cell Lung Cancer A549 Cells to Adriamycin. *Phytomedicine* 63, 153000.

Murase, T., Misawa, K., Haramizu, S., Minegishi, Y., and Hase, T. (2010). Nootkatone, a Characteristic Constituent of Grapefruit, Stimulates Energy Metabolism and Prevents Diet-Induced Obesity by Activating AMPK. *Am. J. Physiol. Endocrinol. Metab.* 299, E266–E275. doi:10.1152/ajpendo.00774.2009

Musolino, V., Gliozzi, M., Scarano, F., Bosco, F., Scicchitano, M., Nucera, S., et al. (2020). Bergamot Polyphenols Improve Dyslipidemia and Pathophysiological Features in a Mouse Model of Non-alcoholic Fatty Liver Disease. *Sci. Rep.* 10 (1), 2565–2579. doi:10.1038/s41598-020-59485-3

Smith, B. K., Marcinko, K., Desjardins, E. M., Lally, J. S., Ford, R. J., and Steinberg, G. R. (2016). Treatment of Nonalcoholic Fatty Liver Disease: Role of AMPK. *Am. J. Physiol. Endocrinol. Metab.* 311 (4), E730–E740. doi:10.1152/ajpendo.00225.2016

Trefts, E., and Shaw, R. J. (2021). AMPK: Restoring Metabolic Homeostasis over Space and Time. *Mol. Cell* 81 (18), 3677–3690. doi:10.1016/j.molcel.2021.08.015

Wang, Y., Wang, M., Xu, M., Li, T., Fan, K., Yan, T., et al. (2018). Nootkatone, a Neuroprotective Agent from Alpiniae Oxyphyllae Fructus, Improves Cognitive Impairment in Lipopolysaccharide-Induced Mouse Model of Alzheimer's Disease. *Int. Immunopharmacol.* 62, 77–85. doi:10.1016/j.intimp.2018.06.042

Yan, H., Gao, Y., and Zhang, Y. (2017). Inhibition of JNK Suppresses Autophagy and Attenuates Insulin Resistance in a Rat Model of Nonalcoholic Fatty Liver Disease. *Mol. Med. Rep.* 15 (1), 180–186. doi:10.3892/mmr.2016.5966

Yan, H., Gao, Y. Q., Zhang, Y., Wang, H., Liu, G. S., and Lei, J. Y. (2018). Chlorogenic Acid Alleviates Autophagy and Insulin Resistance by Suppressing JNK Pathway in a Rat Model of Nonalcoholic Fatty Liver Disease. *J. Biosci.* 43 (2), 287–294. doi:10.1007/s12038-018-9746-5

Yan, T., Li, F., Xiong, W., Wu, B., Xiao, F., He, B., et al. (2021). Nootkatone Improves Anxiety- and Depression-like Behavior by Targeting Hyperammonemia-Induced Oxidative Stress in D-Galactosamine Model of Liver Injury. *Environ. Toxicol.* 36 (4), 694–706. doi:10.1002/tox.23073

Yong, Z., Ruiqi, W., Hongji, Y., Ning, M., Chenzuo, J., Yu, Z., et al. (2021). Mangiferin Ameliorates HFD-Induced NAFLD through Regulation of the AMPK and NLRP3 Inflammasome Signal Pathways. *J. Immunol. Res.* 2021, 1–17. doi:10.1155/2021/4084566

Younossi, Z., Anstee, Q. M., Marietti, M., Hardy, T., Henry, L., Eslam, M., et al. (2018). Global Burden of NAFLD and NASH: Trends, Predictions, Risk Factors and Prevention. *Nat. Rev. Gastroenterol. Hepatol.* 15 (1), 11–20. doi:10.1038/nrgastro.2017.109

Zamani-Garmsiri, F., Hashemnia, S. M. R., Shabani, M., Bagherieh, M., Emamgholipour, S., and Meshkani, R. (2021). Combination of Metformin and Genistein Alleviates Non-alcoholic Fatty Liver Disease in High-Fat Diet-Fed Mice. *J. Nutr. Biochem.* 87, 108505. doi:10.1016/j.jnutbio.2020.108505

Zeng, L., Tang, W. J., Yin, J. J., and Zhou, B. J. (2014). Signal Transductions and Nonalcoholic Fatty Liver: a Mini-Review. *Int. J. Clin. Exp. Med.* 7 (7), 1624–1631.

Zhang, L., Yang, M., Ren, H., Hu, H., Boden, G., Li, L., et al. (2013). GLP-1 Analogue Prevents NAFLD in ApoE KO Mice with Diet and Acrp30 Knockdown by Inhibiting C-JNK. *Liver Int.* 33 (5), 794–804. doi:10.1111/liv.12120

Zhong, X., Huang, M., Kim, H. G., Zhang, Y., Chowdhury, K., Cai, W., et al. (2020). SIRT6 Protects against Liver Fibrosis by Deacetylation and Suppression of SMAD3 in Hepatic Stellate Cells. *Cell Mol. Gastroenterol. Hepatol.* 10 (2), 341–364. doi:10.1016/j.jcmgh.2020.04.005

Zhu, X., Bian, H., Wang, L., Sun, X., Xu, X., Yan, H., et al. (2019). Berberine Attenuates Nonalcoholic Hepatic Steatosis through the AMPK-SREBP-1c-SCD1 Pathway. *Free Radic. Biol. Med.* 141, 192–204. doi:10.1016/j.freeradbiomed.2019.06.019

Conflict of Interest: The authors declare that the research was conducted in the absence of any commercial or financial relationships that could be construed as a potential conflict of interest.

Publisher's Note: All claims expressed in this article are solely those of the authors and do not necessarily represent those of their affiliated organizations, or those of the publisher, the editors, and the reviewers. Any product that may be evaluated in this article, or claim that may be made by its manufacturer, is not guaranteed or endorsed by the publisher.

frontiers | Frontiers in Pharmacology

TYPE Original Research
PUBLISHED 29 August 2022
DOI 10.3389/fphar.2022.925264

OPEN ACCESS

EDITED BY
Menghao Huang,
Indiana University school of medicine, United States

REVIEWED BY
Hu Li,
Chinese Academy of Medical Sciences and Peking Union Medical College, China
Guijie Chen,
Nanjing Agricultural University, China
Lili Qu,
University of Connecticut Health Center, United States

*CORRESPONDENCE
Zhenrui Huang,
huangzhenrui@gdaas.cn
Wenjuan Zhang,
zwj2080@126.com

†These authors have contributed equally to this work.

SPECIALTY SECTION
This article was submitted to Gastrointestinal and Hepatic Pharmacology, a section of the journal Frontiers in Pharmacology

RECEIVED 21 April 2022
ACCEPTED 13 July 2022
PUBLISHED 29 August 2022

CITATION
Zhou C, Zhang W, Lin H, Zhang L, Wu F, Wang Y, Yu S, Peng X, Cheng W, Li M, Pan X, Huang Z and Zhang W (2022), Effect of theaflavin-3,3′-digallate on leptin-deficient induced nonalcoholic fatty liver disease might be related to lipid metabolism regulated by the Fads1/PPARδ/Fabp4 axis and gut microbiota. *Front. Pharmacol.* 13:925264. doi: 10.3389/fphar.2022.925264

Effect of theaflavin-3,3′-digallate on leptin-deficient induced nonalcoholic fatty liver disease might be related to lipid metabolism regulated by the Fads1/PPARδ/Fabp4 axis and gut microbiota

Cheng Zhou[1†], Wenji Zhang[2†], Hui Lin[3], Luyun Zhang[1], Fan Wu[1], Yan Wang[1], Susu Yu[1], Xinyue Peng[1], Wenli Cheng[1], Min Li[1], Xiaoying Pan[2], Zhenrui Huang[2*] and Wenjuan Zhang[1*]

[1]Department of Public Health and Preventive Medicine, School of Medicine, Jinan University, Guangzhou, China, [2]Guangdong Provincial Engineering & Technology Research Center for Tobacco Breeding and Comprehensive Utilization, Key Laboratory of Crop Genetic Improvement of Guangdong Province, Crops Research Institute, Guangdong Academy of Agricultural Sciences, Guangzhou, China, [3]Department of Radiation Oncology, Guangdong Provincial People's Hospital, Guangdong Academy of Medical Sciences, Guangzhou, China

Nonalcoholic fatty liver disease (NAFLD), one of the risk factors for hepatitis, cirrhosis, and even hepatic carcinoma, has been a global public health problem. The polyphenol compound theaflavin-3,3′-digallate (TF3), mainly extracted from black tea, has been reported to produce an effect on hypoglycemic and antilipid deposition *in vitro*. In our study, we further investigated the function and novel mechanisms of TF3 in protecting NAFLD *in vivo*. By using leptin-deficient obese (ob/ob) mice with NAFLD symptoms, TF3 treatment prevented body weight and waistline gain, reduced lipid accumulation, and alleviated liver function injury, as well as decreased serum lipid levels and TG levels in livers in ob/ob mice, observing no side effects. Furthermore, the transcriptome sequencing of liver tissue showed that TF3 treatment corrected the expression profiles of livers in ob/ob mice compared with that of the model group. It is interesting to note that TF3 might regulate lipid metabolism *via* the Fads1/PPARδ/Fabp4 axis. In addition, 16S rRNA sequencing demonstrated that TF3 increased the abundance of *Prevotellaceae_UCG-001*, *norank_f_Ruminococcaceae*, and *GCA-900066575* and significantly decreased that of *Parvibacter*. Taken together, the effect of TF3 on NAFLD might be related to lipid metabolism regulated by the Fads1/PPARδ/Fabp4 axis and gut microbiota. TF3 might be a promising candidate for NAFLD therapy.

KEYWORDS

TF3, nonalcoholic fatty liver disease, RNA sequencing, 16S rRNA, lipid metabolism

Introduction

Nonalcoholic fatty liver disease (NAFLD), also called metabolic-associated fatty liver disease (MAFLD) (Eslam et al., 2020), affected approximately one quarter of the global adult population (Younossi et al., 2018). Considering the increasing morbidity of obesity and diabetes (Cotter and Rinella, 2020), the incidence of NAFLD has been increasing in recent years, and metabolic diseases were associated with greater NAFLD risk (Perumpail et al., 2017), which means NAFLD could place a heavier economic burden on health in the global societies. As a common chronic liver disease, NAFLD has a broad spectrum of clinical manifestations; simple steatosis could progress into nonalcoholic steatohepatitis, fibrosis, cirrhosis, and hepatocellular carcinoma (Manne et al., 2018; Liu et al., 2022). As the most widely prescribed lipid-lowering drugs, statins can be safely used to treat dyslipidemia in patients with NAFLD/NASH (Easl Easd And Easo, 2016; Chalasani et al., 2018). Their limited use is mainly attributed to hepatotoxicity such as asymptomatic raised aminotransferases (Nascimbeni et al., 2019), along with myalgia, hemorrhagic stroke, cognitive decline, peripheral neuropathy, insomnia, cataract, etc. (Mancini et al., 2011). Although trial evidence supports the efficacy of some diabetes drugs in patients with NAFLD or NASH, pioglitazone (Sanyal et al., 2010) might significantly increase weight, and metformin (Anushiravani et al., 2019) had no substantial impact on liver disease. At present, there is no specific treatment for NAFLD in clinic; thus, the effective drugs need to be actively explored.

Theaflavin-3,3′-digallate (TF3) was formed from the oxidation of selected pairs of catechins during tea processing and was one of the polyphenols in black tea. TF3, together with theaflavin (TF1), theaflavin-3-gallate (TF2A), theaflavin-3′-gallate (TF2B), belongs to the theaflavin (TF) category. They have the beneficial health effects and pharmacological activities (Wu et al., 2011; Fatima et al., 2013). As a more active monomer, TF3 has anticancer (Gao et al., 2019), cellular antioxidant (Jiang et al., 2021), and antibacterial (Wang S. et al., 2019) biological activities. Oral administration of a TF3-rich complex was reported to significantly decrease the adiposity index, enhance the insulin-sensitive index, inhibit the hepatic lipase activity, and slightly reduce leptin levels in livers in an obese Sprague-Dawley rat model (Jin et al., 2013). At a recent time, the effect of TFs extracted and purified from black tea was studied in high-fat diet–induced obese mice, and the results demonstrated that gavage administration of TFs might exert antihyperglycemic and lipid-lowering effects by inhibiting the synthesis and accumulation of lipids in the liver with activation of related pathways. Compared to other monomers of theaflavins, TF3 was proved to be the best choice (Cai et al., 2021). Our previous research *in vitro* also reported that TF3 is the best one among the theaflavin constituents in alleviating hepatocyte lipid deposition through activating an AMPK signaling pathway by inhibiting plasma kallikrein (Zhang et al., 2020). However, as a polyhydroxylated polyphenol, TF3 can associate with surrounding water molecules, forming a large hydration shell around the TF3 molecule, which makes it difficult to utilize through the transcellular transport (Lambert and Yang, 2003). Some studies reported that TF3 had poor systematic bioavailability through gavage or oral administration (Mulder et al., 2001; Henning et al., 2006). Therefore, the intraperitoneal injection is a feasible direction to enhance the bioavailability in animal experiments.

Hence, in this study, the effects of TF3 on NAFLD were assessed in an ob/ob mouse model by intraperitoneal injection treatment to improve bioavailability and find the novel regulatory mechanism through the preliminary "gut–liver" interaction at the individual level. With the maturity of bioinformatics, transcriptome sequencing and 16S rRNA sequencing have been used here for gene expression analysis to reveal the overall biological characteristics. Our study would further explore TF3 as a promising natural drug to prevent and treat NAFLD.

Materials and methods

Mice and treatment

The 5 specific pathogen-free male C57BL/6J and 25 ob/ob mice (7 weeks old) (Beijing, SCXK 2019-0008) were purchased from Beijing Huafukang Biotechnology Co., Ltd. (Beijing, China). These mice were housed in a 12/12-h light and dark cycle at a constant temperature (22°C ± 2°C) and provided with standard chow diet and free water in Ruiye Model Animal Biotechnology Co., Ltd. (Guangzhou, China) (Guangdong, SYXK 2020-0218). After 7 days of adaptive feeding, C57BL/6J mice were assigned to the control group with saline (WT), and ob/ob mice were randomized into five groups ($n = 5$): the model group with saline (ob/ob), the positive group with polyene phosphatidyl choline of 3000 μL/kg body weight (ob/ob + PPC), low TF3 group with the dose of 5 mg/kg body weight (ob/ob + L-TF3), middle TF3 group with the dose of 10 mg/kg body weight (ob/ob + M-TF3), and high TF3 group with the dose of 20 mg/kg body weight (ob/ob + H-TF3). The intraperitoneal injection administration was performed every day for 4 weeks. The body weight and food intake of mice were recorded every day, and the waist circumference was measured every 3 days. At the end of the experiment, the stool samples were taken before all mice were sacrificed. The whole blood samples were from retro-orbital blood collection and left at room temperature for at least 30 min and then separated by centrifugation (2,500 rpm for 20 min) to obtain serum. A small portion of the freshly isolated and weighed liver was fixed in 4% paraformaldehyde, and the remaining liver and sera were frozen immediately in liquid nitrogen and then were stored at −80°C until they were to

be used. The adipose tissue (epididymal, perirenal, subcutaneous, and brown fats) samples as well as other organs were also isolated, collected, weighed, and then stored at −80°C for further analysis.

Biochemical and histopathological analyses

The biochemical indicators in serum were measured using reagent kits of triglyceride (TG) (A110-1-1), total cholesterol (TC) (A111-1-1), high-density lipoprotein cholesterol (HDL-c) (A112-1-1), low-density lipoprotein cholesterol (LDL-c) (A113-1-1), free fatty acids (FFA) (A042-2-1), alanine aminotransferase (ALT) (C009-2-1), and aspartate aminotransferase (AST) (C010-2-1) from Nanjing Jiancheng Bioengineering Institute (Nanjing, China). The TG levels in the liver were detected using the same reagent kit as serum. The fixed liver tissues were embedded in paraffin. Sections with a thickness of 5 μm were obtained and stained using hematoxylin and eosin (H&E). All sections were observed under a motorized multifunctional upright fluorescence microscope (DM6000B, Leica, Germany).

Transcriptome sequencing and bioinformatics analysis

Total RNA was extracted from the mouse liver tissue samples, and the concentration and purity were detected using NanoDrop 2000. RNA integrity was detected using agarose gel electrophoresis, and RIN value was determined using Agilent 2100. The mRNA was isolated from total RNA through utilizing magnetic beads with Oligo (dT) to perform A-T base pairing with the ploy-A tail at the 3′ end of eukaryotic mRNA. Fragmentation buffer was added to screen out the short-sequence fragments of mRNA, that is, those approximately 300 bp. Then, first-strand cDNA and second-strand cDNA were sequentially synthesized. The Illumina Novaseq 6000 System was used for sequencing. Before sequencing, the library was enriched, 15 cycles of PCR were used for amplification, and 2% agarose gels were used to recover the target bands. A TBS380 Mini-Fluorometer was used for quantification. Clusters were generated by bridge PCR amplification on a cBot System (Illumina). The transcriptome information was analyzed on the online platform of Majorbio Cloud Platform (www.majorbio.com). To identify the differentially expressed genes (DEGs) of liver tissues, those that had Fold Change ≥ 1.5 and adjusted $p < 0.05$ were considered statistically significant. Gene Ontology (GO) and Kyoto Encyclopedia of Genes and Genomes (KEGG) enrichment analyses were performed to explore the biological functions of the DEGs and pathways they enriched significantly. The Benjamini–Hochberg (B-H) multiple test correction method was used to correct the false positives (adjusted $p < 0.05$).

16S rRNA sequencing and bioinformatics analysis

Total community DNA extracted from the stool samples of mice was used for PCR amplification. Then, PCR amplification products were detected and quantified using the QuantiFluor-ST™ blue fluorescence quantification system (Promega). The purified amplicons were combined in equimolar masses and sequenced on the Illumina MiSeq PE300 platform (Illumina, San Diego, United States). After subsampling each sample to an equal sequencing depth (39,800 reads per sample) and clustering for the next analysis, the alpha diversities of the gut microbiota in samples were calculated using the observed richness (sobs) and the diversity (shannon) index. The Good's coverage and rarefaction curves were used to determine whether the sequencing amount was sufficient. Beta diversity was determined using the OTUs from each sample, and the similarity between samples was calculated using the unweighted unifrac and represented in principal co-ordinate analysis (PCoA). Welch's *t* test was performed to obtain species with significant differences between two groups. The data of 16S rRNA sequencing were also analyzed on the online platform of Majorbio Cloud Platform (www.majorbio.com).

Statistical analysis

The data were presented as the mean ± standard deviation. Differential analysis was performed using SPSS 20.0 with the significance criterion set at $p < 0.05$. Student's *t* test was used to assess the differences between two groups. One-way analysis of variance with Dunnett's *post hoc* test and a nonparametric test were utilized for comparisons among multiple groups. Figures were generated using GraphPad Prism 8.3.0 or Majorbio Cloud Platform.

Results

Effect of theaflavin-3,3′-digallate on growth parameters and organ coefficients of nonalcoholic fatty liver disease in ob/ob mice

To observe the effect of TF3 on NAFLD, we found that the final body weight and waistline, that is, body weight gain and waistline gain, of ob/ob mice in the model group both were higher than those of mice in the control group ($p < 0.01$ or $p < 0.001$). In comparison with those in the model group, these growth parameters all significantly reduced in the M-TF3 and H-TF3 groups with *p* values less than 0.01 or 0.001, respectively (Figures 1A–D). In particular, body weight gain in the H-TF3

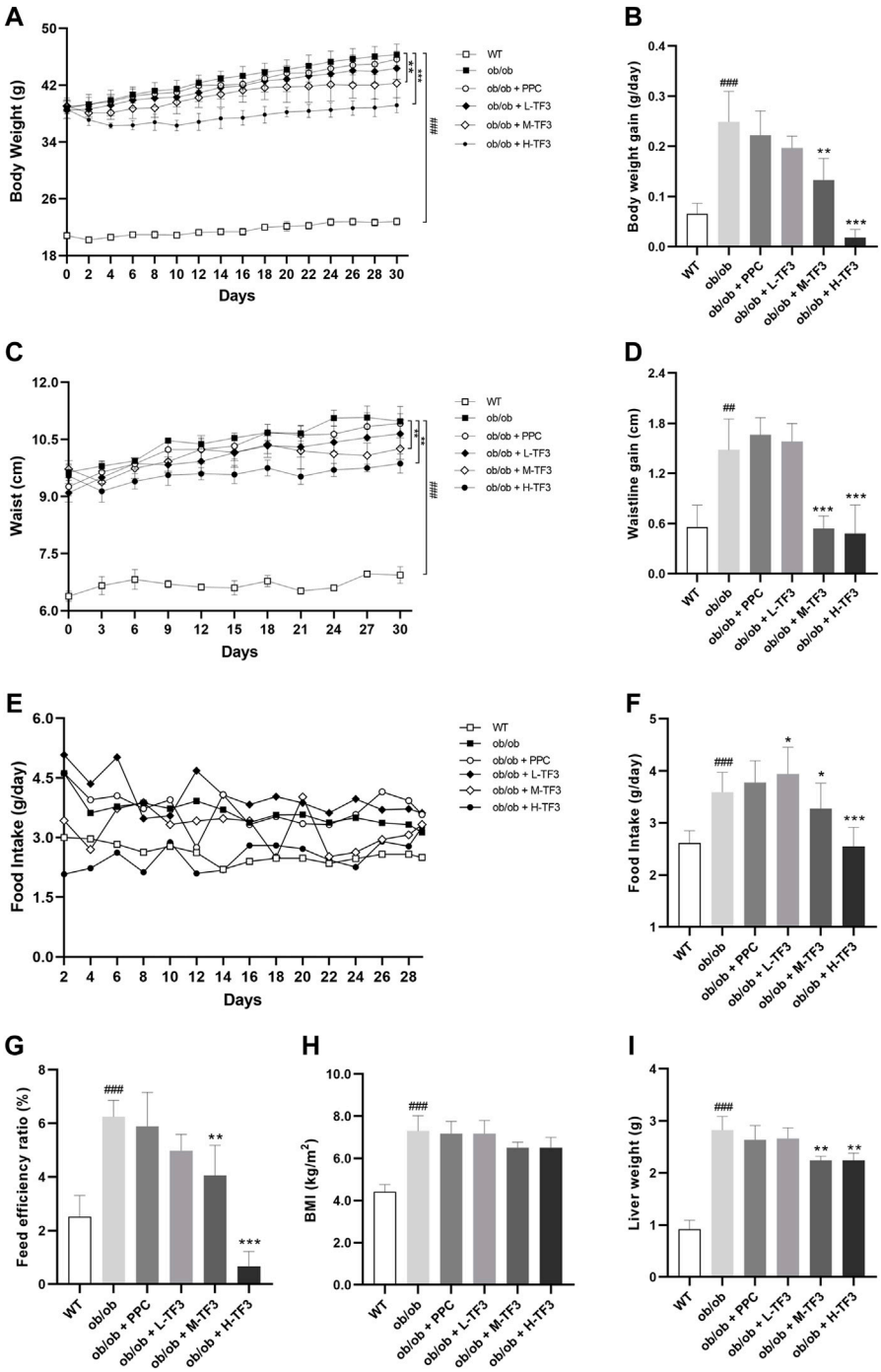

FIGURE 1
Body weight, waistline, food intake, BMI, and liver weight. **(A)** The trend of weight change within 4 weeks. **(B)** Body weight gain. **(C)** The trend of waistline changes within 4 weeks. **(D)** Waistline gain. **(E)** The trend of food intake changes within 4 weeks. **(F)** Average daily food intake. **(G)** Feed efficiency ratio. Feed efficiency ratio (%) = body weight gain (g/day)/food intake (g/day) × 100%. **(H)** BMI. **(I)** Liver weight. All data are shown as the mean or mean ± standard deviation (n = 5). Statistical significance: $^{\#}p < 0.05$, $^{\#\#}p < 0.01$, $^{\#\#\#}p < 0.001$ vs. the WT group. $^{*}p < 0.05$, $^{**}p < 0.01$, $^{***}p < 0.001$ vs. the ob/ob group.

group was only 1/14 of that in the ob/ob group. In Figures 1E, F, significant differences were observed in the average daily food intake between all the TF3 groups and the ob/ob group. We find it interesting that L-TF3 treatment made food intake increased ($p < 0.05$), while M-TF3 and H-TF3 treatment decreased food intake ($p < 0.05$ and $p < 0.001$, respectively). Moreover, the feed

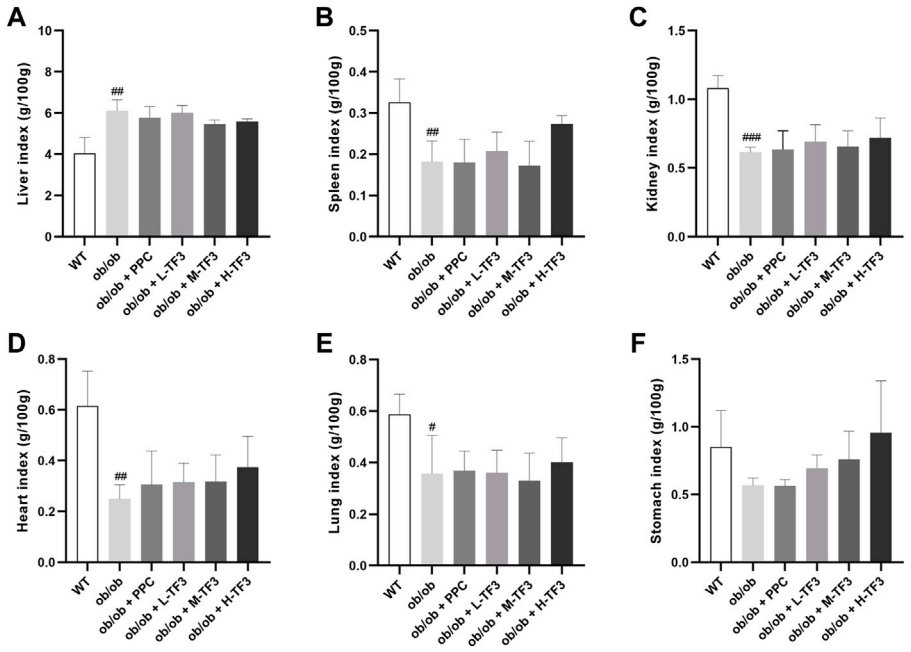

FIGURE 2
Organ coefficients. **(A)** Liver index. **(B)** Spleen index. **(C)** Kidney index. **(D)** Heart index. **(E)** Lung index. **(F)** Stomach index. All data are shown as the mean ± standard deviation (n = 5). Statistical significance: $^{\#}p < 0.05$, $^{\#\#}p < 0.01$, $^{\#\#\#}p < 0.001$ vs. the WT group.

efficiency ratio declined from 6.2 to 0.7% in ob/ob mice with H-TF3 treatment ($p < 0.001$). The M-TF3 groups also exhibited a decrease in feed efficiency ratio compared with the ob/ob group ($p < 0.01$) (Figure 1G). In contrast, the BMI was not observed to have a significant change in the TF3 groups and ob/ob group from Figure 1H ($p > 0.05$). Liver weight in the M-TF3 and H-TF3 groups was lighter than that in the ob/ob group ($p < 0.01$) (Figure 1I). The organ coefficients showed no significant difference in all ob/ob mice ($p > 0.05$) (Figures 2A–F). The viability of mice was not affected, except that the mice in the H-TF3 group had slightly less smooth hair during adaptation within the first 3 days of administration, but it recovered quickly.

Theaflavin-3,3′-digallate decreased fat accumulation of nonalcoholic fatty liver disease in ob/ob mice

Although the epididymal adipose tissue (EAT), subcutaneous adipose tissue (SAT), perirenal adipose tissue (PAT), and brown adipose tissue had been weighted in the experimental groups and model group, the relative weight of EAT in the H-TF3 group was significantly lower than that in the ob/ob group with $p < 0.01$, and white adipose tissue (WAT, the sum of EAT, SAT, and PAT) (g/100 g body weight) decreased in the M-TF3 and H-TF3 groups with $p < 0.05$ and $p < 0.001$, respectively (Figures 3A–E).

Theaflavin-3,3′-digallate attenuated liver tissue variation of nonalcoholic fatty liver disease in ob/ob mice

Liver size in ob/ob mice dramatically increased with a much lighter color than that in wild mice, which might indicate a higher fat content. The mice in the M-TF3 and H-TF3 groups were seen with obviously smaller liver size than that of the ob/ob group. These changes were improved sequentially as the dose of TF3 increases. M-TF3 and H-TF3 treatment made liver size smaller and deepened the color (Figure 3F). H&E staining of pathological slice observation showed prominent diffuse hepatic steatosis with nuclear condensation, cytoplasmic looseness, and increased fat vacuoles in ob/ob mice compared to wild mice. M-TF3 and H-TF3 treatment significantly reversed these changes (Figure 3G). Taken together, TF3 changed the appearance of the liver and alleviated hepatic steatosis in ob/ob mice.

Theaflavin-3,3′-digallate reduced blood lipid, liver function injury, and hepatic triglyceride of nonalcoholic fatty liver disease in ob/ob mice

TF3 significantly decreased the levels of TC and LDL-c in the M-TF3 and H-TF3 treatment group compared to the ob/ob

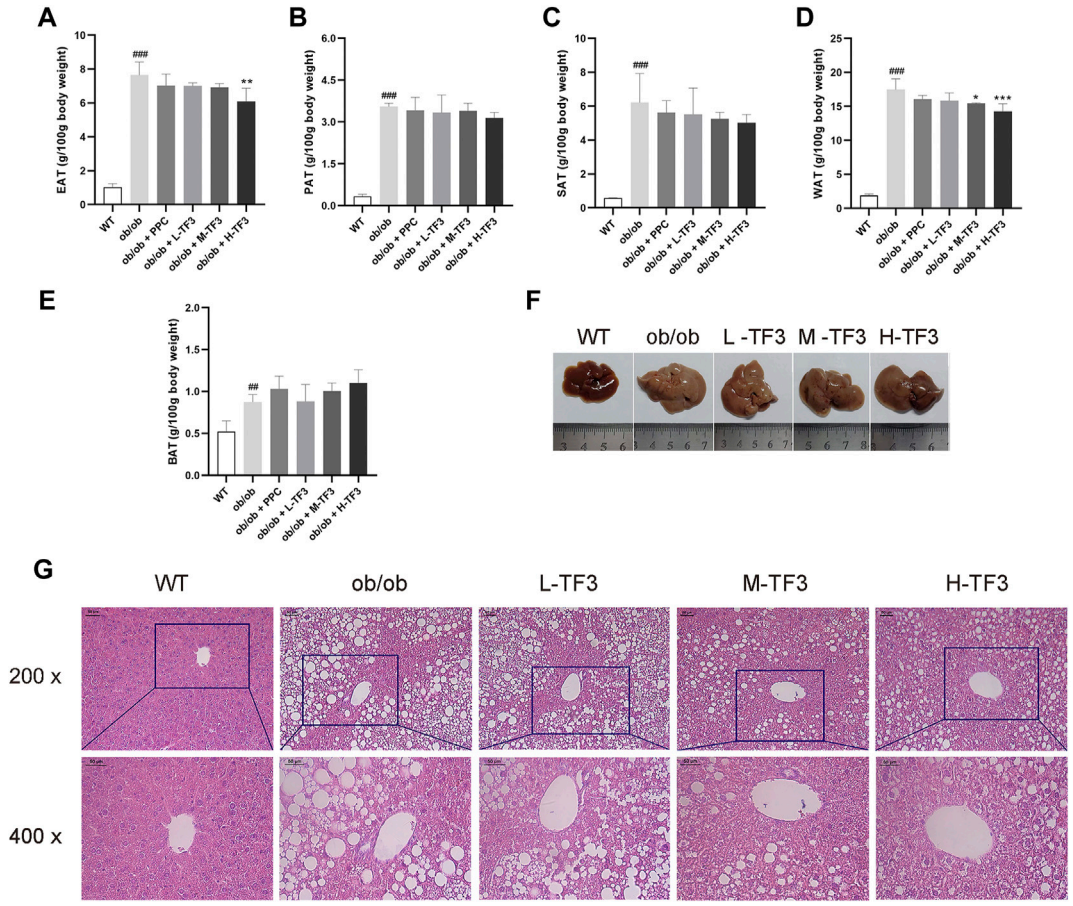

FIGURE 3
Weight of adipose tissue, hepatic appearance, and hematoxylin and eosin (H&E) staining. **(A)** Weight of epididymal adipose tissue. **(B)** Weight of subcutaneous adipose tissue. **(C)** Weight of perineal adipose tissue. **(D)** Weight of white adipose tissue; white adipose tissue was the sum of subcutaneous, perineal, and epididymal adipose tissue. **(E)** Weight of brown adipose tissue. **(F)** Liver appearance. **(G)** The representative image of the liver slides in H&E staining (scale bar, 50 μm for ×200 and ×400 magnification). All data are shown as the mean ± standard deviation (n = 5). Statistical significance: $^{\#}p < 0.05$, $^{\#\#}p < 0.01$, $^{\#\#\#}p < 0.001$ vs. the WT group. $^{*}p < 0.05$, $^{**}p < 0.01$, $^{***}p < 0.001$ vs. the ob/ob group.

group. TC ($p < 0.01$) and LDL-c ($p < 0.001$) in H-TF3 mice were lower than TC ($p < 0.05$) and LDL-c ($p < 0.01$) in M-TF3 mice. In contrast, obvious difference in TG ($p < 0.01$), HDL-c ($p < 0.05$), and FFA ($p < 0.05$) were observed only by H-TF3 supplementation compared with the ob/ob mice (Figures 4A–E). The elevated ALT and AST were also significantly decreased in the M-TF3 and H-TF3 intervention group compared to those in the ob/ob model group with dose-dependent trends (Figures 4F, G). AST ($p < 0.05$) and ALT ($p < 0.01$) in the M-TF3 group and AST ($p < 0.01$) and ALT ($p < 0.01$) in the H-TF3 group were 28.0% and 45.7% and 45.4% and 60.9% lower than those in the ob/ob group, respectively. In particular, the level of ALT in the H-TF3 group was close to that in the normal wild mice. H-TF3 treatment also reversed the elevated hepatic TG ($p < 0.01$) level induced by ob/ob obese mice (Figure 4H).

Theaflavin-3,3′-digallate regulated the hepatic gene expression profile

Based on the sequencing results of the WT, ob/ob, and H-TF3 groups, the sequencing quality was high and the sequencing depth was sufficient for transcriptome analysis (Supplementary Table S1). The expression distribution (Figure 5A) and principal component analysis (Figure 5B) indicated that biological reproducibility between samples was enough to subsequent analysis. Differential expression analysis and a Venn plot showed that there were 1,942 DEGs in the WT vs. ob/ob comparison including 988 upregulated DEGs and 954 downregulated DEGs. Moreover, 1,050 DEGs included 497 upregulated DEGs and 553 downregulated DEGs in the ob/ob vs. H-TF3 comparison (Figure 5C). These DEGs were subjected to additional bioinformatics analysis by being created

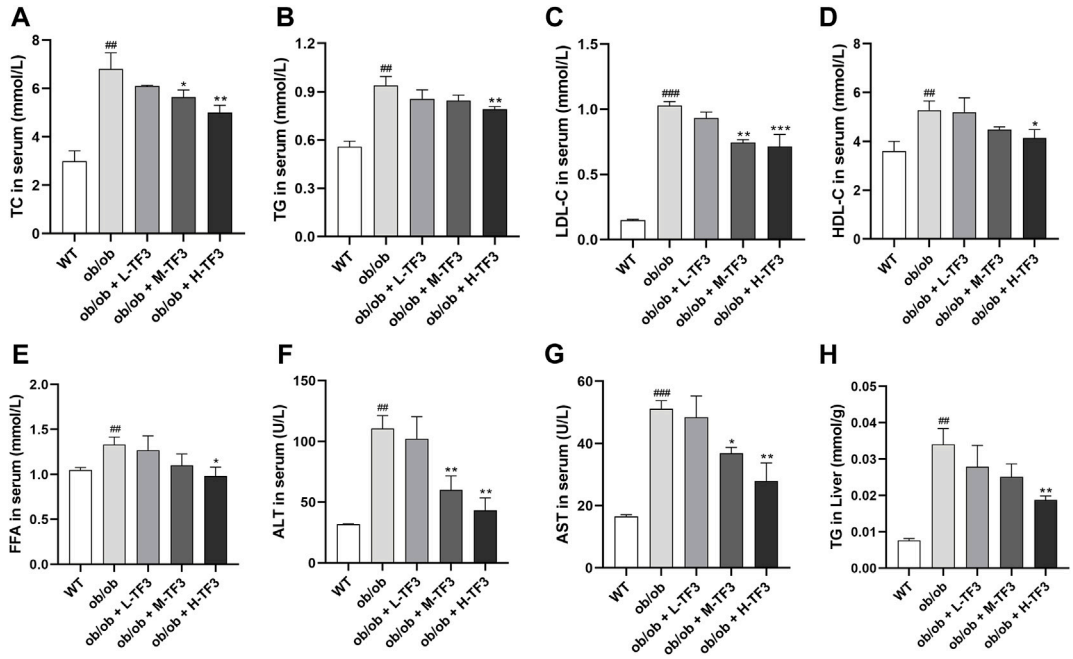

FIGURE 4
Biochemical parameters. **(A)** Total cholesterol (TC) level in serum. **(B)** Triglyceride (TG) level in serum. **(C)** Low-density lipoprotein cholesterol (LDL-c) level in serum. **(D)** High-density lipoprotein cholesterol (HDL-c) level in serum. **(E)** Free fatty acid (FFA) level in serum. **(F)** Alanine aminotransferase (ALT) level in serum. **(G)** Aspartate aminotransferase (AST) level in serum. **(H)** TG level in liver. Each parameter was repeated three times independently. All data are shown as the standard deviation ($n = 3$). Statistical significance: $^{\#}p < 0.05$, $^{\#\#}p < 0.01$, $^{\#\#\#}p < 0.001$ vs. the WT group. $^{*}p < 0.05$, $^{**}p < 0.01$, $^{***}p < 0.001$ vs. the ob/ob group.

as target gene sets. The MA plots showed the distribution of upregulated and downregulated DEGs in two comparison groups (Figures 5D, E).

GO and KEGG enrichment analyses were performed in target gene sets. GO terms with the top 20 enrichment degrees showed that the cholesterol transport, sterol transport, regulation of lipid storage, and fatty acid derivative metabolic process were closely related to NAFLD in obese mice (Figure 6A). KEGG enrichment analysis showed that the upregulated DEGs of the WT and ob/ob groups were mainly enriched in pathways of fatty acid elongation and steroid hormone biosynthesis, fatty acid metabolism, metabolic pathways, peroxisome proliferator-activated receptor (PPAR) signaling pathway, and biosynthesis of unsaturated fatty acids pathways (Figure 6B). In addition, the downregulated DEGs were enriched in steroid hormone biosynthesis, metabolic pathways, and cholesterol metabolism (Figure 6C). In the ob/ob and H-TF3 groups, the DEGs were primarily distributed in the pathways of regulation of lipid storage, secondary alcohol biosynthetic process, energy reserve metabolic process, and steroid biosynthetic and metabolic process (Figure 6D). KEGG enrichment analysis showed that downregulated DEGs between the ob/ob group and the H-TF3 group were mainly enriched in the PPAR signaling pathway (Figure 6E), while upregulated DEGs were mostly distributed in metabolic pathways, type I diabetes mellitus, steroid biosynthesis, bile secretion, etc. (Figure 6F). These results suggested that metabolic pathways and the PPAR signaling pathway might be crucial pathways producing an effect on NAFLD in this study. Moreover, 77 DEGs of metabolic pathways in the ob/ob vs. H-TF3 group were selected to create a histogram of KEGG analysis. It is interesting to note that they were mainly annotated to the lipid metabolism process including biosynthesis of unsaturated fatty acids (Fads1, Tecr, Scd1, and Elovl1), arachidonic acid and linoleic acid metabolism (Cyp4f14, Cyp1a2, and Cyp2c70), and steroid biosynthesis (Fdft1, Tm7sf2, Ebp, Dhcr7). These genes were significantly upregulated in ob/ob mice with TF3 treatment. In the PPAR signaling pathway, the expression of Fabp4, Plin4, Lpl, and Acadm was decreased, while that of Ppard encoding peroxisome proliferator-activated receptors δ (PPARδ) was increased. Based on the above results, we supposed that TF3 treatment might alleviate NAFLD through lipid metabolism regulated by the Fads1/PPARδ/Fabp4 axis.

Theaflavin-3,3′-digallate altered gut microbiota structure

The results of 16S rRNA demonstrated that the Sobs and Shannon indices showed no significant difference between the

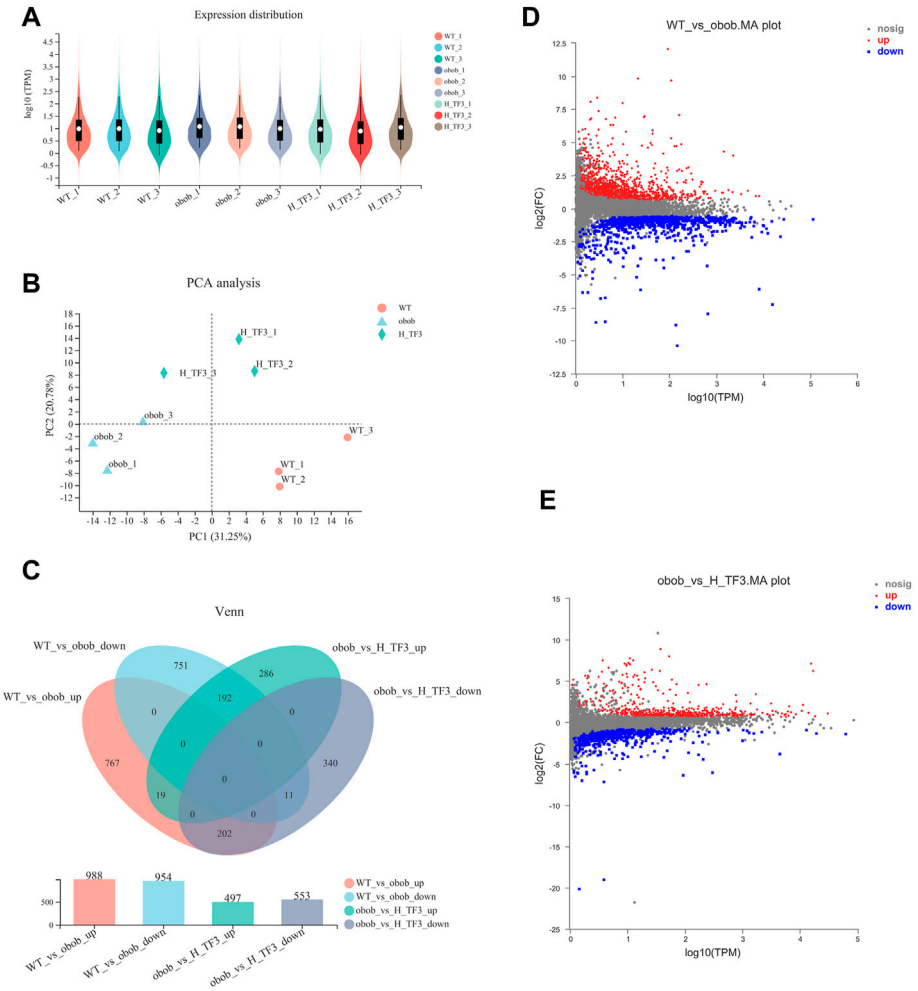

FIGURE 5
Comparison of gene expression (n = 3). **(A)** Violin plot showed gene expression distribution of each sample. **(B)** Principal component analysis (PCA) of gene expression profiles of three groups in liver tissue. **(C)** Venn diagram summarized gene changes in expression in various gene sets. **(D)** MA plot represented upregulated and downregulated genes in the WT vs. ob/ob comparison group. **(E)** MA plot represented upregulated and downregulated genes in the ob/ob vs. H-TF3 comparison group.

WT and ob/ob groups. In ob/ob obese mice, no significant effect on the richness and diversity of the gut microbiota was observed compared to that in wild mice (Figure 7A). In contrast, the Sobs and Shannon indices were both significantly increased with H-TF3 treatment compared with those in the ob/ob mice group (Figure 7B), indicating that H-TF3 could enhance the richness and diversity of the gut microbiota. The Good's coverage was up to 99% in each sample, and the rarefaction curves showed clear asymptotes (Figure 7C), which together indicated that the depth of sequencing data was sufficient and adequately covered most of the microbial diversity information in the sample. Moreover, PCoA revealed that the gut microbiota composition was different among the three groups (Figure 7D). To assess specific changes in the gut microbiota, we compared the relative abundance at the genus level. The relative abundance of *Odoribacter*, *Prevotellaceae_UCG-003*, *unclassified_f__Eggerthellaceae*, and *Prevotellaceae_Ga6A1_group* was significantly increased, whereas the relative abundance of *Christensenellaceae_R-7_group* and *Ruminococcus* was decreased in that ob/ob group compared with those in the WT group ($p < 0.05$) (Figure 7E). In contrast, the relative abundance of *Prevotellaceae_UCG-001*, *norank_f__Ruminococcaceae*, and *GCA-900066575* was significantly increased, and that of *Parvibacter* was significantly decreased in the H-TF3 group compared with those in the ob/ob group ($p < 0.05$) (Figure 7F). Gut microbiota in ob/ob mice differentiated from that of WT group mice. TF3 treatment changed gut microbiota composition in ob/ob mice.

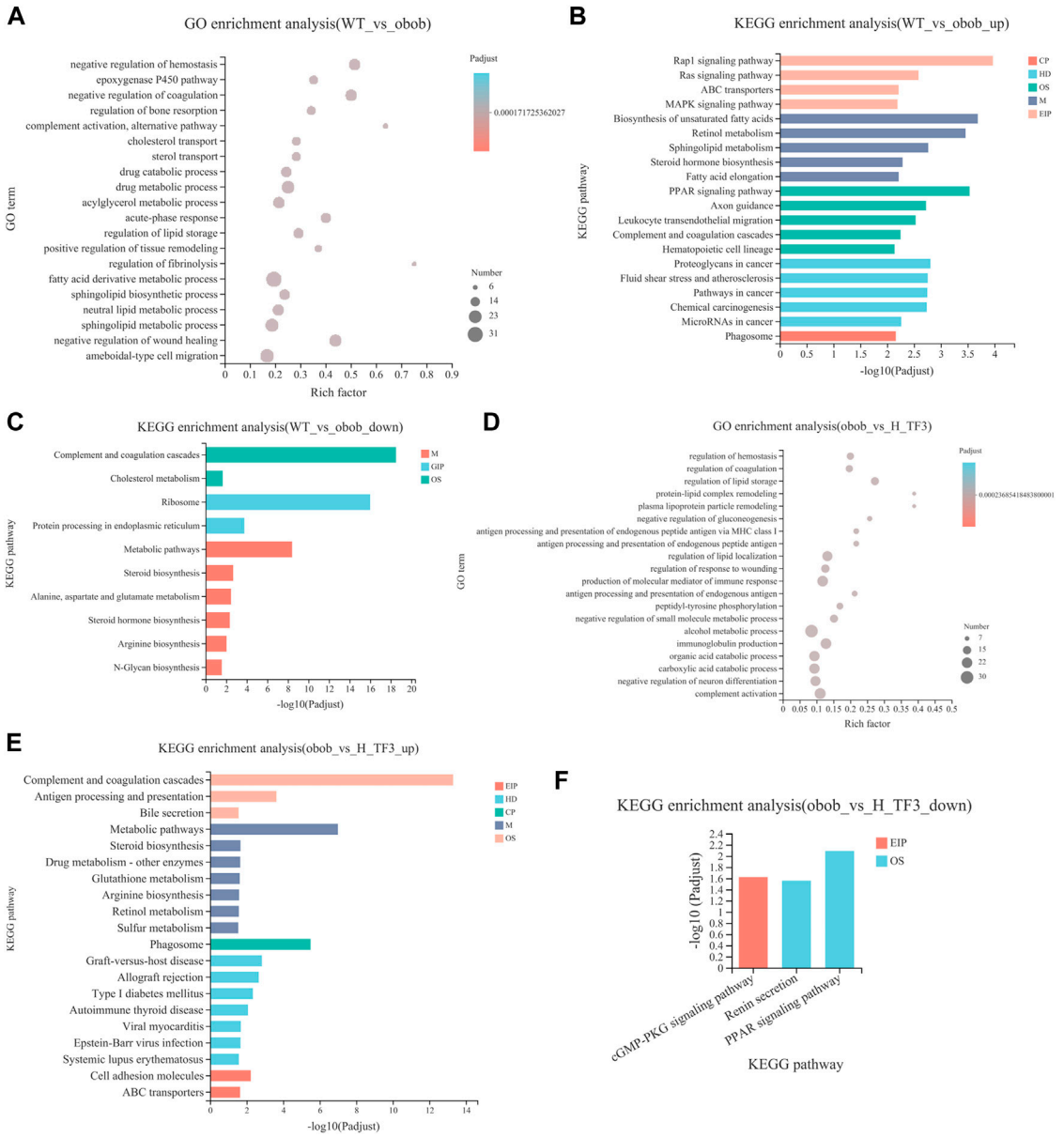

FIGURE 6
GO and KEGG enrichment analyses of DEGs between WT vs. ob/ob and ob/ob vs. H-TF3 comparison group (n = 3). **(A)** Top 20 enriched GO terms from DEGs in the WT vs. ob/ob group. **(B)** Top 20 enriched KEGG pathways from upregulated DEGs in the WT vs. ob/ob group. **(C)** Enriched KEGG pathways from downregulated DEGs in the WT vs. ob/ob group. **(D)** Top 20 enriched GO terms from DEGs in the ob/ob vs. H-TF3 group. **(E)** Top 20 enriched KEGG pathways from upregulated DEGs in the ob/ob vs. H-TF3 group. **(F)** Enriched KEGG pathways from downregulated DEGs in the ob/ob vs. H-TF3 group.

Associations between the gut microbiota composition and biochemical indicators and candidate genes

The expression of the 11 DEGs involved in lipid metabolism and 5 DEGs in the PPAR signaling pathway were reversed by H-TF3 treatment in ob/ob mice with significant difference (adjusted $p < 0.05$). Their differences in expression are shown in Figure 8A and Table 1. For further correlation analysis, 16 DEGs served as candidate genes that potentially functioned after TF3 treatment in NAFLD. The correlation between liver candidate genes and gut microbiota are shown in a Spearman

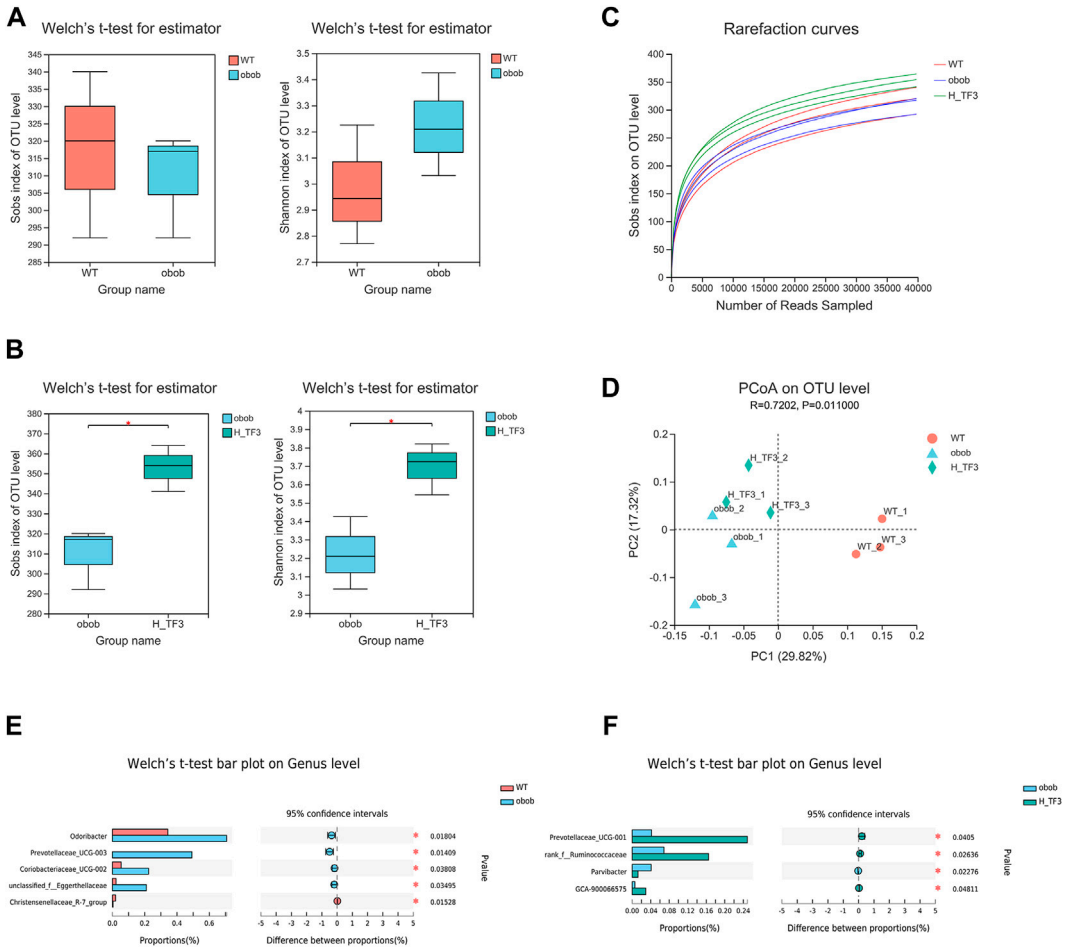

FIGURE 7
Different gut microbiota composition in the WT vs. ob/ob group and the ob/ob vs. H-TF3 comparison group (n = 3). **(A)** Alpha diversity index (Sobs and Shannon) compared between the WT and ob/ob groups. **(B)** Alpha diversity index (Sobs and Shannon) compared between the ob/ob and H-TF3 groups. **(C)** Rarefaction curves. **(D)** Beta diversity analysis. Principal coordinates analysis (PCoA) based on unweighted unifrac at the OTU level among the three groups. **(E)** Bar plot showed the different gut microbiota at the genus level in the WT and ob/ob groups using Welch's t test. **(F)** Bar plot showed the different gut microbiota at the genus level in the ob/ob and H-TF3 groups using Welch's t test. Statistical significance: $^*p < 0.05$.

correlation heatmap (Figure 8B). The relative abundance of *norank_f__Ruminococcaceae* genus exhibited a strong correlation with the expression of Cyp1a2, Dhcr7, Cyp4f14, Tm7sf2, Fads1, Ebp, Scd1, Tecr, Lpl, and Fabp4 ($p < 0.05$), especially those genes involved in the Fads1/PPARδ/Fabp4 signaling axis. We find it interesting that the relative abundance of *Alistipes* also showed a significantly positive correlation with the expression of some candidate genes, including Cyp2c70, Dhcr7, Tm7sf2, Fads1, Ebp, Scd1, Fdft1, Elovl1, and Tecr ($p < 0.05$). In addition, the correlation between biochemical parameters and intestinal flora are shown in a Spearman correlation heatmap (Figure 8C). The relative abundance of *norank_f__Ruminococcaceae* exhibited a significantly negative correlation with serum TC, TG, LDL-c, and FFA ($p < 0.05$). The relative abundance of *Akkermansia* was negatively correlated with the level of TC, HDL-c, FFA, and ALT in serum ($p < 0.05$). Preliminary correlation analyses demonstrated that TF3 might have a multidimensional effect on NAFLD mitigation.

Discussion

The lipid-lowering effects of theaflavin monomer TF3 have been authenticated *in vitro and vivo* in the recent 5 years, although there are only a few studies. Our previous study first confirmed that TF3 relieved hepatocyte lipid deposition through the novel plasma kallikrein/AMPK signaling pathway in FFA-induced hepatic HepG2 cells (Zhang et al., 2020). A recent study reported that TF3 could ameliorate obesity in

TABLE 1 List of candidate genes (obob_vs._H_TF3).

Gene name	Gene description	Regulation
Ppard	peroxisome proliferator activator receptor delta	up
Cyp2c70	cytochrome P450, family 2, subfamily c, polypeptide 70	up
Cyp1a2	cytochrome P450, family 1, subfamily a, polypeptide 2	up
Plin4	perilipin 4	down
Dhcr7	7-dehydrocholesterol reductase	up
Fabp4	fatty acid binding protein 4, adipocyte	down
Cyp4f14	cytochrome P450, family 4, subfamily f, polypeptide 14	up
Tm7sf2	transmembrane 7 superfamily member 2	up
Lpl	lipoprotein lipase	down
Fdft1	farnesyl diphosphate farnesyl transferase 1	up
Ebp	phenylalkylamine Ca^{2+} antagonist (emopamil) binding protein	up
Fads1	fatty acid desaturase 1	up
Tecr	trans-2,3-enoyl-CoA reductase	up
Scd1	stearoyl-Coenzyme A desaturase 1	up
Acadm	acyl-Coenzyme A dehydrogenase, medium chain	down
Elovl1	elongation of very long chain fatty acids	up

high-fat diet–induced mice by oral administration for 9 weeks through the signaling pathway of SIRT6/AMPK/SREBP-1/FASN. Even if the bioavailability of TF3 is considered poor, the beneficial effects were observed in the experimental design (Cai et al., 2021). In this NAFLD-related study, considering the lower bioavailability, the intraperitoneal injection administration of TF3 was applied to the ob/ob mouse model with more homogeneous phenotype. We found that TF3 rapidly produced beneficial effects based on the changes of weight and waistline in 1 week without bouncing until the end of the experiment. The results of the 4-week experiment gave us a reason to believe that TF3 has an obviously stable and effective therapeutic effect. Compared with oral administration for 9 weeks, intraperitoneal injection administration greatly shortened time and cost as well as improved the efficiency of animal experiment. Moreover, we found that the Fads1/PPARδ/Fabp4 signaling axis might be a new therapeutic target for NAFLD in the current study.

TF3 improved NAFLD in ob/ob mice. As expected, TF3 supplement decreased body weight, body weight gain, waistline, waistline gain in obese mice with food intake reduction. Effect of TF3 on phenotype was possibly related to suppression on appetite, which is in accord with the fact that black tea drinking makes people consume less food (Carter and Drewnowski, 2012). The organ coefficients were not obviously affected by TF3 treatment, indicating that TF3 is a relatively safe pharmacological ingredient. We could draw a conclusion of hepatic steatosis improving from histopathological analysis, which consisted of phenotypic changes in mice. The EAT with lighter weight was observed; it was an important organ for TG accumulation and many adipokines secretion (Corton et al., 1994). According to the results of biochemical indicators, TF3 had protective effects by decreasing the serum lipid and TG levels in the liver and could restore the activity of the liver function enzymes of AST and ALT.

The hepatic transcriptomics analysis indicated that metabolic pathways and the PPAR signaling pathway might be crucial pathways producing the effect of TF3. Metabolic pathways included biosynthesis of unsaturated fatty acids, arachidonic acid and linoleic acid metabolism, and steroid biosynthesis. The results are similar with the mechanism of turmeric in preventing hyperlipidemia in mice (Wang et al., 2021). Moreover, we proposed that TF3 produced an effect on NAFLD by regulating lipid metabolism *via* the Fads1/PPARδ/Fabp4 signaling axis. First, TF3 acted on upstream Fads1 and then activated PPARδ and downstream Fabp4. Fatty acid desaturase 1 encoded by Fads1 is one of the rate-limiting enzymes in the polyunsaturated fatty acid (PUFA) desaturation pathway (Martinelli et al., 2008). Patients with NAFLD had pathological changes associated with the depletion of PUFA; the higher expression of Fads1 protects liver from lipid accumulation (Araya et al., 2010; Athinarayanan et al., 2021). Moreover, Fads1 is specifically involved in catalyzing the conversion of dihomo-gamma-linolenic acid to arachidonic acid (Martinelli et al., 2008). Arachidonic acid and linoleic acid both belong to unsaturated fatty acids. Arachidonic acid is an important ω-6 PUFA, which is the most widely distributed endogenous active substance *in vivo*. A study reported that *Sagittaria sagittifolia* polysaccharide exerted preventive protection against high-fat diet–induced NAFLD by interfering with arachidonic acid metabolism (Deng et al., 2020). We find it interesting that the epoxyeicosatrienoic acids (EETs) are products of arachidonic acid and can be catalyzed by cytochrome P450 epoxygenases, in

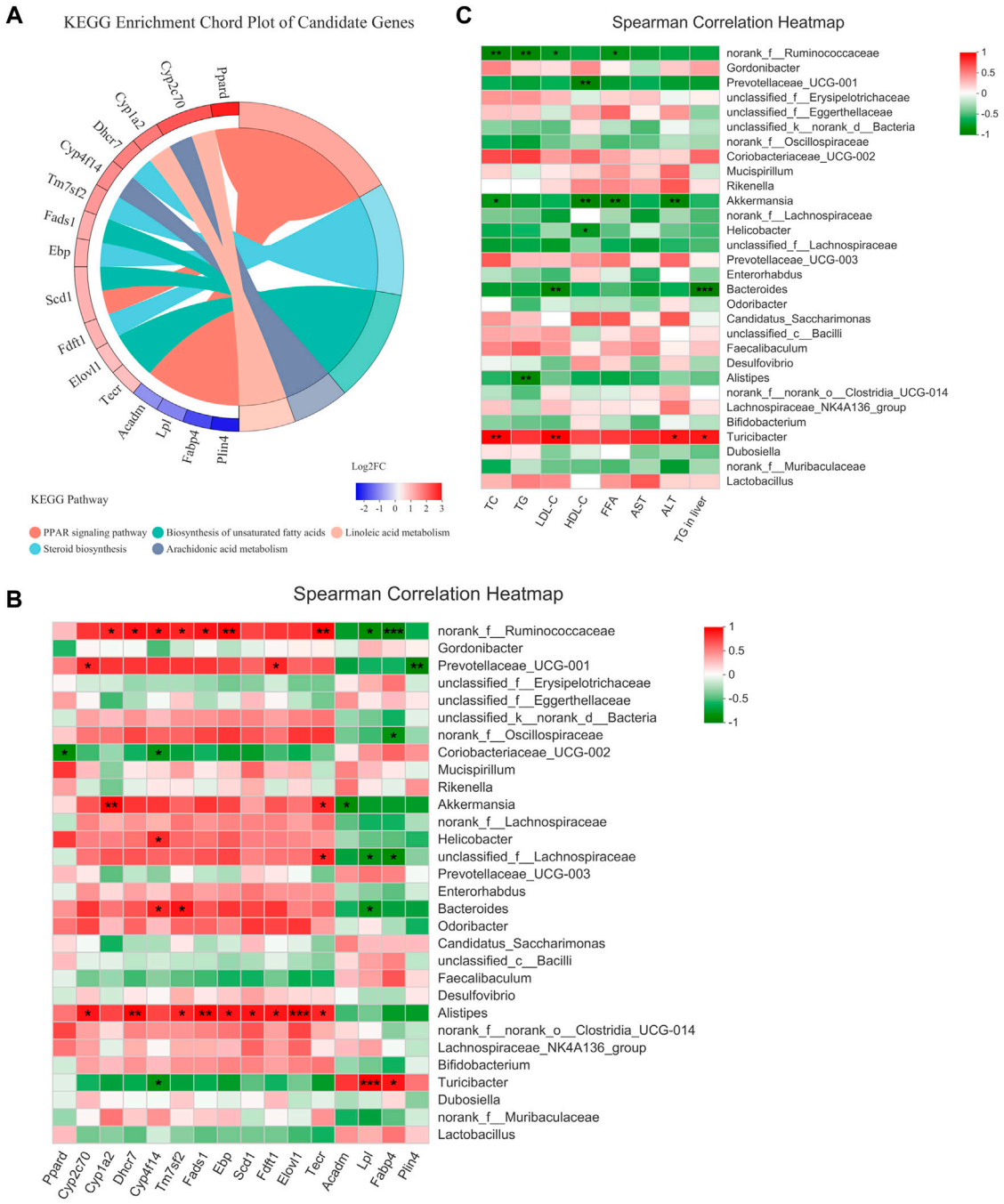

FIGURE 8
Candidate genes and Spearman correlation heatmap (n = 3). **(A)** KEGG enrichment chord plot of candidate genes. Left of plot is the regulation and fold change of expression; right is KEGG pathways. **(B)** The correlation between the gut microbiota and candidate genes. **(C)** The correlation between the gut microbiota and serum biochemical parameters. Statistical significance: $^{*}p < 0.05$, $^{**}p < 0.01$.

line with the increased expression of Cyp4f14, CYP1a2, and Cyp2c70 in this study. EETs and their metabolites can activate peroxisome proliferator-activated receptors α (PPARα) and peroxisome proliferator-activated receptors γ (PPARγ) in the PPAR signaling pathway (Wang X. et al., 2019). The PPAR signaling pathway is actively involved in the regulation of lipid metabolism, glucose homeostasis, cell proliferation, and adipocyte differentiation (Hu N. et al., 2021). The PPARδ is one of ligand-activated transcription factors that can be activated by the ligand of unsaturated fatty acids. PPARs (PPARα, PPARδ,

and PPARγ) stimulate lipid and glucose utilization by increasing mitochondrial function and fatty acid desaturation pathways (Montaigne et al., 2021). Therefore, we speculated that arachidonic acid might be an activator of PPARδ. About downstream Fabp4, it encoded fatty acid-binding protein 4 controlled by most notably PPARγ, PPARδ, and FFA (Haunerland and Spener, 2004). Fabp4 bind long-chain FFA and are specifically expressed in adipocyte (Thompson et al., 2018). Although the underlying molecular mechanisms of Fabp4 expression and activity have not been fully elucidated, Omega-3 fatty acids were reported to decrease the expression and consecutive secretion of Fabp4, which had a positive effect on anti-obesity and reversal of insulin resistance (Furuhashi et al., 2016; Chung et al., 2021). Based on above, we supposed that the Fads1/PPARδ/Fabp4 signaling axis might be a direct target pathway of TF3 to reduce lipid accumulation, providing a more theoretical basis for further drug development and clinical application.

Apart from signaling axis-related genes, TF3 also regulated some other gene expressions related to NAFLD. Plin4, Lpl, and Acadm were also critical target genes of PPARs in the PPAR signaling pathway. Their expression decreased after TF3 treatment. With the progression of NAFLD, the Lpl/Fabp4/Cpt1 molecule axis and controlled fatty acid metabolism were generally upregulated since the NASH phase (Yang et al., 2021). Hence, Plin4, Lpl, and Acadm might produce beneficial effects on preventing the progression of NAFLD to nonalcoholic steatohepatitis. In addition, the increased expression of Fdft1, Tm7sf2, Ebp, and Dhcr7, involved in cholesterol biosynthesis, might indirectly promote primary bile acid biosynthesis. Bile acid supplementations and agonists for specific targets played an important role in decreasing lipid accumulation and treating metabolic liver disorders (Liu H. et al., 2016; Evangelakos et al., 2021). For example, obeticholic acid, the steroidal agonist of farnesoid X receptor, became the most promising drug for MAFLD/steatohepatitis (Younossi et al., 2019). These genes might exert a synergistic effect with the Fads1/PPARδ/Fabp4 signaling axis in TF3.

The gut microbiota plays a crucial role in NAFLD mitigation through various mechanisms such as energy absorption and storage, promoting insulin resistance and choline deficiency and interfering with bile acid metabolism (Blaut, 2015; Wang et al., 2020). Hence, we analyzed the changes of the gut microbiota in NAFLD with TF3 supplement and found that the community richness and diversity of the gut microbiota increased. This is similar to the infusions of green tea, oolong tea, and black tea (Liu Z. et al., 2016); in addition, another tea polyphenol (epigallocatechin-3-gallate) treatment (Ushiroda et al., 2019) suppressed fatty liver disease by improving gut dysbiosis or increasing the diversity of the gut microbiota or altered its structure in obese mice. Our analysis demonstrated that *Prevotellaceae_UCG-001*, *norank_f__Ruminococcaceae* and *GCA-900066575* were significantly increased and *Parvibacter* was decreased in the H-TF3 group compared with those in the ob/ob group at the genus level. *Ruminococcaceae* are butyrate-producing bacteria. Butyrate is a kind of short-chain fatty acid (SCFA) produced from resistant starch, dietary fiber, and low-digestible polysaccharides by the microbiota in the colon and distal small intestine via fermentation (Kau et al., 2011; Zhou et al., 2017). Butyric acid protected against HFD-induced hepatic steatosis, inflammation, and liver injury (Zhou et al., 2017). *Prevotellaceae_UCG-001* also produces SCFAs, which stimulates glucagon secretion and increases satiety to regulate fat synthesis and cholesterol in the liver and inhibit weight gain (Maljaars et al., 2008; Wang M. et al., 2019). Previous studies had shown that high-fat diet–induced obese mice had a higher abundance of *GCA-900066575* than wild mice (Li et al., 2020; Hu Q. et al., 2021). However, we found that the abundance of *GCA-900066575* increased in the H-TF3 group rather than in ob/ob obese mice. A study also reported that α-linolenic acid could alleviate fatty liver and increase the abundance of *GCA-900066575* (Gao et al., 2020). *Parvibacter* is a beneficial bacterium, but its abundance reduced rather than increased, as expected, in the TF3 group (Li et al., 2022). TF3 mainly increased the abundance of SCF-producing bacteria to synergistically reduce fat accumulation and hepatic steatosis. It is worth mentioning that we found that TF3 could modulate gut microbiota composition *in vivo* even by intraperitoneal injection.

Accumulating evidence has pointed out the importance of the gut–liver axis in the development of liver disease. According to the correlation between the gut microbiota and candidate genes involved in lipid metabolism and PPAR signaling pathways, biochemical parameters, we supposed that the changes of the gut microbiota might be related to the Fads1/PPARδ/Fabp4 signaling axis. They further decreased lipid levels and liver injury together in NAFLD with TF3 supplement. However, the mechanism is still unclear. Their interaction requires further research. Bile acid metabolism, gut microbial metabolites such as lipopolysaccharide (LPS), and gut barrier dysfunction contribute to chronic liver disease by abnormal regulation of the gut–liver axis (Schneider et al., 2018; An et al., 2022). In a subsequent study, we will deeply explore the mechanism of the gut–liver axis in TF3, clarify the pharmacological effects, and provide more detailed clinical data for the drug development of TF3 in preventing and curing NAFLD.

Conclusion

It was demonstrated that TF3 was a safe and effective pharmacological ingredient for relieving NAFLD in the ob/ob mice model. The weight and waistline, fat accumulation, serum lipid, liver injury, and hepatic TG were alleviated by TF3 treatment. The beneficial effect of TF3 on NAFLD might be related to lipid metabolism regulated by the Fads1/PPARδ/Fabp4 axis and gut microbiota. The Spearman

correlation indicated that the gut microbiota might associate with the hepatic Fads1/PPARδ/Fabp4 signaling axis. Their interaction requires further research. TF3 might be a promising drug for clinical use to improve NAFLD.

Data availability statement

The datasets presented in this study can be found in online repositories. The names of the repository/repositories and accession number(s) can be found in the following: https://www.ncbi.nlm.nih.gov/, PRJNA824024; https://www.ncbi.nlm.nih.gov/, PRJNA824955.

Ethics statement

The animal study was reviewed and approved by the Animal Ethical Experimentation Committee of Jinan University.

Author contributions

CZ, LZ, FW, YW, SY, XP, WC, and ML collected the data. CZ performed the data analysis and interpreted the data, performed majority of the experiments, and prepared the draft. WIZ designed the research, provided guidance, and revised the draft. WUZ directed the study's analytic strategy and revised the manuscript. HL, XP, and ZH reviewed the manuscript. All authors contributed to the article and approved the submitted version.

Funding

This work was supported by the National Natural Science Foundation of China (grant number 81903319); the Natural Science Foundation of Guangdong Province of China (grant number 2021A1515011220); the Administration of Traditional Chinese Medicine of Guangdong Province of China (grant number 20211008); the Special Fund for Scientific Innovation Strategy-Construction of High Level Academy of Agriculture Science (grant number R2018YJ-YB3002, R2019YJ-QG001); the Top Young Talents of Guangdong Hundreds of Millions of Projects of China (grant number 87316004); The Foundation of Director of Crops Research Institute, Guangdong Academy of Agricultural Sciences (grant number 202205); the Outstanding Young Scholar of Double Hundred Talents of Jinan University of China; and the National Natural Science Foundation of China (grant number 81473014).

Conflict of interest

The authors declare that the research was conducted in the absence of any commercial or financial relationships that could be construed as a potential conflict of interest.

Publisher's note

All claims expressed in this article are solely those of the authors and do not necessarily represent those of their affiliated organizations, or those of the publisher, the editors, and the reviewers. Any product that may be evaluated in this article, or claim that may be made by its manufacturer, is not guaranteed or endorsed by the publisher.

Supplementary material

The Supplementary Material for this article can be found online at: https://www.frontiersin.org/articles/10.3389/fphar.2022.925264/full#supplementary-material

References

An, L., Wirth, U., Koch, D., Schirren, M., Drefs, M., Koliogiannis, D., et al. (2022). The role of gut-derived lipopolysaccharides and the intestinal barrier in fatty liver diseases. *J. Gastrointest. Surg.* 26, 671–683. doi:10.1007/S11605-021-05188-7

Anushiravani, A., Haddadi, N., Pourfarmanbar, M., and Mohammadkarimi, V. (2019). Treatment options for nonalcoholic fatty liver disease: A double-blinded randomized placebo-controlled trial. *Eur. J. Gastroenterol. Hepatol.* 31, 613–617. doi:10.1097/Meg.0000000000001369

Araya, J., Rodrigo, R., Pettinelli, P., Araya, A. V., Poniachik, J., and Videla, L. A. (2010). Decreased liver fatty acid delta-6 and delta-5 desaturase activity in obese patients. *Obes. (Silver Spring)* 18, 1460–1463. doi:10.1038/Oby.2009.379

Athinarayanan, S., Fan, Y. Y., Wang, X., Callaway, E., Cai, D., Chalasani, N., et al. (2021). Fatty acid desaturase 1 influences hepatic lipid homeostasis by modulating the pparα-fgf21 Axis. *Hepatol. Commun.* 5, 461–477. doi:10.1002/Hep4.1629

Blaut, M. (2015). Gut microbiota and energy balance: Role in obesity. *Proc. Nutr. Soc.* 74, 227–234. doi:10.1017/S0029665114001700

Cai, X., Liu, Z., Dong, X., Wang, Y., Zhu, L., Li, M., et al. (2021). Hypoglycemic and lipid lowering effects of theaflavins in high-fat diet-induced obese mice. *Food Funct.* 12, 9922–9931. doi:10.1039/D1fo01966j

Carter, B. E., and Drewnowski, A. (2012). Beverages containing soluble fiber, caffeine, and green tea catechins suppress hunger and lead to less energy consumption at the next meal. *Appetite* 59, 755–761. doi:10.1016/J.Appet.2012.08.015

Chalasani, N., Younossi, Z., Lavine, J. E., Charlton, M., Cusi, K., Rinella, M., et al. (2018). The diagnosis and management of nonalcoholic fatty liver disease: Practice guidance from the American association for the study of liver diseases. *Hepatology* 67, 328–357. doi:10.1002/Hep.29367

Chung, J. Y., Hong, J., Kim, H. J., Song, Y., Yong, S. B., Lee, J., et al. (2021). White adipocyte-targeted dual gene silencing of fabp4/5 for anti-obesity, anti-inflammation and reversal of insulin resistance: Efficacy and comparison of administration routes. *Biomaterials* 279, 121209. doi:10.1016/J.Biomaterials.2021.121209

Corton, J. M., Gillespie, J. G., and Hardie, D. G. (1994). Role of the amp-activated protein kinase in the cellular stress response. *Curr. Biol.* 4, 315–324. doi:10.1016/S0960-9822(00)00070-1

Cotter, T. G., and Rinella, M. (2020). Nonalcoholic fatty liver disease 2020: The state of the disease. *Gastroenterology* 158, 1851–1864. doi:10.1053/J.Gastro.2020.01.052

Deng, X., Ke, X., Tang, Y., Luo, W., Dong, R., Ge, D., et al. (2020). Sagittaria sagittifolia polysaccharide interferes with arachidonic acid metabolism in non-alcoholic fatty liver disease mice via Nrf2/Ho-1 signaling pathway. *Biomed. Pharmacother.* 132, 110806. doi:10.1016/J.Biopha.2020.110806

Easl Easd And Easo (2016). Easl-easd-easo clinical practice guidelines for the management of non-alcoholic fatty liver disease. *Obes. Facts* 9, 65–90. doi:10.1159/000443344

Eslam, M., Newsome, P. N., Sarin, S. K., Anstee, Q. M., Targher, G., Romero-Gomez, M., et al. (2020). A new definition for metabolic dysfunction-associated fatty liver disease: An international expert consensus statement. *J. Hepatol.* 73, 202–209. doi:10.1016/J.Jhep.2020.03.039

Evangelakos, I., Heeren, J., Verkade, E., and Kuipers, F. (2021). Role of bile acids in inflammatory liver diseases. *Semin. Immunopathol.* 43, 577–590. doi:10.1007/S00281-021-00869-6

Fatima, M., Kesharwani, R. K., Misra, K., and Rizvi, S. I. (2013). Protective effect of theaflavin on erythrocytes subjected to *in vitro* oxidative stress. *Biochem. Res. Int.* 2013, 649759. doi:10.1155/2013/649759

Furuhashi, M., Hiramitsu, S., Mita, T., Omori, A., Fuseya, T., Ishimura, S., et al. (2016). Reduction of circulating Fabp4 level by treatment with omega-3 fatty acid ethyl esters. *Lipids Health Dis.* 15, 5. doi:10.1186/S12944-016-0177-8

Gao, X., Chang, S., Liu, S., Peng, L., Xie, J., Dong, W., et al. (2020). Correlations between A-linolenic acid-improved multitissue homeostasis and gut microbiota in mice fed A high-fat diet. *Msystems* 5, e0039120. doi:10.1128/Msystems.00391-20

Gao, Y., Yin, J., Tu, Y., and Chen, Y. C. (2019). Theaflavin-3, 3'-digallate suppresses human ovarian carcinoma ovcar-3 cells by regulating the checkpoint kinase 2 and P27 Kip1 pathways. *Molecules* 24, E673. doi:10.3390/Molecules24040673

Haunerland, N. H., and Spener, F. (2004). Fatty acid-binding proteins-insights from genetic manipulations. *Prog. Lipid Res.* 43, 328–349. doi:10.1016/J.Plipres.2004.05.001

Henning, S. M., Aronson, W., Niu, Y., Conde, F., Lee, N. H., Seeram, N. P., et al. (2006). Tea polyphenols and theaflavins are present in prostate tissue of humans and mice after green and black tea consumption. *J. Nutr.* 136, 1839–1843. doi:10.1093/Jn/136.7.1839

Hu, N., Chen, C., Wang, J., Huang, J., Yao, D., and Li, C. (2021a). Atorvastatin ester regulates lipid metabolism in hyperlipidemia rats via the ppar-signaling pathway and hmgcr expression in the liver. *Int. J. Mol. Sci.* 22, 11107. doi:10.3390/Ijms222011107

Hu, Q., Niu, Y., Yang, Y., Mao, Q., Lu, Y., Ran, H., et al. (2021b). Polydextrose alleviates adipose tissue inflammation and modulates the gut microbiota in high-fat diet-fed mice. *Front. Pharmacol.* 12, 795483. doi:10.3389/Fphar.2021.795483

Jiang, Y., Jin, W., Li, J., and Huang, Q. (2021). Associations between caseinophosphopeptides and theaflavin-3, 3'-digallate and their impact on cellular antioxidant activity. *Food Funct.* 12, 7390–7401. doi:10.1039/D1fo01413g

Jin, D., Xu, Y., Mei, X., Meng, Q., Gao, Y., Li, B., et al. (2013). Antiobesity and lipid lowering effects of theaflavins on high-fat diet induced obese rats. *J. Funct. Foods* 5, 1142–1150. doi:10.1016/J.Jff.2013.03.011

Kau, A. L., Ahern, P. P., Griffin, N. W., Goodman, A. L., and Gordon, J. I. (2011). Human nutrition, the gut microbiome and the immune system. *Nature* 474, 327–336. doi:10.1038/Nature10213

Lambert, J. D., and Yang, C. S. (2003). Cancer chemopreventive activity and bioavailability of tea and tea polyphenols. *Mutat. Res.* 523-524, 201–208. doi:10.1016/S0027-5107(02)00336-6

Li, H., Liu, F., Lu, J., Shi, J., Guan, J., Yan, F., et al. (2020). Probiotic mixture of lactobacillus plantarum strains improves lipid metabolism and gut microbiota structure in high fat diet-fed mice. *Front. Microbiol.* 11, 512. doi:10.3389/Fmicb.2020.00512

Li, Y., Bai, D., Lu, Y., Chen, J., Yang, H., Mu, Y., et al. (2022). The crude guava polysaccharides ameliorate high-fat diet-induced obesity in mice via reshaping gut microbiota. *Int. J. Biol. Macromol.* 213, 234–246. doi:10.1016/J.Ijbiomac.2022.05.130

Liu, H., Pathak, P., Boehme, S., and Chiang, J. L. (2016a). Cholesterol 7α-hydroxylase protects the liver from inflammation and fibrosis by maintaining cholesterol homeostasis. *J. Lipid Res.* 57, 1831–1844. doi:10.1194/Jlr.M069807

Liu, Y., Zheng, J., Hao, J., Wang, R. R., Liu, X., Gu, P., et al. (2022). Global burden of primary liver cancer by five etiologies and global prediction by 2035 based on global burden of disease study 2019. *Cancer Med.* 11, 1310–1323. doi:10.1002/Cam4.4551

Liu, Z., Chen, Z., Guo, H., He, D., Zhao, H., Wang, Z., et al. (2016b). The modulatory effect of infusions of green tea, oolong tea, and black tea on gut microbiota in high-fat-induced obese mice. *Food Funct.* 7, 4869–4879. doi:10.1039/C6fo01439a

Maljaars, P. W., Peters, H. P., Mela, D. J., and Masclee, A. A. (2008). Ileal brake: A sensible food target for appetite control. A review. *Physiol. Behav.* 95, 271–281. doi:10.1016/J.Physbeh.2008.07.018

Mancini, G. B., Baker, S., Bergeron, J., Fitchett, D., Frohlich, J., Genest, J., et al. (2011). Diagnosis, prevention, and management of statin adverse effects and intolerance: Proceedings of A Canadian working group consensus conference. *Can. J. Cardiol.* 27, 635–662. doi:10.1016/J.Cjca.2011.05.007

Manne, V., Handa, P., and Kowdley, K. V. (2018). Pathophysiology of nonalcoholic fatty liver disease/nonalcoholic steatohepatitis. *Clin. Liver Dis.* 22, 23–37. doi:10.1016/J.Cld.2017.08.007

Martinelli, N., Girelli, D., Malerba, G., Guarini, P., Illig, T., Trabetti, E., et al. (2008). Fads genotypes and desaturase activity estimated by the ratio of arachidonic acid to linoleic acid are associated with inflammation and coronary artery disease. *Am. J. Clin. Nutr.* 88, 941–949. doi:10.1093/Ajcn/88.4.941

Montaigne, D., Butruille, L., and Staels, B. (2021). Ppar control of metabolism and cardiovascular functions. *Nat. Rev. Cardiol.* 18, 809–823. doi:10.1038/S41569-021-00569-6

Mulder, T. P., Van Platerink, C. J., Wijnand Schuyl, P. J., and Van Amelsvoort, J. M. (2001). Analysis of theaflavins in biological fluids using liquid chromatography-electrospray mass spectrometry. *J. Chromatogr. B Biomed. Sci. Appl.* 760, 271–279. doi:10.1016/S0378-4347(01)00285-7

Nascimbeni, F., Pellegrini, E., Lugari, S., Mondelli, A., Bursi, S., Onfiani, G., et al. (2019). Statins and nonalcoholic fatty liver disease in the era of precision medicine: More friends than foes. *Atherosclerosis* 284, 66–74. doi:10.1016/J.Atherosclerosis.2019.02.028

Perumpail, B. J., Khan, M. A., Yoo, E. R., Cholankeril, G., Kim, D., and Ahmed, A. (2017). Clinical epidemiology and disease burden of nonalcoholic fatty liver disease. *World J. Gastroenterol.* 23, 8263–8276. doi:10.3748/Wjg.V23.I47.8263

Sanyal, A. J., Chalasani, N., Kowdley, K. V., Mccullough, A., Diehl, A. M., Bass, N. M., et al. (2010). Pioglitazone, vitamin E, or placebo for nonalcoholic steatohepatitis. *N. Engl. J. Med.* 362, 1675–1685. doi:10.1056/Nejmoa0907929

Schneider, K. M., Albers, S., and Trautwein, C. (2018). Role of bile acids in the gut-liver Axis. *J. Hepatol.* 68, 1083–1085. doi:10.1016/J.Jhep.2017.11.025

Thompson, K. J., Austin, R. G., Nazari, S. S., Gersin, K. S., Iannitti, D. A., and Mckillop, I. H. (2018). Altered fatty acid-binding protein 4 (Fabp4) expression and function in human and animal models of hepatocellular carcinoma. *Liver Int.* 38, 1074–1083. doi:10.1111/Liv.13639

Ushiroda, C., Naito, Y., Takagi, T., Uchiyama, K., Mizushima, K., Higashimura, Y., et al. (2019). Green tea polyphenol (Epigallocatechin-3-Gallate) improves gut dysbiosis and serum bile acids dysregulation in high-fat diet-fed mice. *J. Clin. Biochem. Nutr.* 65, 34–46. doi:10.3164/Jcbn.18-116

Wang, M., Wang, R., Li, L., Yan, Y., Jia, S., Jiang, H., et al. (2021). Quantitative proteomics of plasma and liver reveals the mechanism of turmeric in preventing hyperlipidemia in mice. *Food Funct.* 12, 10484–10499. doi:10.1039/D1fo01849c

Wang, M., Wichienchot, S., He, X., Fu, X., Huang, Q., and Zhang, B. (2019a). *In vitro* colonic fermentation of dietary fibers: Fermentation rate, short-chain fatty acid production and changes in microbiota. *Trends Food Sci. Technol.* 88, 1–9. doi:10.1016/j.tifs.2019.03.005

Wang, S., Wang, Y., Wang, Y., Duan, Z., Ling, Z., Wu, W., et al. (2019b). Theaflavin-3, 3'-digallate suppresses biofilm formation, acid production, and acid tolerance in Streptococcus mutans by targeting virulence factors. *Front. Microbiol.* 10, 1705. doi:10.3389/Fmicb.2019.01705

Wang, X., Li, L., Wang, H., Xiao, F., and Ning, Q. (2019c). Epoxyeicosatrienoic acids alleviate methionine-choline-deficient diet-induced non-alcoholic steatohepatitis in mice. *Scand. J. Immunol.* 90, E12791. doi:10.1111/Sji.12791

Wang, Y., Dilidaxi, D., Wu, Y., Sailike, J., Sun, X., and Nabi, X. H. (2020). Composite probiotics alleviate type 2 diabetes by regulating intestinal microbiota and inducing glp-1 secretion in Db/Db mice. *Biomed. Pharmacother.* 125, 109914. doi:10.1016/J.Biopha.2020.109914

Wu, Y. Y., Li, W., Xu, Y., Jin, E. H., and Tu, Y. Y. (2011). Evaluation of the antioxidant effects of four main theaflavin derivatives through chemiluminescence and dna damage analyses. *J. Zhejiang Univ. Sci. B* 12, 744–751. doi:10.1631/Jzus.B1100041

Yang, H., Deng, Q., Ni, T., Liu, Y., Lu, L., Dai, H., et al. (2021). Targeted inhibition of lpl/fabp4/cpt1 fatty acid metabolic Axis can effectively prevent the progression of nonalcoholic steatohepatitis to liver cancer. *Int. J. Biol. Sci.* 17, 4207–4222. doi:10.7150/Ijbs.64714

Younossi, Z., Anstee, Q. M., Marietti, M., Hardy, T., Henry, L., Eslam, M., et al. (2018). Global burden of nafld and nash: Trends, predictions, risk factors and prevention. *Nat. Rev. Gastroenterol. Hepatol.* 15, 11–20. doi:10.1038/Nrgastro.2017.109

Younossi, Z. M., Ratziu, V., Loomba, R., Rinella, M., Anstee, Q. M., Goodman, Z., et al. (2019). Obeticholic acid for the treatment of non-alcoholic steatohepatitis: Interim analysis from A multicentre, randomised, placebo-controlled phase 3 trial. *Lancet* 394, 2184–2196. doi:10.1016/S0140-6736(19)33041-7

Zhang, W., An, R., Li, Q., Sun, L., Lai, X., Chen, R., et al. (2020). Theaflavin Tf3 relieves hepatocyte lipid deposition through activating an ampk signaling pathway by targeting plasma kallikrein. *J. Agric. Food Chem.* 68, 2673–2683. doi:10.1021/Acs.Jafc.0c00148

Zhou, D., Pan, Q., Xin, F. Z., Zhang, R. N., He, C. X., Chen, G. Y., et al. (2017). Sodium butyrate attenuates high-fat diet-induced steatohepatitis in mice by improving gut microbiota and gastrointestinal barrier. *World J. Gastroenterol.* 23, 60–75. doi:10.3748/wjg.v23.i1.60

Advantages of publishing in Frontiers

OPEN ACCESS
Articles are free to read for greatest visibility and readership

FAST PUBLICATION
Around 90 days from submission to decision

HIGH QUALITY PEER-REVIEW
Rigorous, collaborative, and constructive peer-review

TRANSPARENT PEER-REVIEW
Editors and reviewers acknowledged by name on published articles

Frontiers
Avenue du Tribunal-Fédéral 34
1005 Lausanne | Switzerland

Visit us: www.frontiersin.org
Contact us: frontiersin.org/about/contact

REPRODUCIBILITY OF RESEARCH
Support open data and methods to enhance research reproducibility

DIGITAL PUBLISHING
Articles designed for optimal readership across devices

FOLLOW US
@frontiersin

IMPACT METRICS
Advanced article metrics track visibility across digital media

EXTENSIVE PROMOTION
Marketing and promotion of impactful research

LOOP RESEARCH NETWORK
Our network increases your article's readership